Aus dem Cécile und Oskar Vogt-Institut für Hirnforschung
der Heinrich-Heine-Universität Düsseldorf

Zytoarchitektonische Analyse und probabilistische Karten zur Untersuchung von Sprache

Dissertation

zur Erlangung des Doktorgrades Doctor rerum medicarum „Dr. rer. med.“
der Medizinischen Fakultät der Heinrich-Heine-Universität Düsseldorf

vorgelegt von
Nina Unger
(2024)

Als Inauguraldissertation gedruckt mit Genehmigung der
Medizinischen Fakultät der Heinrich-Heine-Universität Düsseldorf

gez.:
Dekan: Prof. Dr. med. Nikolaj Klöcker
Gutachter/innen: Prof. Dr. med. Katrin Amunts, Prof. Dr. med. Simon Eickhoff

"It’s rather unlikely that psychology, on its own,
will arrive at the real, lawful characterization of the structure of the mind,
as long as it neglects the anatomy of the organ of the mind."

(Paul Flechsig, 1896)

Publikationen

Teile dieser Arbeit wurden veröffentlicht:

Publikationen in Peer-Reviewed Journals:

1. **Unger, N.**, Haeck, M., Eickhoff, S. B., Camilleri, J. A., Dickscheid, T., Mohlberg, H., Bludau, S., Caspers, S., & Amunts, K. (2023). Cytoarchitectonic mapping of the human frontal operculum – New correlates for a variety of brain functions. *Frontiers in Human Neuroscience, 17,* 1087026. https://doi.org/10.3389/fnhum.2023.1087026
2. Schiffer, C., Spitzer, H., Kiwitz, K., **Unger, N.**, Wagstyl, K., Evans, A. C., Harmeling, S., Amunts, K., & Dickscheid, T. (2021). Convolutional neural networks for cytoarchitectonic brain mapping at large scale. *NeuroImage, 240,* 118327. https://doi.org/10.1016/j.neuroimage.2021.118327
3. **Unger, N.**, Heim, S., Hilger, D. I., Bludau, S., Pieperhoff, P., Cichon, S., Amunts, K., & Mühleisen, T. W. (2021d). Identification of phonology-related genes and functional characterization of Broca's and Wernicke's regions in language and learning disorders. *Frontiers in Neuroscience, 15,* 680762. https://doi.org/10.3389/fnins.2021.680762

Datenpublikationen – zytoarchitektonische Wahrscheinlichkeitskarten:

4. **Unger, N.,** Bludau. S., Mohlberg, H., Caspers, S., & Amunts, K. (2021a). Probabilistic cytoarchitectonic map of Area OP5 (Frontal Operculum) (v3.2) [Data set]. EBRAINS. DOI: 10.25493/KN1A-YX4
5. **Unger, N.,** Bludau, S., Mohlberg, H., Caspers, S., & Amunts K. (2021b). Probabilistic cytoarchitectonic map of Area OP6 (Frontal Operculum) (v3.2) [Data set]. EBRAINS. DOI: 10.25493/RQKR-WE4
6. **Unger, N.,** Bludau, S., Mohlberg, H., Caspers, S., & Amunts, K. (2021c). Probabilistic cytoarchitectonic map of Area OP7 (Frontal Operculum) (v3.2) [Data set]. EBRAINS. DOI: 10.25493/W2D1-DJF

Konferenzbeiträge – wissenschaftliche Vorträge:

7. **Unger, N**. (04.09.2023). *Cytoarchitectonic mapping of the human frontal operculum – New correlates for a variety of brain functions* [Vortrag]. Retreat 2023 of the iBrain Graduate School, Düsseldorf.
8. **Unger, N.** (26.09.2019). *Cytoarchitectonic analysis and probabilistic maps of the human frontal operculum* [Vortrag]. Vogt-Seminar, Düsseldorf.
9. **Unger, N.** (24.07.2018). *Cytoarchitectonic analysis and probabilistic maps of the human frontal operculum* [Vortrag]. 3rd Annual Meeting of the iBrain Graduate School, Düsseldorf.

Konferenzbeiträge – wissenschaftliche Poster:

10. Bludau, S., Mühleisen, T. W., Pieperhoff, P., Berger, P., **Unger, N.**, Wojtasik, M., Hilger, D. I., Cichon, S., Dickscheid, T., & Amunts, K. (23.06.-03.07.2020). *JuGEx – Bridging the scales between gene expression and cytoarchitecture* [Poster]. 26th Meeting of the Organization of Human Brain Mapping, online.
11. **Unger, N.**, Heim, S., Hilger, D. I., Bludau, S., Pieperhoff, P., Cichon, S., Amunts, K., & Mühleisen, T. W. (21.08.2019). *Candidate genes for phonological processing disorders: A systematic review and expression analysis in Broca's and Wernicke's regions* [Poster]. 11th Annual Meeting der Society for the Neurobiology of Language, Helsinki.
12. **Unger, N.,** Heim, S., Hilger, D. I., Bludau, S., Pieperhoff, P., Cichon, S., Amunts, K., & Mühleisen, T. W. (25.06.-26.06.2019). *Candidate genes for phonological processing disorders: A systematic review and expression analysis in Broca's and Wernicke's regions* [Poster]. 8th INM-ICS Retreat, Jülich.
13. **Unger, N.**, Eickhoff, S. B., Mohlberg, H., Bludau, S., Caspers, S., & Amunts, K. (04.09.2018). *On the trail of language: Cytoarchitectonic analysis and probabilistic maps of the human frontal operculum* [Poster]. Human Brain Project School – The Human Brain Atlas, Düsseldorf.

Zusammenfassung

Sprache ist eine komplexe kognitive Leistung des menschlichen Gehirns, die in Netzwerken ausgeführt wird. In der frühen Sprachforschung lag der Fokus auf den klassischen Sprachareale Broca und Wernicke. Auch heute wird diesen Arealen weiterhin eine Schlüsselrolle zugeschrieben, allerdings weiß man inzwischen, dass weitaus mehr Gehirnareale an der Verarbeitung von Sprache beteiligt sind und es liegt eine Neudefinition der anterioren Sprachregion vor, die u. a. das frontale Operculum (FOp) in unmittelbarer Nähe des Broca-Areals umfasst.

In einer **ersten Publikation** wurden die Areale Op5, Op6 und Op7 im posterioren Bereich des FOp identifiziert. Zytoarchitektonische Wahrscheinlichkeitskarten wurden berechnet und in den Julich-Brain Atlas integriert. Im Rahmen einer multimodalen Charakterisierung des FOp zeigte sich für Area Op6 links die stärkste funktionelle Einbindung in Netzwerke der Musik- und Sprachverarbeitung. Während die Areale Op5-Op7 zunächst mittels eines etablierten beobachterunabhängigen Ansatzes auf Basis statistischer Bildanalyse zytoarchitektonisch kartiert wurden, konnte in einer **zweiten Publikation** ein Deep-Learning-basierter Mapping-Ansatz auf die Areale Op5-Op7 und Area 44+45 angewendet werden. In einer **dritten Publikation** wurden Area 44+45 des Broca-Areals und Area Te3 des Wernicke-Areals hinsichtlich ihrer Genexpression untersucht, wobei der Fokus auf Genen lag, die mit phonologischer Verarbeitung assoziiert sind.

Die gewonnenen zytoarchitektonischen Karten der FOp-Areale Op5-Op7 können zukünftig im klinisch-neurologischen und klinisch-psychiatrischen Bereich sowie für neurowissenschaftliche Fragestellungen eingesetzt werden. Die Studie zur Genexpression in den Arealen 44+45 und Te3 dient als Modell für weitere Gehirnareale, die mit sprachlichen Funktionen assoziiert sind, einschließlich Area Op6 links. Der auf Deep Learning basierende Algorithmus kann ein Impulsgeber zur weiteren Untersuchung relevanter Gehirnareale, Modalitäten oder sprachlicher Faktoren mittels künstlicher Intelligenz sein. Insgesamt trägt das Projekt zur zytoarchitektonischen Analyse von Sprache bei und erweitert das multimodale Wissen über das FOp und die klassischen Sprachareale Broca und Wernicke. Da die Organisation des Gehirns nicht anhand einer einzelnen Modalität erfasst werden kann, sondern auf mehreren organisatorischen Prinzipien und Skalierungen beruht, bietet der EBRAINS Multilevel Human Brain Atlas eine Plattform zur Integration der gewonnenen Daten, als Erweiterung des zytoarchitektonischen Mappings.

Summary

Language is a complex cognitive function of the human brain that is carried out in networks. Early language research focused on classical language areas Broca's and Wernicke's regions. Today, these areas are still considered key, but it is now known that language processing involves far more brain areas than the traditional ones and the anterior language region, including the frontal operculum (FOp) near Broca's region, could be redefined.

In a **first publication**, areas Op5, Op6, and Op7 were identified as part of the posterior FOp. Cytoarchitectonic probability maps were calculated and integrated into the Julich-Brain Atlas. A multimodal characterization of the FOp revealed the most prominent functional integration in music and language processing networks for area Op6 left. While areas Op5-Op7 were initially mapped using a well-established observer-independent cytoarchitectonic approach based on statistical image analysis, a deep-learning-based mapping approach was applied to areas Op5-Op7 and areas 44+45 in a **second publication**. A **third publication** analyzed gene expression in areas 44+45 of Broca's region and area Te3 of Wernicke's region, focusing on genes involved in phonological processing.

In the future, the cytoarchitectonic maps of areas Op5-Op7 of the FOp can be used in clinical neurology and psychiatry as well as for neuroscientific questions. The gene expression study of areas 44+45 and Te3 serves as a model for other brain areas associated with language functions, including area Op6 left. The deep learning-based algorithm can be a potential source of inspiration for further investigation of relevant brain areas, modalities, or linguistic factors using artificial intelligence. Overall, the project contributes to the cytoarchitectonic analysis of language and expands the multimodal knowledge of the FOp and the classical language areas Broca's and Wernicke's regions. Since the organization of the brain cannot be captured by a single modality, but is based on several organizational principles and scales, the EBRAINS Multilevel Human Brain Atlas provides a platform for integrating acquired data as an extension of cytoarchitectonic mapping.

Abkürzungsverzeichnis

3D	Dreidimensional
BA	Brodmann-Areal
CNN	Convolutional Neural Network
EBRAINS	European Brain Research Infrastructures – digitale Forschungsinfrastruktur, geschaffen im Rahmen des von der Europäischen Union finanzierten Human Brain Projects
EEG	Elektroenzephalographie
(f)MRT	(Funktionelle) Magnetresonanztomographie
FOp	Frontales Operculum
GLI	Grauwert-Index (engl., *grey level index*)
JuGEx	Julich Gene Expression Analysis
lvPPA	Primär Progressive Aphasie, logopenische Variante (engl., *logopenic variant of primary progressive aphasia*)
MACM	Meta-analytische Konnektivitätsmodellierung (engl., *meta-analytic connectivity modelling*)
MD	Mahalanobis-Distanz
MNI	Montreal Neurological Institute
MPM	Maximale Wahrscheinlichkeitskarte (engl., *maximum probability map*)
PET	Positronen-Emissions-Tomographie
PMC	Prämotorischer Cortex
POp	Parietales Operculum
PPA	Primär Progressive Aphasie
ROI	Ausgewählter Cortexabschnitt (engl., *region of interest*)
tDCS	Transkranielle Gleichstromstimulation (engl., *transcranial direct current stimulation*)
TMS	Transkranielle Magnetstimulation

Inhaltsverzeichnis

1 Einleitung

Ein wichtiges Ziel der Neurowissenschaften ist die Identifizierung von Gehirnarealen unter Berücksichtigung ihrer genauen Lokalisation und Ausdehnung. Dies kann auf Basis zytoarchitektonischer Analysen erfolgen (Amunts et al., 2020). Die Bestimmung sprachrelevanter Areale der menschlichen Großhirnrinde (Cortex) ist eine notwendige Voraussetzung für die kognitiven Neurowissenschaften und die klinische Sprachforschung (Amunts & Zilles, 2012).

1.1 Klassische Sprachareale Broca und Wernicke

Das Broca- und das Wernicke-Areal wurden Ende des 19. Jahrhunderts von Paul Broca und Carl Wernicke beschrieben und benannt. Sie zeigten einen Zusammenhang zwischen Läsionen in umschriebenen Gehirnregionen und einem durch Aphasie bedingten Verlust von Sprachfunktionen (Sprachproduktion bzw. Sprachverständnis) (Amunts & Zilles, 2012; Zilles & Amunts, 2010). So konnten sie sprachrelevante Areale des Cortex identifizieren und Argumente für eine Spezialisierung der linken Hemisphäre für Sprache aufzeigen (Amunts & Zilles, 2012). Während das Broca-Areal den Bereichen des Pars triangularis und Pars opercularis des posterioren Gyrus frontalis inferior im linken Frontallappen zugeordnet wurde (Amunts & Zilles, 2006), wurde das Wernicke-Areal im Gyrus temporalis superior des linken Temporallappens und im angrenzenden Gyrus supramarginalis lokalisiert (Binder, 2017). Das Broca- und das Wernicke-Areal gelten nach wie vor als „klassische Sprachareale“ und als Schlüsselregionen des Sprachnetzwerks (Friederici, 2017). Anhand der Kartierung Brodmanns (1909), die noch immer breite Anwendung findet (Zilles & Amunts, 2010), kann das Broca-Sprachzentrum den Brodmann-Arealen (BA) 44+45 zugeordnet werden (Amunts & Zilles, 2006; Amunts & Zilles, 2012). Der Bereich des Wernicke-Sprachzentrums kann dem posterioren Teil des BA 22 zugewiesen werden (Morosan et al., 2005).

In Bezug auf die Parzellierung Brocas ist kritisch anzumerken, dass eine mikrostrukturelle Analyse des betrachteten Gehirns nicht durchgeführt wurde. Daher konnte die Lokalisation des Broca-Areals ausschließlich anhand des vorliegenden individuellen Läsionsmusters infolge des Infarktes bestimmt werden (Amunts & Zilles, 2006). Weitere frühe

zytoarchitektonische Karten des Broca-Areals, u. a. von Stengel (1930) und Riegele (1931), wichen bereits von der ursprünglichen Lokalisation ab (Amunts & Zilles, 2012). Parallel dazu wurde an der zytoarchitektonischen Parzellierung Brodmanns (1909) kritisiert, dass sie (i) innerhalb von Sulci liegende Anteile des Cortex unberücksichtigt lässt (Zilles & Amunts, 2010), (ii) ebenfalls auf der linken Hemisphäre eines einzelnen Gehirns basiert (Amunts & Zilles, 2015) und somit die interindividuellen Unterschiede in der Zytoarchitektonik keine Berücksichtigung finden (Lashley & Clark, 1946) sowie (iii) eine mangelnde Beobachterunabhängigkeit, Reproduzierbarkeit und Objektivität aufweist (Bailey & v. Bonin, 1951; Zilles & Amunts, 2010).

Aktuelles zytoarchitektonisches beobachterunabhängiges Mapping bezieht sich für Broca auf Area 44+45 (Amunts et al., 1999; Amunts et al., 2004) und für Wernicke auf Area Te3 (Morosan et al., 2005). Die Tatsache, dass sich diese mikrostrukturellen Korrelate nicht ausschließlich auf die Oberfläche eines Gehirns beziehen (Amunts & Zilles, 2015), sondern auch die exakte Lage innerhalb von Gyri und Sulci im Frontal- bzw. Temporallappen auf Basis mehrerer Gehirne berücksichtigen (Amunts et al., 1999; Amunts et al., 2004; Morosan et al., 2005), spricht für eine unscharfe anatomische Lokalisation der klassischen Sprachareale und der entsprechenden BA (engl., *ill-defined*) (u. a. Tremblay & Dick, 2016).

Während das Broca-Areal heute als wesentlicher Teil der anterioren Sprachregion gilt, ist das Wernicke-Areal wichtiger Bestandteil der posterioren Sprachregion (Amunts & Zilles, 2012). Neben Broca und Wernicke sind weitere Gehirnareale an der Sprachverarbeitung beteiligt. Darüber hinaus ist bekannt, dass Sprache in Netzwerken produziert und verarbeitet wird (Hagoort, 2014). Eine auf Rezeptorarchitektonik beruhende Arbeit (Amunts et al., 2010) stellte eine Neudefinition der anterioren Sprachregion vor, durch Analyse von Area 44+45 (Amunts et al., 1999; Amunts et al., 2004) und kaudal angrenzender (prä-)motorischer Areale sowie des ventral angrenzenden frontalen Cortex. Neben dem klassischen Sprachareal Broca zeigte sich eine Beteiligung des frontalen Operculums (FOp) und des prämotorischen Cortex (PMC), welche nicht als klassische Sprachareale gelten. Verglichen mit dem Mapping von Brodmann (1909) entspricht der Bereich des FOp und des PMC den BA 43+6.

1.2 Bisherige Befunde zur Charakterisierung der Mikrostruktur, Makrostruktur und Funktionen des frontalen Operculums

Mithilfe der quantitativen Autoradiographie sechs ausgewählter Neurotransmitterrezeptoren konnten Amunts et al. (2010) den Bereich des FOp sowie des PMC auf mikrostruktureller Ebene näher charakterisieren. Die Modalität der Rezeptorarchitektonik beschreibt die Verteilung verschiedener Rezeptoren für Neurotransmitter (engl., *„receptor fingerprints"*), die die Gehirnaktivität modulieren. Ihre Profile unterscheiden sich sowohl zwischen den einzelnen Arealen als auch zwischen den verschiedenen Cortexschichten pro Areal (Eickhoff et al., 2007; Zachlod et al., 2023; Zilles et al., 2002). Amunts et al. (2010) identifizierten die Areale Op8 und Op9 des FOp sowie Area 6r1 als Teil des PMC anhand einer abweichenden Rezeptorarchitektonik, die sich wiederum von den klassischen Sprachareale Area 44+45 unterschied. Darüber hinaus konnten Area 44+45 jeweils in zwei Areale und somit feingliedriger als auf Basis der Zytoarchitektonik unterteilt werden (Amunts et al., 2010; Zilles & Amunts, 2018). In Ergänzung dazu zeigten konnektivitätsbasierte Ansätze eine Unterteilung von Area 44+45 sowie des tiefen FOp mit probabilistischem Fasertracking (Anwander et al., 2007; Jung et al., 2017).

Makroanatomisch ist das FOp ein Teil des Frontallappens, der an den Sulcus lateralis angrenzt und den insulären Cortex bedeckt. Es dehnt sich anterior vom parietalen Operculum (POp; Gyrus subcentralis) zum ursprünglichen Broca-Areal aus (Mai et al., 2008). Im Gegensatz zu Area 44+45 ist das FOp phylogenetisch älter (Friederici, 2006) und von der Gehirnoberfläche aus nur partiell sichtbar, da es größtenteils vom Lobus frontalis überdeckt wird (Mai et al., 2008). Das FOp grenzt ventral und medial an Area 44+45 (Friederici, 2017). Es ist mit dem vorderen Teil des Gyrus temporalis superior und dem Sulcus temporalis superior über den Fasciculus uncinatus (ventraler Pfad II) verbunden (Catani et al., 2005; Friederici, 2009; Friederici, 2011).

Frühere Studien zur funktionellen Bildgebung deuteten an, dass das FOp eine breite Beteiligung an sprachlichen Funktionen zeigt. In Bezug auf phonologische Verarbeitung wurde bei der Präsentation gereimter Items ein stärkerer Blood-Oxygenation-Level Dependent Effekt im Bereich des FOp festgestellt als bei der Präsentation sich nicht reimender Items (Hurschler et al., 2013). Bei der Produktion von Silbensequenzen zeigte das FOp eine erhöhte Aktivierung für Sequenzen mit einer höheren phonologischen Komplexität (Bohland & Guenther, 2006). Bei Patient:innen mit Läsionen des FOp links wurde festgestellt, dass sie beim Lesen von Nicht-Wörtern und vergleichbaren phonologischen

Aufgaben weniger akkurat artikulierten (Fiez et al., 2006). In Bezug auf syntaktische Verarbeitung ergab eine funktionelle Magnetresonanztomographie (fMRT)-Studie mit verschiedenen Wortarten, dass die Verarbeitung syntaktisch-relevanter Wörter (Konjunktionen und Adverbien) zu einer erhöhten Aktivität in der unteren Spitze des linken FOp führte (Friederici et al., 2000). In einem weiteren fMRT-Experiment wurde für in der Finite State-Grammatik angeordnete Silben eine höhere Aktivität des FOp nachgewiesen als für Silben entsprechend der Phrasenstrukturgrammatik (Friederici et al., 2006a). Eine ereigniskorrelierte fMRT-Studie zeigte, dass die Verarbeitung von Sätzen mit ungrammatikalischen Wortfolgen zu einer selektiven Aktivierung des tiefen posterioren FOp führte (Friederici et al., 2006b). Neben seiner Beteiligung an Sprache zeigte das FOp eine Assoziation mit der Geschmacksrepräsentation (Chikazoe et al., 2019; Veldhuizen et al., 2011), was sich ebenfalls in Studien mit Makaken zeigte (Rolls et al., 1989). Darüber hinaus war das FOp an einigen kognitiven Funktionen, z. B. der Aufgabenkontrolle (Higo et al., 2011; Quirmbach & Limanowski, 2022), der Wahrnehmung viszeraler Reize (Eickhoff et al., 2006b) und der exekutiven Kontrolle (Novick et al., 2005; Thompson-Schill et al., 1997; für ein Review siehe Gratton et al., 2018) beteiligt.

Da die mikrostrukturellen Korrelate des FOp noch weitgehend unbekannt sind, rezeptorarchitektonische (Amunts et al., 2010), konnektivitätsbezogene (Anwander et al., 2007; Jung et al., 2017) und funktionelle Daten (u. a. Chikazoe et al., 2019; Friederici et al., 2000; Hurschler et al., 2013) jedoch auf eine feinere Unterteilung des FOp hindeuten als die Region der BA 43+6 innerhalb der Karte Brodmanns, wird der posteriore Bereich des FOp in der **ersten Publikation der vorliegenden Arbeit** (Unger et al., 2023) zytoarchitektonisch untersucht. Darüber hinaus soll der Frage nachgegangen werden, welche Rolle das posteriore FOp in der anterioren Sprachregion bzw. im Sprachnetzwerk im engeren Sinne spielt und ob die Region in Gänze an sprachlichen Funktionen beteiligt ist.

1.3 Quantitative zytoarchitektonische Analyse

Im vergangenen Jahrhundert wurden verschiedene kortikale Parzellierungen und Karten vorgelegt, die sich hinsichtlich ihrer Ontologie, der betrachteten Gehirnorganisation, der Anzahl von Arealen und weiterer Aspekte unterschieden (Amunts & Zilles, 2012). Im späten 19. Jahrhundert begann Brodmann mit seiner Arbeit zur Kartierung des Cortex in 43 zytoarchitektonische Areale (Brodmann, 1909) und folgte somit u. a. auf Flechsig (1898), Campbell (1905) und Smith (1907). V. Economo und Koskinas (1925) sowie Sarkisov et al. (1949) der russischen Schule schlossen sich mit ihren zytoarchitektonischen Arbeiten an.

1.3.1 Zytoarchitektonik

Der Cortex umfasst die graue Substanz des Gehirns und bedeckt weite Teile des lateralen und medialen Bereichs der Hirnoberfläche. Der Isocortex ist der phylogenetisch jüngste Bereich des Cortex (Neocortex; Amunts & Zilles, 2012). Er weist eine Breite von 1,5 bis 4,5 mm auf (v. Economo & Koskinas, 1925) und ist meist sechsschichtig (Amunts & Zilles, 2012; Brodmann, 1909). Die horizontalen Schichten (Laminae) werden von Lamina I im äußeren Bereich des Cortex bis Lamina VI an der Rinden-Mark-Grenze mit römischen Ziffern durchnummeriert. Der Neocortex enthält die folgenden Schichten: Molekularschicht (I), äußere Körnerschicht (II), äußere Pyramidenzellschicht (III), innere Körnerschicht (IV), innere Pyramidenzellschicht (V) und multiforme Schicht (VI). Jede Lamina weist charakteristische Zelltypen und eine spezifische Konnektivität mit anderen kortikalen Schichten und Hirnbereichen auf (Amunts & Zilles, 2012).
Die Zytoarchitektonik stellt ein mikrostrukturelles und organisatorisches Grundprinzip des Neocortex und subkortikaler Kerngebiete dar (Amunts & Zilles, 2012), das makroskopischen Landmarken, z. B. in Form von Sulci, nicht zwingend entspricht (Amunts et al., 2007). Basierend auf dem Wissen bisheriger Arbeiten (u. a. Brodmann, 1909; Campbell, 1905; Flechsig, 1898; Sarkisov et al., 1949; Smith, 1907; v. Economo & Koskinas, 1925) existieren mehrere Dutzende bis Hunderte kortikale Bereiche (Amunts & Zilles, 2012). Grundlage für die zytoarchitektonische Analyse sind zellkörpergefärbte histologische Schnitte (Amunts & Zilles, 2012; Brodmann, 1909; Zilles & Amunts, 2010). U. a. v. Economo und Koskinas (1925) entwickelten erste klar definierte quantitative Kriterien zur Unterscheidung kortikaler Areale. Diese berücksichtigten neben der Zusammensetzung, Architektur und Organisation des Cortex

Parameter wie die Zellgröße und -dichte pro Lamina sowie die Cortexdicke (v. Economo & Koskinas, 1925).

1.3.2 Beobachterunabhängige zytoarchitektonische Analyse

Seit Einführung neuer funktioneller und struktureller Bildgebungstechniken in den 1980er-Jahren ergab sich die Anforderung der Registrierung dieser Daten im dreidimensionalen (3D) Raum (Zilles & Amunts, 2010). Zunächst diente die Brodmannsche Karte innerhalb des Talairach-Raumes (Talairach & Tournoux, 1988) als anatomisches Korrelat; zur umfassenden Interpretation gewonnener Daten bestand jedoch weiterer Bedarf an hochauflösenden anatomischen Referenzräumen und -atlanten (Zilles & Amunts, 2010). Im Zuge technischer Weiterentwicklungen entstanden quantitative Methoden zur zytoarchitektonischen Kartierung (Zilles et al., 1978; Zilles et al., 1980; Zilles et al., 1982). Hierbei erwies sich die beobachterunabhängige zytoarchitektonische Analyse nach Schleicher et al. (1999, 2005, 2009) als statistisch valide Methode zur Identifizierung von Arealgrenzen.

Die Quantifizierung zytoarchitektonischer Unterschiede benachbarter Gehirnareale erfolgt durch das Maß der Mahalanobis-Distanz (MD) (Mahalanobis et al., 1949), indem mittlere Profile des Grauwert-Indexes (engl., *grey level index*, GLI) zwischen benachbarten Blöcken (variierende Blockgröße, bestehend aus 10-24 Profilen pro Block) mittels eines Sliding Window Ansatzes betrachtet werden (Bludau et al., 2014; Schleicher et al., 1999; Schleicher et al., 2005). Je größer der Unterschied in der Form zwischen den Profilen benachbarter Blöcke desto größer ihre MD (Überprüfung anhand des Bonferroni-korrigierten Hotelling's T2-Tests ($p < 0{,}001$)). Der Nachweis einer zytoarchitektonischen Grenze wird dann akzeptiert, wenn die MD ein signifikantes Maximum für verschiedene Blockgrößen ergibt und die entsprechende Grenze an vergleichbaren Positionen innerhalb von drei oder mehr benachbarten Hirnschnitten vorliegt (siehe **erste Publikation**, Unger et al., 2023).

1.3.3 Deep-Learning-basierte zytoarchitektonische Analyse

Die Methode nach Schleicher et al. (1999, 2005, 2009) führt zu detaillierten und aussagekräftigen Ergebnissen und etablierte sich als Standard zur Identifizierung von Grenzen zwischen zytoarchitektonischen Arealen innerhalb des Julich-Brain Atlasses

(Amunts et al., 2020). Aufgrund manueller Anteile bringt sie allerdings Durchsatz-Beschränkungen mit sich. Die Entwicklung rein automatisierter Verfahren kann zu einer Erhöhung der zeitlichen Effektivität führen (Kiwitz et al., 2020; Schiffer et al., 2021). Damit ähnlich aussagekräftige und präzise Daten wie durch den bisherigen Mapping-Ansatz (Schleicher et al., 1999; Schleicher et al., 2005; Schleicher et al., 2009) generiert werden können, muss die Methode robust gegenüber der interindividuellen Variabilität des menschlichen Gehirns sein. Zugleich muss das Verfahren sensitiv auf subtile Unterschiede in der Zytoarchitektonik der verschiedenen Hirnregionen reagieren (Schiffer et al., 2021; Spitzer et al., 2017; Spitzer et al., 2018).

Eine automatisierte zytoarchitektonische Analyse zur Parzellierung auf Basis von gefalteten Neuronalen Netzwerken (engl., *Convolutional Neural Networks*, CNNs) stellte sich in ersten Studien unserer Arbeitsgruppe (Spitzer et al., 2017; Spitzer et al., 2018) als eine Möglichkeit zur Analyse von Serien hochauflösender zellkörpergefärbter histologischer Schnitte im visuellen Cortex des menschlichen post-mortem Gehirns „BigBrain“ (Amunts et al., 2013) heraus. Das BigBrain ist ein ultrahochaufgelöstes Modell, das 7.404 gefärbte histologische und 3D-rekonstruierte Schnitte mit 20 µm zellulärer Auflösung enthält. Es dient als Referenzgehirn, in welches neben neuroanatomischen und mikrostrukturellen Daten auch multimodale Informationen integriert werden können (Amunts et al., 2013).

Die Einsetzbarkeit des Deep-Learning-basierten Ansatzes wurde bislang nicht für umfassendere Schnittserien des Cortex untersucht. Da automatisierte und zeitlich effektive Mappingverfahren jedoch für variable funktionelle Systeme und so auch im Bereich des sprachlich-assoziierten Cortex von hoher Relevanz sind, evaluiert die **zweite Publikation der vorliegenden Arbeit** (Schiffer et al., 2021) einen CNN umfassenden Workflow, u. a. für die sprachlich relevanten Areale 44+45 (Amunts et al., 1999; Amunts et al., 2004) sowie für Areale des FOp (Unger et al., 2023).

1.3.4 Julich-Brain-Atlas

Der Julich-Brain Atlas enthält histologisch-zytoarchitektonische 3D-Karten von kortikalen Bereichen und subkortikalen Kerngebieten des menschlichen Gehirns in den Montreal Neurological Institute (MNI)-Referenzräumen Colin27 (Holmes et al., 1998) und ICBM152casym (Evans et al., 2012). Bis 2020 wurden durch 41 Projekte Karten von 248 zytoarchitektonischen Arealen in den Atlas aufgenommen; bestehende Karten

können je nach Bedarf feiner untergliedert werden oder neue Karten können ergänzt werden (Amunts et al., 2020; siehe online, https://julich-brain-atlas.de/).

Zur Erstellung der enthaltenden zytoarchitektonischen Wahrscheinlichkeitskarten erfolgt eine Überlagerung der Kartierung für je 10 post-mortem Gehirne im 3D-Raum. Somit berücksichtigt der Julich-Brain Atlas die natürlich vorkommende interindividuelle Variabilität und es ist möglich, zytoarchitektonische und makroanatomische Variationen hinsichtlich Lokalisation und Ausdehnung einzelner Gehirnregionen einzubeziehen (Amunts et al., 2020).

Anhand von Prozentwerten kann angegeben werden, bei welcher Anzahl der 10 Gehirne pro Voxel ein spezifisches Areal vorliegt (0-100% Überlappung), wodurch Variationen zwischen einzelnen Gehirnen im stereotaktischen Raum berücksichtigt werden können (Amunts et al., 2020). Darüber hinaus zeigen maximale Wahrscheinlichkeitskarten (engl., *maximum probability maps*, MPMs) für jedes spezifische Voxel das Areal an, für das die höchste Wahrscheinlichkeit innerhalb des Voxels besteht (Eickhoff et al., 2005). Nicht gemappte Gebiete werden derzeit durch Lückenkarten (engl., *gap maps*) ausgefüllt (Amunts et al., 2020).

1.4 Multimodale Ansätze

Brodmann (1909) legte durch die zytoarchitektonische Analyse den Grundstein für die Betrachtung des Zusammenhangs zwischen kortikalen Strukturen und Funktionen bzw. Dysfunktionen (Zilles & Amunts, 2010). Während er Struktur-Funktionsbeziehungen in der Monographie von 1909 nur kurz thematisierte, veröffentlichte er einige Jahre später eine umfassendere Übersichtsarbeit (Brodmann, 1914), die Zusammenhänge zwischen zytoarchitektonischer Parzellierung und Läsionen in menschlichen Gehirnen aufzeigte (Zilles & Amunts, 2010). Auf diese Weise bekräftigte Brodmann die Annahme einer Verknüpfung zwischen funktionellen und zytoarchitektonischen Unterschieden innerhalb des Cortex (Amunts & Zilles, 2015; Zilles & Amunts, 2010). Bei einem ersten Vergleich zweier Modalitäten wichen einige der myeloarchitektonischen Grenzen, die Vogt und Vogt (1919) identifizierten, von der zytoarchitektonischen Kartierung Brodmanns (1909) ab; dennoch herrschte im Allgemeinen die Annahme von Kohärenz zwischen myeloarchitektonischer und zytoarchitektonischer Parzellierung (Zilles & Amunts, 2010).

Heute wird davon ausgegangen, dass die Gehirnorganisation nicht anhand einer einzelnen Modalität erfassbar ist, sondern dass dieser mehrere organisatorische Prinzipien zugrunde liegen (Amunts & Zilles, 2015; Eickhoff et al., 2018). Im Gegensatz zu den oft verwendeten MNI-Referenzräumen Colin27 (Holmes et al., 1998) und MNI ICBM 152 (Evans et al., 2012), die sich auf die makroskopische Skala beschränken und für sich genommen keine zusätzlichen funktionellen Informationen liefern, schafft beispielsweise das in **Kapitel 1.3.3** thematisierte Referenzgehirn BigBrain einen mikrostrukturellen Rahmen zur Integration multimodaler Daten und erweitert somit u. a. die Möglichkeiten Brodmanns (Amunts et al., 2013; Amunts & Zilles, 2015). Die Berücksichtigung mehrerer Modalitäten ist wesentlich für die Erstellung eines reproduzierbaren Gehirnatlasses und kann zu einem tieferen Verständnis von Struktur und Funktion ausgewählter Bereiche des Gehirns und ihrer interindividuellen Variabilität führen (Amunts et al., 2014; Glasser et al., 2016; Toga et al., 2006).

1.4.1 Multilevel Human Brain Atlas

Der Julich-Brain Atlas ist Teil des Multilevel Human Brain Atlasses, abrufbar über die Plattform European Brain Research Infrastructures (EBRAINS) des Human Brain Projects und nutzbar mithilfe des Software-Toolpaketes siibra (siehe online, https://atlases.ebrains.eu/viewer/). Die enthaltenden Karten, die sich mit der Zytoarchitektonik auf die Mikroarchitektur bzw. zelluläre Architektur des Cortex beziehen und die die exakte Lokalisation der Areale aufzeigen (siehe **Kapitel 1.3.1**), stellen das Kernstück des Atlasses dar (Amunts et al., 2020). Ein gemeinsamer Referenzraum innerhalb des Multilevel Human Brain Atlasses ermöglicht die Kombination von Daten aus verschiedenen Modalitäten in verschiedenen Maßstäben darzustellen (Amunts et al., 2014; Zachlod et al., 2023). Somit werden die Karten durch multimodale und multiskale Informationen pro Areal ergänzt (Amunts et al., 2013), z. B. durch konnektivitätsbasierte und genomische Fremddaten (siehe **folgende Kapitel 1.4.2 und 1.4.3**). Dies ermöglicht die Gewinnung umfassender neurowissenschaftlicher Erkenntnisse (Amunts et al., 2013).
Der Multilevel Human Brain Atlas kann kontinuierlich an die fortschreitende Kartierung angepasst werden, um neu verfügbare Daten zu integrieren und den Atlas mit umfassenden semantischen Informationen anzureichern. Er ist mit weiteren Atlanten verknüpfbar und steht der wissenschaftlichen Community frei zur Verfügung (Amunts et al., 2020).

1.4.2 Konnektivitätsdaten

Die in **Kapitel 1.2** thematisierte Verteilung der Neurotransmitterrezeptoren hängt eng mit Konnektivitätsmustern zusammen, die für die Rolle eines Areals in größeren Netzwerken relevant sind (Zachlod et al., 2023) und die eine weitere zu betrachtende Modalität darstellen (Anwander et al., 2007; Jung et al., 2017). Es kann zwischen struktureller und funktioneller Konnektivität bzw. Kommunikation im Gehirn unterschieden werden. Während die strukturelle Konnektivität sich auf die Anatomie der Faserbahnen bezieht, handelt es sich bei der funktionellen Konnektivität um die zeitliche Korrelation neuronaler Aktivität von Hirnregionen bei spezifischen Aufgaben bzw. Funktionen (Julich-Brain Atlas, 2023b; Zachlod et al., 2023).
Die für die **erste Publikation** (Unger et al., 2023) betrachteten Daten zur funktionellen Konnektivität des FOp basieren auf einer meta-analytischen Konnektivitätsmodellierung (MACM) (Laird et al., 2009; Robinson et al., 2010). Die Daten zur strukturellen Konnektivität innerhalb des Multilevel Human Brain Atlasses stammen aus der 1000BRAINS-Studie (Caspers et al., 2014) und ermöglichen spezifische Aussagen zur Konnektivität zytoarchitektonischer Areale.

1.4.3 Allen Human Brain Atlas-Daten

Eine weitere Modalität zur Charakterisierung zytoarchitektonischer Areale ist die differentielle Genexpression (Bludau et al., 2018). In einer ersten Studie wurde der Frontalpol (Areale Fp1+Fp2; Bludau et al., 2014) unter diesem Gesichtspunkt untersucht. Es zeigte sich eine signifikante Hochregulierung der Gene *MAOA* und *TAC1* in Area Fp2, verglichen mit Area Fp1 (Bludau et al., 2018). Zum Einsatz kam hierbei das Tool Julich Gene Expression Analysis (JuGEx; Bludau et al., 2018), das Genexpressionsdaten des Allen Human Brain Atlasses (Atlas des Transkriptoms des erwachsenen menschlichen Gehirns; Hawrylycz et al., 2012; Hawrylycz et al., 2015) mit Lokalisationsdaten in Form der zytoarchitektonischen Wahrscheinlichkeitskarten des Julich-Brain Atlasses verknüpft (Bludau et al., 2018). Es ist bekannt, dass der Neocortex ein relativ homogenes Transkriptionsmuster aufweist, jedoch mit deutlichen Merkmalsausprägungen in den primären sensomotorischen Cortices und im Bereich des Frontallappens (Hawrylycz et al., 2012).

Seitens des Allen Institutes war initial vor allem die Korrelation funktioneller und genetischer Gehirndaten angedacht (Hawrylycz et al., 2012). In der Studie von Bludau et al. (2018) wurden kognitive Funktionen untersucht, jedoch nicht speziell Sprachfunktionen. Inwieweit sich z. B. die zytoarchitektonisch distinkten klassischen Sprachareale Broca und Wernicke in Form von Area 44+45 und Area Te3 (Amunts et al., 1999; Amunts et al., 2004; Morosan et al., 2005) hinsichtlich ihrer Expression sprachbezogener Gene unterscheiden, wurde beim Erwachsenen bisher nicht systematisch untersucht. Für das sich entwickelnde Gehirn menschlicher Föten liegen nur wenige Studien vor (Johnson et al., 2009; Lambert et al., 2011). Um die Forschungslücke zu schließen und eine erste sprachrelatierte Studie mit dem Tool JuGEx zu erstellen, betrachtet die **dritte Publikation der vorliegenden Arbeit** (Unger et al., 2021d) die differentielle Expression phonologierelevanter Gene in den zytoarchitektonischen Arealen 44+45 (entspricht Broca) versus Te3 (entspricht Wernicke).

1.5 Ziele der Arbeit

Ziel der **ersten Publikation** (Unger et al., 2023) ist es, das posteriore FOp zytoarchitektonisch zu analysieren und zu segregieren. Hierbei wird die Frage betrachtet, ob der Bereich aus mehreren heterogenen Arealen oder aus einer zusammenhängenden Region besteht. Es folgt die Erstellung von 3D-Karten auf Grundlage der zytoarchitektonischen Kartierung innerhalb von 10 menschlichen post-mortem Gehirnen, um anatomische Unterschiede zwischen den Gehirnen zu berücksichtigen (Amunts et al., 2020). In einem nächsten Schritt sollen, wie in der Studie von Amunts et al. (2004), potenzielle interhemisphärische und geschlechtsspezifische Unterschiede der identifizierten Areale bewertet werden. Um Informationen zu Funktionen der Areale zu gewinnen, erfolgt darauf eine meta-analytische Konnektivitätsmodellierung (MACM) unter Verwendung der BrainMap-Datenbank (Laird et al., 2009; Robinson et al., 2010) und eine Betrachtung ergänzender struktureller Konnektivitätsdaten (1000BRAINS-Studie; Caspers et al., 2014). Darüber hinaus soll geklärt werden, inwieweit das posteriore FOp Teil der anterioren Sprachregion bzw. des Sprachnetzwerks im engeren Sinne ist und ob das vollständige FOp an sprachlichen Funktionen beteiligt ist.

Ziel der **zweiten Publikation** (Schiffer et al., 2021) ist die Erprobung eines neuen Verfahrens zur Deep-Learning-basierten zytoarchitektonischen Analyse in großen Serien histologischer menschlicher post-mortem Gehirnschnitte im BigBrain (Amunts et al., 2013).

Ähnlich wie in Spitzer et al. (2017, 2018) sollen CNNs bereits annotierte Hirnregionen als Trainingsdaten nutzen und die entsprechenden Areale auf weitere Schnitte übertragen. Es sollen mehrere funktionelle Systeme integriert werden, u. a. die neu identifizierten Areale Op5-Op7 (posteriores FOp) sowie Area 44+45 (Broca). In einem nächsten Schritt soll die Evaluation der vorgenommenen automatisierten Kartierung hinsichtlich Qualität und anatomischer Plausibilität erfolgen, um die Anwendbarkeit für die unterschiedlichen kartierten Areale in den histologisch aufbereiteten post-mortem Gehirnen bewerten zu können.

Die **dritte Publikation** (Unger et al., 2021d) nutzt die zytoarchitektonischen Wahrscheinlichkeitskarten der Sprachareale Broca (Area 44+45; Amunts et al., 1999; Amunts et al., 2004) und Wernicke (Area Te3; Morosan et al., 2005). Initiales Ziel ist die Identifizierung von Genen, die laut der Literatur von 2010-2021 bei mehr als einer der Störungen Dyslexie, Dyskalkulie, Sprachentwicklungsstörung und der logopenischen Variante der Primär Progressiven Aphasie (lvPPA) oder bei all diesen Störungen beteiligt sind (definiert als „phonologie-relatierte Gene“). In Bezug auf identifizierte mit phonologischer Verarbeitung assoziierte Gene soll eine Anreicherungsanalyse (engl., *enrichment analysis*) der Genfunktionen erfolgen. Anschließend wird im Rahmen des Hauptvergleichs mit dem Tool JuGEx (Bludau et al., 2018) eine Genexpressionsanalyse für Area 44+45 im Gegensatz zu Area Te3 durchgeführt.

Übergeordnete Zielsetzung der vorliegenden Arbeit ist es, an der Sprachverarbeitung beteiligte Areale mit mikrostruktureller Genauigkeit zu lokalisieren sowie diese multimodal zu charakterisieren. Langfristig sollen die entstehenden und betrachteten zytoarchitektonischen Wahrscheinlichkeitskarten einen Beitrag zum Wissen bzgl. der Funktionalität des Sprachnetzwerkes leisten und in der klinischen Forschung bzw. Versorgung Anwendung finden. Ein positives Votum der Ethikkommission der Medizinischen Fakultät der Heinrich-Heine-Universität Düsseldorf mit der Nr. 4863 zur Durchführung der Studien liegt vor.

2 Publizierte Originalarbeiten

2.1 Unger, N., Haeck, M., Eickhoff, S. B., Camilleri, J. A., Dickscheid, T., Mohlberg, H., Bludau, S., Caspers, S., & Amunts, K. (2023). Cytoarchitectonic mapping of the human frontal operculum – New correlates for a variety of brain functions. ***Frontiers in Human Neuroscience, 17,*** **1087026. https://doi.org/10.3389/fnhum.2023.1087026**

frontiers | Frontiers in Human Neuroscience

TYPE Original Research
PUBLISHED 28 June 2023
DOI 10.3389/fnhum.2023.1087026

OPEN ACCESS

EDITED BY
Maya L. Henry,
The University of Texas at Austin, United States

REVIEWED BY
Olga Kepinska,
University of Vienna, Austria
Andrea Santi,
University College London, United Kingdom

*CORRESPONDENCE
Nina Unger
nina.unger@med.uni-duesseldorf.de

RECEIVED 01 November 2022
ACCEPTED 18 April 2023
PUBLISHED 28 June 2023

CITATION
Unger N, Haeck M, Eickhoff SB, Camilleri JA, Dickscheid T, Mohlberg H, Bludau S, Caspers S and Amunts K (2023) Cytoarchitectonic mapping of the human frontal operculum—New correlates for a variety of brain functions.
Front. Hum. Neurosci. 17:1087026.
doi: 10.3389/fnhum.2023.1087026

Cytoarchitectonic mapping of the human frontal operculum—New correlates for a variety of brain functions

Nina Unger [1,2]*, Martina Haeck[3], Simon B. Eickhoff [4,5], Julia A. Camilleri [4,5], Timo Dickscheid [2,6], Hartmut Mohlberg [2], Sebastian Bludau [2], Svenja Caspers [2,7] and Katrin Amunts [1,2]

[1]Cécile and Oskar Vogt Institute for Brain Research, Medical Faculty and University Hospital Düsseldorf, Heinrich Heine University Düsseldorf, Düsseldorf, Germany, [2]Institute of Neuroscience and Medicine (INM-1), Research Centre Jülich, Jülich, Germany, [3]MEDIAN Klinik Wismar, Wismar, Germany, [4]Institute of Neuroscience and Medicine (INM-7), Research Centre Jülich, Jülich, Germany, [5]Institute for Systems Neuroscience, Medical Faculty and University Hospital Düsseldorf, Heinrich Heine University Düsseldorf, Düsseldorf, Germany, [6]Institute of Computer Science, Heinrich Heine University Düsseldorf, Düsseldorf, Germany, [7]Institute for Anatomy I, Medical Faculty and University Hospital Düsseldorf, Heinrich Heine University Düsseldorf, Düsseldorf, Germany

The human frontal operculum (FOp) is a brain region that covers parts of the ventral frontal cortex next to the insula. Functional imaging studies showed activations in this region in tasks related to language, somatosensory, and cognitive functions. While the precise cytoarchitectonic areas that correlate to these processes have not yet been revealed, earlier receptorarchitectonic analysis resulted in a detailed parcellation of the FOp. We complemented this analysis by a cytoarchitectonic study of a sample of ten postmortem brains and mapped the posterior FOp in serial, cell-body stained histological sections using image analysis and multivariate statistics. Three new areas were identified: Op5 represents the most posterior area, followed by Op6 and the most anterior region Op7. Areas Op5-Op7 approach the insula, up to the circular sulcus. Area 44 of Broca's region, the most ventral part of premotor area 6, and parts of the parietal operculum are dorso-laterally adjacent to Op5-Op7. The areas did not show any interhemispheric or sex differences. Three-dimensional probability maps and a maximum probability map were generated in stereotaxic space, and then used, in a first proof-of-concept-study, for functional decoding and analysis of structural and functional connectivity. Functional decoding revealed different profiles of cytoarchitectonically identified Op5-Op7. While left Op6 was active in music cognition, right Op5 was involved in chewing/swallowing and sexual processing. Both areas showed activation during the exercise of isometric force in muscles. An involvement in the coordination of flexion/extension could be shown for

10.3389/fnhum.2023.1087026

the right Op6. Meta-analytic connectivity modeling revealed various functional connections of the FOp areas within motor and somatosensory networks, with the most evident connection with the music/language network for Op6 left. The new cytoarchitectonic maps are part of Julich-Brain, and publicly available to serve as a basis for future analyses of structural-functional relationships in this region.

KEYWORDS

Julich-Brain Atlas, BigBrain, cerebral cortex, cytoarchitecture, language, music, frontal operculum, probability maps

1. Introduction

Broca's and Wernicke's regions are considered to be key regions of language processing (Grodzinsky and Friederici, 2006; Grodzinsky and Santi, 2008; Friederici, 2011; DeWitt and Rauschecker, 2013; Binder, 2017; Friederici, 2017). Broca's region with areas 44 and 45 (Amunts et al., 1999, 2004) can be found in the left inferior frontal gyrus (IFG) and is part of the anterior language region. Wernicke's region (including posterior part of area 22) (Morosan et al., 2005) is located in the left superior temporal gyrus and is part of the posterior language region (Amunts and Zilles, 2012). Broca's and Wernicke's regions are connected through the arcuate fascicle and the left superior longitudinal fascicle (dorsal pathway II) as well as through the extreme capsule fiber system (ventral pathway I) [Catani et al., 2005; Friederici, 2009, 2011, 2012; Fernández-Miranda et al., 2015, for reviews see Bernal and Ardila (2009) and Bernard et al. (2019)].

Language networks comprise a large number of brain regions [for a review see Hagoort, 2014]. It has been emphasized that Broca's region is heterogeneous and consists of multiple, functionally distinct components (Hagoort, 2019; Fedorenko and Blank, 2020). The hypothesis was formulated that the dorsal language system, which includes area 44 and the posterior part of the superior temporal gyrus is complemented by the ventral language system, consisting of area 45 and the anterior part of the superior temporal gyrus (Skeide et al., 2016). Moreover, the anterior language region does not only consist of Broca's region in a narrow sense, but may include neighboring areas of the ventral frontal cortex (Hagoort, 2014). These findings can be interpreted in the sense that the classical Broca and Wernicke regions might be anatomically ill-defined and should be replaced by more accurate descriptions (Tremblay and Dick, 2016). This also implies, however, a need to study the anatomical neighbors of classically defined Broca's and Wernicke's regions with respect to their structure and putative function in language processing.

Research from our own group has proposed a new segregation of the broader anterior language region that goes beyond classical areas 44 and 45 (Amunts et al., 2010). Using quantitative receptor autoradiography of major neurotransmitter receptors, areas 44 and 45 and neighboring areas including caudally adjacent motor/premotor areas and ventrally adjacent ventral frontal cortex have been analyzed. Areas 44 and 45 have been further subdivided (each into two areas), and new areas in the frontal operculum (FOp) and premotor cortex have been identified (Amunts et al., 2010; Zilles and Amunts, 2018). Recent maps of areas Op8 and Op9 of the FOp (Saal et al., 2021a,b), which are located rostro-ventrally to areas 44 and 45 have confirmed this concept. These areas show a specific receptor architecture, distinct from classical language areas 44 and 45. Along the same line, connectivity-based analysis and probabilistic fiber tracking showed a subdivision of areas 44 and 45, and the deep FOp (Anwander et al., 2007; Jung et al., 2017). The FOp is connected with the anterior part of the superior temporal gyrus and the superior temporal sulcus via the uncinate fascicle (ventral pathway II) (Catani et al., 2005; Friederici, 2009, 2011). Furthermore, areas of the FOp seem to be phylogenetically older than areas 44 and 45 (Friederici, 2006), which is also in line with the assumption that the FOp region is functionally distinct.

The FOp has been discussed in the context of language: It seems to be mainly involved in the processing of phonological and syntactical information, both in healthy subjects and in patients with language disorders. For phonological processing, a stronger blood-oxygen-level-dependent response in the FOp was reported during auditory rhyme processing (rhymed trials) compared to non-rhymed trials (Huschler et al., 2013). In case of syllable sequence production, the FOp showed an increased activation for stimuli with a higher phonological complexity (Bohland and Guenther, 2006). Patients with left FOp lesions were found to perform less accurately in reading non-words and comparable phonological tasks (Fiez et al., 2006). A functional magnetic resonance imaging (fMRI) study (Friederici et al., 2000) reported an increased activity in the lower tip of the left FOp during a syntactic judgment task (deciding whether a stimulus belongs to nouns or to function words, e.g., conjunction or preposition) compared with a semantic judgment task (deciding whether a stimulus belongs to concrete or abstract words). Here, non-prototypical members of word types (concrete function words, e.g., because or if as well as abstract nouns, e.g., pain) were reported to show higher activation and neural resources compared with prototypical word type members (concrete nouns, e.g., house as well as abstract function words, e.g., on or above) (Friederici et al., 2000). Another fMRI experiment on syntax reported local specific activations in the left FOp during a task of transition processing, i.e., the evaluation concerning transitional dependencies (Friederici et al., 2006a). An event-related fMRI study

demonstrated that processing of sentences with ungrammatical word orders lead to a selective engagement of the more posterior deep FOp (Friederici et al., 2006b). In addition to its involvement in language, the FOp seems to play a role for gustatory representation, task control, and the perception of visceral stimuli (Eickhoff et al., 2006b; Higo et al., 2011; Veldhuizen et al., 2011; Chikazoe et al., 2019; Quirmbach and Limanowski, 2022) as well as executive control [(Thompson-Schill et al., 1997; Novick et al., 2005), for a review see Gratton et al. (2018)], according to activation patterns reported for this region. It would be plausible to assume that such diversity of function is not supported by a single brain region, but by several.

Some language processing functions have been shown to differ between genders. For example, in terms of rhyming, an echo-planar fMRI study showed a lateralized activity in the left IFG in male participants, but not females. In contrast, the pattern of activation in females showed more diffuse involvement of the left and right IFG, which was interpreted by the authors as evidence for organizational differences between genders in phonological processing (Shaywitz et al., 1995). To our knowledge, existing studies on gender differences in language mostly consider Broca's region, while neighboring regions, e.g., FOp, have not been addressed. However, the structural correlates of the differences and whether they also affect the FOp are largely unknown.

The FOp and its cytoarchitectonic parcellation have not been addressed so far. The map of Brodmann (1909) showed Brodmann's area (BA) 43 as the posterior neighbor of Broca's region; it is located at the inferior edge of the postcental gyrus and superior to the lateral fissure as well as in the cingulate region of the cortex (see **Figure 1A**). The Brodmann map, however, does not show any details of the cortex within the sulci or any parcellation details ventrally to BA 44, BA 45, and BA 47. The cytoarchitectonic map of von Economo and Koskinas (1925) described the subcentral area PF*D*, area FB_{op} of the frontal lobe, the opercular intermediate frontal area FCD_{op}, and area FD_{op} as possible anatomical correlates for the posterior part of the FOp (**Figure 1D**). Nevertheless, both maps share the problem that they represent 2D schematic drawings of the lateral surface of the brain, but do not well disclose cortical areas that are obscured by the bulging cortex of the (lateral) frontal cortex. More recent maps of Petrides and Pandya (1994), designated the area anterior to the central sulcus as area 6 (6VR and 6VC). Öngür et al. (2003) described a precentral opercular area (PrCO) adjacent to the insular cortex and located in the inside of the lateral fissure representing parts of the FOp. A more detailed view into the complex 3D geometry of the FOp is necessary to study the spatial relationships of the IFG, the FOp, and the neighboring insula. This became possible in the BigBrain model, a histological representation of cell body stained sections at 20 μm isotropic spatial resolution (Amunts et al., 2013; see **Figures 1B, C, E, F**).

Because of these open questions and the lack of precise microstructural maps that would be instrumental in further developing the concept of an anterior language region, the aim of the study was (a) to analyze the posterior part of the FOp and its segregation, (b) to generate 3D maps based on cytoarchitectonic

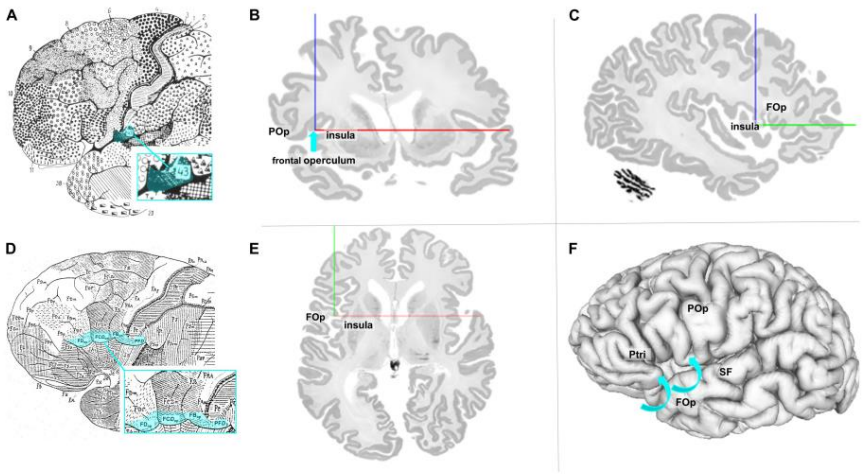

FIGURE 1
(A) Modified cytoarchitectonic map of Brodmann (1909), including BA 43 (blue highlighted). Details of the cortex within the sulci or areas ventrally to areas 44, 45, and 47 were not shown by Brodmann. Area 43 (highlighted in blue) is located slightly posterior to the referred area. **(B)** Coronal section of the BigBrain (Amunts et al., 2013). The blue arrow points to the macroanatomic location of lefthemispheric FOp. POp, parietal operculum. **(C)** Sagittal section of the BigBrain with annotations of the FOp and the insula. **(D)** Modified cytoarchitectonic mapping of von Economo and Koskinas (1925) with highlighted areas FD_{op}, FCD_{op}, FB_{op}, and PF*D*, localized at the ventral end of the frontal lobe. **(E)** Axial section of the BigBrain with annotations of the FOp and the insula. **(F)** View of the left surface of the BigBrain. The blue arrows show that the FOp is also found below the brain surface. POp, parietal operculum; Ptri, triangular part of the inferior frontal gyrus; SF, Silvian fissure. Physical coordinates (cursor) for panels **(B,C,E,F)**: −38.637 mm/22.526 mm/0.444 mm (https://atlases.ebrains.eu/viewer).

10.3389/fnhum.2023.1087026

mapping in a sample of ten brains to take into account variations in anatomy between brains (Amunts and Zilles, 2015), (c) to evaluate potential interhemispheric and gender differences, and (d) to perform meta-analytic connectivity modeling (MACM) using the BrainMap database (Laird et al., 2009; Robinson et al., 2010), considering complementary connectivity data, to gain further insights into the functions of the areas.

2. Materials and methods

2.1. Histological and image processing

Ten human postmortem brains were analyzed (five females and five males; **Supplementary Table 1**), which were obtained via the body donor program of the Anatomical Institute of the Heinrich Heine University Düsseldorf. Written informed consent from body donors was obtained. The donors had no clinical history of neurological or psychiatric diseases. The study was performed according to the guidelines of the Ethics Committee of the University of Düsseldorf (#4863).

The brains were extracted within less than 24 h after death and fixed in 4% formalin or in Bodian's fixative for at least 6 months, and further processed. A MRI scan of each brain was obtained using a 1.5-T Siemens scanner (Erlangen, Germany) using a T1-weighted 3D FLASH sequence (flip angle: 40°, repetition time: 40 ms, time echo: 5 ms). The scans served as undistorted references for subsequent 3D reconstruction. The brains were then embedded in paraffin and serially sectioned in the coronal plane (Polycut E, Reichert-Jung, Germany; thickness = 20 µm). Each 15th section (distance between mounted sections: 300 µm) was stained for cell bodies (Merker, 1983). The whole procedure and subsequent mapping, cytoarchitectonic analysis, and the computation of cytoarchitectonic probability maps (see sections 2.1–2.5) is in detail described in Amunts et al. (2020).

2.2. Observer-independent identification of cytoarchitectonic borders based on the gray level index (GLI)

Cytoarchitectonic borders between areas of the FOp were identified using image analysis and statistical tools (Schleicher et al., 1999, 2005, 2009). Hereby, rectangular regions of interest (ROIs) (**Figure 2A**) were identified in the images of the histological sections, and scanned in a mosaic like pattern. For this purpose, a

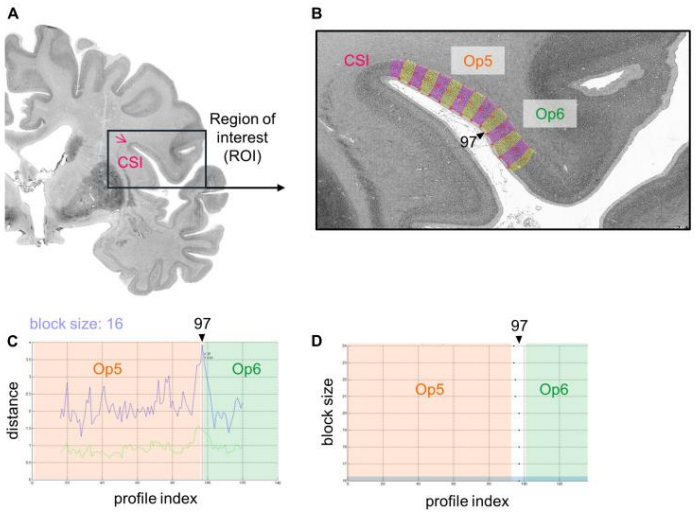

FIGURE 2
Analysis of a cytoarchitectonic border between Op5 and Op6, right hemisphere using an observer-independent mapping approach (Schleicher et al., 1999). **(A)** A region of interest (ROI) was identified (black box), which covered the whole extent of the FOp including the circular sulcus of the insula (CSI). It was scanned in a mosaic like pattern. Measurements were transformed into a gray level index (GLI) image that showed the volume fraction of cell bodies. **(B)** Equidistant traverses perpendicular to the outer and inner contour line were calculated (pink and yellow lines, changing after every 10th traverse). GLI profiles along these traverses displayed laminar changes in cytoarchitecture. CSI, circular sulcus of the insula. **(C)** The Mahalanobis distance (MD) (Mahalanobis et al., 1949) was used as a measure to quantify dissimilarity in shape of GLI profiles between neighboring areas (see upper blue curve; lower green curve: Euclidean distance function) (Schleicher et al., 2000). By means of a sliding window technique, profiles with different block sizes were moved along the cortical ribbon. For the specific block size 16, MD reaches a significant local maximum at the border between areas Op5 and Op6, at profile position 97. **(D)** Resulting significant maxima of the MD function showed profile positions with potential cytoarchitectonic borders (in the example, at profile position 97). In case MD resulted in significant maxima for different block sizes at similar profile positions [Blue marked block size: Block size 16 from panel **(C)**] and in case this border was found in three comparable positions in a minimum of three adjacent brain sections, a peak was accepted as a cytoarchitectonical border.

high-resolution CCD-Camera (Axiocam MRm, ZEISS, Germany) was used, combined with an optical light microscope (Axioplan 2 imaging, ZEISS, Germany). ROIs of every 60^{th} histological section were digitized with an in-plane resolution of 1.02 μm per pixel in both hemispheres with ZEISS image analysis software Axiovision (Version 4.6, ZEISS, Germany). Digitized ROIs were transformed into gray level index (GLI) images using an in-house software written in Matlab (The MathWorks, Inc., Natick, MA, USA) (Schleicher et al., 2005, 2009; Bludau et al., 2014). The intensities of the pixels of a GLI image correspond to the volume fraction of stained cell bodies, ranging from 0% to 100% (Wree et al., 1982; Schleicher et al., 2000).

Outer (border between layers I and II) and inner contour lines (border between layer VI and the white matter) were drawn manually in each GLI image using Matlab scripts. Equidistant traverses were generated perpendicular to the two contour lines (**Figure 2B**; Schleicher et al., 1999, 2000, 2009). GLI profiles running along these curvilinear traverses quantified laminar changes in the volume fraction of cell bodies, i.e., the regional cytoarchitecture (Schleicher et al., 2009). A feature vector with ten elements was calculated including the mean GLI, center of gravity, standard deviation, skewness, and kurtosis of the original profile, and the same features of its first derivative. Individual and local variations of cortical thickness were normalized by length normalization to compensate for differences in thickness of the cortex between brains, areas, and geometry (Schleicher et al., 1999).

The Mahalanobis distance (MD) (Mahalanobis et al., 1949) was used to quantify dissimilarities in the shape of mean GLI profiles between neighboring blocks of profiles as measures of cytoarchitectonic differences between brain areas (Schleicher et al., 2005). To increase the robustness of the MD calculation, a number of profiles (range: 10–24 profiles) was grouped into blocks of profiles. Afterward, the MD between adjacent blocks was calculated. A sliding window technique was used to systematically move the different blocks along the cortical ribbon of the ROI. The profile blocks were shifted by one profile at a time (Schleicher et al., 1999, 2005). The larger the difference in shape between profiles of adjacent blocks, the larger was their MD.

A significant maximum of the Mahalanobis distance (Bonferroni-corrected Hotelling's T2 test) indicated a cytoarchitectonic border between two adjacent cortical areas (**Figure 2C**). A border was accepted if the MD resulted in a significant maximum for different block sizes (**Figure 2D**) and the border was found at comparable positions in three or more adjacent brain sections. Subsequently, each border passed a quality control to exclude "artificial borders," e.g., due to blood vessels, wrinkles, or other artifacts (Schleicher et al., 1999).

2.3. Hierarchical cluster analysis of area-specific cytoarchitecture

By performing a Matlab-based hierarchical cluster analysis, we aimed to determine the degree of cytoarchitectonic similarities and/or dissimilarities between FOp areas compared with areas 44 and 45 (Amunts et al., 1999, 2004). For each area, 10–15 consecutive GLI profiles were selected, coming from three sections per hemisphere and brain. Profiles from the left and right hemispheres of Op5-Op7 were merged in the present study, since no volumetric differences between left and right hemispheres were found (see section 3.4). For each profile, a ten-element feature vector was calculated to enable quantification of similarity/dissimilarity between the different areas (Schleicher et al., 2005). Hierarchical clustering of these feature vectors was performed using the Euclidean distance and the Ward linkage method (Ward, 1963). Cytoarchitectonic similarity between two areas was reflected by a low Euclidean distance, whereas cytoarchitectonic dissimilarity was associated with a higher Euclidean distance. The results were visualized in a hierarchical dendrogram (**Figure 5**).

2.4. 3D cytoarchitectonic probability maps in stereotaxic reference space and maximum probability maps (MPMs)

Delineations of FOp areas were manually transferred onto corresponding digitized sections (1,200 dpi high-resolution). Afterward, they were 3D reconstructed in each of the 10 postmortem brains. Images of the brains and their areas were then registered to the T1-weighted single-subject brain Colin27 of the MNI reference space and the ICBM152casym space (Holmes et al., 1998; Evans et al., 2012). The identified areas were superimposed in the two reference spaces, and 3D continuous probabilistic maps were generated (Amunts et al., 2020). Briefly, after calculating a linear affine transformation [7 degrees of freedom (DOF): 3 translations, 3 rotations, 1 isotropic scaling] as well as a non-linear transformation vector field (3 translations for every voxel of the data set) with optimized parameters for the MRI signal of the *in vivo* reference data set and the 3D reconstructed histologic postmortem brain data, the transformations of histological data sets were stored and then applied to the mapped cytoarchitectonic regions per set of reconstructed postmortem data. For this purpose, the calculated transformations for the whole brain were applied to all regions mapped in the 10 postmortem brains and superimposed in the reference space. Volume files were used to store the resulting probabilistic cytoarchitectonic maps. In the next step, the probabilistic values were projected onto a cortical surface model of the reference brain, computed with FreeSurfer, and a surface-based representation of the cytoarchitectonic maps was computed (Amunts et al., 2020). The maps showed, for each voxel of the reference brain, the probability that a cortical area was located at a given position of the reference space. Thereby, intersubject anatomical variability of cortical areas was quantified. Subsequently, a maximum probability map (MPM) was calculated (Eickhoff et al., 2005), which assigned each voxel of the reference brain to the cortical area with the highest probability in the respective voxel.

2.5. Volumetric analysis

The volumes of each FOp area were calculated per hemisphere and brain, considering the individual shrinkage-corrected volume for each brain and area. Beforehand, shrinkage factors were

calculated as the ratio between the brain volume before and after the histological processing procedure (Amunts et al., 2020). In order to compare volumes of areas from brains with different size, the volume of each area was additionally normalized using the individual total brain volume (normalized volume = shrinkage-corrected individual area volume/shrinkage-corrected individual whole-brain volume). Thus, relative volume ratios were used for volume calculation to allow comparability between different brains.

The shrinkage corrected and normalized mean volumes for the different areas were tested for hemisphere and gender differences using a non-parametric pair-wise permutation test. The null distribution was evaluated with Monte Carlo simulation (1,000,000 iterations). Differences were considered to be significant if they were larger than 95% of values under the null-hypothesis [$p < 0.05$, false discovery rate (FDR) corrected for multiple comparisons] (Eickhoff et al., 2007; Bludau et al., 2014).

2.6. Functional decoding of areas Op5, Op6, and Op7

To functionally characterize areas Op5-Op7, we used a MACM based analysis on the BrainMap database[1] (Fox and Lancaster, 2002; Laird et al., 2005). MPMs of left and right areas Op5, Op6, and Op7 in MNI ICBM 152 reference space were defined as volumes of interest (VOIs). The BrainMap database contains 3D coordinates as results from published task-related neuroimaging experiments combined with meta-data describing "behavioral domains" and "paradigm classes" (Laird et al., 2009).

The following BrainMap Sleuth search criteria were used to filter for matching functional imaging studies with 3D peak coordinates: At the level of imaging modality, fMRI and positron emission tomography data of healthy subjects were considered, with at least one activation focus. Deactivations were excluded. Only normal mapping studies (no interventions and no group comparison) were considered (Laird et al., 2011). The search criteria led to a total number of 2,620 matching functional neuroimaging experiments at the time of analysis for further evaluation. No preselection of taxonomic categories was applied.

Analysis of meta-data involved the acquisition of all detectable functions by the over-representation of behavioral domains and paradigm classes in the experiments activating each VOI relative to the BrainMap database (Eickhoff et al., 2011). Whereas behavioral domains refer to mental processes of six neural main categories and related subcategories (cognition, action, perception, emotion, interoception, pharmacology), paradigm classes refer to single experimental tasks [(Laird et al., 2009), available online, http://www.brainmap.org/taxonomy/]. Bar charts visualized activated behavioral domains and paradigm classes for each examined VOI with its respective probability likelihood ratio. For this, forward and reverse inference were applied. Forward inference describes the probability of observing activity in a brain region, taking into account knowledge of a predefined behavioral domain or paradigm class. Reverse inference describes the probability of a particular behavioral domain or paradigm class, given activation in a VOI. Significance was established with a binomial test [$p < 0.05$, FDR corrected for multiple comparisons] (Laird et al., 2009; Eickhoff et al., 2011).

2.7. Functional and structural connectivity of areas Op5, Op6, and Op7

In a first step, we integrated functional connectivity using MACM, and aimed to analyze whole-brain co-activation patterns of Op5-Op7 left/right. Therefore, MACM analyses were performed using the activation likelihood estimation algorithm. To analyze the functional connectivity (co-activation) of each FOp area, concordant activation foci were determined per area from reported neuroimaging activation data obtained from BrainMap (Eickhoff et al., 2011). Due to spatial uncertainty of neuroimaging data, we modeled the foci as probability distributions. As a result, MACM generated coincided whole-brain co-activation maps for each FOp area (peak x-y-z coordinates in stereotaxic reference space). They were displayed on the MNI ICBM 152 brain template. To define a null-distribution reflecting a random spatial assignment of experiments, a permutation test with 10,000 repetitions was used ($p < 0.05$, FDR corrected) (Eickhoff et al., 2016). To analyze equal and differing co-activation patterns of Op5–Op7, we carried out a conjunction analysis and a contrast analysis (Nichols et al., 2005). The conjunction analysis is based on identifying brain areas that are activated by task A and task B or combined tasks (Price and Friston, 1997; Nichols et al., 2005). In further application, it included overlap of the six single MACM co-activation maps and enabled us to investigate which brain regions demonstrated co-activation with all three opercular areas Op5, Op6, and Op7, or combinations of the areas. The contrast analysis was performed by voxel-wise calculation of differences between co-activation maps of individual MACM analyses. The analysis was conducted to demonstrate differing functional connectivity between two respective VOIs as well as to highlight unique functions for each area per hemisphere (Eickhoff et al., 2011).

In a second step, we studied the structural connectivity of bilateral areas Op5, Op6, and Op7 using connectivity data of the population-based German cohort study 1000BRAINS (Caspers et al., 2014). Connectivity data can be accessed online via 3D atlas viewer "siibra-explorer" of the Human Brain Project's EBRAINS research infrastructure.[2] In the 1000BRAINS study, structural connectivity was analyzed on the basis of diffusion-weighted MRI obtained in a 3T MR scanner (sequence parameters of two datasets: b = 1,000 s/mm^2 and 60 diffusion-weighted volumes; b = 2700 s/mm^2 and 120 diffusion-weighted volumes, both at an isotropic resolution of 2.4 mm) (Caspers and Schreiber, 2021). Whole-brain connectivity matrices based on brain regions included in the Julich-Brain cytoarchitectonic maps were used as representations of the variability of fiber tracts, i.e., structural connectivity, in the 1000BRAINS population sample (Caspers et al., 2014).

1 http://brainmap.org

2 https://atlases.ebrains.eu/viewer

10.3389/fnhum.2023.1087026

3. Results

3.1. Cytoarchitecture of areas Op5–Op7 and distinction from neighboring areas

Three new cytoarchitectonic areas were identified, which differed in their microstructure. Op5 showed a prominent internal granular layer IV. Layer IV was thinner in areas Op6 and Op7. I.e., area Op5 is a granular area, while Op6 and Op7 are dysgranular. Details about cytoarchitectonic criteria for Op5, Op6, and Op7 can be found in **Table 1**.

Area Op5 showed a rather prominent laminar pattern (**Figure 3A**). Layer III revealed a gradient in pyramidal cell size from superficial (smaller cells) to deep parts (larger cells), with largest cell size in the lower layer III. In addition, Op5 showed large pyramidal cells in layer V. Layer IV was broad and densely packed, with a higher cell density than in layer V. The borders of layer IV to layers III and V were well defined.

Area Op6 was distinct from Op5 and Op7 by a somewhat lower overall cell density (**Figure 3B**). Op6 showed more pronounced vertical columns than the other two areas. Layer II showed a high cell density, and its border to layer III was clearly visible. Layer IV was intermingled by pyramidal cells from layers III and V. Prominent and elongated pyramidal cells were found in layer V. Layers IIIc and IV had a higher cell density than layer V. Layer VI was broad, with numerous small cells.

Area Op7 differed from Op5 and Op6 by its densely packed layers IIIc, IV, and the upper layer V (**Figure 3C**). In contrast, layers IIIa+b and lower layer V of Op7 showed a lower cell density. Large pyramidal cells were found in lower layer III and layer V. The transition to the white matter was blurred, mainly because of the low cell density in the lower portion of layer VI.

The cytoarchitectonic differences between the three Op-areas and neighboring areas were captured by the observer-independent mapping procedure, and the localization of borders were proven by multivariate statistics (see section 2). Exemplary cytoarchitectonic borders between areas Op5 and Op6 are shown in **Figures 4A, B**, and between Op6 and Op7 in **Figures 4C, D**.

A cluster analysis (**Figure 5**) further quantified similarities and dissimilarities between the areas. It showed that areas Op6 and Op7 as the two dysgranular areas were most similar to each other, while area Op5 as granular area was distinct. In the diagram, areas 44 and 45 were separated from the three FOp areas, and located on another branch of the hierarchical cluster tree. This indicates a greater cytoarchitectonic difference between areas 44 and 45 to the FOp than within Op5–Op7.

In comparison, the neighboring parietal, opercular area OP4 (dysgranular) (Eickhoff et al., 2006c) showed a smaller size of pyramidal cells in the lower layer III and a lower cell density in layers III and V (**Figure 6A**). The main difference between area Op5 and the insular area Id4 (dysgranular) (Quabs et al., 2021a) was that layer III of Id4 was more sparsely populated with cells than layer III of Op5 (**Figure 6B**). The comparison of areas Op6 and premotor cortex revealed a weak laminar differentiation of area 6r1, i.e., all cortical layers from layer II to VI showed an approximately similar cell packing density (Amunts et al., 2010; **Figure 6C**). Like area 44, both areas Op6 and Op7 contained large pyramidal cells in layer III. However, they did not reach the size of pyramidal cells of area 44 (deep layer III and layer V) (**Figures 6D, E**). Compared with area Op7, area Op8 (Saal et al., 2021a) revealed a faint but recognizable layer IV in comparison with the prominent horizontal stripes of Op7 consisting of layers IIIc, IV, and Va. In adjacent layers, Op7 showed a lower cell density, and Op8 a higher cell density (especially in the lower layer III and in the upper layer V) (**Figure 6F**). The comparison of areas Op7 and Id6 (dysgranular) (Quabs et al., 2021b) revealed that pyramidal cells of layer IIIc had a higher dispersion, while the horizontal stripe in area Id6 appeared broader than in Op7 (Quabs et al., 2022; **Figure 6G**). In contrast to area Id7, Op7 showed a higher density of pyramidal cells in deep layer III and a higher packing of layer VI (Grodzinsky et al., 2020; **Figure 6H**).

TABLE 1 Cytoarchitectonic characteristics of opercular areas Op5, Op6, and Op7.

Area	Cytoarchitectonic characteristics
Op5	• Rather granular cytoarchitectonic area • Distinct horizontal lamination • Gradient in pyramidal cell size of layer III • Large pyramids in layers III and V • Broad layer IV with a high cell density and well defined borders to layers III and V • Large-sized pyramidal cells in layers IIIc and V adjusting directly to layer IV • High cell density in layer VI
Op6	• Dysgranular cytoarchitectonic area • Lower overall cell density compared with areas Op5 and Op7 • Poor cell density apart from layers IIIc and IV • Arrangement of cells mainly in columns • Border between layer II and layer III clear cut due to a high amount of cells in layer II • Layer IV not clearly visible due to intermingling with pyramidal cells from layers III and V • Prominent large sized and elongated pyramidal cells in layer V • Thick layer VI with numerous small cells
Op7	• Dysgranular cytoarchitectonic area • High cell density of layer IIIc, layer IV and the upper layer V • Lower cell density of layers IIIa + b and the lower layer V of Op7 • Large-sized pyramidal cells within the lower layer III and layer V • Blurred transition with the white matter, mainly because of the low cell density in the lower portion of layer VI

10.3389/fnhum.2023.1087026

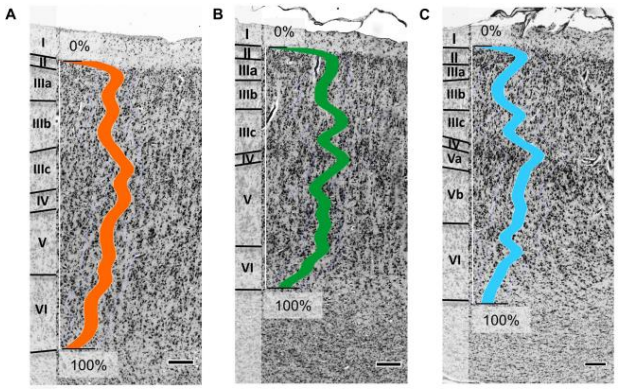

FIGURE 3
Cytoarchitecture of areas Op5 **(A)**, Op6 **(B)**, and Op7 **(C)** (Op5 and Op6 taken from brain BC20, right hemisphere; Op7 taken from brain BC21, right hemisphere). The colored lines indicate the mean gray level index (GLI) profiles of areas Op5 (orange line), Op6 (green line), and Op7 (blue line) for a range from 0% (outer contour line, border between layers I and II) and 100% (inner contour line, border between layer VI and the white matter). Roman numbers indicate the cortical layers. Scale bars = 200 μm.

3.2. Topography of areas Op5, Op6, and Op7

Areas Op5-Op7 occupied the posterior part of the FOp, and approached the insula, up to the circular sulcus of the insula (CSI). The borders between Op5 and Op6 as well as between Op6 and Op7 were always located lateral to the CSI, and never reached the medial wall (**Figure 7** for the location of areas Op5–Op7 on consecutive sections).

Main parts of the three FOp-areas were located in the depths of the lateral fissure. In six of the 20 hemispheres, Op5 extended a few millimeters to the free brain surface (subcentral gyrus; two left hemispheres, four right hemispheres). In all hemispheres, Op5 reached the CSI and was located medially and anterior to area OP4. The border between Op5 and Op6 was in the ventral wall of the FOp.

In all 20 hemispheres, Op6 extended a few millimeters to the free brain surface (precentral gyrus/IFG). Op6 adjoined Op5 anteriorly and Op7 posteriorly. Lateral neighbors of Op6 were premotor area 6r1 and area 44 in caudo-rostral direction. Op7 reached the free brain surface in none of the hemispheres, but always was buried in the sulcus. Op7 was laterally adjacent to the insular cortex. Furthermore, Op7 was medially and posteriorly adjacent to area 44 and to the anterior part of the FOp (mainly Op8, more rarely Op9) (Saal et al., 2021a,b). Like the border between Op5 and Op6, the border between Op6 and Op7 was located in the depth of the fissure.

The medial neighbor of areas Op5, Op6, and Op7 was the anterior insula (Op5/Op6: Id4, Id6; Op7: Id6, Id7) (Grodzinsky et al., 2020; Quabs et al., 2021a,b). In some hemispheres, the posterior part of area Op5 was located medially to OP3 (Eickhoff et al., 2006c). Areas Op5-Op7 were mainly arranged in anterior-posterior direction. This localization did not differ between male and female brains.

3.3. Cytoarchitectonic 3D maps and intersubject variability

Intersubject variability in extent and location of areas Op5, Op6, and Op7 was quantified in the probability maps (**Figure 8**). The superimposition of all ten brains resulted in probabilistic maps, whereby the color coding from dark blue to red corresponds to an increasing overlap, or decreasing intersubject variability. Centers of gravity in 3D space for the left and right hemispheres are listed in **Table 2**; they did not differ between male and female brains.

The MPM reveals small parts of Op5 at the subcentral gyrus, while Op6 occupied parts of the precentral gyrus (**Figure 8C**). Op7 remained consistently within the lateral fissure. Cytoarchitectonic maps are shown also as surface representations in the reference brain Colin27 (Evans et al., 2012), to give a better impression of the extent of the areas in the depth of the brain. All data are part of the Julich-Brain Atlas (Amunts et al., 2020), and publicly available via the Human Brain Atlas of the EBRAINS research infrastructure of the Human Brain Project[3].

3.4. Volumes of areas Op5, Op6, and Op7

Areas Op5 and Op6 were about the same size, while area Op7 was the smallest area among the three. The intersubject variability of volume was most prominent for area Op6 and least prominent for area Op7 (see **Table 3** for individual volumes per hemisphere). The shrinkage-corrected volumes did neither differ between hemispheres or sexes (all $p > 0.05$; see **Table 4** and **Figure 9**).

3 https://www.humanbrainproject.eu/en/explore-the-brain

10.3389/fnhum.2023.1087026

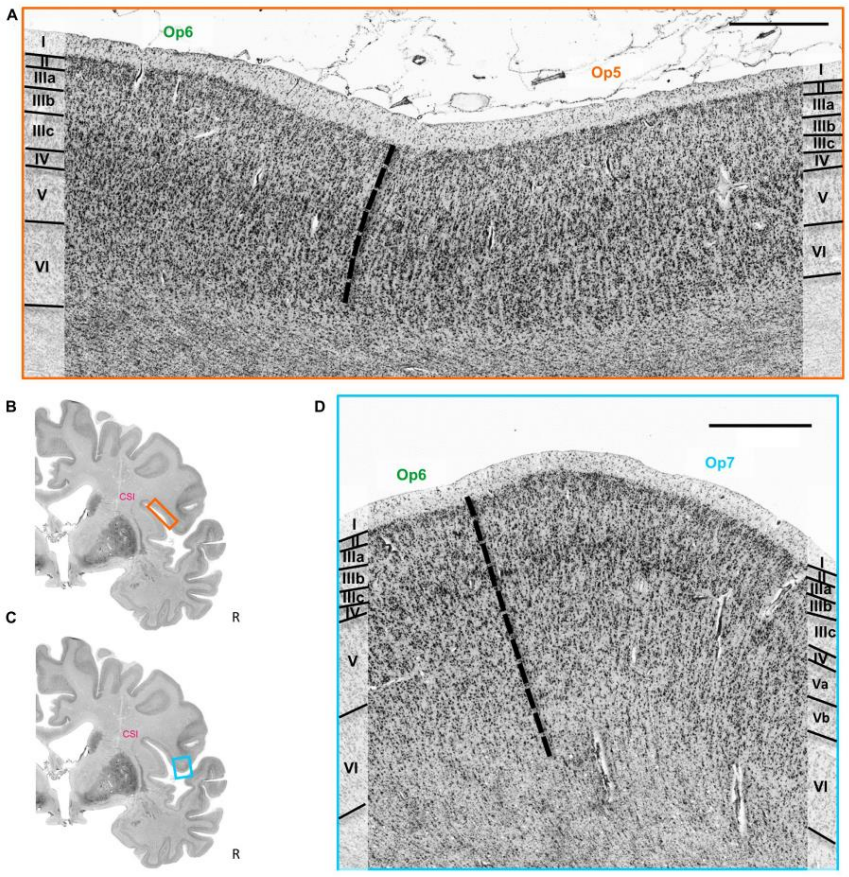

FIGURE 4
(A) Cytoarchitectonic border (dashed line) between the areas Op5 and Op6. Roman numbers indicate cortical layers. CSI = circular sulcus of the insula. Scale bar = 1000 μm. **(B)** Localization of the brain section in panel **(A)**. **(C)** Localization of the brain section in panel **(D)**. **(D)** Cytoarchitectonic border (dashed line) between the areas Op6 and Op7. Roman numbers indicate the cortical layers. CSI, circular sulcus of the insula. Scale bar = 1000 μm.

3.5. Functional profiles of Op5, Op6, and Op7

Based on the BrainMap database, area-specific functions of Op5, Op6, and Op7 were analyzed. Related Sleuth search results from the BrainMap database can be found in **Supplementary Table 2**. All results of the behavioral domain category as well as of the paradigm class category can be found in **Table 5**.

The following functional profiles were found: Op6 left was involved in music cognition, whereas Op5 right was active in chewing/swallowing and sexual processing. Both areas together showed an activation in isometric force of muscles. Op6 right showed an activation in flexion/extension.

3.6. Functional and structural connectivity on areas Op5, Op6, and Op7

The conjunction analysis of MACM revealed that areas Op5–Op7 showed co-activational connectivity with area 44 (Broca's region), with the parietal operculum (POp), with areas of the temporal lobe as well as with parts of the somatosensory cortex (**Figure 10A**). The contrast analysis of MACM showed differences in co-activation by comparing two of the new opercular maps. An overview of all MACM results is summarized in **Supplementary Table 3**. Areas of co-activational clustering were connected with the cytoarchitectonically defined areas of the Julich-Brain Atlas 2.9 (Amunts et al., 2020; **Supplementary Tables 3–4**).

10.3389/fnhum.2023.1087026

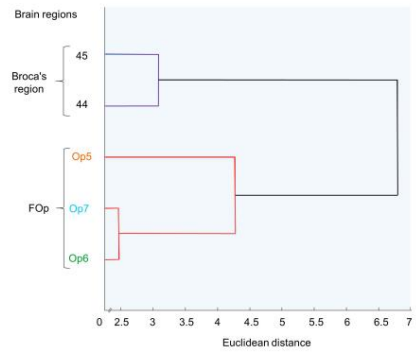

FIGURE 5
Hierarchical cluster analysis of areas Op5, Op6, Op7, and areas 44 and 45. Op6 and Op7 are similar to each other and form a cluster, distinct from Op5. Areas 44 and 45 form a distinct cluster.

Op5 left showed co-activations with area 1 (Geyer et al., 1999, 2000), area 2 (Grefkes et al., 2001), area 3b (Geyer et al., 1999, 2000), area Id4 (Quabs et al., 2022), and area OP3 (Eickhoff et al., 2006a,c) in the left hemisphere as well as with area Id6 (Quabs et al., 2022) in the right hemisphere. Op5 right showed co-activations with areas 3a (Geyer et al., 1999, 2000), 3b, 4a (Geyer et al., 1996), 4p (Geyer et al., 1996), and OP1 (Eickhoff et al., 2006a,c) in the left hemisphere and with areas OP3 and OP4 (Eickhoff et al., 2006a,c) in the right hemisphere. Additional co-activations were detected for Op5 right with 6ma (Ruan et al., 2018), 6mp (Ruan et al., 2018), the medial geniculate body (Kiwitz et al., 2022), and Id4 in both hemispheres.

Op6 left showed co-activations with area 44 (Amunts et al., 1999, 2004), area Id6, area FG1 (Caspers et al., 2013), and area FG2 (Caspers et al., 2013), in the left hemisphere as well as with areas hIP1 (Choi et al., 2006), hIP3 (Scheperjans et al., 2008a,b), and PFm (inferior parietal lobule, IPL) (Caspers et al., 2006, 2008) in the right hemisphere. Further co-activations existed with areas 6ma and FG4 (Lorenz et al., 2017) in both hemispheres. For Op6 right, co-activations with areas 6mp, OP1, OP4, PF (IPL) (Caspers et al., 2006, 2008) and PFcm (IPL) (Caspers et al., 2006, 2008) right as well as with bilateral area 6ma could be observed.

Op7 left showed co-activations with areas 33 (Palomero-Gallagher et al., 2015) and Id7 (Grodzinsky et al., 2020) in the right hemisphere as well as with area Id6 in both hemispheres. Further co-activations could be observed for Op7 right with OP1 right as well as with bilateral areas Id6 and Id7.

In comparison to the MACM results, the structural connectivity analysis based on the 1000BRAINS study (results in alphabetical order) revealed structural connectivity of Op5 left with Id4, Id6, Ig3 (Quabs et al., 2022), OP1, OP3, and OP4 in the left hemisphere. For Op5 right, there was structural connectivity with areas 3b, 4a, 6d1 (Sigl et al., 2021a), 6d2 (Sigl et al., 2021b), 6ma, Id4, Id5 (Quabs et al., 2022), Id6, Id7, OP1-OP4, PF, PFcm, PFm, PFop (IPL) (Caspers et al., 2006, 2008), and PFt (IPL) (Caspers et al., 2006, 2008) in the right hemisphere. For Op6 left, structural connectivity could be observed with areas 1, 4a, 44, 45 (Amunts et al., 1999, 2004), Id2 (Quabs et al., 2022), Id5-Id7, Ig3, Op8 (Saal et al., 2021a), Op9 (Saal et al., 2021b), PF, PFcm, PFm, PFop, PFt, and TE 2.2

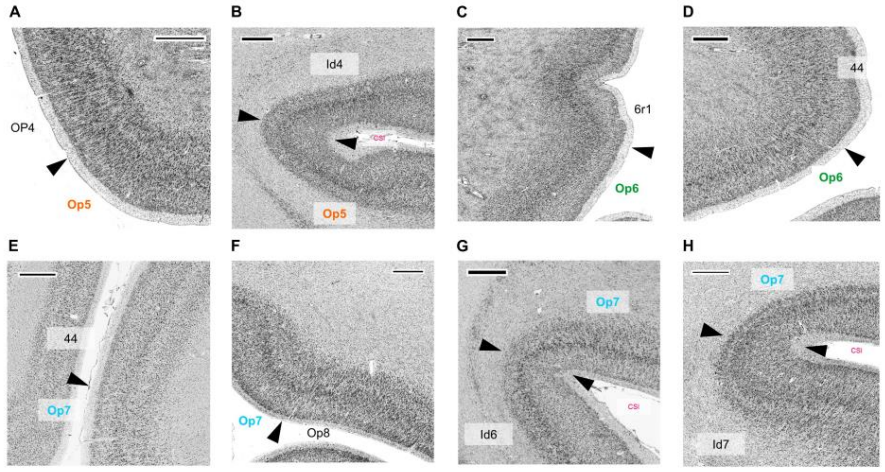

FIGURE 6
Cytoarchitectonic borders between areas Op5 and OP4 (Eickhoff et al., 2006a,c) **(A)**, between area Op5 and insular area Id4 (Quabs et al., 2021a) **(B)**, between area Op6 and premotor area 6r1, which is not yet mapped **(C)**, between area Op6 and area 44 (Amunts et al., 1999, 2004) **(D)**, between area Op7 and area 44 **(E)**, between areas Op7 and Op8 (Saal et al., 2021a) **(F)**, between areas Op7 and Id6 (Quabs et al., 2021b) **(G)**, and between area Op7 and Id7 (Grodzinsky et al., 2020) **(H)**. CSI, circular sulcus of the insula. Scale bars = 1,000 μm.

10.3389/fnhum.2023.1087026

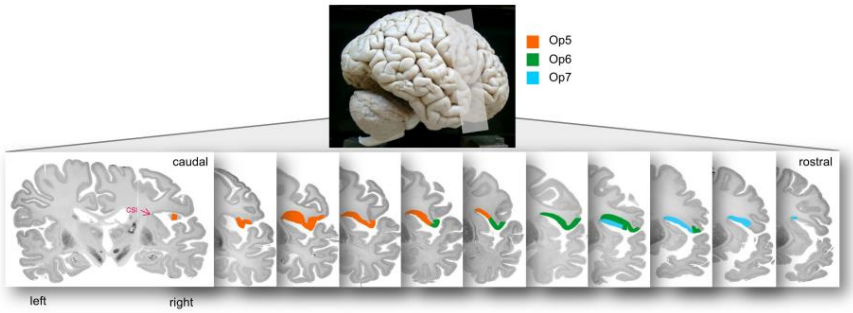

FIGURE 7
Localization of areas Op5, Op6, and Op7 in the right hemisphere of brain BC20 in serial coronal sections. The opercular areas Op5–Op7 approached to the insula up to the circular sulcus of the insula (CSI), which is highlighted with the pink arrowhead in the most posterior section. The upper lateral view of the brain illustrates the range of sectioning.

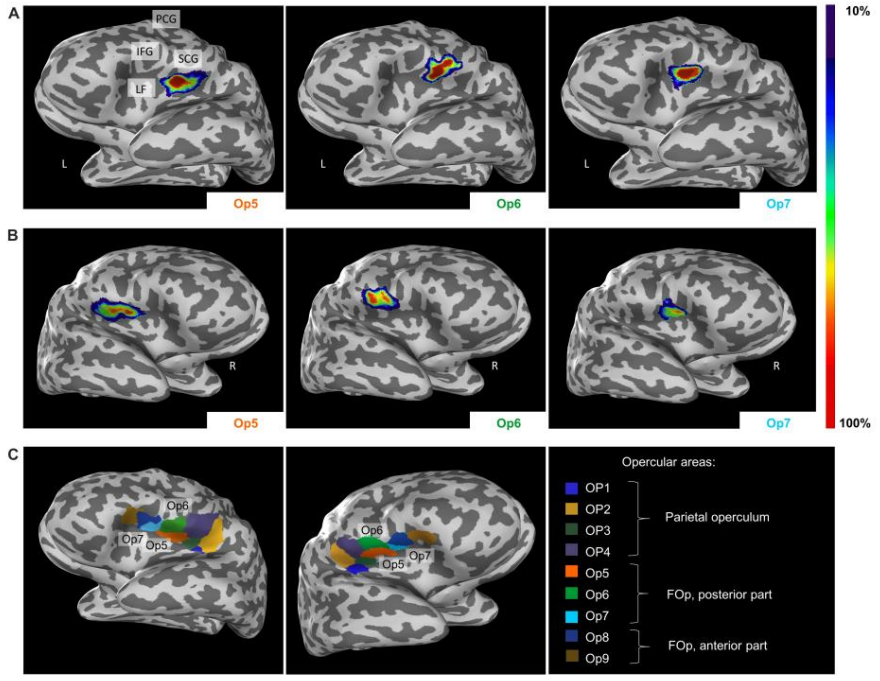

FIGURE 8
Lateral view from the left **(A)** and the right side **(B)** of the cytoarchitectonic probabilistic maps of the delineated areas Op5, Op6, and Op7 (MNI-Colin27 reference space, inflated view, Julich-Brain Atlas https://julich-brain-atlas.de/). The number of overlapping brains per voxel is color-coded. IFG, inferior frontal gyrus; LF, lateral fissure; PCG, precentral gyrus; SCG, subcentral gyrus. **(C)** Left-hemispheric and right-hemispheric maximum probability maps (MPMs) of areas Op5–Op7 in MNI-Colin27 reference space. The visualization also includes neighboring areas OP1–OP4 and Op8–Op9. Presentation of the MPMs on inflated brains to visualize also areas in sulci.

10.3389/fnhum.2023.1087026

TABLE 2 Coordinates of the centers of gravity for FOp areas Op5, Op6, and Op7 in MNI ICBM 152 space (upper table section) and anatomical MNI Colin27 space (lower table section) separated for the left and right hemisphere.

Center of gravity coordinates in MNI ICBM 152 space						
Area	Left hemisphere			Right hemisphere		
	X Sagittal	Y Coronal	Z Horizontal	X Sagittal	Y Coronal	Z Horizontal
Op5	−47	−5	13	45	−1	12
Op6	−52	5	6	52	8	5
Op7	−40	10	9	37	14	10
Center of gravity coordinates in anatomical MNI Colin 27 space of continuous probability maps						
Area	Left hemisphere			Right hemisphere		
	X Sagittal	Y Coronal	Z Horizontal	X Sagittal	Y Coronal	Z Horizontal
Op5	−47	−4	13	46	−2	12
Op6	−52	5	7	54	6	5
Op7	−39	10	11	39	12	10

TABLE 3 Size of Op5, Op6, and Op7 in both hemispheres.

Area	V_{mean} [mm^3] ± SD [mm^3]	
	Left hemisphere	Right hemisphere
Op5	1,059.98 ± 305.97	1,142.91 ± 453.18
Op6	1,281.77 ± 545.07	1,139.33 ± 415.07
Op7	525.32 ± 190.34	509.79 ± 313.81

Mean values (V_{means}) of the corrected volumes with associated standard deviations (SD) for Op5, Op6, and Op7, separated for the left and right hemispheres. Histologic volumes were corrected using the individual shrinkage factor of each individual brain.

(Morosan et al., 2005) in the left hemisphere as well as with 6d1 and 6d2 in both hemispheres. For Op6 right, there was structural connectivity with areas 6d1, 6d2, 6d3 (Sigl et al., 2021c), 6ma, Id4, OP4, PFm, PFop, PFt, and PGa (Caspers et al., 2006, 2008) right. For Op7 left remained structural connectivity with Id6 left. For Op7 right, there was structural connectivity with Id5 and Id6 right. Selected functional and structural connectivity results, specifically for area Op6 left, can be found in **Figures 10B, C**.

4. Discussion

The present study revealed a new microstructural parcellation of the posterior FOp in the human brain based on cytoarchitectonic differences and introduced 3D maps of the three new areas Op5, Op6, and Op7. Cytoarchitectonic borders were identified using image analysis and statistical criteria, to make them reproducible. The new areas were cytoarchitectonically distinct from the adjacent insula and other surrounding areas. The varying location and extent of the FOp-areas were reflected in cytoarchitectonic probabilistic maps in the MNI-Colin27 and the MNI ICBM 152 space, which enable analyses and comparisons with *in vivo* neuroimaging data serving as anatomical reference. No significant differences in the volumes, localization of areas Op5-Op7 in space,

TABLE 4 Volume of areas Op5–Op7 of the human FOp in each hemisphere of the 10 postmortem brains.

Brain	Areal volume [mm^3]						Sum
	Op5 left	Op5 right	Op6 left	Op6 right	Op7 left	Op7 right	
BC4	880.64	673.62	862.81	582.65	337.48	280.21	3,617.41
BC5	918.83	362.48	1,084.69	1,488.09	181.44	671.16	4,706.69
BC6	1,129.95	1,032.09	1,530.89	1,039.16	681.33	564.37	5,977.80
BC7	905.44	1,745.84	2,324.69	1,842.41	413.13	1,254.46	8,485.98
BC8	1,185.68	1,052.69	1,236,78	701,92	487.63	233.74	4898.44
BC9	404.81	1,038.41	774.47	781.92	438.48	177.97	3,616.06
BC10	1,087.60	1,234.67	2,061.01	1,204.37	578.37	661.69	6,827,71
BC12	1,195.72	1,029.52	700.63	1,013.90	616.89	430.58	4,987.24
BC20	1,453.47	1,376.31	957.07	1,078.14	704.52	499.13	6,068.64
BC21	1,437.65	1,883.46	1,284.70	1,660.74	813.97	324.63	7,405.14
Mean	1,059.98	1,142.91	1,281.77	1,139.33	525.32	509.79	5,659.11
SD	305.971	453.18	545.07	415.07	190.34	313.81	2,223.43

10.3389/fnhum.2023.1087026

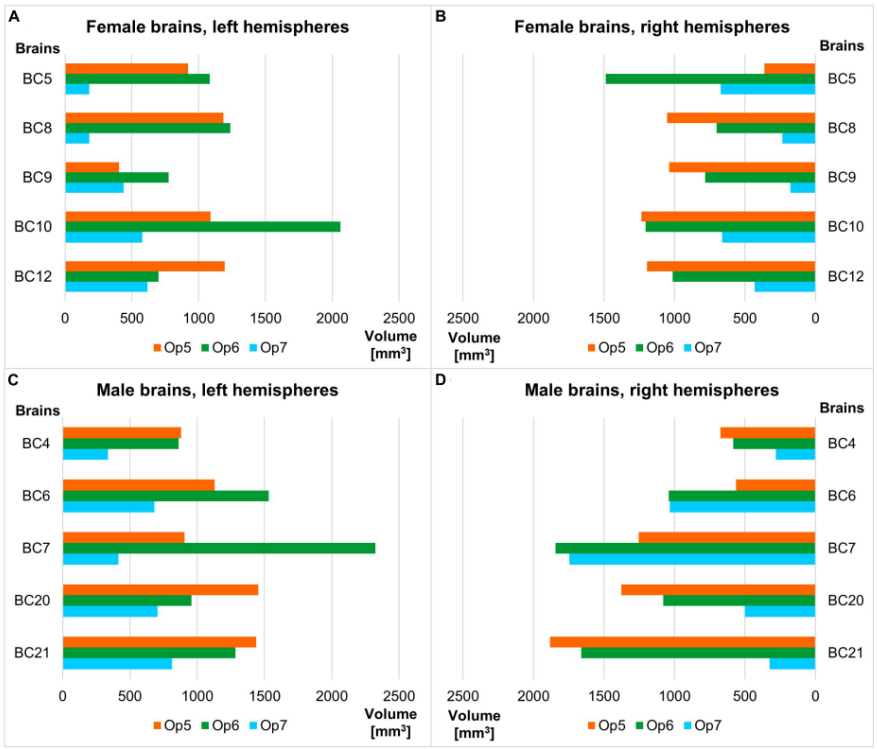

FIGURE 9
Volume of areas Op5–Op7 of the human FOp in each hemisphere of the ten postmortem brains sorted by female **(A,B)** and male brains **(C,D)**, each by left and right hemisphere. Analyses revealed no significant volume difference between sexes nor between hemispheres (all $p > 0.05$).

TABLE 5 Behavioral domains and paradigm classes of Op5, Op6, and Op7 left and right ($p < 0.05$, FDR corrected) represented by colored boxes per hemisphere.

Behavioral domain	Op5		Op6		Op7	
	LH	RH	LH	RH	LH	RH
Cognition.Music						
Interoception sexuality						
Perception somesthesis.Pain						
Paradigm class	**Op5**		**Op6**		**Op7**	
	LH	RH	LH	RH	LH	RH
Music comprehension						
Flexion/Extension						
Chewing/Swallowing						
Sexual arousal/Gratification						
Isometric force						
Pain monitor/Discrimination						

LH, left hemisphere; RH, right hemisphere.

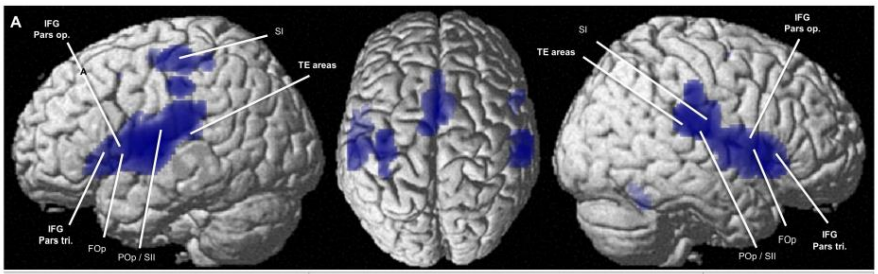

B

Language-related brain areas – showing connectivity with area Op6 left		Exemplary functions	Reference(s) from Julich-Brain Atlas (Amunts et al., 2020)
Area 44 left	Broca's region	Language production and perception; phonological and syntactical processing; verbal fluency; spontaneous speech; semantic processing; word production	Amunts et al. (1999, 2004)
Area 45 left			
Area Id2 left	Anterior insula	Responses to somatosensoric stimuli (Kurth et al., 2010)	Quabs et al. (2022)
Area Id5 left		Multifunctional integration, e.g. interoception, sensorimotorics, cognition, and social-emotional processing	Quabs et al. (2022)
Area Id6 left		Cognitive functions such as attention (Kurth et al., 2010)	Quabs et al. (2022)
Area Id7 left		Syntactical language processing	Grodzinsky et al. (2020)
Area Ig3 left		Gustatory perception (Kurth et al., 2010)	Quabs et al. (2022)
Area Op8 left	Frontal operculum, anterior part	Language processing	Saal et al. (2021a)
Area Op9 left		Language processing	Saal et al. (2021b)
Area TE 2.2 left	Primary auditory cortex	Processing of auditory stimuli	Morosan et al. (2005)

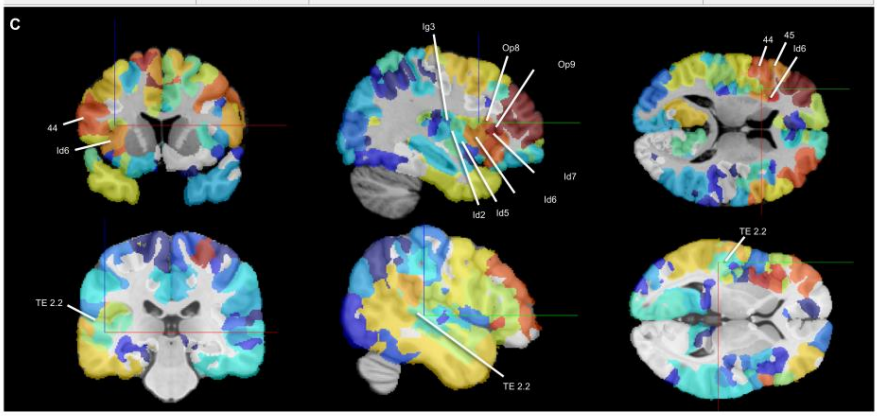

FIGURE 10
(A) Areas Op5–Op7: Results of the conjunction analysis displayed on the cortical surface (MNI ICBM 152 reference brain) (Nichols et al., 2005) proving combined co-activation of the areas Op5-Op7 calculated by meta-analytic connectivity modeling (MACM) (Eickhoff et al., 2011). The analysis revealed that areas Op5-Op7 showed co-activational connectivity with area 44 (Broca's region), with the FOp, and with the TE areas. Also with the POp and and with parts of the somatosensory cortex, all FOp areas showed co-activational connectivity. FOp = frontal operculum; IFG Pars op. = inferior frontal gyrus, opercular part; IFG Pars tri. = inferior frontal gyrus, triangular part; POp/SII = parietal operculum/secondary somatosensory cortex; SI = primary somatosensory cortex; TE areas = auditory cortex in the temporal lobe. **(B)** Area Op6 left: Language-related brain areas that showed connectivity with area Op6 left in the present study and thus were connected with the FOp in a network. For full connectivity results, see **Supplementary Tables 3**, **4**. Additional reference: Kurth et al. (2010)—for citation, see **Supplementary material**. **(C)** Structural connectivity of area Op6 left: Frontal, sagittal, and coronal sections in the MNI ICBM 152 reference space (two different cutting heights). Marked are areas associated with selected functions including language, which show a structural connectivity to Op6 left. Level of structural connectivity to Op6 left from the 1000BRAINS cohort (Caspers et al., 2014) is indicated by coloring of areas red (high structural connectivity) to blue (low structural connectivity). Physical coordinates (cursor) for upper **(C)**: −36.095 mm/10.771 mm/12.499 mm; Physical coordinates (cursor) for lower **(C)**: −51.450 mm/−29.050 mm/2.100 mm (https://atlases.ebrains.eu/viewer).

or with respect to their relationship to sulci and gyri were found between male and female brains.

The present study confirmed our hypothesis that the FOp is composed of several cytoarchitectonic areas that are distinct in microstructure and connectivity (Anwander et al., 2007; Amunts et al., 2010; Friederici, 2017). By evaluating MACM and structural connectivity results and by comparing co-activations and functional specifics of the co-activated areas, we identified distinct functions, with Op6 left being involved in music cognition and wider music/language-relevant networks. Combined with Op5 right, Op6 left was also active in a task of isometric force of muscles. Op5 right showed involvement in chewing/swallowing and sexual processing, while Op6 right was active in flexion/extension.

4.1. Comparison of new maps of Op5-Op7 with other maps of the FOp

The present results supplement earlier findings of our group based on receptorarchitectonic analyses (Amunts et al., 2010), and go beyond the parcellation of the FOp in historical maps, proposed, for example, by Brodmann (1909) and von Economo and Koskinas (1925). Brodmann described BA 43 and BA 6 near the central sulcus as two homogeneous areas, but his drawing only shows the brain surface. The new Op5 of the present study most likely corresponds to the rostral part of BA 43 (Brodmann, 1909). Areas Op6 and Op7 seemed to correspond to the caudal part of BA 6, partially adjacent to BA 43 (Brodmann, 1909). The putative anatomical correlates for Op5-Op7 in the maps of von Economo and Koskinas (1925) are most probably areas PF*D*, FB_{op}, FCD_{op}, and FD_{op}. However, the pattern of segregation is not the same. While Op5 may mainly be assigned to the rostral part of PF*D* and to the caudal part of FB_{op}, areas Op6 and Op7 seem to correspond to the rostral part of FB_{op}, to area FCD_{op}, and to the most caudal part of FD_{op} (von Economo and Koskinas, 1925). Clearly, a more thorough comparison with previous maps would require aligning them to the same reference space, which is not an option.

More recent maps of the human prefrontal cortex of Petrides and Pandya (1994) showed an extended area 6 in the peri-Sylvian region, adjacent to the central sulcus. Area 6 of Petrides and Pandya (1994) consisted of the areas 6VR and 6VC (in anterior-posterior direction). Area PrCO of Öngür et al. (2003) most probably corresponds to areas Op6 and Op7, based on their description of an area anterior to the central sulcus within the lateral fissure.

In accordance to previous findings (e.g., Keller et al., 2009), no anatomical asymmetry or lateralization of the FOp in favor of the left hemisphere could be found for Op5–Op7. This is different from the finding of an anatomical asymmetry of area 44. In area 44, a left-hemispheric asymmetry in volume could be observed providing a putative structural correlate for lateralization of speech (Amunts et al., 1999).

4.2. Functional decoding of areas Op5, Op6, and Op7

The MACM analyses revealed a contribution of left Op6 to music cognition. This is in correspondence with earlier studies showing an association of the entire FOp with rhythm perception (Limb et al., 2006), musical priming (intonation judgments) (Tillmann et al., 2003), and song complexity (Brown et al., 2004). The present analysis also showed a co-activation of Op6 left with area 44 in the left hemisphere. 1000BRAINS data confirmed this by showing structural connectivity of Op6 left with left area 44 and additionally, with left area 45. As for the FOp, there was evidence for Broca's region being involved in music processing (Levitin and Menon, 2003), which fits in that music and language are both based on syntactic rules that are complex, hierarchically-structured, and based on implicitly existing structural norms (Kunert et al., 2015).

For right area Op5, the MACM analysis indicated a connection to interoception of sexuality. A perfusion fMRI investigation about male sexual activity showed that the whole FOp is a brain region correlated with measures of sexual behavior (Georgiadis et al., 2010). The FOp was also mentioned as neuroanatomical correlate of penile erection when viewing photographic stimuli (Moulier et al., 2006). MACM revealed co-activations between area Op5 right and areas 3a, 3b, 4a, 4p, the medial geniculate body, Id4, OP1, and OP3, which corresponds largely (except the precentral gyrus) to the areas that have been associated with sexual behavioral measures (Georgiadis et al., 2010). Blood oxygen level-dependent effects described by Moulier et al. (2006), however, confirmed also the precentral co-activations for the FOp shown by MACM, and were also reflected in the structural connectivity data considered. At the same time, the underlying cytoarchitecture did not differ between male and female brains. A larger sample size might be necessary to reveal such differences, which would go beyond the scope of the present study.

For right area Op5, functional decoding with MACM revealed an association with chewing/swallowing. This is in agreement to a study of Lowell et al. (2009), where an involvement of the FOp in overt swallowing was revealed. The POp, the supplementary motor area, and several parts of the thalamus also showed activation for the swallowing task in the study, which fits to the co-activations of the right Op5 with the medial geniculate body as well as with areas OP1, OP3, and OP4 in MACM. Further co-activations for right Op5 could be observed with motor areas 4a, 4p, 6ma, 6mp, and Id4. The relationship to motor areas was further confirmed by the analysis of structural connectivity, which was demonstrated for area OP2, motor areas 6d1, 6d2, and parts of the inferior parietal lobule (PF, PFcm, PFm, PFop, and PFt).

For Op6 left as well as for Op5 right, the MACM analysis revealed a functional involvement in studies of isometric force of muscles. A study by Ward and Frackowiak (2003) about age-dependent changes in neural correlates during an isometric hand grip task showed age-varying activations in the FOp. For Op6 left, the MACM analysis showed also correlations with other areas involved in the "grasping circuit" as described by Ward and Frackowiak (2003), including area 44 left as well as areas hIP1 and hIP3 of the intraparietal sulcus. Structural connectivity data affirmed connections of left Op6 to left area 44. Furthermore, it showed structural connections to areas 1 and 4a in combination with parts of area 6 and the IPL, being relevant for motor functions (Caspers et al., 2006, 2008).

For right area Op6, the MACM analysis indicated activation during flexion/extension. In a study in which older participants

had to perform a bimanual flexion/extension task, the FOp was one of the activated areas (Goble et al., 2010). The fact that MACM showed co-activation for Op6 right with areas 6ma, 6mp, OP1, and OP4 fits to activations of motor area and SII region that were additionally mentioned by Goble et al. (2010). In addition to motor area 6 and the POp, by including structural connectivity, connections to the area Id4 and IPL areas were found.

4.3. Specificity of areas Op5-Op7 in music/language versus other functions

The analyses with BrainMap suggested that left area Op6 is involved in music-related functions, which has also been reported for Broca's region (Chiang et al., 2018). Op6, in particular, shows cytoarchitectonic similarities with neighboring area 44: Both are dysgranular, with large pyramidal cells in layers III and V (although a bit smaller in Op6 than in BA 44). Furthermore, both areas showed functional co-activations with each other according to the present MACM. The analysis of the structural connectivity of left Op6 based on the 1000BRAINS study indicated that it is connected with left areas 44 and 45. Similarities in music perception and syntactic processing of language have been discussed (Kunert et al., 2015), and one might argue that Op6 is also involved in both. Similar to connections of Broca's region with the superior temporal gyrus [(Catani et al., 2005; Friederici, 2009, 2011, 2012; Fernández-Miranda et al., 2015), for reviews see Bernal and Ardila (2009) and Bernard et al. (2019)], the connection of Op6 left with left area TE 2.2 of the extended Wernicke's region could indicate a supporting role of Op6 left in the language network.

Although both FOp and Broca's region support music and language functions (e.g., Golestani and Zatorre, 2004; Friederici et al., 2006a; Grodzinsky and Friederici, 2006; Zysset et al., 2007; Ventura-Campos et al., 2013; Chai et al., 2016), left Op6 is also functionally distinct from Broca's region. In terms of syntactic processing, for example, studies by Friederici and colleagues showed that the left FOp is involved in building local phrase structures (noun phrases, verb phrases as well as prepositional phrases), while Broca's region has been shown to support the computation of dependency relation between constituents of a sentence and to play a crucial role in the processing of syntactically complex sentence hierarchies (Grodzinsky, 2000; Friederici et al., 2003, 2006a; Friederici, 2006; Grodzinsky and Friederici, 2006).

Previously reported differences on functional and connectivity-based heterogeneity between the genders regarding phonology (Shaywitz et al., 1995) could not be verified on a microstructural level, neither by the hierarchical cluster analysis nor by the volume analysis. Again, the relatively small sample size in this mapping study represents a limitation for such type of analysis.

Interestingly, the study confirmed an involvement of the identified opercular areas in functional networks different from language and music processing. Area Op5 right was associated with sexual processing based on functional decoding and multiple connections have been found with the POp. This finding may indicate a role of Op5 right in the cortical somatosensory networks. Eickhoff et al. (2006b) discussed that the parietal opercular cortex receives various sensory information and integrates them into an interoceptive perception of the body's condition (Eickhoff et al., 2006b). In addition, areas Op5 and Op6 seem to be part of motor control networks. Functional integration of chewing/swallowing, isometric force of muscles, and flexion/extension was reflected by structural connections of area Op5 right to areas 6d1, 6d2, and 6ma as well as of area Op6 left to areas 6d1 and 6d2. In terms of swallowing, also connections to the POp (areas OP1 OP3, and OP4) were relevant (Lowell et al., 2009). Area Op5 is a (rostral) direct neighbor of the POp, which is associated with somesthesis, while Op6 is a direct (ventral) neighbor of area 44 linked to music and language and area 6 linked to motor functions. Thus, it could be hypothesized that the posterior part of the FOp could also serve a kind of transition zone between these areas.

4.4. Data availability

The new maps of areas Op5, Op6, and Op7 are openly available in different reference spaces (MNI-Colin27 and MNI ICBM 152 reference spaces) and as surface representation. The maps are part of the Julich-Brain Atlas[4] and can be explored using the 3D atlas viewer "siibra-explorer" and other tools of the siibra toolsuite of the EBRAINS research infrastructure (see footnote 2) of the Human Brain Project. They can be downloaded as part of the Julich-Brain 2.9 cytoarchitectonic maps,[5] or as individual datasets [Op5,[6] (Unger et al., 2021a); Op6,[7] (Unger et al., 2021b); Op7,[8] (Unger et al., 2021c)]. Areas Op5-Op7 were also mapped in the BigBrain (brain BC20) (Amunts et al., 2013), and maps are also available in the BigBrain space. For each map, region-specific datasets are linked via the EBRAINS Knowledge Graph[9] and the siibra toolsuite (siibra-explorer hosted at https://atlases.ebrains.eu/viewer; siibra-python client: https://siibra-python.readthedocs.io).

4.5. Conclusion

The present study provided a comprehensive cytoarchitectonic description and maps of the posterior part of the FOp consisting of areas Op5, Op6, and Op7. The areas not only proved to be different in terms of cytoarchitecture, but also showed functional differences, which corresponds to prior receptor studies. Op6 left was shown to play a role in music processing, and a role in the broader language networks could be assumed. While sexual sensations could be assigned to Op5 right, motor connections could be found for Op5 and Op6. Thus, the present study was able to characterize the posterior part of the FOp more

4 https://julich-brain-atlas.de/
5 https://doi.org/10.25493/VSMK-H94
6 https://doi.org/10.25493/KN1A-YX4
7 https://doi.org/10.25493/RQKR-WE4
8 https://doi.org/10.25493/W2D1-DJF
9 https://kg.ebrains.eu/search

precisely, both structurally and functionally. The openly available maps will serve as a tool to decode the function of this region in more detail.

Data availability statement

The datasets presented in this study can be found in online repositories. The names of the repository/repositories and accession number(s) can be found in the article/ **Supplementary material**.

Ethics statement

The studies involving human participants were reviewed and approved by the Ethics Committee of the Medical Faculty of the Heinrich Heine University Düsseldorf (permission #4863). Written informed consent for participation was not required for this study in accordance with the national legislation and the institutional requirements.

Author contributions

NU performed and calculated cytoarchitectonic characterization, statistical border detection of the human FOp areas, and statistics with support by KA, SC, and SB. MH contributed to cytoarchitectonic mapping. KA designed the study and supervised all aspects of the study. NU prepared hierarchical cluster analysis and SB computed it. HM computed the volumetric analysis and NU and SB made the final analyses. HM calculated the probabilistic maps and MPMs. NU estimated the functional characterization and wrote the first draft of the manuscript. SBE, JAC, and TD conducted the MACM analysis and subsequently interpreted by NU. All authors performed the discussion of results, writing, and editing of the manuscript.

Funding

This work had received funding from the European Union's Horizon 2020 Research and Innovation Programme under Grant Agreement Nos. 785907 (HBP SGA2) and 945539 (HBP SGA3).

Acknowledgments

We thank René Hübbers and Ulrich Opfermann-Emmerich for technical assistance. In addition, we also thank Peter Pieperhoff for transformation of the maps of Op5-Op7 from Colin27 space to the ICBM152casym space.

Conflict of interest

The authors declare that the research was conducted in the absence of any commercial or financial relationships that could be construed as a potential conflict of interest.

Publisher's note

All claims expressed in this article are solely those of the authors and do not necessarily represent those of their affiliated organizations, or those of the publisher, the editors and the reviewers. Any product that may be evaluated in this article, or claim that may be made by its manufacturer, is not guaranteed or endorsed by the publisher.

Supplementary material

The Supplementary Material for this article can be found online at: https://www.frontiersin.org/articles/10.3389/fnhum.2023.1087026/full#supplementary-material

References

Amunts, K., and Zilles, K. (2012). Architecture and organizational principles of Broca's region. *Trends Cogn. Sci.* 16, 418–426. doi: 10.1016/j.tics.2012.06.005

Amunts, K., and Zilles, K. (2015). Architectonic mapping of the human brain beyond Brodmann. *Neuron* 88, 1086–1107. doi: 10.1016/j.neuron.2015.12.001

Amunts, K., Lenzen, M., Friederici, A. D., Schleicher, A., Morosan, P., Palomero-Gallagher, N., et al. (2010). Broca's region: Novel organizational principles and multiple receptor mapping. *PLoS Biol.* 8:e1000489. doi: 10.1371/journal.pbio.1000489

Amunts, K., Lepage, C., Borgeat, L., Mohlberg, H., Dickscheid, T., Rousseau, M.-É., et al. (2013). BigBrain: An ultrahigh-resolution 3D human brain model. *Science* 340, 1472–1475. doi: 10.1126/science.1235381

Amunts, K., Mohlberg, H., Bludau, S., and Zilles, K. (2020). Julich-Brain: A 3D probabilistic atlas of the human brain's cytoarchitecture. *Science* 369, 988–992. doi: 10.1126/science.abb4588

Amunts, K., Schleicher, A., and Zilles, K. (2004). Outstanding language competence and cytoarchitecture in Broca's speech region. *Brain Lang.* 89, 346–353. doi: 10.1016/S0093-934X(03)00360-2

Amunts, K., Schleicher, A., Bürgel, U., Mohlberg, H., Uylings, H. B. M., and Zilles, K. (1999). Broca's region revisited: Cytoarchitecture and intersubject variability. *J. Comp. Neurol.* 412, 319–341. doi: 10.1002/(SICI)1096-9861(19990920)412:2<319::AID-CNE10>3.0.CO;2-7

Anwander, A., Tittgemeyer, M., Von Cramon, D. Y., Friederici, A. D., and Knösche, T. R. (2007). Connectivity-based parcellation of Broca's area. *Cereb. Cortex* 17, 816–825. doi: 10.1093/cercor/bhk034

Bernal, B., and Ardila, A. (2009). The role of the arcuate fasciculus in conduction aphasia. *Brain* 132, 2309–2316. doi: 10.1093/brain/awp206

Bernard, F., Zemmoura, I., Ter Minassian, A., Lemée, J.-M., and Menei, P. (2019). Anatomical variability of the arcuate fasciculus: A systematical review. *Surg. Radiol. Anat.* 41, 889–900. doi: 10.1007/s00276-019-02244-5

Binder, J. R. (2017). Current controversies on Wernicke's area and its role in language. *Curr. Neurol. Neurosci. Rep.* 17:58. doi: 10.1007/s11910-017-0764-8

Bludau, S., Eickhoff, S. B., Mohlberg, H., Caspers, S., Laird, A. R., Fox, P. T., et al. (2014). Cytoarchitecture, probability maps and functions of the human frontal pole. *Neuroimage* 93(Pt 2), 260–275. doi: 10.1016/j.neuroimage.2013.05.052

Bohland, J. W., and Guenther, F. H. (2006). An fMRI investigation of syllable sequence production. *Neuroimage* 32, 821–841. doi: 10.1016/j.neuroimage.2006.04.173

Brodmann, K. (1909). *Vergleichende Lokalisationslehre der Großhirnrinde*. Leipzig: Barth.

Brown, S., Martinez, M. J., Hodges, D. A., Fox, P. T., and Parsons, L. M. (2004). The song system of the human brain. *Cogn. Brain Res.* 20, 363–375. doi: 10.1016/j.cogbrainres.2004.03.016

Caspers, J., Zilles, K., Eickhoff, S. B., Schleicher, A., Mohlberg, H., and Amunts, K. (2013). Cytoarchitectonical analysis and probabilistic mapping of two extrastriate areas of the human posterior fusiform gyrus. *Brain Struct. Funct.* 218, 511–526. doi: 10.1007/s00429-012-0411-8

Caspers, S., and Schreiber, J. (2021). *HBP data descriptor: 1000BRAINS study, connectivity data (v1.1)*. Available online at: https://search.kg.ebrains.eu/instances/83407c06-b494-4307-861e-d06a5aecdf8a (accessed July 10, 2022).

Caspers, S., Eickhoff, S. B., Geyer, S., Scheperjans, F., Mohlberg, H., Zilles, K., et al. (2008). The human inferior parietal lobule in stereotaxic space. *Brain Struct. Funct.* 212, 481–495. doi: 10.1007/s00429-008-0195-z

Caspers, S., Geyer, S., Schleicher, A., Mohlberg, H., Amunts, K., and Zilles, K. (2006). The human inferior parietal cortex: Cytoarchitectonic parcellation and interindividual variability. *Neuroimage* 33, 430–448. doi: 10.1016/j.neuroimage.2006.06.054

Caspers, S., Moebus, S., Lux, S., Pundt, N., Schütz, H., Mühleisen, T. W., et al. (2014). Studying variability in human brain aging in a population-based German cohort-rationale and design of 1000BRAINS. *Front. Aging Neurosci.* 6:149. doi: 10.3389/fnagi.2014.00149

Catani, M., Jones, D. K., and Ffytche, D. H. (2005). Perisylvian language networks of the human brain. *Ann. Neurol.* 57, 8–16. doi: 10.1002/ana.20319

Chai, X. J., Berken, J. A., Barbeau, E. B., Soles, J., Callahan, M., Chen, J.-K., et al. (2016). Intrinsic functional connectivity in the adult brain and success in second-language learning. *J. Neurosci.* 36, 755–761. doi: 10.1523/JNEUROSCI.2234-15.2016

Chiang, J. N., Rosenberg, M. H., Bufford, C. A., Stephens, D., Lysy, A., and Monti, M. M. (2018). The language of music: Common neural codes for structured sequences in music and natural language. *Brain Lang.* 185, 30–37. doi: 10.1016/j.bandl.2018.07.003

Chikazoe, J., Lee, D. H., Kriegeskorte, N., and Anderson, A. K. (2019). Distinct representations of basic taste qualities in human gustatory cortex. *Nat. Commun.* 10:1048. doi: 10.1038/s41467-019-08857-z

Choi, H.-J., Zilles, K., Mohlberg, H., Schleicher, A., Fink, G. R., Armstrong, E., et al. (2006). Cytoarchitectonic identification and probabilistic mapping of two distinct areas within the anterior ventral bank of the human intraparietal sulcus. *J. Comp. Neurol.* 495, 53–69. doi: 10.1002/cne.20849

DeWitt, I., and Rauschecker, J. P. (2013). Wernicke's area revisited: Parallel streams and word processing. *Brain Lang.* 127, 181–191. doi: 10.1016/j.bandl.2013.09.014

Eickhoff, S. B., Lotze, M., Wietek, B., Amunts, K., Enck, P., and Zilles, K. (2006b). Segregation of visceral and somatosensory afferents: An fMRI and cytoarchitectonic mapping study. *Neuroimage* 31, 1004–1014. doi: 10.1016/j.neuroimage.2006.01.023

Eickhoff, S. B., Schleicher, A., Zilles, K., and Amunts, K. (2006c). The human parietal operculum. I. Cytoarchitectonic mapping of subdivisions. *Cereb. Cortex* 16, 254–267. doi: 10.1093/cercor/bhi105

Eickhoff, S. B., Amunts, K., Mohlberg, H., and Zilles, K. (2006a). The human parietal operculum. II. Stereotaxic maps and correlation with functional imaging results. *Cereb. Cortex* 16, 268–279. doi: 10.1093/cercor/bhi106

Eickhoff, S. B., Bzdok, D., Laird, A. R., Roski, C., Caspers, S., Zilles, K., et al. (2011). Co-activation patterns distinguish cortical modules, their connectivity and functional differentiation. *Neuroimage* 57, 938–949. doi: 10.1016/j.neuroimage.2011.05.021

Eickhoff, S. B., Nichols, T. E., Laird, A. R., Hoffstaedter, F., Amunts, K., Fox, P. T., et al. (2016). Behavior, sensitivity, and power of activation likelihood estimation characterized by massive empirical simulation. *Neuroimage* 137, 70–85. doi: 10.1016/j.neuroimage.2016.04.072

Eickhoff, S. B., Paus, T., Caspers, S., Grosbras, M.-H., Evans. A. C., Zilles, K., et al. (2007). Assignment of functional activations to probabilistic cytoarchitectonic areas revisited. *Neuroimage* 36, 511–521. doi: 10.1016/j.neuroimage.2007.03.060

Eickhoff, S. B., Stephan, K. E., Mohlberg, H., Grefkes, C., Fink, G. R., Amunts, K., et al. (2005). A new SPM toolbox for combining probabilistic cytoarchitectonic maps and functional imaging data. *Neuroimage* 25, 1325–1335. doi: 10.1016/j.neuroimage.2004.12.034

Evans, A. C., Janke, A. L., Collins, D. L., and Baillet, S. (2012). Brain templates and atlases. *Neuroimage* 62, 911–922. doi: 10.1016/j.neuroimage.2012.01.024

Fedorenko, E., and Blank, I. A. (2020). Broca's area is not a natural kind. *Trends Cogn. Sci.* 24, 270–284. doi: 10.1016/j.tics.2020.01.001

Fernández-Miranda, J. C., Wang, Y., Pathak, S., Stefaneau, L., Verstynen, T., and Yeh, F.-C. (2015). Asymmetry, connectivity, and segmentation of the arcuate fascicle in the human brain. *Brain Struct. Funct.* 220, 1665–1680. doi: 10.1007/s00429-014-0751-7

Fiez, J. A., Tranel, D., Seager-Frerichs, D., and Damasio, H. (2006). Specific reading and phonological processing deficits are associated with damage to the left frontal operculum. *Cortex* 42, 624–643. doi: 10.1016/s0010-9452(08)70399-x

Fox, P. T., and Lancaster, J. L. (2002). Mapping context and content: The BrainMap model. *Nat. Rev. Neurosci.* 3, 319–321. doi: 10.1038/nrn789

Friederici, A. D. (2006). Broca's area and the ventral premotor cortex in language: Functional differentiation and specificity. *Cortex* 42, 472–475. doi: 10.1016/s0010-9452(08)70380-0

Friederici, A. D. (2009). Pathways to language: Fiber tracts in the human brain. *Trends Cogn. Sci.* 13, 175–181. doi: 10.1016/j.tics.2009.01.001

Friederici, A. D. (2011). The brain basis of language processing: From structure to function. *Physiol. Rev.* 91, 1357–1392. doi: 10.1152/physrev.00006.2011

Friederici, A. D. (2012). Language development and the ontogeny of the dorsal pathway. *Front. Evol. Neurosci.* 4:3. doi: 10.3389/fnevo.2012.00003

Friederici, A. D. (2017). *Language in our brain: The origins of a uniquely human capacity*. Cambridge, MA: MIT Press.

Friederici, A. D., Bahlmann, J., Heim, S., Schubotz, R. I., and Anwander, A. (2006a). The brain differentiates human and non-human grammars: Functional localization and structural connectivity. *Proc. Natl. Acad. Sci. U.S.A.* 103, 2458–2463. doi: 10.1073/pnas.0509389103

Friederici, A. D., Fiebach, C. J., Schlesewsky, M., Bornkessel, I. D., and Von Cramon, D. Y. (2006b). Processing linguistic complexity and grammaticality in the left frontal cortex. *Cereb. Cortex* 16, 1709–1717. doi: 10.1093/cercor/bhj106

Friederici, A. D., Opitz, B., and Von Cramon, D. Y. (2000). Segregating semantic and syntactic aspects of processing in the human brain: An fMRI investigation of different word types. *Cereb. Cortex* 10, 698–705. doi: 10.1093/cercor/10.7.698

Friederici, A. D., Rüschemeyer, S.-A., Hahne, A., and Fiebach, C. J. (2003). The role of left inferior frontal and superior temporal cortex in sentence comprehension: Localizing syntactic and semantic processes. *Cereb. Cortex* 13, 170–177. doi: 10.1093/cercor/13.2.170

Georgiadis, J. R., Farrell, M. J., Boessen, R., Denton, D. A., Gavrilescu, M., Kortekaas, R., et al. (2010). Dynamic subcortical blood flow during male sexual activity with ecological validity: A perfusion fMRI study. *Neuroimage* 50, 208–216. doi: 10.1016/j.neuroimage.2009.12.034

Geyer, S., Ledberg, A., Schleicher, A., Kinomura, S., Schormann, T., Bürgel, U., et al. (1996). Two different areas within the primary motor cortex of man. *Nature* 382, 805–807. doi: 10.1038/382805a0

Geyer, S., Schleicher, A., and Zilles, K. (1999). Areas 3a, 3b, and 1 of human primary somatosensory cortex: 1. Microstructural organization and interindividual variability. *Neuroimage* 10, 63–83. doi: 10.1006/nimg.1999.0440

Geyer, S., Schormann, T., Mohlberg, H., and Zilles, K. (2000). Areas 3a, 3b, and 1 of human primary somatosensory cortex: 2. Spatial normalization to standard anatomical space. *Neuroimage* 11, 684–696. doi: 10.1006/nimg.2000.0548

Goble, D. J., Coxon, J. P., Van Impe, A., De Vos, J., Wenderoth, N., and Swinnen, S. P. (2010). The neural control of bimanual movements in the elderly: Brain regions exhibiting age-related increases in activity, frequency-induced neural modulation, and task-specific compensatory recruitment. *Hum. Brain Mapp.* 31, 1281–1295. doi: 10.1002/hbm.20943

Golestani, N., and Zatorre, R. J. (2004). Learning new sounds of speech: Reallocation of neural substrates. *Neuroimage* 21, 494–506. doi: 10.1016/j.neuroimage.2003.09.071

Gratton, C., Sun, H., and Petersen, S. E. (2018). Control networks and hubs. *Psychophysiology* 55:e13032. doi: 10.1111/psyp.13032

Grefkes, C., Geyer, S., Schormann, T., Roland, P., and Zilles, K. (2001). Human somatosensory area 2: Observer-independent cytoarchitectonic mapping, interindividual variability, and population map. *Neuroimage* 14, 617–631. doi: 10.1006/nimg.2001.0858

Grodzinsky, Y. (2000). The neurology of syntax: Language use without Broca's area. *Behav. Brain Sci.* 23, 1–21. doi: 10.1017/s0140525x00002399

Grodzinsky, Y., and Friederici, A. D. (2006). Neuroimaging of syntax and syntactic processing. *Curr. Opin. Neurobiol.* 16, 240–246. doi: 10.1016/j.conb.2006.03.007

Grodzinsky, Y., and Santi, A. (2008). The battle for Broca's region. *Trends Cogn. Sci.* 12, 474–480. doi: 10.1016/j.tics.2008.09.001

Grodzinsky, Y., Deschamps, I., Pieperhoff, P., Iannilli, F., Agmon, G., Loewenstein, Y., et al. (2020). Logical negation mapped onto the brain. *Brain Struct. Funct.* 225, 19–31. doi: 10.1007/s00429-019-01975-w

Hagoort, P. (2014). Nodes and networks in the neural architecture for language: Broca's region and beyond. *Curr. Opin. Neurobiol.* 28, 136–141. doi: 10.1016/j.conb.2014.07.013

Hagoort, P. (2019). The neurobiology of language beyond single-word processing. *Science* 366, 55–58. doi: 10.1126/science.aax0289

Higo, T., Mars, R. B., Boorman, E. D., Buch, E. R., and Rushworth, M. F. S. (2011). Distributed and causal influence of frontal operculum in task control. *Proc. Natl. Acad. Sci. U.S.A.* 108, 4230–4235. doi: 10.1073/pnas.1013361108

Holmes, C. J., Hoge, R., Collins, L., Woods, R., Toga, A. W., and Evans, A. C. (1998). Enhancement of MR images using registration for signal averaging. *J. Comput. Assist. Tomogr.* 22, 324–333. doi: 10.1097/00004728-199803000-00032

Huschler, M. A., Liem, F., Jäncke, L., and Meyer, M. (2013). Right and left perisylvian cortex and left inferior frontal cortex mediate sentence-level rhyme detection in spoken language as revealed by sparse fMRI. *Hum. Brain Mapp.* 34, 3182–3192. doi: 10.1002/hbm.22134

Jung, J., Cloutman, L. L., Binney, R. J., and Lambon Ralph, M. A. (2017). The structural connectivity of higher order association cortices reflects human functional brain networks. *Cortex* 97, 221–239. doi: 10.1016/j.cortex.2016.08.011

Keller, S. S., Crow, T., Foundas, A., Amunts, K., and Roberts, N. (2009). Broca's area: Nomenclature, anatomy, typology and asymmetry. *Brain Lang.* 109, 29–48. doi: 10.1016/j.bandl.2008.11.005

Kiwitz, K., Brandstetter, A., Schiffer, C., Bludau, S., Mohlberg, H., Omidyeganeh, M., et al. (2022). Cytoarchitectonic maps of the human metathalamus in 3D space. *Front. Neuroanat.* 16:837485. doi: 10.3389/fnana.2022.837485

Kunert, R., Willems, R. M., Casasanto, D., Patel, A. D., and Hagoort, P. (2015). Music and language syntax interact in Broca's area: An fMRI study. *PLoS One* 10:e0141069. doi: 10.1371/journal.pone.0141069

Laird, A. R., Eickhoff, S. B., Fox, P. M., Uecker, A. M., Ray, K. L., Saenz, J. J. Jr., et al. (2011). The BrainMap strategy for standardization, sharing, and meta-analysis of neuroimaging data. *BMC Res. Notes* 4:349. doi: 10.1186/1756-0500-4-349

Laird, A. R., Eickhoff, S. B., Kurth, F., Fox, P. M., Uecker, A. M., Turner, J. A., et al. (2009). ALE meta-analysis workflows via the BrainMap database: Progress towards a probabilistic functional brain atlas. *Front. Neuroinform.* 3:23. doi: 10.3389/neuro.11.023.2009

Laird, A. R., Lancaster, J. J., and Fox, P. T. (2005). BrainMap: The social evolution of a human brain mapping database. *Neuroinformatics* 3, 65–77. doi: 10.1385/ni:3:1:065

Levitin, D. J., and Menon, V. (2003). Musical structure is processed in "language" areas of the brain: A possible role for Brodmann Area 47 in temporal coherence. *Neuroimage* 20, 2142–2152. doi: 10.1016/j.neuroimage.2003.08.016

Limb, C. J., Kemeny, S., Ortigoza, E. B., Rouhani, S., and Braun, A. R. (2006). Left hemispheric lateralization of brain activity during passive rhythm perception in musicians. *Anat. Rec. Pt. A Discov. Mol. Cell Evol. Biol.* 288A, 382–389. doi: 10.1002/ar.a.20298

Lorenz, S., Weiner, K. S., Caspers, J., Mohlberg, H., Schleicher, A., Bludau, S., et al. (2017). Two new cytoarchitectonic areas on the human mid-fusiform gyrus. *Cereb. Cortex* 27, 373–385. doi: 10.1093/cercor/bhv225

Lowell, S. Y., Poletto, C. J., Knorr-Chung, B. R., Reynolds, R. C., Simonyan, K., and Ludlow, C. L. (2009). Sensory stimulation activates both motor and sensory components of the swallowing system. *Neuroimage* 42, 285–295. doi: 10.1016/j.neuroimage.2008.04.234

Mahalanobis, P. C., Majumdar, D. N., and Rao, C. R. (1949). Anthropometric survey of the united provinces, 1941: A statistical study. *Sankhyā Indian J. Stat.* 9, 89–324.

Merker, B. (1983). Silver staining of cell bodies by means of physical development. *J. Neurosci. Methods.* 9, 235–241. doi: 10.1016/0165-0270(83)90086-9

Morosan, P., Schleicher, A., Amunts, K., and Zilles, K. (2005). Multimodal architectonic mapping of human superior temporal gyrus. *Anat. Embryol.* 210, 401–406. doi: 10.1007/s00429-005-0029-1

Moulier, V., Mouras, H., Pélégrini-Issac, M., Glutron, D., Rouxel, R., Grandjean, B., et al. (2006). Neuroanatomical correlates of penile erection evoked by photographic stimuli in human males. *Neuroimage* 33, 689–699. doi: 10.1016/j.neuroimage.2006.06.037

Nichols, T., Brett, M., Andersson, J., Wager, T., and Poline, J.-B. (2005). Valid conjunction inference with the minimum statistic. *Neuroimage* 25, 653–660. doi: 10.1016/j.neuroimage.2004.12.005

Novick, J. M., Trueswell, J. C., and Thompson-Schill, S. L. (2005). Cognitive control and parsing: Reexamining the role of Broca's area in sentence comprehension. *Cogn. Affect. Behav. Neurosci.* 5, 263–281. doi: 10.3758/cabn.5.3.263

Öngür, D., Ferry, A. T., and Price, J. L. (2003). Architectonic subdivision of the human orbital and medial prefrontal cortex. *J. Comp. Neurol.* 460, 425–449. doi: 10.1002/cne.10609

Palomero-Gallagher, N., Eickhoff, S. B., Hoffstaedter, F., Schleicher, A., Mohlberg, H., Vogt, B. A., et al. (2015). Functional organization of human subgenual cortical areas: Relationship between architectonical segregation and connectional heterogeneity. *Neuroimage* 115, 177–190. doi: 10.1016/j.neuroimage.2015.04.053

Petrides, M., and Pandya, D. (1994). "Comparative architectonic analysis of the human and the macaque frontal cortex," in *Handbook of neuropsychology*, eds F. Boller and J. Grafman (Amsterdam: Elsevier), 17–58.

Price, C. J., and Friston, K. J. (1997). Cognitive conjunction: A new approach to brain activation experiments. *Neuroimage* 5, 261–270. doi: 10.1006/nimg.1997.0269

Quabs, J., Caspers, S., Bludau, S., Mohlberg, H., and Amunts, K. (2021a). *Probabilistic cytoarchitectonic map of area Id4 (insula) (v5.1) [data set]*. Jülich: EBRAINS. doi: 10.25493/6495-07U

Quabs, J., Caspers, S., Bludau, S., Mohlberg, H., and Amunts, K. (2021b). *Probabilistic cytoarchitectonic map of area Id6 (insula) (v5.1) [data set]*. Jülich: EBRAINS. doi: 10.25493/PVEY-DPX

Quabs, J., Caspers, S., Schöne, C., Mohlberg, H., Bludau, S., Dickscheid, T., et al. (2022). Cytoarchitecture, probability maps and segregation of the human insula. *Neuroimage* 260:119453. doi: 10.1016/j.neuroimage.2022.119453

Quirmbach, F., and Limanowski, J. (2022). A crucial role of the frontal operculum in task-set dependent visuomotor performance monitoring. *eNeuro.* 9, 1–12. doi: 10.1523/eneuro.0524-21.2021

Robinson, J. L., Laird, A. R., Glahn, D. C., Lovallo, W. R., and Fox, P. T. (2010). Metaanalytic connectivity modeling: Delineating the functional connectivity of the human amygdala. *Hum. Brain Mapp.* 31, 173–184. doi: 10.1002/hbm.20854

Ruan, J., Bludau, S., Palomero-Gallagher, N., Caspers, S., Mohlberg, H., Eickhoff, S. B., et al. (2018). Cytoarchitecture, probability maps, and functions of the human supplementary and pre-supplementary motor areas. *Brain Struct. Funct.* 223, 4169–4186. doi: 10.1007/s00429-018-1738-6

Saal, M., Bludau, S., Mohlberg, H., Caspers, S., and Amunts, K. (2021a). *Probabilistic cytoarchitectonic map of area OP8 (frontal operculum) (v6.2) [data set]*. Jülich: EBRAINS. doi: 10.25493/1CTC-2GS

Saal, M., Bludau, S., Mohlberg, H., Caspers, S., and Amunts, K. (2021b). *Probabilistic cytoarchitectonic map of area OP9 (frontal operculum) (v6.2) [data set]*. Jülich: EBRAINS. doi: 10.25493/9TCJ-JZ3

Scheperjans, F., Eickhoff, S. B., Hömke, L., Mohlberg, H., Hermann, K., Amunts, K., et al. (2008a). Probabilistic maps, morphometry, and variability of cytoarchitectonic areas in the human superior parietal cortex. *Cereb. Cortex* 18, 2141–2157. doi: 10.1093/cercor/bhm241

Scheperjans, F., Hermann, K., Eickhoff, S. B., Amunts, K., Schleicher, A., and Zilles, K. (2008b). Observer-independent cytoarchitectonic mapping of the human superior parietal cortex. *Cereb. Cortex* 18, 846–867. doi: 10.1093/cercor/bhm116

Schleicher, A., Amunts, K., Geyer, S., Kowalski, T., Schormann, T., Palomero-Gallagher, N., et al. (2000). A stereological approach to human cortical architecture: Identification and delineation of cortical areas. *J. Chem. Neuroanat.* 20, 31–47. doi: 10.1016/s0891-0618(00)00076-4

Schleicher, A., Amunts, K., Geyer, S., Morosan, P., and Zilles, K. (1999). Observer-independent method for microstructural parcellation of cerebral cortex: A quantitative approach to cytoarchitectonics. *Neuroimage* 9, 165–177. doi: 10.1006/nimg.1998.0385

Schleicher, A., Morosan, P., Amunts, K., and Zilles, K. (2009). Quantitative architectural analysis: A new approach to cortical mapping. *J. Autism Dev. Disord.* 39, 1568–1581. doi: 10.1007/s10803-009-0790-8

Schleicher, A., Palomero-Gallagher, N., Morosan, P., Eickhoff, S. B., Kowalski, T., De Vos, K., et al. (2005). Quantitative architectural analysis: A new approach to cortical mapping. *Anat. Embryol.* 210, 373–386. doi: 10.1007/s00429-005-0028-2

Shaywitz, B. A., Shaywltz, S. E., Pugh, K. R., Constable, R. T., Skudlarski, P., Fulbright, R. K., et al. (1995). Sex differences in the functional organization of the brain for language. *Nature* 373, 607–609. doi: 10.1038/373607a0

Sigl, B., Caspers, S., Bludau, S., Mohlberg, H., Eickhoff, S. B., and Amunts, K. (2021a). *Probabilistic cytoarchitectonic map of area 6d1 (PreCG) (v7.1) [data set]*. Jülich: EBRAINS. doi: 10.25493/KSY8-H3F

Sigl, B., Caspers, S., Bludau, S., Mohlberg, H., Eickhoff, S. B., and Amunts, K. (2021b). *Probabilistic cytoarchitectonic map of area 6d2 (PreCG) (v7.1) [data set]*. Jülich: EBRAINS. doi: 10.25493/WJQ5-HWC

Sigl, B., Caspers, S., Bludau, S., Mohlberg, H., Eickhoff, S. B., and Amunts, K. (2021c). *Probabilistic cytoarchitectonic map of area 6d3 (SFS) (v7.1) [data set]*. Jülich: EBRAINS. doi: 10.25493/D41S-AG7

Skeide, M. A., Brauer, J., and Friederici, A. D. (2016). Brain functional and structural predictors of language performance. *Cereb. Cortex* 26, 2127–2139. doi: 10.1093/cercor/bhv042

Thompson-Schill, S. L., D'Esposito, M., Aguirre, G. K., and Farah, M. J. (1997). Role of left inferior prefrontal cortex in retrieval of semantic knowledge: A reevaluation. *Proc. Natl. Acad. Sci. U.S.A.* 94, 14792–14797. doi: 10.1073/pnas.94.26.14792

Tillmann, B., Janata, P., and Bharucha, J. J. (2003). Activation of the inferior frontal cortex in musical priming. *Cogn. Brain Res.* 16, 145–161. doi: 10.1016/s0926-6410(02)00245-8

Tremblay, P., and Dick, A. S. (2016). Broca and Wernicke are dead, or moving past the classic model of language neurobiology. *Brain Lang.* 162, 60–71. doi: 10.1016/j.bandl.2016.08.004

Unger, N., Bludau, S., Mohlberg, H., Caspers, S., and Amunts, K. (2021a). *Probabilistic cytoarchitectonic map of area OP5 (frontal operculum) (v3.2) [data set]*. Jülich: EBRAINS. doi: 10.25493/KN1A-YX4

Unger, N., Bludau, S., Mohlberg, H., Caspers, S., and Amunts, K. (2021b). *Probabilistic cytoarchitectonic map of area OP6 (frontal operculum) (v3.2) [data set]*. Jülich: EBRAINS. doi: 10.25493/RQKR-WE4

Unger, N., Bludau, S., Mohlberg, H., Caspers, S., and Amunts, K. (2021c). *Probabilistic cytoarchitectonic map of area OP7 (frontal operculum) (v3.2) [data set]*. Jülich: EBRAINS. doi: 10.25493/W2D1-DJF

Veldhuizen, M. G., Albrecht, J., Zelano, C., Boesveldt, S., Breslin, P., and Lundström, J. N. (2011). Identification of human gustatory cortex by activation likelihood estimation. *Hum. Brain Mapp.* 32, 2256–2266. doi: 10.1002/hbm.21188

Ventura-Campos, N., Sanjuán, A., González, J., Palomar-García, M.-Á., Rodríguez-Pujadas, A., Sebastián-Gallés, N., et al. (2013). Spontaneous brain activity predicts learning ability of foreign sounds. *J. Neurosci.* 33, 9295–9305. doi: 10.1523/jneurosci.4655-12.2013

von Economo, C., and Koskinas, G. (1925). *Die Cytoarchitektonik der Hirnrinde des erwachsenen Menschen*. Wien: Springer Verlag.

Ward, J. H. Jr. (1963). Hierarchical grouping to optimize an objective function. *J. Am. Stat. Assoc.* 58, 236–244. doi: 10.1080/01621459.1963.10500845

Ward, N. S., and Frackowiak, R. S. J. (2003). Age-related changes in the neural correlates of motor performance. *Brain* 126, 873–888. doi: 10.1093/brain/awg071

Wree, A., Schleicher, A., and Zilles, K. (1982). Estimation of volume fractions in nervous tissue with an image analyzer. *J. Neurosci. Methods* 6, 29–43. doi: 10.1016/0165-0270(82)90014-0

Zilles, K., and Amunts, K. (2018). Cytoarchitectonic and receptorarchitectonic organization in Broca's region and surrounding cortex. *Curr. Opin. Behav. Sci.* 21, 93–105. doi: 10.1016/j.cobeha.2018.02.011

Zysset, S., Schroeter, M. L., Neumann, J., and Von Cramon, D. Y. (2007). Stroop interference, hemodynamic response and aging: An event-related fMRI study. *Neurobiol. Aging* 28, 937–946. doi: 10.1016/j.neurobiolaging.2006.05.008

2.2 Schiffer, C., Spitzer, H., Kiwitz, K., Unger, N., Wagstyl, K., Evans, A. C., Harmeling, S., Amunts, K., & Dickscheid, T. (2021). Convolutional neural networks for cytoarchitectonic brain mapping at large scale. ***NeuroImage, 240,*** **118327. https://doi.org/10.1016/j.neuroimage.2021.118327**

NeuroImage 240 (2021) 118327

Contents lists available at ScienceDirect

NeuroImage

journal homepage: www.elsevier.com/locate/neuroimage

Convolutional neural networks for cytoarchitectonic brain mapping at large scale

Christian Schiffer[a,b,*], Hannah Spitzer[c], Kai Kiwitz[d], Nina Unger[d], Konrad Wagstyl[e], Alan C. Evans[f], Stefan Harmeling[g], Katrin Amunts[a,d], Timo Dickscheid[a,b]

[a] Institute of Neuroscience and Medicine (INM-1), Research Centre Jülich, Germany
[b] Helmholtz AI, Research Centre Jülich, Germany
[c] Institute of Computational Biology, Helmholtz Zentrum München, Germany
[d] Cécile & Oscar Vogt Institute for Brain Research, University Hospital Düsseldorf, Heinrich-Heine-University Düsseldorf, Germany
[e] Wellcome Centre for Human Neuroimaging, University College London, London, United Kingdom
[f] Department of Neurology & Neurosurgery, Montréal Neurological Institute (MNI), McGill University, Montréal, Canada
[g] Institute of Computer Science, Heinrich-Heine-University Düsseldorf, Germany

ARTICLE INFO

Keywords:
Cytoarchitecture
Deep learning
Segmentation
Histology
Human brain
Brain mapping
Cortex

ABSTRACT

Human brain atlases provide spatial reference systems for data characterizing brain organization at different levels, coming from different brains. Cytoarchitecture is a basic principle of the microstructural organization of the brain, as regional differences in the arrangement and composition of neuronal cells are indicators of changes in connectivity and function. Automated scanning procedures and observer-independent methods are prerequisites to reliably identify cytoarchitectonic areas, and to achieve reproducible models of brain segregation. Time becomes a key factor when moving from the analysis of single regions of interest towards high-throughput scanning of large series of whole-brain sections. Here we present a new workflow for mapping cytoarchitectonic areas in large series of cell-body stained histological sections of human postmortem brains. It is based on a Deep Convolutional Neural Network (CNN), which is trained on a pair of section images with annotations, with a large number of un-annotated sections in between. The model learns to create all missing annotations in between with high accuracy, and faster than our previous workflow based on observer-independent mapping. The new workflow does not require preceding 3D-reconstruction of sections, and is robust against histological artefacts. It processes large data sets with sizes in the order of multiple Terabytes efficiently. The workflow was integrated into a web interface, to allow access without expertise in deep learning and batch computing. Applying deep neural networks for cytoarchitectonic mapping opens new perspectives to enable high-resolution models of brain areas, introducing CNNs to identify borders of brain areas.

1. Introduction

Human brain atlases provide a spatial framework for localizing information retrieved from neuroscientific studies of different brains, addressing brain organization from different angles and including different data modalities. The cerebral cortex of the brain is organized into cortical areas, which each have a specific functional role. They can be identified in cell body stained sections based on cytoarchitecture. Regional differences in the spatial arrangement and composition of the cells covary with changes in connectivity and function Goulas et al. (2018). Cytoarchitectonic borders can be identified in microscopic scans of histological brain sections, based on the analysis of the arrangement and distribution of cells, their different morphology and size, as well as differences in the appearance and relative thickness of cortical layers. Such criteria have been formulated for the first time more than a century ago to map the cerebral cortex, and still serve as guidelines for cytoarchitectonic analysis Amunts and Zilles (2015). Different approaches have been proposed in the past to identify positions of borders in a reliable manner Annese et al. (2004); Schleicher et al. (1999); Schmitt and Böhme (2002). The de-facto standard for identifying borders of cytoarchitectonic areas in the human cerebral cortex is a method based on multivariate statistical image analysis Schleicher et al. (1999), which has been applied for the identification of more than 200 areas to date Amunts et al. (2020). To map the whole extent of an area in both hemispheres, and to capture its intersubject variability through studies in large samples, however, is extremely time- and labor-intensive: Cytoarchitectonic maps need to aggregate properties across many histological sections and multiple brains. To address this challenge, mapping

* Corresponding author at: Institute of Neuroscience and Medicine (INM-1), Research Centre Jülich, Jülich, Germany.
E-mail address: c.schiffer@fz-juelich.de (C. Schiffer).

https://doi.org/10.1016/j.neuroimage.2021.118327.
Received 25 November 2020; Received in revised form 5 May 2021; Accepted 30 June 2021
Available online 2 July 2021.

includes a subset of histological sections (every 15–60ths section, i.e. 0.3 mm to 1.2 mm distance between sections) of ten human postmortem brains resulting in analyses of several hundred sections per area, which corresponds to a workload in the order of one or even several person years per area Amunts et al. (2020).

Recent high-throughput scanning devices and powerful compute resources enable a much higher degree of automation in digitalization and analysis of whole human brain sections at microscopical resolution. Technological progress has made it possible to 3D-reconstruct a complete postmortem brain at 20 micron spatial resolution with more than 7000 sections - the BigBrain Amunts et al. (2013). This high-resolution brain model opens the possibility to produce complete maps of cytoarchitectonic areas at full microscopic resolution, and to cover large image stacks with brain areas extending across thousands of sections. Hereby, each section image has up to 120,000 × 80,000 pixels image size each. In order to address these challenges, a method is required, which

1. automatically classifies brain areas based on cytoarchitectonic criteria,
2. handles series with thousands of 2D images of histological sections with data in the Giga- to Terabyte range,
3. is robust against histological artefacts, which are inevitable in large section series,
4. provides stable results independently of the cutting plane, e.g. when changes in the cutting direction relative to the brain tissue prevents analysis of the 6-layered structure of the cerebral cortex (in the following referred to as *oblique cuts*), and
5. can be operated and supervised by neuroscience experts without requiring advanced computer science skills.

Previous experience in cytoarchitectonic mapping has shown that the identification of brain areas considers multiple parameters. This is true for traditional visual inspection using a light microscope, as well as for automated mapping approaches. It involves complex multi-scale texture patterns, from the level of neurons up to a level of cortical layers and areas. However, several parameters that can be used for identification of cortical areas heavily depend on the cutting plane of the histological sections with respect to the orientation of cortical columns. The highly folded cerebral cortex of the human brain hereby poses particular challenges, since brain areas may appear in a very different way in dependence on the cutting angle. Thus, brain mapping needs to operate in a variable data space, where no restrictions should be made on the orientation of the cutting plane relative to the course of cortical layers and the brain surface. In addition, automated brain mapping needs to consider variation in tissue quality and staining, as well as histological artefacts. Finally, automated mapping methods must take into account variations in cytoarchitecture between different brains and lead to identical parcellations, even if interindividual differences in cytoarchitecture are large.

Previous work on automated cytoarchitectonic area segmentation (Spitzer et al., 2017; 2018) proposes to use Convolutional Neural Networkss (CNNss) for automatic segmentation of multiple cytoarchitectonic areas across multiple human brains. This is a remarkably challenging task, as the model needs to be robust against the considerable interindividual variability of the human brain, inevitable histological artefacts, variations in staining, and oblique cuts, to name only a few of the constraints. At the same time, it has to be highly sensitive to variations of cytoarchitecture in different brain areas, which may be subtle. This may result in a need for large amounts of training data, which is difficult to cover. Consequently, such generalized segmentation models are still subject to active research.

We here propose a new workflow for cytoarchitectonic mapping of a *target area* across large or complete series of histological human brain sections with a high degree of automation. The workflow is illustrated in Fig. 1. Following a "divide & conquer" approach, the full extent of a target brain area *a* is subdivided into intervals of sections, which are enclosed by annotations created at approximately regular section intervals. Separate CNNss are then trained for each interval, using the enclosing annotations as training data. This results in a set of *local segmentation models*, each specialized to automatically map only the tissue sections which fall into the corresponding interval. By training local models for each interval of target area *a*, an interactive workflow is obtained that allows an expert to label cytoarchitectonic areas in full stacks of histological sections with minimal manual annotation, aided by Deep Learning, and at a speed that matches high throughput image acquisition.

In this work, we

1. introduce a method to automatically map cytoarchitectonic brain areas across large series of histological human brain sections (Section 2),
2. evaluate its precision on 18 cytoarchitectonic areas from the BigBrain dataset Amunts et al. (2013) to investigate its applicability to a wide range of different brain areas,
3. assess its precision for two areas in three brains with variable staining protocols Amunts et al. (2013, 2000); Ding et al. (2016) to investigate robustness against interindividual differences and different staining procedures, and
4. create highly detailed and complete 3D maps of four areas in the BigBrain dataset[1] and evaluate their anatomical plausibility.[2]

2. Materials and methods

2.1. GLI-based mapping of cytoarchitectonic areas for training and validation

Our proposed method requires annotations of the target area at roughly regular intervals in approximately 1% of sections in the stack. Such annotations consist of localizations of areal borders in the section, and are defined using the well-established GLI-based mapping procedure described in Schleicher et al. (1999). This approach starts by scanning the histological images and by building a Gray Level Index (GLI) image Schleicher et al. (1999). The GLI is a measure of the volume fraction of cell bodies Wree et al. (1982). In a next step, profiles extending from the cortical surface to the white matter border are extracted along Laplacians, which reflect laminar changes in the volume fraction of cell bodies, and thus encode cytoarchitecture. These Laplacians reflect an important feature of cortical cytoarchitecture, i.e. its columnar structure Schleicher et al. (2000). The cortical surface and the white matter border are manually identified. Using a sliding window procedure across the cortical ribbon, the similarity of blocks of profiles is being estimated by the Mahalanobis distance, a multi-variate distance measure, at each position, that is combined with a Hotelling's *t*-test for checking significance. Borders between areas are indicated by significant peaks in the Mahalanobis distance function. The positions of borders are then labeled in the image. These borders are then used as a basis for the network training and validation.

2.2. Datasets

The datasets used in this study comprise image series of histological sections of three human brains, which have been stained for neuronal cell bodies Amunts et al. (2020); Ding et al. (2016). The brains vary in terms of cytoarchitecture and folding pattern, as well as staining properties, presence of histological artifacts and other features (Fig. 2). Areas have been mapped in the past (cf. Section 2.1) using at least every 60th section of the series. These maps provide the basis to train the neural network models and to perform automatic segmentation in previously unseen, close by sections.

[1] https://www.bigbrainproject.org

[2] The maps are released in the public domain as part of the multilevel human brain atlas in the EBRAINS platformhttps://www.ebrains.eu

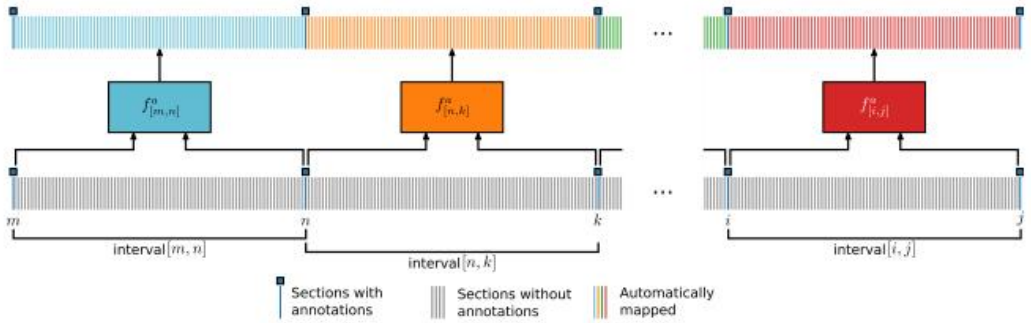

Fig. 1. Setup of our workflow. Images of histological sections are depicted as thin vertical bars, neural network models are depicted as colored boxes. The full extent of sections containing a target brain area a (sections m to j, bottom row) is subdivided into section intervals, which are defined by annotations at regular intervals (blue squares, $m, n, k, \ldots$). One local segmentation model $f^a_{[m,n]}$ is trained for each interval enclosed by a pair of annotations $[m, n]$. After training, each model is applied to automatically map sections falling into the corresponding interval. (For interpretation of the references to color in this figure legend, the reader is referred to the web version of this article.)

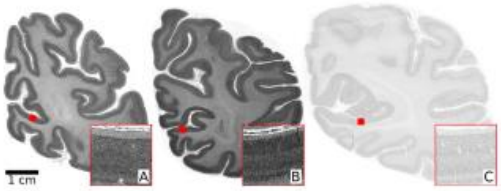

Fig. 2. Example images of cell body stained histological human brain sections taken from datasets B20(A), B01(B) and AAHB (C). All sections were sampled from a comparable region of the occipital lobe. Differences arise from intersubject variability and variations in staining and histological processing protocols. Locations of detail views (2 mm × 2 mm) are marked with red squares. For B20and B01, only the right hemisphere is shown. AAHB only includes a single hemisphere. Cerebellum was removed from B20and AAHB for visualization. Scale bar: 1cm (same for all three sections). (For interpretation of the references to color in this figure legend, the reader is referred to the web version of this article.)

The first dataset - denoted as B20- is based on the original histological sections of the publicly available microscopic 3D model BigBrain (Amunts et al., 2013). The dataset consists of images of 7404 coronal sections with a thickness of 20 µm. A modified Merker stain Merker (1983) was used to stain cell bodies. A subset of sections was scanned at 1 µm resolution using a high-throughput light-microscopic scanner (TissueScope HS, Huron Digital Pathology Inc.). Annotations based on the GLI-based method (Section 2.1) at an interval of approximately 60 sections (≈ 1.2 mm) were obtained for 18 cortical areas, belonging to different functional systems:

1. Visual areas $hOc1$, $hOc2$ (Amunts et al., 2000), $hOc3v$ (Rottschy et al., 2007) and $hOc5$ (Malikovic et al., 2007). Additional annotations at an interval of approximately 30 (0.6 mm) sections were created for $hOc5$, as well as on a small set of sections containing $hOc3v$ (Kiwitz et al., 2019a; 2019b; 2020a; 2020b).
2. Areas of the frontal operculum $Op5$, $Op6$ and $Op7$ Unger et al. (2020a, 2020b, 2020c).
3. Areas 44 and 45 of Broca's region (Amunts et al., 1999; 2004) in the inferior frontal gyrus.
4. Areas $hIP5$, $hIP6$, $hIP7$ and $hIP8$ (Richter et al., 2019) in the intraparietal sulcus.
5. Supplementary motor area SMA and pre-supplementary motor area $preSMA$ Ruan et al. (2018).
6. Premotor areas $6d1$, $6d2$ and $6d3$ Sigl (2018); Sigl et al. (2019a, 2019b, 2019c).

The BigBrain dataset has been fully reconstructed at 20 µm Amunts et al. (2013) and therefore opens the possibility to investigate the 3D consistency of the computed maps after transformation into the reconstructed space.

Brain areas differ in cytoarchitecture, as well as in size and in how much the morphology of an area changes across a series of consecutive brain sections. This has implications for the amount of annotations required to capture the relevant properties of certain areas. For example, $hOc1$ is large and shows only moderate changes across consecutive sections. In comparison, $hOc5$ is considerably smaller, and $hOc3v$ changes considerably across consecutive sections (see Fig. 10, C-F), resulting in a need for more annotations to capture their structure.

The second dataset - B01- has also been used for mapping in the past, whereby every 15th section of the whole series of sections was stained and digitized. This brain was 3D reconstructed with a spatial resolution of 1 mm isotropic Amunts et al. (2020). Annotations for visual areas $hOc1$ and $hOc2$ at an interval of approximately every 60th section (Amunts et al., 2000) in a subset of sections have been used. This dataset serves to investigate robustness against intersubject variability, while the lab protocol is similar to the one used for B20.

The third dataset - AAHB-, comes from the *Allen Adult Human Brain Atlas* Ding et al. (2016). It includes 106 unevenly spaced, publicly available sections. In contrast to the first two series of images, it differs in thickness (50 µm), and the staining method (Nissl staining). Annotations are provided for cortical and subcortical gray matter according to a modified Brodmann scheme on one hemisphere (cf. (Ding et al., 2016)). This dataset is used to investigate robustness of the proposed method against variable lab protocols and delineation criteria with respect to areas $hOc1$ and $hOc2$, which correspond to *"primary visual cortex (striate cortex, area V1/17)"* (identifier 10269) and *"parastriate cortex (area V2, area 18)"* (identifier 10271), respectively, in the Allen ontology.

2.3. Local segmentation models

Annotations of cytoarchitectonic areas based on GLI mapping (Section 2.1) were used to train CNNss, which we refer to as *local segmentation models*. Each local segmentation model $f^a_{[s_1,s_2]}$ was trained on two sections s_1 and s_2 (the *training sections*) with available annotations for a target area a. Trained local segmentation models were then applied

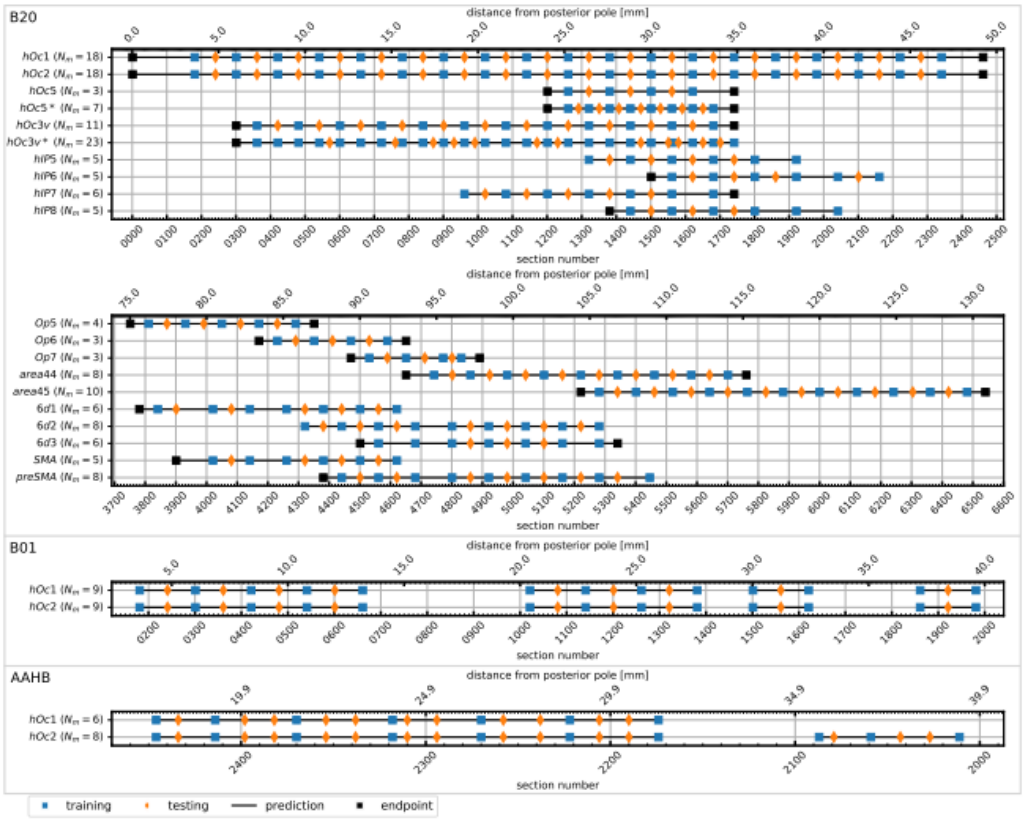

Fig. 3. Training and test sections from available annotations across stacks of histological sections. Consecutive pairs of training sections (blue squares) induce one local segmentation model. For example, model $f^{B20-hOc1}_{[181,301]}$ was trained on sections 181 and 301 of dataset B20, segments area $hOc1$ in the full interval $[182, 300]$, and was tested on Section 2.1. N_m denotes the number of trained local segmentation models. $*$ marks experiments performed with a smaller training interval. (For interpretation of the references to color in this figure legend, the reader is referred to the web version of this article.)

to "fill the gaps", i.e. to automatically segment the target area in sections enclosed by the respective training sections s_1 and s_2 (Fig. 1). The focus on a single target area and a spatially restricted stack of consecutive sections reduces cytoarchitectonic and morphological variations that need to be captured by the respective models, which we expect to result in improved performance compared to training models for multiple areas or a wider range of sections as proposed in Spitzer et al. (2017).

We trained local segmentation models for 18 cytoarchitectonic areas in B20and two areas in each of B01and AAHB. Fig. 3 gives an overview of sections used for the individual areas. Most local segmentation models were trained on two training sections with annotations at ~ 2.4 mm distance, corresponding to ~ 120 sections for B20 and B01 and 48 sections for AAHB. Additional local segmentation models with a reduced interval size of 60 sections (1.2 mm) were trained for areas $hOc3v$ and $hOc5$ to account for highly variable morphology ($hOc3v$, see Fig. 10, C-F) and small area size ($hOc5$). For B01and AAHB, local segmentation models were trained only for ranges of sections where annotations were available at the required interval. Segmentations of the outer most parts of cytoarchitectonic areas which were not enclosed by training sections (i.e. Sections 1 to 181 for $hOc1$ in B20) were processed using the closest available local segmentation model. For example, model $f^{B20-hOc1}_{[181,301]}$ was also applied to the section interval $[1, 181]$.

2.4. Neural network architecture

For local segmentation models, the modified U-Net architecture (Ronneberger et al., 2015) proposed by Spitzer et al. (2017) was extended into a multi-scale neural network model (Fig. 5, C). U-Nets have proven to be very powerful for many applications in biomedical image segmentation (e.g. (Çiçek et al., 2016; Milletari et al., 2016)). They consist of an encoder and decoder branch, which are linked by skip-connections between layers of corresponding spatial resolution to allow recovery of fine-grained details during upsampling. Compared to the U-Net (Ronneberger et al., 2015), the modified architecture (Spitzer et al., 2017) employs additional encoder layers and a different number of filters to make processing of large image patches computationally tractable. To show the benefit of using a multi-scale variant of U-Nets, three network variants were used: A high-resolution encoder network (HR), a low-resolution network (LR), and a combined multi-scale architecture (MS).

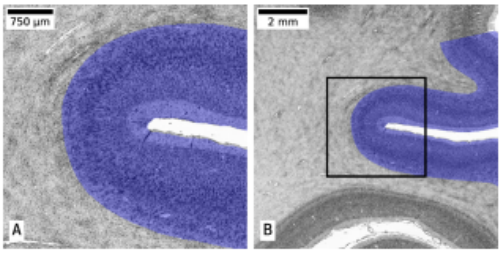

Fig. 4. Typical input patches for the proposed MSarchitecture. A high-resolution image patch (A, 2 µm per pixel) resolves fine-grained microstructural texture, while a lower resolution image patch (B, 16 µm per pixel) provides more information on macroanatomical context. The black rectangle indicates the position of patch (A) inside patch (B). Expert annotations of area *hOc2* are overlayed in blue. (For interpretation of the references to color in this figure legend, the reader is referred to the web version of this article.)

High-resolution encoder architecture (HR *)*

The architecture proposed in Spitzer et al. (2017) was used as base architecture (Fig. 5, A). A *high-resolution encoder* E_{HR} receives high-resolution input patches with a size of 2025×2025 pixels at 2 µm pixel resolution ($4.05 \times 4.05\,\mathrm{mm}^2$, Fig. 4, A) and enables recognition of fine-grained microstructural textures. It consists of six convolutional blocks, with the number of filters set to $\{16, 32, 64, 64, 128, 128\}$ respectively. All but the last block are followed by a max-pooling operation with pool size 2 and stride 2. The first layer of the first block in E_{HR} uses a filter size of 5 and a stride of 4, which increases the receptive field while keeping memory consumption and computational effort tangible. All remaining convolutional layers of E_{HR} use a kernel size of 3 and stride 1. Following (Spitzer et al., 2018), we initialize E_{HR} from a network that has been pre-trained on a self-supervised task, specifically on predicting the geodesic distance along the brain surface between image patches from the BigBrain dataset. This auxiliary task has been shown to promote extraction of distinctive cytoarchitectonic features. The decoder consists of four convolutional blocks with the number of filters set to $\{128, 64, 64, 32\}$ respectively. Each block is preceded by an upsampling block, which consists of a nearest neighbor upsampling with kernel size 2 and stride 2, followed by a zero-padded convolutional layer with kernel size 2 and stride 1. All convolutional operations in the network are followed by batch normalization Ioffe and Szegedy (2015) and Rectified Linear Unit (ReLU) non-linearity.

Multi-scale network architecture (MS *)*

The multi-scale network architecture was obtained by attaching a *low-resolution encoder* E_{LR} as a second branch to HR, which receives lower resolution image patches with a size of 682×682 pixels at 16 µm pixel resolution ($10.912 \times 10.912\,\mathrm{mm}^2$), centered at the same location as E_{HR} patches (Fig. 4). This branch allows to learn features at the scale of local cortical folding patterns. Although such macroscopic features are not generally representative of cytoarchitecture in human brains, as they vary largely between individuals (Amunts and Zilles, 2015), they are appropriate in the present setting due to the locality of the network models. E_{LR} is based on E_{HR}, and composed of six convolutional blocks with the same number of filters as E_{HR}. All convolutional filters use a filter size of 3 and a stride of 1. Convolutional layers in the first block use a dilation rate of 1, while all other convolutional layers within E_{LR} use a dilation rate of 2 to enlarge the receptive field.

Low-resolution encoder architecture (LR *)*

The third architecture is based on HR, but replaces the encoder E_{HR} with E_{LR} (Fig. 5, B). By design, this model can only recognize macroscopic tissue features, and no detailed cytoarchitectonic properties at the level of cell bodies.

2.5. Training strategy

Stochastic gradient descent with Nesterov momentum (Sutskever et al., 2013) was used as optimizer for training the neural network models. Training was performed for 3000 iterations. The learning rate was initially set to 0.01 and decreased by a factor of 0.5 after 1000, 1400, 1800, 2200 and 2600 iterations. Momentum was set to 0.9. Categorical cross-entropy with a weight decay of 0.0001 was used as loss function.

Background class labels

Spitzer et al. (2017) reported convergence problems when training models with a single background class that includes both white and gray matter components, resulting in a mix of tissue parts with very high and very low similarity to the target area under the same classification label. Thus, the general background class was split into separate labels for gray matter (cor) and white matter (wm), resulting in a semantic segmentation problem with the four classes bg, wm, cor, and the target area a. For splitting the background class into wm and cor, different strategies were used for each dataset:

1. For B20, a volumetric tissue classification presented in Lewis et al. (2014) was projected onto the 2D histological sections using transformations provided by the authors of Amunts et al. (2013).
2. For B01, the gray white matter segmentation described in Spitzer et al. (2017) was used.
3. For AAHB, the respective delineations available from the Allen ontology Ding et al. (2016) were used.

Patchwise training

The full resolution scans of the whole-brain sections are by far too large to be used for training. Thus, a patchwise training procedure as also proposed in Ronneberger et al. (2015), Spitzer et al. (2017, 2018) was employed. However, due to the locality of local segmentation models, patches were sampled only in the direct proximity of the target brain area a, to effectively teach the models to distinguish a from its immediate surroundings. Only pixels with a distance of 5 mm or less to any pixel annotated as a were considered as potential center points for training patches.

Data augmentation

The following data augmentations were employed to simulate most frequently observed variations in the data: Both at test and training time, images were rotated by multiples of 90 degrees so that the y axis of coronal sections matches approximately the cranial direction. Random rotation by an angle sampled from a uniform distribution with support $[-45, 45]$ were applied to account for small differences in rotation angle. Intensity variations were addressed by random pixel intensity augmentation with the function $f(x) = \alpha x^{\gamma} + \beta$. The same intensity transformation is applied to all pixels of a training patch. Parameters were chosen from uniform distributions with $\alpha \sim U[0.9, 1.1]$, $\beta \sim U[-0.2, +0.2]$ and $\gamma \sim U[0.8, 1.214]$. The range of each parameter was empirically chosen to reflect natural variations occurring in the data.

Implementation

Training was performed on the supercomputer *JURECA*[3] at the Jülich Supercomputing Centre at Research Centre Jülich (JSC) Krause and Thörnig (2018). Each compute node was equipped with four NVidia K80 GPUs with 12 Gigabyte of VRAM, 2 Intel Xeon E5-2680 v3 Haswell CPUs (12 2.5 GHz cores with hyperthreading each) and 128 Gigabyte of RAM (Krause and Thörnig, 2018). Training of one model occupied one GPU node, using all 4 GPUs and all 48 threads. Of the available 48 threads, 4 were assigned to one GPU each to coordinate the training process, while the remaining 44 threads read training patches from disk in a streaming fashion, applied data

[3] https://www.fz-juelich.de/ias/jsc/EN/Expertise/Supercomputers/JURECA/JURECA_node.html

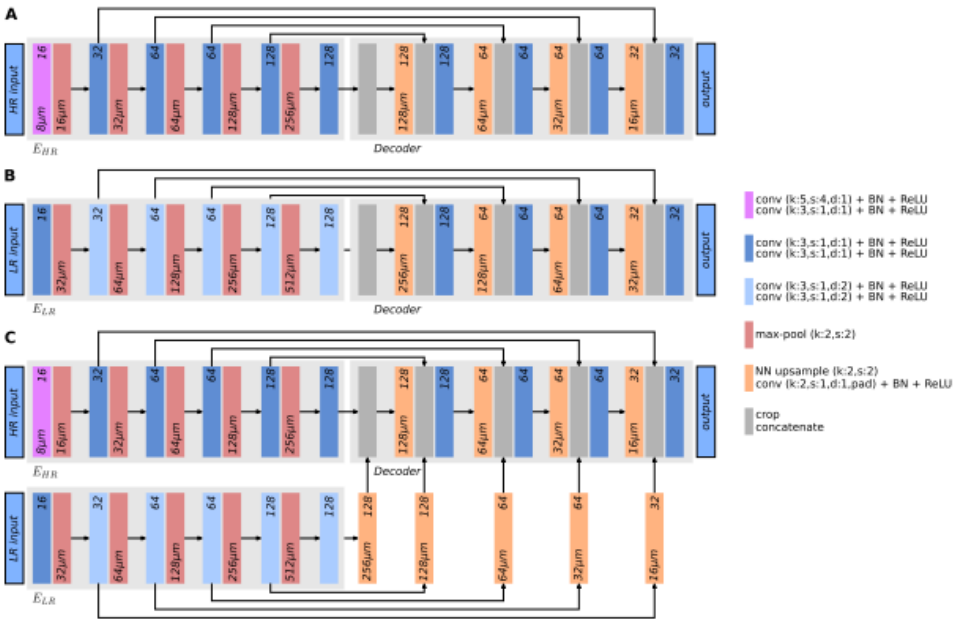

Fig. 5. Illustration of investigated neural network architectures. *A:* High-resolution architecture (HR) from (Spitzer et al., 2017), which can capture fine-grained microstructural textures. *B:* Low-resolution architecture (LR), which can capture macroscopic tissue features. *C:* Proposed multi-scale architecture (MS) to capture both fine and coarse grained tissue features. E_{HR} is pre-initialized with weights of the self-supervised network proposed in Spitzer et al. (2018). Numbers at the top of each block denote the number of filters used in the convolutional layers of this block. Numbers at the bottom denote the physical output spacing in µm per pixel for layers which change the physical spacing of the features.

augmentation and sent data to the training threads. Inter-process communication was implemented based on Message Passing Interface (MPI) using *mpi4py* (Dalcin et al., 2011). Training was implemented using *TensorFlow* (Abadi et al., 2016). Distributed training was performed using *Horovod* (Sergeev and Del Balso, 2018) and synchronous distributed stochastic gradient descent. Batch size was set to 16 image patches per GPU, resulting in a total effective batch size of 64 patches per iteration. The linear learning rate scaling rule for distributed training proposed in Goyal et al. (2017) was employed, scaling the learning rate by the number of GPUs.[4] Batch normalization statistics were computed independently for each GPU and not averaged during training. Software code is publicly available [5].

2.6. Web-based interactive workflow for efficient cytoarchitectonic mapping

The proposed workflow was implemented as an interactive web application (Fig. 6) to provide direct user control over the segmentation workflow through a web browser.[6] The application allows entering annotations in a sparse set of reference sections, controlling the training workflow on a remote cluster, and efficiently inspecting predicted segmentations in the complete stack of histological sections. It does not require in-depth expertise in Deep Learning and/or batch computations.

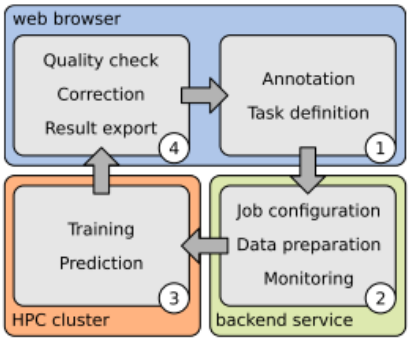

Fig. 6. Overview of the mapping workflow. The user starts by creating annotations (*1*) of a brain area *a* using the web-based annotation tool *microdraw*, and defines training tasks by specifying which annotations should be used to train local segmentation models (Section 2.5). Annotations and task definitions are then submitted to a backend web service (*2*) which prepares the data for training and submits a job to a HPC cluster. Training and subsequent prediction are performed on the HPC system (*3*). Obtained results can be viewed directly in *microdraw* for quality control (*4*). The user may decide to export results of sufficient quality for subsequent processing steps (e.g. 3D reconstruction), manually refine the predictions directly in *microdraw*, or repeat the workflow with additional annotations to improve performance.

[4] Since we use a relatively small number of employed GPUs however, we do not apply the initial learning rate warm up phase described in Goyal et al. (2017).

[5] Code available at https://jugit.fz-juelich.de/c.schiffer/atlas

[6] Code available at https://jugit.fz-juelich.de/c.schiffer/atlasui

Technically, it is designed as an extension of the web based annotation tool *microdraw* [7], combined with a novel backend service that controls data exchange and job supervision on an ssh-accessible compute cluster. We used the workflow on the JURECA supercomputer at the Jülich Supercomputing Center (JSC). It uses common and freely available software components, and is portable to other sites, potentially requiring site-specific adjustments to account for differences in the software stack, scheduling system and data access.

The workflow typically iterates through the following steps:

1. The user enters annotations for a target brain area a in two tissue sections s_1 and s_2, enclosing a local stack interval of ≈ 100 sections using *microdraw*, and this way defines a local segmentation model $f^a_{[s_1,s_2]}$ (Section 2.3).
2. A training task for the local segmentation model is submitted as a job to a GPU cluster at the push of a button, using default parameters (Section 2.5). It does not require any further configuration. Training typically takes 70 min on one compute node of the JURECA supercomputer. Multiple jobs can be submitted in parallel, if the cluster allows.
3. After training, predictions for all sections in the interval are automatically generated. For a large area like $hOc1$, this takes approximately 30 min for 120 sections. Computed segmentations are automatically displayed in the web frontend once they become available. Data synchronization between the web server and compute nodes is handled by the backend service.
4. After inspecting the segmentation quality, the user can choose to enter additional training data, either reducing the size of the current interval or initiating the next interval in the stack.

2.7. Validation framework and strategy

Additional sections with annotations in between the training sections were used for validating performance of local segmentation models on sections that were not seen during training (orange diamonds in Fig. 1). Segmentations of these test sections were quantitatively evaluated using the F1 score (also known as Dice score or Sørensen-Dice index), computed as the harmonic mean of precision of recall. Auxiliary labels added to ensure convergence (Section 2.5) were excluded from F1 score calculation, as the focus lies on segmentation performance for target area a.

Similar to the proximity sampling strategy employed for training (Section 2.5), segmentations on sections not seen during training were only created and evaluated in the approximate region containing a on the respective sections. These approximate regions were determined by projection of the closest reference annotations for a to the image in question using conventional linear image registration based on robust image features as in Dickscheid et al. (2019).

The benefit of a multi-scale architecture was investigated by training separate local segmentation models with neural network architectures HR, LR and MS for all areas in B20. For HRand MS, the high-resolution encoder E_{HR} was initialized with the weights of the network from Spitzer et al. (2018). Furthermore, the performance of multiple local segmentation models, each trained on a local subset of sections as described in Section 2.3, was compared to the performance of one single model trained on all annotations available for a target area a in the following way: For each target area in the B20 dataset, one model was trained using the union of all training sections of the local segmentation models (blue squares in Fig. 1), using the same training strategy as for local segmentation models. We conducted these experiments using HR, LR and MS architectures, and denote models trained on the whole stack as HR (ALL), LR (ALL)and MS (ALL), respectively, again pre-initializing the high-resolution encoder E_{HR} with weights from Spitzer et al. (2018)

[7] http://microdraw.pasteur.fr

The robustness of the proposed method against intersubject variability in brain structure and differences in staining protocols was investigated by training local segmentations models (with MS architecture) for areas $hOc1$ and $hOc2$ in datasets B01 and AAHB. To better understand the roles of the low and high-resolution branches (E_{LR} and E_{HR}) in the MSarchitecture, an experiment similar to occlusion sensitivity analysis (Zeiler and Fergus, 2014) was performed: Using model $f^{hOc2}_{[901,1021]}$ which implements the MSarchitecture, we investigated how predictions change when we set the input patch for either E_{LR} or E_{HR} to zero, effectively preventing information extraction using the respective branch.

2.8. Generating high-resolution 3D cytoarchitectonic maps in the BigBrain dataset

Non-linear transformations described in Amunts et al. (2013); Omidyeganeh et al. (2020) from 2D histological sections into 3D reconstructed space available for the BigBrain dataset Amunts et al. (2013) were used to generate 3D maps for areas $hOc1$, $hOc2$, $hOc3v$ and $hOc5$ from 2D segmentations produced by our method. Segmentations were obtained using the workflow described in Section 2.3 and checked for quality by an expert (e.g. plausibility and consistency across consecutive sections). For areas $hOc3v$ and $hOc5$, results of segmentation models trained with a training interval size of 1.2 mm were used for reconstruction (marked with $*$ in Fig. 3). Between 8% ($hOc3v$) and 23% ($hOc1$) of sections containing the investigated areas were not used for reconstruction due to histological artifacts (e.g. resulting from long-term storage or staining inhomogeneities). Segmentations that passed the quality check were transformed into the 3D reconstructed space. Excluded sections were replaced by interpolations from neighboring sections, using Laplacian fields as proposed in Schober et al. (2016).

Resulting 3D maps were smoothed using a median filter with kernel size $11 \times 11 \times 11$ pixel to compensate for small artefacts. The size of the filter was chosen to match the expected precision of annotations at boundaries (not higher than 100 µm), translating to 5 voxels at the target resolution of 20 µm. Furthermore, connected component analysis on the smoothed volume was performed to determine and remove spurious false positive predictions outside the target area, relying on the assumption that cytoarchitectonic areas are continuous in 3D. Only components with a minimum volume of 27 mm^3 (3 mm × 3 mm × 3 mm) were kept. Effects of median filtering and connected component filtering are illustrated in Fig. 7.

To assess the improvement in 3D consistency and anatomical plausibility gained by the proposed workflow, a reference reconstruction of area $hOc1$ was computed, which performs a direct 3D interpolation between reference annotations obtained by GLI mapping. This reference reconstruction does not use the local segmentation models, and relies only on reference annotations and 3D reconstruction. It was computed by transforming the annotations of the training sections (blue squares in Fig. 3) into the 3D reconstructed space, and filling the gaps by Laplacian field interpolation (Schober et al., 2016).

The anatomical consistency of 3D reconstructed maps was further evaluated by computing their volume and surface area, which were then compared to reference values from Amunts et al. (2000). The volume of each area was computed by counting the total number of labeled voxels and multiplying the result by the physical size of each voxel.

The surface area was computed by first extracting a closed surface mesh of each area using the marching cubes algorithm Lewiner et al. (2003). The subset of mesh vertices lying on the pial surface was then determined by including all triangles where the cortical depth Bok (1929) was smaller than 0.25. To obtain the cortical depth of each mesh vertex, the procedure described in Leprince et al. (2015) was applied to the cortical ribbon defined by the gray and white matter segmentation provided with the BigBrain model (Lewis et al., 2014). The result was a volumetric dataset with voxels in the white matter labelled 1, voxels outside the brain labelled

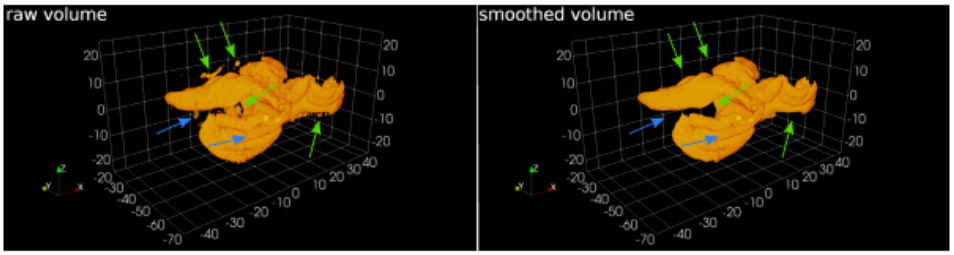

Fig. 7. Effects of median filtering and connected component filtering using the example of *hOc*1. Median filtering smooths the volume and removed small errors originating from registration errors or incorrect predictions (blue arrows). Filtering of small connected components removed small clusters of false positives from the volume (green arrows). Axes x, y and z correspond to left-to-right, posterior-to-anterior and ventral-to-dorsal directions, respectively. Axis labels are specified in mm and correspond to positions in the 3D reconstructed BigBrain space. See Fig. 14 for more images of *hOc*1 from different viewing angles. (For interpretation of the references to color in this figure legend, the reader is referred to the web version of this article.)

0, and voxels inside the isocortex labelled with values between 0 and 1, representing their cortical depth according to the equivolumetric model (Bok, 1929). Cortical depths of mesh vertices were then looked up in this volume. Finally, the surface area of the pial surface for each cytoarchitectonic area was computed by summing up the area of all triangles associated to the pial surface.

Both volume and surface area measurements were corrected for tissue shrinkage Amunts et al. (2000). The volume-based shrinkage factor for B20has been determined in Amunts et al. (2005) based on the fresh weight and the volume after histological processing as $f_V = 1.931$. From this, an area-based (2D) shrinkage factor of $f_A = f_V^{2/3} = 1.551$ was derived.

3. Results

Differences in performance were observed depending on the network architecture (HR, LR, MS), the training setting (global vs. local segmentation models), the considered brain area, as well as the distance between annotated brain sections.

All architectures except for LR (ALL) show comparably good performance for *hOc*1. For most areas however, LR and MS achieved higher performance than other investigated models. For areas *hOc*3*v* and *hOc*5, where additional models were trained with reduced distance between training sections (indicated by ∗ in Fig. 8), performance of LRand MSincreased when reducing the distance between training sections, while only minor improvements were observed for the remaining architectures.

Representative image patches segmented by the MSarchitecture for each investigated area extracted from test sections of B20are shown in Fig. 9. True positive, false positive and false negative predictions are indicated in green, red and blue, respectively. A large share of incorrectly classified pixels belonged to cortical regions with highly oblique cutting angles (Fig. 10 B, C). While large rifts tended to be excluded from the prediction (Fig. 10, A), smaller rifts or tissue foldings were correctly segmented as surrounding area (Fig. 9, A, D, E, G, O).

Scores obtained for areas *hOc*1 and *hOc*2 were overall consistent across different brain samples (Fig. 11). In all three cases, scores obtained for *hOc*2 were lower compared to *hOc*1. Lowest median F1 score for *hOc*2 was obtained for B20, along with an increased variance. Example patches showing the border between *hOc*1 and *hOc*2 on test sections extracted from approximately identical brain regions in the three datasets are shown in Fig. 12.

Models trained on all sections (HR (ALL), LR (ALL), MS (ALL)) obtained lower mean and median F1 scores than their locally trained counterparts HR, LR, and MS (Table 1). LR (ALL) and HR (ALL) showed comparable performance, MS (ALL) performed slightly better. The lowest

Table 1
F1 score statistics computed across all areas and test sections in the B20dataset obtained by the different network architectures HR, LRand MS(trained on local intervals), as well as HR (ALL), LR (ALL)and MS (ALL)(trained on all annotated sections per area). Higher mean/median values and lower standard deviation mean better performance.

model	median	mean	std
HR(all)	0.5319	0.5680	0.2075
LR(all)	0.5648	0.5533	0.1723
MS(all)	0.5869	0.6020	0.1973
HR	0.6294	0.6130	0.2105
LR	0.7439	0.7036	0.1865
MS	0.7469	0.7200	0.1825

scoring local model HR performs better than the highest scoring global model MS (ALL). Both LR and MS resulted in higher mean and median F1 scores than HR, with lower standard deviations. Highest mean and median performance was obtained by MS (Table 1, Fig. 8).

Setting the input patch of either E_{LR} or E_{HR} to zero provides indication on the influence of different scales in the proposed MSarchitecture (Fig. 13): Having access to only low-resolution image information, the model still identifies the approximate location of area *hOc*2, but with poorly defined borders. Using only high-resolution information, the model captures finer details, but has difficulties localizing the area correctly. When the model has access to both high- and low-resolution information, this results in better agreement with the reference annotations.

Locations, orientations and shapes of reconstructed 3D maps (computed using steps described in Section 2.8) were anatomically plausible and consistent (Fig. 14). The 3D map of *hOc*5 showed partially missing extremal ends along the posterior anterior axis. Volume and surface estimates from the 3D maps reported in Table 2 corresponded well with the numbers reported in Amunts et al. (2000). Surface areas of *hOc*1, *hOc*2 and *hOc*5 were largely confirmed with the reference values, as well as the volumes derived from automatic segmentations of areas *hOc*1 and *hOc*2. The reconstructed volume of area *hOc*5 stood out by being considerably smaller than the reference volume.

Comparison of corresponding 3D reconstructions of area *hOc*1 (Fig. 14 E vs. F) showed that the proposed approach provided anatomically more consistent results than direct spatial interpolation of GLI-based annotations, while both build on the same annotation effort. 3D interpolation produced abrupt transitions in anterior-posterior direction

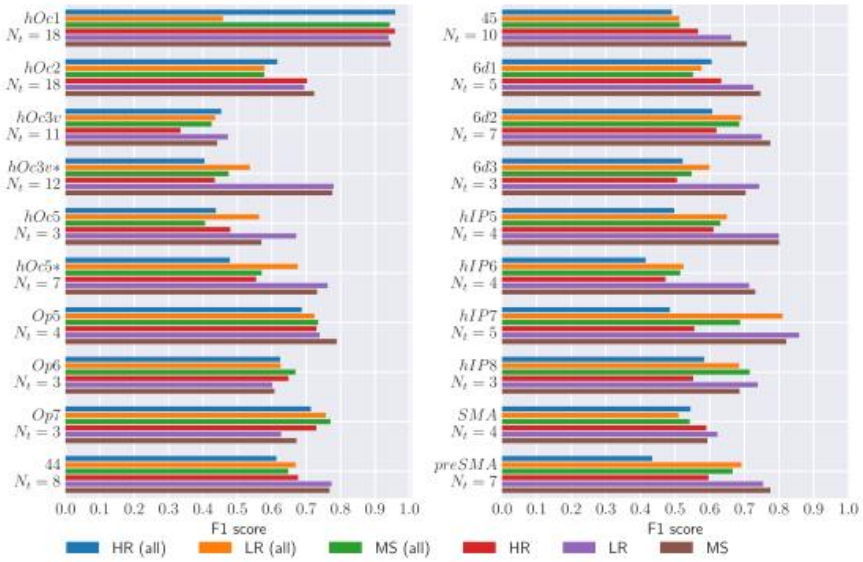

Fig. 8. Median F1 scores for HR (ALL), LR (ALL), MS (ALL), HR, LRand MS per investigated brain area in dataset B20. N_t denotes the number of test sections for which F1 scores were computed for a particular area. * indicates where training of local segmentation models was performed with reduced distance between training sections. Higher values denote better performance.

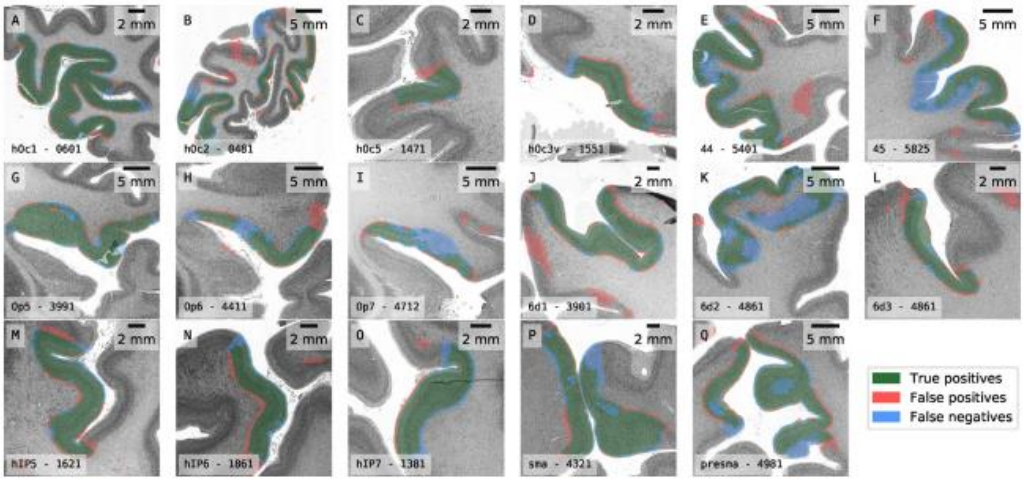

Fig. 9. Example image patches and corresponding model predictions extracted from test sections of B20segmented using the proposed MSarchitecture. One image patch is shown for each investigated cytoarchitectonic area. Colors green, red and blue indicate true positive, false positive and false negative predictions, respectively. (For interpretation of the references to color in this figure legend, the reader is referred to the web version of this article.)

(Fig. 14, F, 1) and only captured structures already contained in the reference annotations, leading to inconsistencies near fine-grained morphological structures (e.g. Fig. 14 F, 2 and 3). The proposed method often produced reasonable segmentations for sections outside the training interval (Fig. 14, E, 1), which interpolation cannot provide by definition.

4. Discussion

In this work, we proposed a novel Deep Learning based workflow to create segmentations of cytoarchitectonic areas in large series of histological human brain sections using only a limited set of manually created annotations. We evaluated this approach across different cytoar-

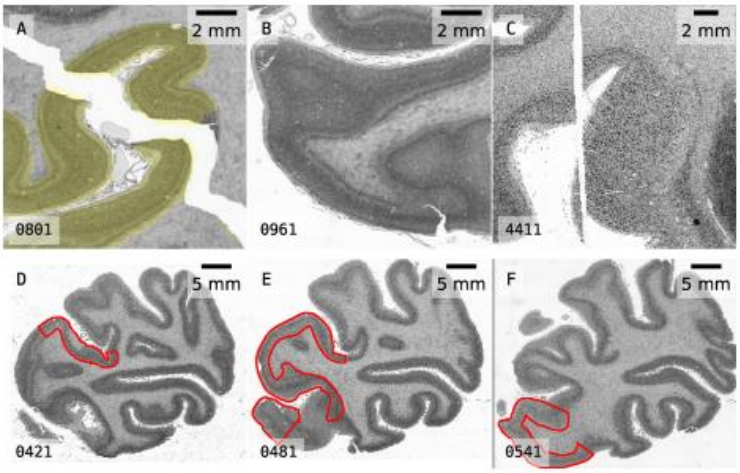

Fig. 10. Image patches extracted from B20showing common challenges encountered during manual and automated cytoarchitectonic mapping. *A:* Mechanical damages resulting from histological processing. Prediction for *hOc*1 shown in yellow demonstrate handling of larger mechanical damages. *B:* Region where the cutting angle is highly oblique, leading to partial or full occlusion of cortical layer structure (*oblique cuts*). *C:* Mechanically damaged and obliquely cut tissue. *C-F:* Example illustrating highly variable morphology of area *hOc3v* (highlighted in red) across 120 histological sections in B20. (For interpretation of the references to color in this figure legend, the reader is referred to the web version of this article.)

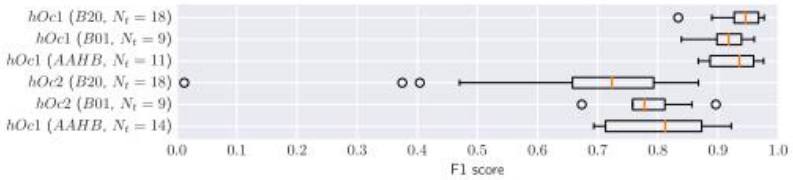

Fig. 11. F1 scores for segmentations of *hOc*1 and *hOc*2 obtained by the MSarchitecture on test sections of datasets B20, B01 and AAHB. N_t denotes the number of test sections for which F1 scores were computed for a particular area.

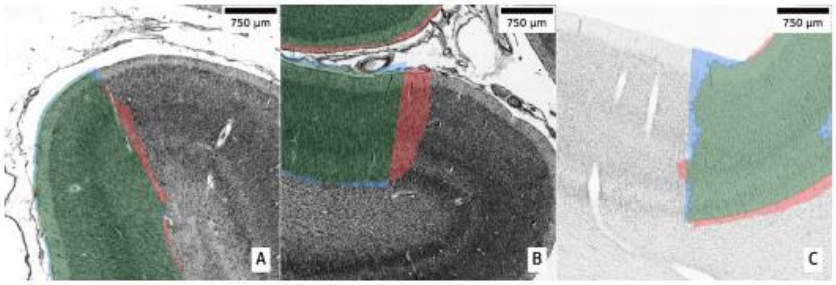

Fig. 12. Example patches and typical segmentation results extracted from test sections in datasets B20 (A), B01 (B) and AAHB (C). All three patches show the segmentation of *hOc*2 obtained by a local segmentation model with MSarchitecture. Patches were extracted at the border between *hOc*1 and *hOc*2 and in comparable regions of the respective brain. Colors green, red and blue indicate true positive, false positive and false negative predictions, respectively (see also legend in Fig. 9). (For interpretation of the references to color in this figure legend, the reader is referred to the web version of this article.)

chitectonic areas, brain samples and staining protocols. As a concrete use case, we then applied it to create high-resolution 3D maps of areas *hOc*1, *hOc*2, *hOc3v* and *hOc*5 in the BigBrain Amunts et al. (2013).

4.1. Quality of derived 3D maps in the BigBrain

The proposed method produced 3D maps with a high degree of anatomical consistency and identified cytoarchitectonic areas precisely in the histological brain sections. Partially missing extremal ends remain a challenge, as seen in anterior-posterior direction of *hOc*5. Such parts are often difficult to identify even using manual methods. Therefore, training data for such extremal ends is difficult to obtain. The segmentation of extremal ends could potentially be addressed by providing additional GLI-based mappings (at the cost of additional annotation effort), or by an explicit shape-based inference step on top of the pixel segmentation. The 3D map of *hOc*1 created with the proposed method is superior to the map obtained by direct spatial interpolation between GLI-based annotations. Methods based on 3D interpolation inherit any

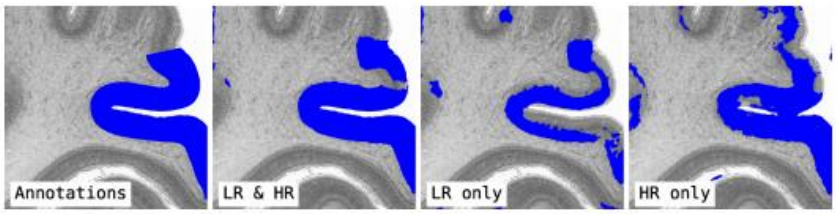

Fig. 13. Reference annotations and predictions of area *hOc*2 (blue) for an example patch from section 961 of the B20dataset. Predictions were obtained by using both low- and high-resolution information (`LR & HR`), only low-resolution (`LR only`), and only high-resolution information (`HR only`). The input image patch for E_{HR} and E_{LR} was set to zero to investigate the role of low- and high-resolution image information, respectively. Predictions were created with model $f^{hOc2}_{[961,1021]}$ using the MSarchitecture. (For interpretation of the references to color in this figure legend, the reader is referred to the web version of this article.)

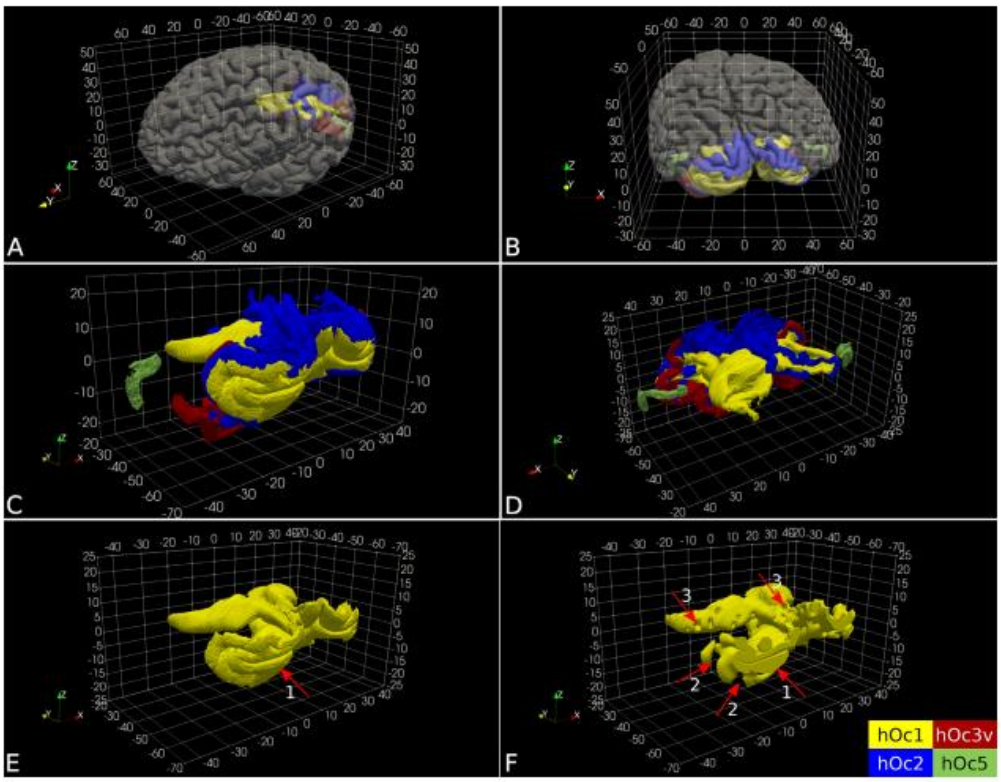

Fig. 14. 3D maps of visual cytoarchitectonic areas *hOc*1 (yellow), *hOc*2 (blue), *hOc*3*v* (red) and *hOc*5 (green), obtained by transforming the independent 2D segmentations generated by the proposed method into the 3D reconstructed space of the B20dataset. *A*+*B*: Spatial embedding of reconstructed areas into the 3D reconstructed BigBrain volume. *C*+*D*: Detailed view of reconstructed cytoarchitectonic areas. *E*+*F*: Comparison of *hOc*1 reconstructed based on our proposed method (E) and based on an interpolation between annotations in the reconstructed space, using Laplacian fields as proposed in Schober et al. (2016) (F). Arrows in F) mark example locations demonstrating shortcomings of the interpolation based reconstruction. Axes x, y and z correspond to left-to-right, posterior-to-anterior and ventral-to-dorsal directions, respectively. Axis labels are specified in mm and correspond to positions in the 3D reconstructed BigBrain space. (For interpretation of the references to color in this figure legend, the reader is referred to the web version of this article.)

Table 2
Estimated volumes (in mm^3) and surface areas (in mm^2) of brain areas derived from the full 3D maps in the 3D reconstructed space of the B20 dataset. Reference mean μ and standard deviation σ were computed based on male subjects from (Amunts et al., 2000). Shrinkage corrected of volumes and surface areas was performed using correction factors $f_V = 1.931$ and $f_A = 1.551$ respectively (Amunts et al., 2005).

area	volume	corrected	μ	σ	z-score
*hOc*1	9019.30	17416.27	18042.2	2464.39	−0.25
*hOc*2	6448.60	12452.26	12634.2	2862.84	−0.06
*hOc*3*v*	1974.76	3813.26	n.a.	n.a.	n.a.
*hOc*5	304.10	587.21	1144.4	406.53	−1.37
area	surface	corrected	μ	σ	z-score
*hOc*1	6891.03	10685.76	12213.0	2225.55	−0.69
*hOc*2	6749.64	10466.52	10390.4	2925.37	0.03
*hOc*3*v*	2142.04	3321.62	n.a.	n.a.	n.a.
*hOc*5	319.79	495.89	450.2	135.92	0.34

error in the alignment of consecutive sections, making them inappropriate for stacks with only linear or no 3D reconstruction. The proposed method does not assume any prior 3D reconstruction - in fact its outputs might be used to guide image registration with landmarks.

4.2. Practical usefulness of the implemented workflow

The presented method showed good robustness against intersubject variability and different histological processing protocols. Thus it largely overcomes the need for brain or area specific parameter adjustments, which makes it well suited to be used as a self-contained tool for neuroscientists. Consequently, it was possible to implement it into a web application that provides a practical mapping workflow for end users from different disciplines. The web application is currently used by five neuroscientists in our institute for their research projects, without requiring support from a computer scientist. The interactive workflow enables efficient mapping of brain areas across full series of histological sections, en par with high throughput microscopy. Such efficiency of mapping was previously impossible in our experience. To give a concrete example, we consider that a trained expert typically needs 30–60 min to identify cytoarchitectonic borders for one cortical area on a single tissue section. Using the established GLI-based mapping approach (see Section 2.1), this would translate to an approximate effort of 150 work days (8 h per day) to map *hOc*1 across the whole stack of 2461 sections. In comparison, the proposed method required annotation of only 18 sections to generate precise segmentations of the complete stack, corresponding to approximately 9 working hours. Altogether, including quality checks and computations, the presented workflow allows precise mapping of a large brain area in the order of 1–2 weeks - a task that would require almost a year of work with previously established methods.

Although the workflow provides a high degree of automation, we still recommend final inspection of results by an expert to ensure optimal quality. The interactive web application presented in Section 2.6 assists users with such quality control, by displaying predictions and allowing immediate correction of remaining errors with significantly less effort than annotating images from scratch. Of course, the typical amount of necessary manual corrections is an important indicator for the usefulness of the tool in practice. In our experience from mapping a whole range of different human brain regions, quality control and manual corrections typically take in the order of few hours per brain area, which may include several thousand sections.

Nevertheless, the need for manual supervision could be further reduced by investigating into methods for identifying prediction errors. Such methods could directly inform the user where additional annotations could help to further optimize the results, thereby realizing an active learning (Settles, 2009) scheme.

4.3. Ability to distinguish higher associative areas

In contrast to primary areas such as the primary visual cortex *hOc*1, so called higher associative areas have a less distinct cytoarchitecture, and less prominently differ from their neighbouring areas. Such observation lead Bailey and von Bonin to the conclusion that it is almost impossible to reliably distinguish such areas from each other, and to define borders between them (Bailey and von Bonin, 1951). This view is not supported any more due to the possibility to identify cytoarchitectonic borders in a reliable and reproducible way (for an overview see (Zilles and Amunts, 2010)). However, the fact that intersubject differences between identical areas of different brains may exceed cytoarchitectonic differences between two neighboring areas in one and the same brain creates challenges for modern brain mapping (Amunts et al., 1999).

Atzeni et al. (2018) also addressed automated mapping of histology. They segmented brain structures in a serial stack of human brain sections from the Allen Human Brain Atlas (Ding et al., 2016) (dataset AAHB used in our experiments). They used annotations from Ding et al. (2016) on a small set of sections at regular intervals, in order to train a probabilistic model that combines multi-atlas segmentation with a CNNs to segment the remaining sections. Compared to the present work however, their approach is restricted to brain structures that can be recognized at a resolution of 250 µm. The authors confirm in their paper that more subtle classes, in particular subdivisions of the isocortex, introduce excessive noise with their approach. The method presented here segmented both *hOc*1 and *hOc*2 in the same dataset with high accuracy by including more fine-grained texture features into the models, thus going clearly beyond this restriction.

4.4. Effect of the local segmentation models

Previous work on automatic cytoarchitectonic brain mapping using machine learning emphasized the importance of strategies for efficient exploitation of available training data and prior information. This includes incorporating probabilistic priors from brain atlases Spitzer et al. (2017) and self-supervised learning Spitzer et al. (2018). The key idea of the present paper is to use multiple local segmentation models, each of which focuses on a spatially restricted subset of sections in one specific brain area. In order to maximize practical benefit, we make an explicit design decision not to aim for a general classification model of multiple brain areas and brains. The benefit of such local segmentations models is confirmed by our experiments, which showed significantly improved performance of HR, LR, and MS compared to their globally trained counterparts HR (ALL), LR (ALL)and MS (ALL).

A major advantage of the local segmentation models is the ability to flexibly adjust the distance between training sections to account for regions with particularly simple or complex properties. This has been demonstrated for the challenging areas *hOc*5 and *hOc*3*v*, where a reduction of the distance between training sections from 120 (2.4 mm) to 60 (1.2 mm) improved precision to a satisfactory level while keeping the annotation effort tractable.

Distance reduction results in major performance gains when using local segmentation models LRor MS, but only minor gains when using globally trained models LR (ALL) or MS (ALL). This suggests that local segmentation models make more efficient use of the additional training data.

In a similar fashion, larger areas or areas with distinct cytoarchitectonic features (e.g. *hOc*1) can be segmented with a coarser set of training sections, in this case reducing annotation effort.

The availability of expert annotations limits our ability to evaluate the effect of reducing distance between annotated sections. The results of our experiments for areas *hOc*3*v* and *hOc*5 suggest, that the optimal distance between annotated sections depends on the cytoarchitectural and morphological complexity of a brain area. The proposed interactive

workflow allows users to add annotations incrementally until satisfied with the segmentation.

On the downside of local models, hyperparameter assessment (e.g. for learning rate or model architecture) is not straightforward when training multiple models on different training sets and evaluating them on individual test sets. Model performance needs to be evaluated across several areas, sections and brains, which can be computationally expensive and lead to a slow development process.

4.5. Effect of the multi-scale model architecture

Macroscopic features of the cerebral cortex (e.g. folding patterns) vary between individual brains. While the location of gyri and sulci can provide guidance for localizing brain areas, such coarse landmarks cannot generally be used to precisely predict cytoarchitectonic borders (Amunts and Zilles, 2015; Fischl et al., 2008; Im and Grant, 2019; Lebenberg et al., 2018). Consequently, established methods for identifying cytoarchitectonic areas rely on high-resolution microscopic information Schleicher et al. (1999); Spitzer et al. (2017, 2018). In contrast, the proposed local segmentation models are able to exploit macroscopic features for improving segmentation performance, thanks to their specialization on only a part of a specific brain area from one individual brain. This can be seen from the higher scores produced by the LR and MS architectures for local segmentations models (Table 1), and by the lack of such an effect for models trained on all sections of a brain area (HR (ALL), LR (ALL), MS (ALL)). Microscopic resolution features further contribute to the performance of the local segmentation models, as verified by a Wilcoxon signed-rank test (Wilcoxon, 1945) ($p = .0011$) which confirms that the multi-scale approach of MS further improves the performance compared to LR. However, this is a relatively small effect compared to the improvement between HR and MS. We can therefore assume that macroscopic information is more relevant than microscopic information in the strictly local setting.

For further understanding the influence of the two scales in the model, it is helpful to compare predictions obtained when occluding (i.e. setting to zero) either the microscopic or macroscopic inputs in a MS model: Using only low-resolution inputs, the model is still able to approximately locate the area, but fails to capture the fine details. On the other hand, a model restricted to see only high-resolution inputs struggles to correctly locate the area. This confirms our assumption that the MS model mostly uses low-resolution inputs for localization and high-resolution inputs for local refinement. While the results of this experiment cover only a specific setting (e.g. model, area and input location), they give us some confidence that the model works as expected.

4.6. Failure mode analysis

The predictions produced by the proposed model typically include some remaining errors (Figs. 9, 12), which require careful interpretation.

Close to brain region boundaries, it must be noted that the GLI-based reference annotations enforce straight lines to model the border, which reflects the vertical arrangement of neurons in columns as a major principle in cortical organization (Schleicher et al., 2000; 1999). This may lead to discrepancies with the present segmentations, that do not enforce such constraints (see for example Fig. 12). In fact the location of the boundary is not determined down to the single pixel, and as a consequence, pixel-level metrics have a somewhat limited significance there.

Many of the remaining classification errors further coincide with highly oblique cutting angles of the tissue. As also reported in (Schleicher et al., 1999; Spitzer et al., 2017; 2018), identification of cortical areas is almost impossible at such angles, because the laminar composition of the cortex is then almost invisible in the 2D section. In such cases, experts would consult adjacent sections to identify areas, which the proposed method cannot do. An extension of the method considering multiple adjacent sections for classification might be able to overcome this issue.

Whether or not remaining segmentation errors are critical in practice depends on the availability of postprocessing methods for correcting them. In the experiments that we carried out, the precise 3D reconstruction of the BigBrain dataset could be used for removing spurious errors (Section 2.8). However, if no precise 3D reconstruction is available, the manual effort for quality control of predictions and any necessary error corrections increases. For such settings, it would be beneficial to develop additional heuristics to identify errors, e.g. for detecting inter-section inconsistencies from only approximate section alignments.

5. Conclusion

A novel method based on Convolutional Neural Networks (CNNss) was introduced for automated mapping of cytoarchitectonic areas in large series of histological human brain sections. Segmentation models were trained for segmentation of different cytoarchitectonic areas in histological stacks obtained from three different brain samples. A key idea is to train separate local segmentation models based on annotations of one specific target area in only two training sections, to focus the learning process on microscopic and macroscopic tissue features close to the training sections. Local segmentation models enable exploitation of low-resolution macroscopic information and significantly improve performance over globally trained models. After training, local segmentation models were able to accurately segment sections in between their respective training sections. By concatenating results from multiple local segmentation models, segmentations for complete brain areas can be obtained. The proposed method opens up new possibilities to map complete stacks of histological human brain sections in a highly automated fashion, and thus provides an important basis for building high-resolution human brain maps for datasets like BigBrain. To the best of our knowledge, the maps of areas $hOc1$, $hOc2$, $hOc3v$ and $hOc5$ computed for the BigBrain model using this method are the first high-resolution 3D maps of human cytoarchitectonic areas created from full stacks of histological sections at cellular resolution. These maps enable precise studies of area-specific morphological and columnar features at microscopic resolution, and in combination with existing cortical layer maps (Wagstyl et al., 2020) an investigation into layer-specific aspects of each region. Dense maps further enable straightforward mapping from the volume to the whole brain mesh surface, which in turn facilitates comparison with other modalities, especially in-vivo imaging. They represent an important contribution for using BigBrain as a microscopic resolution reference space, since they provide direct links to probabilistic cytoarchitectonic reference parcellations at the macroscopic scale (Amunts et al., 2020) that are widely used in neuroimaging studies. As such, our work makes an important contribution to linking neuroscientific findings across spatial scales.

Ethics Statement

The study carried out requires no separate ethical approvals. Postmortem brains were obtained in accordance to legal and ethical regulations and guidelines. Brain tissue for datasets B01 and B20 was obtained through the body donor program of the department of anatomy of the Heinrich Heine University Düsseldorf and with approval of the ethics committee of the medical faculty of the Heinrich Heine University Düsseldorf. Brain tissue for dataset AAHB was obtained from the University of Maryland Brain and Tissue Bank and with approval by the Human Investigation Committees and Institutional Ethics Committees of the University of Maryland.

Declaration of Competing Interest

The authors declare no competing interests.

Credit authorship contribution statement

Christian Schiffer: Conceptualization, Methodology, Software, Validation, Formal analysis, Investigation, Data curation, Writing - original draft, Writing - review & editing, Visualization. **Hannah Spitzer:** Conceptualization, Methodology, Software, Writing - review & editing. **Kai Kiwitz:** Data curation, Validation, Writing - review & editing. **Nina Unger:** Data curation, Validation, Writing - review & editing. **Konrad Wagstyl:** Software, Writing - review & editing. **Alan C. Evans:** Resources, Writing - review & editing, Funding acquisition. **Stefan Harmeling:** Writing - review & editing, Supervision. **Katrin Amunts:** Conceptualization, Investigation, Validation, Writing - review & editing, Supervision, Project administration, Resources, Funding acquisition. **Timo Dickscheid:** Conceptualization, Methodology, Supervision, Writing - original draft, Writing - review & editing, Project administration, Funding acquisition.

Acknowledgments

This project received funding from the European Union's Horizon 2020 Research and Innovation Programme, grant agreements 785907 (HBP SGA2) and 945539 (HBP SGA3), from the Helmholtz Association's Initiative and Networking Fund through the Helmholtz International BigBrain Analytics and Learning Laboratory (HIBALL) under the Helmholtz International Lab grant agreement InterLabs-0015, and from Priority Program 2041 (SPP 2041) "Computational Connectomics" of the German Research Foundation (DFG). This work was further supported by the German Federal Ministry of Education and Research (BMBF) and the Max Planck Society for the Advancement of Science through their joint initiative between German Universities and German Research Organizations Computing time was granted through JARA on the supercomputer JURECA at Jülich Supercomputing Centre (JSC) as part of the project CJINM16.

Supplementary material

Supplementary material associated with this article can be found, in the online version, at 10.1016/j.neuroimage.2021.118327.

References

Abadi, M., Barham, P., Chen, J., Chen, Z., Davis, A., Dean, J., Devin, M., Ghemawat, S., Irving, G., Isard, M., 2016. TensorFlow: a system for large-scale machine learning. In: 12th USENIX Symposium on Operating Systems Design and Implementation OSDI 16, pp. 265–283.

Amunts, K., Kedo, O., Kindler, M., Pieperhoff, P., Mohlberg, H., Shah, N.J., Habel, U., Schneider, F., Zilles, K., 2005. Cytoarchitectonic mapping of the human amygdala, hippocampal region and entorhinal cortex: intersubject variability and probability maps. Anat. Embryol. 210 (5–6), 343–352. doi:10.1007/s00429-005-0025-5.

Amunts, K., Lepage, C., Borgeat, L., Mohlberg, H., Dickscheid, T., Rousseau, M.-É., Bludau, S., Bazin, P.-L., Lewis, L.B., Oros-Peusquens, A.-M., Shah, N.J., Lippert, T., Zilles, K., Evans, A.C., 2013. BigBrain: an ultrahigh-resolution 3D human brain model. Science 340 (6139), 1472–1475. doi:10.1126/science.1235381.

Amunts, K., Malikovic, A., Mohlberg, H., Schormann, T., Zilles, K., 2000. Brodmann's areas 17 and 18 brought into stereotaxic space—where and how variable? Neuroimage 11 (1), 66–84. doi:10.1006/nimg.1999.0516.

Amunts, K., Mohlberg, H., Bludau, S., Zilles, K., 2020. Julich-Brain: a 3D probabilistic atlas of the human brain's cytoarchitecture. Science doi:10.1126/science.abb4588.

Amunts, K., Schleicher, A., Bürgel, U., Mohlberg, H., Uylings, H.B.M., Zilles, K., 1999. Broca's region revisited: cytoarchitecture and intersubject variability. J. Comp. Neurol. 412 (2), 319–341. doi:10.1002/(SICI)1096-9861(19990920)412:2<319::AID-CNE10>3.0.CO;2-7.

Amunts, K., Schleicher, A., Zilles, K., 2004. Outstanding language competence and cytoarchitecture in Broca's speech region. Brain Lang. 89 (2), 346–353. doi:10.1016/S0093-934X(03)00360-2.

Amunts, K., Zilles, K., 2015. Architectonic mapping of the human brain beyond brodmann. Neuron 88 (6), 1086–1107. doi:10.1016/j.neuron.2015.12.001.

Annese, J., Pitiot, A., Dinov, I.D., Toga, A.W., 2004. A myelo-architectonic method for the structural classification of cortical areas. Neuroimage 21 (1), 15–26. doi:10.1016/j.neuroimage.2003.08.024.

Atzeni, A., Jansen, M., Ourselin, S., Iglesias, J.E., 2018. A probabilistic model combining deep learning and multi-atlas segmentation for semi-automated labelling of histology. In: Frangi, A.F., Schnabel, J.A., Davatzikos, C., Alberola-López, C., Fichtinger, G. (Eds.), Medical Image Computing and Computer Assisted Intervention – MICCAI 2018, vol. 11071. Springer International Publishing, pp. 219–227. doi:10.1007/978-3-030-00934-2_25.

Bailey, P., von Bonin, G., 1951. The isocortex of man. Urbana 3.

Bok, S.T., 1929. Der Einfluß der in den Furchen und Windungen auftretenden Krümmungen der Großhirnrinde auf die Rindenarchitektur. Zeitschrift für die gesamte Neurologie und Psychiatrie 121 (1), 682. doi:10.1007/BF02864437.

Çiçek, Ö., Abdulkadir, A., Lienkamp, S.S., Brox, T., Ronneberger, O., 2016. 3D U-Net: learning dense volumetric segmentation from sparse annotation. In: International Conference on Medical Image Computing and Computer-Assisted Intervention. Springer, pp. 424–432.

Dalcin, L.D., Paz, R.R., Kler, P.A., Cosimo, A., 2011. Parallel distributed computing using Python. Adv. Water Resour. 34 (9), 1124–1139. doi:10.1016/j.advwatres.2011.04.013.

Dickscheid, T., Haas, S., Bludau, S., Glock, P., Huysegoms, M., Amunts, K., 2019. Towards 3D reconstruction of neuronal cell distributions from histological human brain sections. Future Trends HPC Disruptive Scenario 34, 223.

Ding, S.-L., Royall, J.J., Sunkin, S.M., Ng, L., Facer, B.A.C., Lesnar, P., Guillozet-Bongaarts, A., McMurray, B., Szafer, A., Dolbeare, T.A., Stevens, A., Tirrell, L., Benner, T., Caldejon, S., Dalley, R.A., Dee, N., Lau, C., Nyhus, J., Reding, M., Riley, Z.L., Sandman, D., Shen, E., van der Kouwe, A., Varjabedian, A., Write, M., Zollei, L., Dang, C., Knowles, J.A., Koch, C., Phillips, J.W., Sestan, N., Wohnoutka, P., Zielke, H.R., Hohmann, J.G., Jones, A.R., Bernard, A., Hawrylycz, M.J., Hof, P.R., Fischl, B., Lein, E.S., 2016. Comprehensive cellular-resolution atlas of the adult human brain. J. Comp. Neurol. 524 (16), 3127–3481. doi:10.1002/cne.24080.

Fischl, B., Rajendran, N., Busa, E., Augustinack, J., Hinds, O., Yeo, B.T., Mohlberg, H., Amunts, K., Zilles, K., 2008. Cortical folding patterns and predicting cytoarchitecture. Cereb. Cortex 18 (8), 1973–1980.

Goulas, A., Zilles, K., Hilgetag, C.C., 2018. Cortical gradients and laminar projections in mammals. Trends Neurosci. 41 (11), 775–788. doi:10.1016/j.tins.2018.06.003.

Goyal, P., Dollár, P., Girshick, R., Noordhuis, P., Wesolowski, L., Kyrola, A., Tulloch, A., Jia, Y., He, K., 2017. Accurate, large minibatch SGD: training imagenet in 1 h. arXiv preprint arXiv:1706.02677.

Im, K., Grant, P.E., 2019. Sulcal pits and patterns in developing human brains. Neuroimage 185, 881–890.

Ioffe, S., Szegedy, C., 2015. Batch normalization: accelerating deep network training by reducing internal covariate shift. In: International Conference on Machine Learning, pp. 448–456.

Kiwitz, K., Schiffer, C., Dickscheid, T., Amunts, K., 2019. Reference delineations of area hOc1 (V1, 17, CalcS) in individual sections of the BigBrain [Data set]. EBRAINS doi:10.25493/3GSV-T4A.

Kiwitz, K., Schiffer, C., Dickscheid, T., Amunts, K., 2019. Reference delineations of area hOc2 (V2, 18) in individual sections of the BigBrain [Data set]. EBRAINS doi:10.25493/8MKD-D77.

Kiwitz, K., Schiffer, C., Dickscheid, T., Amunts, K., 2020. Reference delineations of area hOc3v (LingG) in individual sections of the BigBrain [Data set]. EBRAINS doi:10.25493/DBZG-QZ.

Kiwitz, K., Schiffer, C., Dickscheid, T., Malikovic, A., Amunts, K., 2020. Reference delineations of area hOc5 (LOC) in individual sections of the BigBrain [Data set]. EBRAINS doi:10.25493/4027-K9Y.

Krause, D., Thörnig, P., 2018. JURECA: Modular supercomputer at Jülich supercomputing centre. J. Large-Scale Res. Facil. JLSRF 4, A132. doi:10.17815/jlsrf-4-121-1.

Lebenberg, J., Labit, M., Auzias, G., Mohlberg, H., Fischer, C., Rivière, D., Duchesnay, E., Kabdebon, C., Leroy, F., Labra, N., Poupon, F., Dickscheid, T., Hertz-Pannier, L., Poupon, C., Dehaene-Lambertz, G., Hüppi, P.S., Amunts, K., Dubois, J., Mangin, J.-F., 2018. A framework based on sulcal constraints to align preterm, infant and adult human brain images acquired in vivo and post mortem. Brain Struct. Funct. 223 (9), 4153–4168. doi:10.1007/s00429-018-1735-9.

Leprince, Y., Poupon, F., Delzescaux, T., Hasboun, D., Poupon, C., Rivière, D., 2015. Combined Laplacian-equivolumic model for studying cortical lamination with ultra high field MRI (7 T). In: 2015 IEEE 12th International Symposium on Biomedical Imaging (ISBI), pp. 580–583. doi:10.1109/ISBI.2015.7163940.

Lewiner, T., Lopes, H., Vieira, A.W., Tavares, G., 2003. Efficient implementation of marching cubes' cases with topological guarantees. J. Graphics Tools 8 (2), 1–15. doi:10.1080/10867651.2003.10487582.

Lewis, L., Lepage, C., Fournier, M., Zilles, K., Amunts, K., Evans, A.C., 2014. BigBrain: initial tissue classification and surface extraction. 20th Annual Meeting of the Organization for Human Brain Mapping (OHBM).

Malikovic, A., Amunts, K., Schleicher, A., Mohlberg, H., Eickhoff, S.B., Wilms, M., Palomero-Gallagher, N., Armstrong, E., Zilles, K., 2007. Cytoarchitectonic analysis of the human extrastriate cortex in the region of V5/MT+: aprobabilistic, stereotaxic map of area hOc5. Cereb. Cortex 17 (3), 562–574. doi:10.1093/cercor/bhj181.

Merker, B., 1983. Silver staining of cell bodies by means of physical development. J. Neurosci. Methods 9 (3), 235–241. doi:10.1016/0165-0270(83)90086-9.

Milletari, F., Navab, N., Ahmadi, S.-A., 2016. V-Net: fully convolutional neural networks for volumetric medical image segmentation. In: 2016 Fourth International Conference on 3D Vision (3DV). IEEE, pp. 565–571.

Omidyeganeh, M., Lepage, C., Wagstyl, K., Spitzer, H., Dickscheid, T., Amunts, K., Evans, A., 2020. Non-linear registration of 1 µm histology sections into 3D 20 µm BigBrain space. 26th Annual Meeting of the Organization for Human Brain Mapping.

Richter, M., Amunts, K., Mohlberg, H., Bludau, S., Eickhoff, S.B., Zilles, K., Caspers, S., 2019. Cytoarchitectonic segregation of human posterior intraparietal and adjacent parieto-occipital sulcus and its relation to visuomotor and cognitive functions. Cereb. Cortex 29 (3), 1305–1327. doi:10.1093/cercor/bhy245.

Ronneberger, O., Fischer, P., Brox, T., 2015. U-Net: convolutional networks for biomedical image segmentation. In: International Conference on Medical Image Computing and Computer-Assisted Intervention. Springer, pp. 234–241.
Rottschy, C., Eickhoff, S.B., Schleicher, A., Mohlberg, H., Kujovic, M., Zilles, K., Amunts, K., 2007. Ventral visual cortex in humans: cytoarchitectonic mapping of two extrastriate areas. Hum. Brain Mapp. 28 (10), 1045–1059. doi:10.1002/hbm.20348.
Ruan, J., Bludau, S., Palomero-Gallagher, N., Caspers, S., Mohlberg, H., Eickhoff, S.B., Seitz, R.J., Amunts, K., 2018. Cytoarchitecture, probability maps, and functions of the human supplementary and pre-supplementary motor areas. Brain Struct. Funct. 223 (9), 4169–4186. doi:10.1007/s00429-018-1738-6.
Schleicher, A., Amunts, K., Geyer, S., Kowalski, T., Schormann, T., Palomero-Gallagher, N., Zilles, K., 2000. A stereological approach to human cortical architecture: identification and delineation of cortical areas. J. Chem. Neuroanat. 20, 31–47. doi:10.1016/S0891-0618(00)00076-4.
Schleicher, A., Amunts, K., Geyer, S., Morosan, P., Zilles, K., 1999. Observer-independent method for microstructural parcellation of cerebral cortex: a quantitative approach to cytoarchitectonics. Neuroimage 9 (1), 165–177. doi:10.1006/nimg.1998.0385.
Schmitt, O., Böhme, M., 2002. A robust transcortical profile scanner for generating 2-D traverses in histological sections of richly curved cortical courses. Neuroimage 16 (4), 1103–1119. doi:10.1006/nimg.2002.1159.
Schober, M., Axer, M., Huysegoms, M., Schubert, N., Amunts, K., Dickscheid, T., 2016. Morphing image masks for stacked histological sections using Laplace's equation. In: Tolxdorff, T., Deserno, T.M., Handels, H., Meinzer, H.-P. (Eds.), Bildverarbeitung Für Die Medizin 2016. Springer, pp. 146–151. doi:10.1007/978-3-662-49465-3_27.
Sergeev, A., Del Balso, M., 2018. Horovod: fast and easy distributed deep learning in TensorFlow. arXiv preprint arXiv:1802.05799.
Settles, B., 2009. Active Learning Literature Survey. Computer Sciences Technical Report. University of Wisconsin–Madison.
Sigl, B., 2018. Zytoarchitektur, Netzwerke und Funktionen der Areale des menschlichen dorsolateralen prämotorischen Kortex - Komponenten motorischer Planung und Kandidat für das Frontale Augenfeld Dissertation.
Sigl, B., Bludau, S., Mohlberg, H., Eickhoff, S.B., Amunts, K., 2019a. Interpolated 3D map of area 6d1 (PreCG) in the BigBrain [Data set].. EBRAINS doi:10.25493/K0X6-KKB.
Sigl, B., Bludau, S., Mohlberg, H., Eickhoff, S.B., Amunts, K., 2019b. Interpolated 3D map of area 6d2 (PreCG) in the BigBrain [Data set].. EBRAINS doi:10.25493/8WSN-JQ8.
Sigl, B., Bludau, S., Mohlberg, H., Eickhoff, S.B., Amunts, K., 2019c. Interpolated 3D map of area 6d3 (PreCG) in the BigBrain [Data set].. EBRAINS doi:10.25493/B87N-ZDX.
Spitzer, H., Amunts, K., Harmeling, S., Dickscheid, T., 2017. Parcellation of visual cortex on high-resolution histological brain sections using convolutional neural networks. In: 2017 IEEE 14th International Symposium on Biomedical Imaging (ISBI 2017). IEEE, pp. 920–923. doi:10.1109/ISBI.2017.7950666.
Spitzer, H., Kiwitz, K., Amunts, K., Harmeling, S., Dickscheid, T., 2018. Improving cytoarchitectonic segmentation of human brain areas with self-supervised siamese networks. In: Medical Image Computing and Computer Assisted Intervention – MICCAI 2018. Springer International Publishing, pp. 663–671.
Sutskever, I., Martens, J., Dahl, G., Hinton, G., 2013. On the importance of initialization and momentum in deep learning. In: International Conference on Machine Learning, pp. 1139–1147.
Unger, N., Bludau, S., Mohlberg, H., Caspers, S., Amunts, K., 2020a. Probabilistic cytoarchitectonic map of area OP5 (Frontal Operculum) (v2.0) [Data set]. EBRAINS doi:10.25493/TWFH-BJZ.
Unger, N., Bludau, S., Mohlberg, H., Caspers, S., Amunts, K., 2020b. Probabilistic cytoarchitectonic map of area OP6 (Frontal Operculum) (v2.0) [Data set]. EBRAINS doi:10.25493/41KE-8HT.
Unger, N., Bludau, S., Mohlberg, H., Caspers, S., Amunts, K., 2020c. Probabilistic cytoarchitectonic map of area OP7 (Frontal Operculum) (v2.0) [Data set]. EBRAINS doi:10.25493/T2M3-2ST.
Wagstyl, K., Larocque, S., Cucurull, G., Lepage, C., Cohen, J.P., Bludau, S., Palomero–Gallagher, N., Lewis, L.B., Funck, T., Spitzer, H., 2020. BigBrain 3D atlas of cortical layers: cortical and laminar thickness gradients diverge in sensory and motor cortices. PLoS Biol. 18 (4), e3000678.
Wilcoxon, F., 1945. Individual comparisons by ranking methods. Biometrics Bull. 1 (6), 80–83. doi:10.2307/3001968.
Wree, A., Schleicher, A., Zilles, K., 1982. Estimation of volume fractions in nervous tissue with an image analyzer. J. Neurosci. Methods 6 (1), 29–43. doi:10.1016/0165-0270(82)90014-0.
Zeiler, M.D., Fergus, R., 2014. Visualizing and understanding convolutional networks. In: European Conference on Computer Vision. Springer, pp. 818–833.
Zilles, K., Amunts, K., 2010. Centenary of Brodmann's map–conception and fate. Nat. Rev. Neurosci. 11 (2), 139–145. doi:10.1038/nrn2776.

2.3 Unger, N., Heim, S., Hilger, D. I., Bludau, S., Pieperhoff, P., Cichon, S., Amunts, K., & Mühleisen, T. W. (2021). Identification of phonology-related genes and functional characterization of Broca's and Wernicke's regions in language and learning disorders. ***Frontiers in Neuroscience, 15,*** **680762. https://doi.org/10.3389/fnins.2021.680762**

frontiers in Neuroscience

ORIGINAL RESEARCH
published: 03 September 2021
doi: 10.3389/fnins.2021.680762

OPEN ACCESS

Edited by:
Silvia Pellegrini,
University of Pisa, Italy

Reviewed by:
Claudio V. Mello,
Oregon Health and Science University, United States
Amaia Carrion-Castillo,
Basque Center on Cognition, Brain and Language, Spain

***Correspondence:**
Thomas W. Mühleisen
t.muehleisen@fz-juelich.de

†ORCID:
Nina Unger
orcid.org/0000-0001-5388-8814
Stefan Heim
orcid.org/0000-0002-5818-8355
Dominique I. Hilger
orcid.org/0000-0003-3360-5754
Sebastian Bludau
orcid.org/0000-0001-6173-9050
Peter Pieperhoff
orcid.org/0000-0001-6166-8926
Sven Cichon
orcid.org/0000-0002-9475-086X
Katrin Amunts
orcid.org/0000-0001-5828-0867
Thomas W. Mühleisen
orcid.org/0000-0002-6057-5952

Specialty section:
This article was submitted to Neurogenomics, a section of the journal Frontiers in Neuroscience

Received: *15 March 2021*
Accepted: *04 August 2021*
Published: *03 September 2021*

Citation:
Unger N, Heim S, Hilger DI, Bludau S, Pieperhoff P, Cichon S, Amunts K and Mühleisen TW (2021) Identification of Phonology-Related Genes and Functional Characterization of Broca's and Wernicke's Regions in Language and Learning Disorders. Front. Neurosci. 15:680762. doi: 10.3389/fnins.2021.680762

Identification of Phonology-Related Genes and Functional Characterization of Broca's and Wernicke's Regions in Language and Learning Disorders

Nina Unger[1,2,3†], Stefan Heim[2,4,5†], Dominique I. Hilger[2†], Sebastian Bludau[2†], Peter Pieperhoff[2†], Sven Cichon[2,6,7†], Katrin Amunts[1,2,5†] and Thomas W. Mühleisen[1,2,6†]*

[1] *Cécile and Oskar Vogt Institute for Brain Research, Medical Faculty, University Hospital Düsseldorf, Heinrich Heine University Düsseldorf, Düsseldorf, Germany,* [2] *Institute of Neuroscience and Medicine (INM-1), Research Centre Jülich, Jülich, Germany,* [3] *Department of Neurology, Medical Faculty, RWTH Aachen University, Aachen, Germany,* [4] *Department of Psychiatry, Psychotherapy and Psychosomatics, Medical Faculty, RWTH Aachen University, Aachen, Germany,* [5] *JARA-Brain, Jülich-Aachen Research Alliance, Jülich, Germany,* [6] *Department of Biomedicine, University of Basel, Basel, Switzerland,* [7] *Institute of Medical Genetics and Pathology, University Hospital Basel, Basel, Switzerland*

Impaired phonological processing is a leading symptom of multifactorial language and learning disorders suggesting a common biological basis. Here we evaluated studies of dyslexia, dyscalculia, specific language impairment (SLI), and the logopenic variant of primary progressive aphasia (lvPPA) seeking for shared risk genes in Broca's and Wernicke's regions, being key for phonological processing within the complex language network. The identified "phonology-related genes" from literature were functionally characterized using Atlas-based expression mapping (JuGEx) and gene set enrichment. Out of 643 publications from the last decade until now, we extracted 21 candidate genes of which 13 overlapped with dyslexia and SLI, six with dyslexia and dyscalculia, and two with dyslexia, dyscalculia, and SLI. No overlap was observed between the childhood disorders and the late-onset lvPPA often showing symptoms of learning disorders earlier in life. Multiple genes were enriched in Gene Ontology terms of the topics learning (*CNTNAP2, CYFIP1, DCDC2, DNAAF4, FOXP2*) and neuronal development (*CCDC136, CNTNAP2, CYFIP1*, *DCDC2*, *KIAA0319*, *RBFOX2*, *ROBO1*). Twelve genes showed above-average expression across both regions indicating moderate-to-high gene activity in the investigated cortical part of the language network. Of these, three genes were differentially expressed suggesting potential regional specializations: *ATP2C2* was upregulated in Broca's region, while *DNAAF4* and *FOXP2* were upregulated in Wernicke's region. *ATP2C2* encodes a magnesium-dependent calcium transporter which fits with reports about disturbed calcium and magnesium levels for dyslexia and other communication disorders. *DNAAF4* (formerly known as *DYX1C1*) is involved in neuronal migration supporting the hypothesis of disturbed migration in dyslexia. *FOXP2* is a transcription factor that regulates a number of genes

involved in development of speech and language. Overall, our interdisciplinary and multi-tiered approach provided evidence that genetic and transcriptional variation of *ATP2C2*, *DNAAF4*, and *FOXP2* may play a role in physiological and pathological aspects of phonological processing.

Keywords: development, phonology, gene expression, Broca's area, Wernicke's area

INTRODUCTION

Developmental language and learning disorders severely impair children's abilities in speaking, reading, writing, calculating, and combinations thereof (American Psychiatric Association, 2013). One cognitive domain commonly involved in the majority of these disorders is phonological processing which refers to the analysis and synthesis of the sound structure of spoken and written language (phonological awareness), phonological representations and the rapid access (rapid automatized naming) or memorizing (phonological working memory) thereof. The different phonological domains are highly inter-correlated and part of the shared construct of phonological processing.

At the behavioral level, patients with dyslexia, dyscalculia, or specific language impairment (SLI) show deficits in key domains of phonological processing such as phonological awareness, phonological working memory, and/or speeded access to phonological codes during rapid automatized naming, as summarized in **Supplementary Table 1**. Dyslexia is primarily associated with impaired phonological awareness (Steinbrink et al., 2008; Pennington and Bishop, 2009; Hasselhorn et al., 2010; Child et al., 2019). This, like rapid automatized naming, may be considered as a predictive factor for early-onset dyslexia (Thompson et al., 2015). In addition, dyslexia patients perform poorly on phonological working memory (De Carvalho et al., 2014; Child et al., 2019) and show deficits in phonological representations leading to difficulties in phoneme awareness and phonological coding (Pennington and Bishop, 2009). In dyscalculia, connections between phonological processing and arithmetic abilities can be observed (De Smedt and Boets, 2010; Raghubar et al., 2010; De Smedt, 2018). The phonological working memory was identified to serve as a short-time buffer for mathematical operations based on the triple code model which codes numbers as numerals, number words, and abstract numerosities (Dehaene, 1992; Dehaene et al., 2003; Träff and Passolunghi, 2015; Pollack and Ashby, 2018). Patients with SLI, especially with a speech sound disorder, exhibit an inadequate phonological realization and use of particular phonemes in spontaneous speech due to impaired phonological awareness abilities and a lower quality of phonological representations (Lewis et al., 2011; Claessen and Leitão, 2012; American Psychiatric Association, 2013). Some studies also showed lower scores in SLI in phonological working memory increasing the language difficulties (Torrens and Yagüe, 2016).

In addition to impaired phonological processing with effects on language, reading, and mathematical abilities early in life, phonological deficits may have an onset late in life, e.g., in patients with primary progressive aphasia, a progressive neurodegenerative disease (Magnin et al., 2016). The logopenic variant of primary progressive aphasia (lvPPA) was included in this research for this reason and due to high comorbidity with developmental learning disorders meaning that lvPPA patients have a higher probability for these disorders in childhood (Rogalski et al., 2008). Like children with SLI, adults with lvPPA exhibit phonological paraphasias, i.e., errors in the phonological realization of a word, in spontaneous speech as well as in naming (Gorno-Tempini et al., 2011). One central mechanism for these lvPPA symptoms is a deficit of phonological working memory. In addition, alterations in phonological representations may be observable (Gorno-Tempini et al., 2008; Henry et al., 2016).

Phonological processing is related to the language areas of the fronto-temporal network, in particular Broca's region (opercular and triangular parts of the left inferior frontal gyrus) and Wernicke's region (left inferior parietal lobule and posterior superior temporal gyrus; Müller and Knight, 2006; Rogalsky and Hickok, 2011; Hartwigsen, 2015, 2016; Binder, 2017; Klaus and Hartwigsen, 2019; Yi et al., 2019; Hartwigsen et al., 2020). Broca's and Wernicke's regions represent central nodes of the phonological processing network, which are integrated into phonological processes in phonological production as well as in phonological perception (Heim et al., 2003; Indefrey and Levelt, 2004; Friederici, 2011; Indefrey, 2011; Hagoort and Indefrey, 2014). While Broca's region is associated with phonological word fluency, phonological decisions, and the phonological loop (Heim et al., 2008, 2009a,b; Aboitiz et al., 2010; Liakakis et al., 2011; Katzev et al., 2013; Wagner et al., 2014; Klaus and Hartwigsen, 2019), Wernicke's region is involved in phonological speech perception and auditory word-form recognition (Buchsbaum et al., 2001; DeWitt and Rauschecker, 2013). Both regions are connected by the language-relevant pathways, arcuate fasciculus and superior longitudinal fasciculus (Catani et al., 2005; Friederici, 2009, 2011, 2012; Friederici and Gierhan, 2013). Both fasciculi are associated with the transport of order information as a part of the phonological loop (Papagno et al., 2017) and the arcuate fasciculus is also involved in automatic repetition (Catani et al., 2005; Berthier et al., 2012; Papagno et al., 2017). Furthermore, a high functional connectivity between Broca's and Wernicke's regions based on the arcuate fasciculus leads to a higher linguistic performance, e.g., in phonological word learning (López-Barroso et al., 2013).

Functional resonance imaging and diffusion tensor imaging studies suggested that Broca's and Wernicke's regions are affected in patients with SLI, dyslexia, dyscalculia, and also the lvPPA (McCrone, 2002; Sonty et al., 2007; Heim et al., 2010; Verhoeven et al., 2012; Dinkel et al., 2013). In children with SLI, an abnormal connection between both regions was reported in contrast to age-matched controls, i.e., a significantly reduced mean fractional anisotropy was shown in the superior longitudinal fasciculus

(Verhoeven et al., 2012). Dyslexia patients showed lower activations in Broca's region during phonological decision tasks as well as in Wernicke's region during auditory discrimination tasks (Heim et al., 2010). In dyscalculia patients, both regions are the common regions for the interaction of phonological processing and mathematical abilities (Pollack and Ashby, 2018). Additionally, reduced connectivity between Wernicke's region and the intraparietal sulcus was found in dyscalculia patients (McCrone, 2002). Moreover, Broca's region was excessively activated in dyscalculia patients during a calculation task (Dinkel et al., 2013). In lvPPA patients, Sonty et al. (2007) reported a lower effective connectivity (dysfunctional network interaction) between Broca's and Wernicke's regions.

Twin studies suggest that reading and language skills are heritable, with influences from both genetic factors and environmental factors (Hensler et al., 2010; Wadsworth et al., 2010; Tosto et al., 2017; Rice et al., 2020). Similar to developmental disorders, primary progressive aphasia also has a genetic component (Henry and Gorno-Tempini, 2010; Kim et al., 2016). Yet, there are no systematic approaches published that relate genes to the domains of phonological processing, but rather only to isolated phonological features within language and/or learning disorders or the physiological language. Furthermore, there is no study about a specific expression analysis of language-related genes in Broca's and Wernicke's regions of the adult human brain. However, two studies investigated the developing brain using data-driven, whole-transcriptome approaches to identify profiles of regionally co- or differentially expressed genes. Johnson et al. (2009) screened different brain regions in human fetuses including the perisylvian cortex (ventrolateral prefrontal, motor-somatosensory, parietal association, temporal auditory), where *FOXP2* showed a modest upregulation. Lambert et al. (2011) directly screened precursor structures of Broca's and Wernicke's regions in the fetal brain and found several *FOXP2* regulated genes among the differentially expressed genes. An overview of the other recent studies on Broca's and Wernicke's regions in humans and model organisms is provided by **Supplementary Table 2**.

Given that the named language and/or learning disorders in childhood and late adulthood have commonalities in (a) phonological processing deficits as one cognitive signature, (b) repercussions in the neural processing circuits for phonology, and (c) genetic predispositions, we wanted to investigate whether there is a specific genetic contribution to general phonological processing principles for dyslexia, dyscalculia, SLI, and lvPPA. For this purpose, we developed a workflow to integrate clinical, neuroanatomical, and genetic knowledge about phonological processing abilities in these disorders (**Figure 1**). First, we performed a screening of the literature for potentially candidate genes for phonological processing ("phonology-related genes") shared between the disorders. We then characterized these genes by enrichment analysis of gene functions and expression analysis in the two key regions involved in phonological processing (Broca's and Wernicke's regions) using a new computational tool (JuGEx, Bludau et al., 2018) for the joint statistical analysis of microstructural variability (Julich-Brain Atlas; Amunts et al., 2020) and transcriptional variability (Hawrylycz et al., 2012, 2015; Allen Human Brain Atlas, 2013) in adult human brains.

MATERIALS AND METHODS

Literature Evaluation Process

The following criteria were used to screen the literature and had to be fulfilled: (a) Publication date between 01/01/2010 and 23/05/2021, (b) investigation of at least one of the disorders dyslexia, dyscalculia, SLI, and lvPPA, (c) report of at least one human gene as significant original/replicated result ($p < 0.05$), (d) report of at least one gene as a risk factor for a disorder or trait/phenotype related with the disorder, (e) sample containing more than one individual (no single-case study), (f) sample of European origin to reduce a potential influence of population stratification on our results, (g) study either a linkage analysis, a genome-wide association study (GWAS), or a candidate gene association study.

Criterion (b) was not met if a disorder was named as an attendant symptom of another disorder, e.g., dyslexia as an attendant symptom of tuberous sclerosis. In contrast, articles primarily dealing with specific language and/or learning disorders with additional comorbidities were included, e.g., dyslexia with comorbid attention-deficit hyperactivity disorder. Our criteria referred to the terminology defined by the two most recent Diagnostic and Statistical Manuals of the American Psychiatric Association [DSM-IV (American Psychiatric Association, 1994); DSM-5 (American Psychiatric Association, 2013)] and exact synonyms. Studies investigating the normal variability of a trait in a population sample, e.g., reading skills in a cohort of healthy children, were only included if a direct relation to a corresponding pathology was reported, e.g., in terms of the analysis of risk genes for that pathology.

We performed eleven single searches fully covering the potential combinations of language and/or learning disorders (**Supplementary Table 3**) using PubMed Advanced Search[1] with our search string, composed of clinical categories and genetic terms as described in **Supplementary Table 4**. Each search consisted of two analytical steps: First, a computational text mining of the abstracts and titles from all identified articles using PubTator[2] (Wei et al., 2013). Second, a manual text mining of the full text was performed. Articles were selected for inclusion if they fulfilled all criteria a) to g). Clinical categories found in these articles were summarized in **Supplementary Table 5**. Candidate genes were extracted from research articles, while review articles were excluded from evaluation results because they did not represent original research results. Symbols and names of genes were checked and edited, if necessary, in order to match definitions by the Human Genome Nomenclature Committee[3]. To identify phonology-related genes, we looked for genes that were reported for more than one of the disorders

[1]https://pubmed.ncbi.nlm.nih.gov/advanced
[2]https://www.ncbi.nlm.nih.gov/research/pubtator
[3]https://www.genenames.org

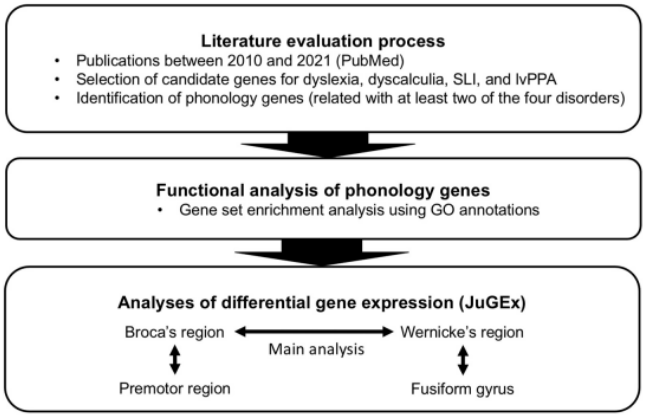

FIGURE 1 | Design of the present study.

using a Venn diagram tool[4]: A phonology-related gene had to be involved in at least two of the four disorders (overlaps).

Functional Enrichment Analysis

Genes were annotated by gene ontology (GO; Gene Ontology Consortium, 2021) using ToppFun, a tool of the ToppGene Suite[5] (Chen et al., 2009). ToppFun was used to find out which GO terms and identifiers (as of 12/03/2021) from the categories "Biological Process," "Molecular Function," or "Cellular Component" were over-represented (enriched) in the list of phonology-related genes from the Venn diagram intersections. The following analytical parameters were chosen: hypergeometric probability mass function as p-value method, Bonferroni corrected q-value < 0.05, gene limits $1 \leq n \leq 2000$, 2 as minimum feature count in the test set. To interpret the relationships of the identified GO terms, we used ancestor charts from QuickGo[6]. These charts are conceptual figures to represent a tree of hierarchically linked GO terms (parental and child terms). Under the same parameters, an enrichment analysis with different pathway annotations was performed with ToppFun which did not yield biologically meaningful significant results possibly due to the small number of candidate genes and/or limited functional annotations for these genes.

Gene Expression Analysis in Cytoarchitectonically Defined Brain Areas

Gene expression differences between pairs of brain regions, technically referred to as volumes of interest (VOIs), were analyzed using the workflow and graphical user interfaces (GUIs) of JuGEx (Bludau et al., 2018). The tool is based on scripts coded in MATLAB (version R2018b, 64 bit; The MathWorks) which are freely accessible (available online[7]). JuGEx integrates regional RNA data from the Allen Human Brain Atlas from three right-handed, two left-handed, and one ambidextrous donors (Hawrylycz et al., 2012) with the three-dimensional cytoarchitectonic probability maps from the Julich-Brain Atlas (Amunts et al., 2020) which are based on observer-independent mapping of cytoarchitectonic areas in ten postmortem brains. Allen Human Brain Atlas and Julich-Brain data are based on brain tissue from deceased adult donors without a psychiatric or neurological diagnosis; the brains did not overlap between both atlas systems (Bludau et al., 2018). The expression data derived from anisotropically distributed tissue samples of Allen Human Brain Atlas and cytoarchitectonic maps from Julich-Brain were registered to the reference space of the Montreal Neuroscience Institute 152 (MNI_{152}) reference brain (Evans et al., 2012). To enable a comparison of gene expression between VOIs in different brains, JuGEx uses relative expression values that were normalized across all regions and six brains from Allen Human Brain Atlas using z-scores (Hawrylycz et al., 2015).

A gene was investigated using the "all-probes mode" which calculates a winsorized mean based on the microarray probes for each gene (Bludau et al., 2018). We considered a p-value smaller than 0.05 as a significant difference between the z-scores of tissue samples in the compared VOIs. The nominal p-values from the permuted n-way analysis of variance (ANOVA) were corrected for multiple comparisons by applying a family-wise error (FWE) correction with the number of analyzed genes ($n = 21$, $p_{FWE} < 0.05$). The permuted n-way ANOVA was repeated 10,000 times with randomly shuffled labels of the analyzed VOIs under the assumption of label exchangeability.

[4]http://bioinformatics.psb.ugent.be/webtools/Venn/

[5]https://toppgene.cchmc.org/enrichment.jsp

[6]https://www.ebi.ac.uk/QuickGO/

[7]https://www.fz-juelich.de/inm/inm-1/jugex

The regional specificity of a gene was defined as significantly higher expression (z-score) in that area (first VOI) compared to another area (second VOI).

Main analysis: In order to define "Broca's region" anatomically, the maps of areas 44 and 45, both cytoarchitectonically described by Amunts et al. (1999, 2004), were merged using JuGEx. We decided to merge both areas considering the spatial resolution of gene expression data in Allen Human Brain Atlas with rather large intervals between sections in relation to the size of the areas. The Te3 map of the Julich-Brain Atlas was used as a proxy for "Wernicke's region," a cytoarchitectonically defined area located in the lateral bulge of the superior temporal gyrus (Morosan et al., 2005). Te3 overlaps in parts with Brodmann's area 22 as defined by Brodmann (1909). Since the left hemisphere is dominant for language in most right- and left-handers (Branch et al., 1964; Mazoyer et al., 2014), we investigated the activity (expression) of potentially functionally relevant candidate genes in the left hemispheres.

Regional specification analysis: To characterize the regional specificity in the frontal lobe, the Julich-Brain maps of premotor areas 6d1, 6d2, and 6d3 were combined and compared with Broca's region. The same was done in the temporal lobe by merging the maps Fg1, Fg2, Fg3, and Fg4 of the fusiform gyrus and by comparing them with Wernicke's region. We considered support for regional specificity if the candidate gene was not significantly upregulated in the non-language areas.

Control analysis: To further evaluate the main analysis, another comparison between Broca's and Wernicke's regions was performed with two additional gene sets. The first set was chosen from the Allen Human Brain Atlas genes and comprised 25 genes, hereafter called "random genes" (**Supplementary Table 6A**). The second set was intentionally taken from the Allen Human Brain Atlas genes and included 14 genes from GWAS of eye, hair, and skin coloration, hereafter called "color genes" (**Supplementary Table 6B**). Both random and color genes were assembled and considered as biological negative controls as described by Bludau et al. (2018).

The following numbers of tissue samples were identified through the aforementioned VOIs in the six brains from Allen Human Brain Atlas using a Julich-Brain map threshold of 20% (this means that only tissue samples were included with a probability of 20% or higher belonging to the corresponding VOIs): left areas 44 and 45 ($n_{\text{tissue samples}} = 25$), left area Te3 ($n_{\text{tissue samples}} = 17$), left areas 6d1, 6d2, and 6d3 ($n_{\text{tissue samples}} = 30$), left areas Fg1, Fg2, Fg3, and Fg4 ($n_{\text{tissue samples}} = 57$). Before statistical analyses, the spatial assignment of tissue samples to maps was manually checked using the "3D visualization" GUI of JuGEx.

The full data of the used maps are provided by the Julich-Brain Atlas *via* the Human Brain Project (available online[8]): Areas 44 (doi: 10.25493/N13Y-Y3F), 45 (doi: 10.25493/K06P-R2S), Te3 (doi: 10.25493/ZZQH-932), 6d1 (doi: 10.25493/KSY8-H3F), 6d2 (doi: 10.25493/WJQ5-HWC), 6d3 (doi: 10.25493/D41S-AG7), Fg1 (doi: 10.25493/RTDM-GK4), Fg2 (doi: 10.25493/N7ZP-17X), Fg3 (doi: 10.25493/F87E-JRA), and Fg4 (doi: 10.25493/MTWF-X4V).

[8]https://search.kg.ebrains.eu/

RESULTS

Phonology-Related Genes From Literature

The literature evaluation process comprised two main steps, a computational text mining of titles, abstracts, and key words, followed by a manual text mining of the whole text body and supplement, to find original research articles and genes (**Figure 2**). The computational text mining of dyslexia, dyscalculia, SLI, and lvPPA literature from the last 11 years using search strings of clinical categories and genetic terms (**Supplementary Table 4**) revealed 643 journal articles. Of these, 98 articles were found more than once, and additional 36 articles were excluded since they were reviews (**Supplementary Table 7A**). Thus, 509 unique research articles provided the basis for further manual text mining which led to the exclusion of another 438 articles that were filtered out with PubTator or did not meet the above mentioned inclusion criteria at whole-text screening. Eventually, 71 research articles remained reporting 77 potential candidate genes (**Supplementary Tables 7B,C**). For the final selection, we put the information of **Supplementary Table 7C** forward to a Venn diagram to seek for overlapping candidate genes from the different disorders (**Figure 3**).

For dyslexia/SLI, we found *ATP2C2* (Newbury et al., 2011; Müller et al., 2017; Martinelli et al., 2021), *CCDC136* (Gialluisi et al., 2014; Adams et al., 2017), *CMAHP* (Eicher et al., 2014), *CMIP* (Newbury et al., 2011; Scerri et al., 2011; Luciano et al., 2018), *CNTNAP2* (Newbury et al., 2011; Peter et al., 2011; Eicher et al., 2013; Luciano et al., 2018), *COL4A2* (Eicher et al., 2013), *FLNC* (Gialluisi et al., 2014; Adams et al., 2017), *FOXP2* (Peter et al., 2011; Wilcke et al., 2012; Eicher et al., 2013; Mozzi et al., 2017; Sánchez-Morán et al., 2018; Doust et al., 2020), *KIAA0319* (Couto et al., 2010; Czamara et al., 2011; Elbert et al., 2011; König et al., 2011; Newbury et al., 2011; Scerri et al., 2011; Cope et al., 2012; Zou et al., 2012; Eicher et al., 2013, 2014; Powers et al., 2013, 2016; Mascheretti et al., 2015; Adams et al., 2017; Carrion-Castillo et al., 2017; Neef et al., 2017; Centanni et al., 2018; Luciano et al., 2018; Sánchez-Morán et al., 2018), *NOP9* (Pettigrew et al., 2016), *RBFOX2* (Gialluisi et al., 2014), *RIPOR2* (Eicher et al., 2014), and *ZNF385D* (Eicher et al., 2013). For dyslexia/dyscalculia, we observed *CYFIP1* (Ulfarsson et al., 2017), *DNAAF4* (Bates et al., 2010; Marino et al., 2011; Paracchini et al., 2011; Mascheretti et al., 2013, 2015; Müller et al., 2017; Luciano et al., 2018), *MYO18B* (Ludwig et al., 2013), *NIPA1* (Ulfarsson et al., 2017), *NIPA2* (Ulfarsson et al., 2017), and *TUBGCP5* (Ulfarsson et al., 2017). For dyslexia/dyscalculia/SLI, we found *DCDC2* (Lind et al., 2010; Czamara et al., 2011; König et al., 2011; Marino et al., 2011, 2012, 2014; Newbury et al., 2011; Scerri et al., 2011; Cope et al., 2012; Eicher et al., 2013, 2014, 2015; Powers et al., 2013, 2016; Cicchini et al., 2015; Gori et al., 2015; Matsson et al., 2015; Adams et al., 2017; Neef et al., 2017; Luciano et al., 2018; Riva et al., 2019) and *ROBO1* (Bates et al., 2011; Mascheretti et al., 2014; Tran et al., 2014; Luciano et al., 2018). From the final

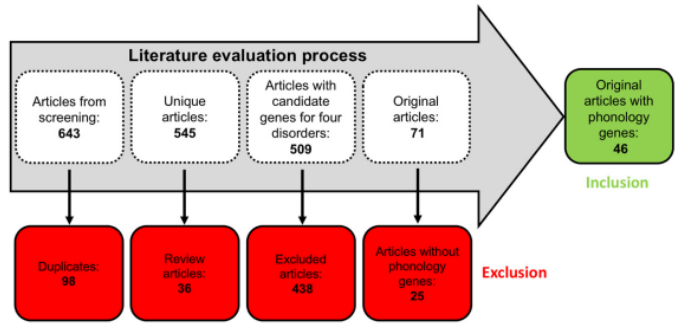

FIGURE 2 | Workflow of the literature evaluation process.

selection of phonology-related candidate genes (**Supplementary Table 7D**), the most significant genetic markers of each gene reported by the original study were extracted and summarized in **Supplementary Table 7E**.

Enrichment Analysis of Phonology-Related Genes

All candidate genes were analyzed for statistical over-representation in GO using ToppFun and the original ancestor charts from GO (Methods section "Functional Enrichment Analysis"). Eleven GO terms showed significant enrichments of phonology-related gene sets that withstood a correction for multiple comparisons (**Table 1**). Total results of this analysis including terms that did not withstand correction are described in **Supplementary Table 8**. The most significant result of the enrichment analysis was the "Biological Process" term "response to auditory stimulus" from the topic *learning*, where we found an enrichment of *CNTNAP2*, *FOXP2*, and *KIAA0319* out of 28 genes from this term (GO:0010996). In hierarchical relationships to this were the child terms "vocal learning" and "response to auditory behavior," where the genes *CNTNAP2* and *FOXP2* were enriched. Within the top eleven results were three additional GO terms which support *learning*. They form a group of terms (cluster), where the neighboring cluster starts at the parent term "cognition" (GO:0050890; enriched genes *CNTNAP2, CYFIP1, DCDC2, DNAAF4, FOXP2*), went over "observational learning" (GO:0098597) and "imitative learning" (GO:0098596) and finally ended this GO term path in "vocal learning."

The second and third most significant GO terms were "dendrite development" (GO:0016358), enriched by *CYFIP1, DCDC2, KIAA0319, RBFOX2*, and *ROBO1*, and "cellular component morphogenesis" (GO:0032989), enriched by *CCDC136, CNTNAP2, CYFIP1, DCDC2, KIAA0319, RBFOX2*, and *ROBO1*, both pointing to *neuronal development* as the second big topic of the enrichment analysis. This finding was complemented by the two terms from the GO category "Cellular Component" "neuron projection membrane" (GO:0032589) and "axolemma" (GO:0030673) and the "Biological Process" category

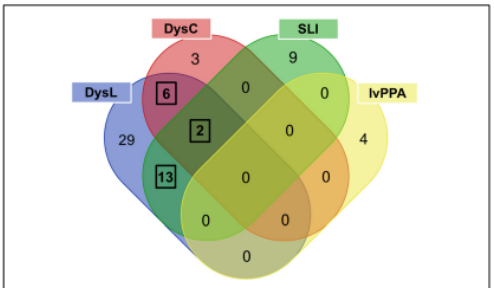

FIGURE 3 | Venn diagram used to determine phonology-related genes from candidate genes overlapping between language and/or learning disorders. The three black frames indicate overlaps of genes associated with at least two disorders. DysL, dyslexia; DysC, dyscalculia; SLI, specific language impairment; lvPPA, logopenic variant of primary progressive aphasia.

term "cell morphogenesis involved in neuron differentiation" (GO:0048667). The only GO term from the "Molecular Function" category among our significant results was "magnesium ion transmembrane transporter activity" (GO:0015095).

Expression of Phonology-Related Genes in Broca's and Wernicke's Regions

In the main analysis, eighteen candidate genes showed similar expression levels in Broca's and Wernicke's regions ($p > 0.05$; **Table 2**). To allow an exploratory classification of these candidates in above-average and below-average expression, we calculated a mean value over all genes using their z-scores from Broca's and Wernicke's regions ($\bar{x} = 0.125$) and found twelve genes expressed above-average (overall mean > 0.125): *ATP2C2, CMAHP, CMIP, CNTNAP2, CYFIP1, DCDC2, DNAAF4, FOXP2, NIPA2, RBFOX2, RIPOR2*, and *TUBGCP5*, while *DCDC2* showed the highest expression (overall mean = 0.573; **Table 2**). Three genes were differentially expressed between both regions:

ATP2C2 showed a higher expression level in Broca's region as compared to Wernicke's region ($p = 0.0291$). *DNAAF4* ($p = 0.0001$) and *FOXP2* ($p = 0.0006$) showed higher expression levels in Wernicke's region, both were stable against correction for multiple comparisons ($p_{FWE} < 0.05$). The fine-mapped expression patterns of the three differentially expressed genes are shown in **Figure 4**.

Two types of follow-up analyses were performed. The regional specificity analysis in the frontal lobe found significantly higher expression levels in Broca's region for *CNTNAP2* ($p = 0.001$) and *DCDC2* ($p = 0.002$), both $p_{FWE} < 0.05$, compared with the language unspecific premotor area (areas 6d1-6d3; **Supplementary Table 9A**); in the temporal lobe, Wernicke's region vs. fusiform gyrus (areas Fg1-Fg4) yielded no significant differential expression ($p > 0.05$; **Supplementary Table 9B**). The control analysis tested random and color genes, each, in Broca's versus Wernicke's regions. Neither of the two analyses demonstrated a differential expression stable against correction (both $p_{FWE} > 0.05$; **Supplementary Tables 9C,D**).

DISCUSSION

Prior studies have been looking for links between risk genes and phonological aspects in individual disorders. Here we went beyond this point and addressed a more fundamental question, i.e., to identify cross-disease candidate phonological genes whose activity (expression level) we wanted to characterize in key regions of the language network using brain atlas-guided expression mapping. To achieve this, our approach comprised three steps. A systematic literature review that identified 21 phonology-related genes for developmental language and/or learning disorders. An expression analysis found that 12 of these genes were active in Broca's and Wernicke's regions, with two genes being more active in Wernicke and one gene being more active in Broca suggesting functional specialization. An enrichment analysis that found out that nine of these genes may contribute to processes of *learning* and *neuronal development*.

Literature Evaluation Identified Candidate Genes for Three Disorders

Our literature evaluation was designed on the assumption that phonological processing may have a common biological basis in the selected disorders, i.e., the "gene overlap hypothesis." At the behavioral level, for example, impairments in working memory (Attout and Majerus, 2015; Gray et al., 2019; Johnson et al., 2020) and in learning ability (Rogalski et al., 2008; Bishop, 2009; Landerl et al., 2009) are evident in dyslexia, dyscalculia, SLI, and lvPPA, in addition to phonological impairment. These aspects are closely linked to phonology. However, since mainly linguistic variables of these disorders were investigated in the underlying studies, there is evidence that all genes can be assigned as phonology-related, although it cannot be assumed that this would be exclusively the case.

Because we based our candidate gene search on findings in cohorts of European ancestry, we had to ignore some potentially interesting candidates from the recent literature. One example was a GWAS of rapid automatized naming and rapid alternating stimulus conducted in Hispanic American and African American

TABLE 1 | Results of the functional enrichment analysis of phonology-related genes.

Term name	Term identifier	GO Category	Hit count query/genome	Phonology-related genes in term genes	*p*-value[#]
Response to auditory stimulus	GO:0010996	Biological Process	3/28	*CNTNAP2, FOXP2, KIAA0319*	**2.67E-06**
Dendrite development	GO:0016358	Biological Process	5/310	*CYFIP1, DCDC2, KIAA0319, RBFOX2, ROBO1*	**1.05E-05**
Cellular component morphogenesis	GO:0032989	Biological Process	7/914	*CCDC136, CNTNAP2, CYFIP1, DCDC2, KIAA0319, RBFOX2, ROBO1*	**1.75E-05**
Vocal learning	GO:0042297	Biological Process	2/7	*CNTNAP2, FOXP2*	**1.95E-05**
Imitative learning	GO:0098596	Biological Process	2/7	*CNTNAP2, FOXP2*	**1.95E-05**
Cognition	GO:0050890	Biological Process	5/375	*CNTNAP2, CYFIP1, DCDC2, DNAAF4, FOXP2*	**2.64E-05**
Observational learning	GO:0098597	Biological Process	2/9	*CNTNAP2, FOXP2*	**3.34E-05**
Cell morphogenesis involved in neuron differentiation	GO:0048667	Biological Process	6/715	*CYFIP1, DCDC2, KIAA0319, RBFOX2, RIPOR2, ROBO1*	**4.86E-05**
Neuron projection membrane	GO:0032589	Cellular Component	3/73	*CNTNAP2, RIPOR2, ROBO1*	**5.69E-05**
Magnesium ion transmembrane transporter activity	GO:0015095	Molecular Function	2/16	*NIPA1, NIPA2*	**1.33E-04**
Axolemma	GO:0030673	Cellular Component	2/21	*CNTNAP2, ROBO1*	**2.12E-04**

[#]*P-value of the underlying hypergeometric probability mass function.*
Bold: p-value stable against correction for multiple comparisons (Bonferroni adjusted q-value < 0.05).

cohorts (Troung et al., 2019). Both parameters are considered as predictors for reading disability and may be relevant for investigating phonological processing. However, we could not consider the genes *RPL7P34* and *RNLS* from this study. The reason is that genomic and transcriptomic variability (in normal and diseased individuals) may be influenced by population stratification, especially common variation is sensible to this, e.g., SNPs mapping to genes or influencing expression. To avoid this bias, we wanted to keep the data sources (study cohorts) as homogenous as possible.

The gene extractions from the consecutive computational and manual text mining were put forward to the overlap analysis (**Figure 3** and **Supplementary Table 7C**) which revealed that the number of common phonology-related genes was 13 for dyslexia/SLI, six for dyslexia/dyscalculia, and two for dyslexia/dyscalculia/SLI, resulting in 21 genes in total (**Supplementary Table 7D**). Hence, three disorders contributed to this result, wherein dyslexia was connected to each phonology-related gene. The fourth language disorder, lvPPA, did not share any of its four genes (*APOE, APP, GRN, MAPT*) with the other disorders. LvPPA is a rare disease in the population and only a small number of putative risk genes are known yet (Gorno-Tempini et al., 2004, 2008). This is an important result and does not contradict our initial hypothesis. We consider it rather informative that the genuine developmental disorders with phonological core aspects cluster together and are somewhat distinct from a neurodegenerative disorder with acute phonological but developmentally more general learning deficits (Gorno-Tempini et al., 2008). We have examined lvPPA with the other disorders because there are two arguments from a clinical point of view: First, lvPPA shows clear phonological symptoms, which is why it belongs to the logopedic disorders. Second, Rogalski et al. (2008), for example, showed that patients with PPA are often affected by learning disorders earlier in life before the late-onset of PPA. The chance of a gene overlap with the more polygenic developmental disorders was therefore smaller. Overall, our evaluation supports the view of different molecular processes underlying lvPPA compared to the investigated developmental disorders.

Gene Enrichment Analysis Implicated Learning and Neuronal Development

Besides the fact that phonological processing is affected in developmental language and/or learning disorders, phonology is the motor for various language learning processes including writing (Treiman, 2017). To explore if phonology-related genes expressed in Broca's and Wernicke's regions acting together in the same Biological Processes, Molecular Functions, and Cellular Components, we performed an enrichment analysis using annotations of gene functions (GO terms). The overall results highlight relationships that can be summarized under the topics *learning* and *neuronal development*. Our findings may

TABLE 2 | Results of the main expression analysis of phonology-related genes.

Gene	Expression levels (mean *z*-score and standard deviation)			*p*-value
	Broca's region ($n_{\text{tissue samples}}$ = 25)	Wernicke's region ($n_{\text{tissue samples}}$ = 17)	Overall mean	
DNAAF4[1]	−0.024 ± 0.193	0.353 ± 0.262	0.129 ± 0.290	**0.0001***
FOXP2	0.270 ± 0.321	0.528 ± 0.254	0.375 ± 0.322	**0.0006***
ATP2C2	0.501 ± 0.242	0.182 ± 0.337	0.372 ± 0.325	**0.0291**
ZNF385D	0.076 ± 0.137	0.012 ± 0.320	0.050 ± 0.231	0.1046
NOP9[2]	−0.237 ± 0.683	−0.082 ± 0.732	−0.174 ± 0.707	0.1533
MYO18B	−0.263 ± 0.464	−0.071 ± 0.657	−0.185 ± 0.558	0.1907
RBFOX2[3]	0.272 ± 0.356	0.139 ± 0.509	0.218 ± 0.430	0.2055
NIPA1	−0.437 ± 0.494	−0.292 ± 0.459	−0.378 ± 0.478	0.2261
CMAHP[4]	0.469 ± 0.241	0.346 ± 0.319	0.419 ± 0.280	0.2643
DCDC2	0.593 ± 0.624	0.543 ± 0.563	0.573 ± 0.601	0.2655
RIPOR2[5]	0.335 ± 0.240	0.433 ± 0.350	0.375 ± 0.293	0.2812
NIPA2	0.444 ± 0.405	0.300 ± 0.303	0.386 ± 0.374	0.2856
CYFIP1	0.222 ± 0.366	0.402 ± 0.477	0.294 ± 0.424	0.4179
CMIP[6]	0.065 ± 0.479	0.126 ± 0.432	0.090 ± 0.461	0.4207
ROBO1	−0.409 ± 0.331	−0.373 ± 0.400	−0.394 ± 0.361	0.4632
CCDC136	−0.309 ± 0.394	−0.368 ± 0.574	−0.332 ± 0.476	0.5643
CNTNAP2	0.507 ± 0.241	0.411 ± 0.305	0.468 ± 0.273	0.6852
COL4A2	0.088 ± 0.563	0.222 ± 0.384	0.142 ± 0.503	0.6864
FLNC	−0.281 ± 0.536	−0.298 ± 0.667	−0.288 ± 0.592	0.7665
TUBGCP5	0.500 ± 0.328	0.493 ± 0.422	0.497 ± 0.369	0.827
KIAA0319	−0.041 ± 0.266	−0.079 ± 0.259	−0.056 ± 0.264	0.8784

Bold: significant p-value (uncorrected).
**P-value stable against correction for multiple comparisons using FWE.*
Previous and alias symbols: [1]DYX1C1; [2]C14orf21; [3]RBM9; [4]CMAH; [5]FAM65B; [6]TCMIP and KIAA1694.

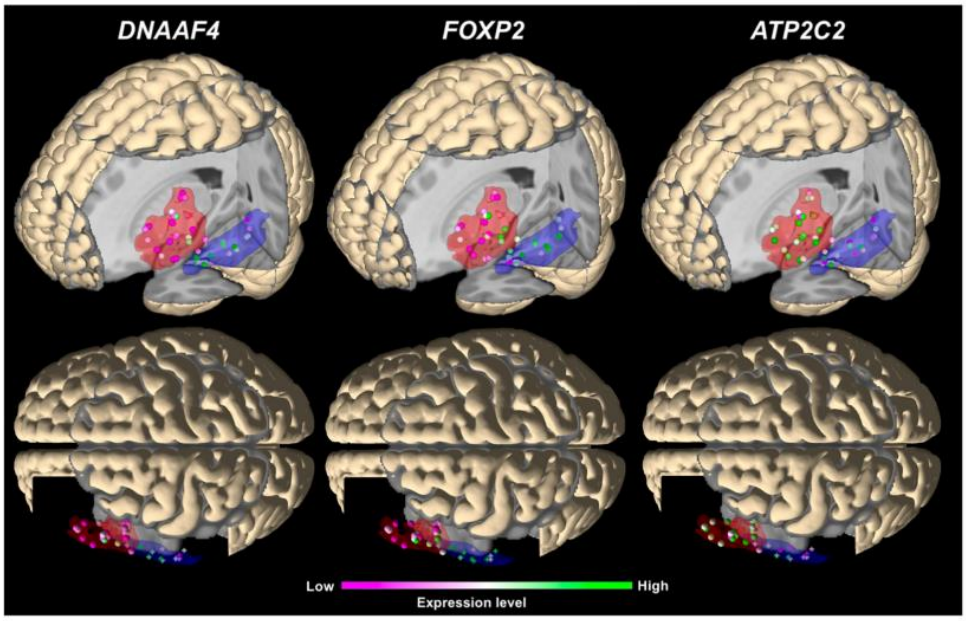

FIGURE 4 | 3D visualization of the main expression analysis using JuGEx in lateral views (top panels) and dorsal views (bottom panels) displaying the three significantly differentially expressed genes: *DNAAF4* and *FOXP2* show higher expression (FWE-corrected) in Wernicke's region and *ATP2C2* in Broca's region. Investigated tissue samples are represented by spheres in the red areas (Broca's region) and crosses in the blue areas (Wernicke's region). RNA expression levels are indicated by z-scores showing ranges between maximal (green) and minimal values (pink).

strengthen the links between phonology and behavioral and/or clinical aspects of the three investigated disorders.

Regarding *learning*, the most significant GO term was "response to auditory stimulus" referring to a process that results in a change in state or activity of a cell or an organism, e.g., gene expression, as a result of an auditory stimulus pointing to the aspect of hearing. In general, auditory processing forms the basis for phonological processing. In case of decreasing auditory performance caused by acquired hearing impairment, studies report a negative influence on phonological representations, for instance, a high working memory capacity was a compensating factor for negative impact of auditory deprivation on phonological processing abilities (Classon et al., 2013). Similar results were found for dyslexia and SLI. In fact, both disorders showed a substantial overlap concerning auditory processing and phonological skills (Fraser et al., 2010). For dyslexia, a link between hearing and reading abilities is known, i.e., changes in brain networks involved in phonological processing lead to deficits in matching speech sounds to their corresponding visual representations (Wallace, 2009).

Another finding of the topic *learning* provides a link between the term "vocal learning," the transcription factor gene *FOXP2*, and one of its prominent transcriptional targets, the cell adhesion and receptor gene *CNTNAP2*, both contributing to all GO terms of the topic *learning*. Since the genes occur in five of eight outcomes, it can be concluded that both genes exert some dominance on result generation. A reason could be that there is plenty of experimental data on both in the literature and databases compared to other genes of our investigation. As *FOXP2* is important in human language development and its disorders, its avian homolog *FoxP2* is thought to play a crucial role in vocal learning and possible deficits in song-learning birds (Jarvis, 2019). *CNTNAP2* was associated with neurodevelopmental disorders including language deficits (Vernes et al., 2008) and variation in language development in the general population (Whitehouse et al., 2011). Recent results suggested that *CNTNAP2* is involved in a developmental cascade of effects in infants where it controls rapid auditory processing leading to early expressive language (Riva et al., 2018).

When comparing the two above-mentioned terms "response to auditory stimulus" and "vocal learning," one gene (*KIAA0319*) only occurred in the term "response to auditory stimulus" and hence was probably the gene that distinguishes both findings. This observation may be interesting since a knock down of

Kiaa0319 expression in a rat model altered cortical responses and sound processing in the auditory cortex which was taken as an analogy for phoneme processing in humans (Centanni et al., 2014). *KIAA0319* encodes a cell adhesion molecule involved in development of the cerebral cortex. In fact, the gene mediates adhesion between migrating neurons and radial glial fibers as well as it regulates the morphology of dendrites (Peschansky et al., 2010). On the question of *KIAA0319* being functionally related to *FOXP2*, there is little literature. In a fMRI study by Pinel et al. (2012) in a reading task in healthy subjects, they found evidence that common genetic variations (SNPs) in both genes may play an important role in language development and in normally developed language networks, but in different cerebral pathways: two *FOXP2* SNPs were associated with variations of activation in the left frontal cortex, while one *KIAA0319* SNP was associated with asymmetry in functional activation of the superior temporal sulcus.

The GO term "dendrite development" was the second most significant enrichment result and addresses the progression of dendrites, from its formation to a mature structure. Five of our candidate genes contributed to this term (*CYFIP1*, *DCDC2*, *KIAA0319*, *RBFOX2*, *ROBO1*). Dendritic extensions propagate electrochemical signals received from other neural cells to the cell body of the neuron. These issues are important constituents of learning and behavior, including synaptic plasticity, and therefore build a strong content-related connection to our first topic (*learning*). *CYFIP1* coordinates the translation of messenger RNA at dendrites (Crespi, 2017). High expression of *CYFIP1* due to gene duplication has been associated with autism (Oguro-Ando et al., 2015). Conversely, low expression by gene deletion was associated with risk of schizophrenia and impaired cognition among otherwise-neurotypical individuals (Stefansson et al., 2008, 2014; Tam et al., 2010). The deletion also affects cognitive, structural, and functional correlates of dyslexia as well as dyscalculia and mediates the strongest risk to the combined disorders (Ulfarsson et al., 2017). A GWAS found association between reading and language skills and SNP rs5995177 in *RBFOX2* (Gialluisi et al., 2014). It encodes an alternative splicing regulator (RNA binding fox-1 homolog 2) involved in brain development (Gehman et al., 2012). A follow-up candidate gene study found a generalized effect of the SNP on cortical thickness in reading- and language-related brain regions of healthy adults (Gialluisi et al., 2017). The rodent homolog of *ROBO1* (*Robo1*) encodes the roundabout guidance receptor 1 which is known for regulating the midline crossing of commissural nerve tracts, a process essential for mammalian brain formation. In family pedigrees from Finland, a rare *ROBO1* haplotype was identified which dominantly co-segregates with the dyslexia diagnosis (Hannula-Jouppi et al., 2005). Individuals who carried this *ROBO1* variant showed dose-dependent impaired interaural interaction suggesting that crossing of the auditory pathways requires an adequate *ROBO1* expression during development (Lamminmäki et al., 2012). *DCDC2* and *KIAA0319* provide experimental evidence for a dual role in both topics. In *neuronal development*, *DCDC2* (doublecortin domain-containing protein 2) is involved in regulating neuronal migration, especially for the cerebral cortex (Galaburda et al., 2006). In *learning*, *DCDC2* was associated with phonological awareness and auditory phonological representations (Goswami, 2011; Eicher et al., 2015). *KIAA0319* (neuronal migration) mediates axon guidance as well as dendrite formation. In this respect, *DCDC2* and *KIAA0319* are among the most studied genes in language and/or learning disorders and future studies of phonological processing that aggregate variation of all five genes seem to be worthwhile.

Expression Analysis Revealed Putative Roles of *ATP2C2*, *DNAAF4*, and *FOXP2*

Expression differences of a gene in two language network regions are not direct evidence for a functional involvement of this gene in phonological processing. However, this arises from combining expression mapping and gene function associated with phonology determined in previous studies. The same is true for associations with disorders, because the expression data from the Allen Human Brain Atlas and mapping data from the Julich-Brain Atlas were collected in brains of people who had no history for neurological or psychiatric disease. Since the Allen expression data do not provide additional genotype data, we cannot directly examine the relationship between genome (genotype), transcriptome (RNA), and phenotype (disease or imaging trait like gray matter volume).

Regarding the main analysis, we found evidence for a significant differential expression of three phonology-related genes. In fact, expression of *ATP2C2* was upregulated in Broca's region, while expression of *DNAAF4* and *FOXP2* was upregulated in Wernicke's region. The regional specification analyses for the frontal and the temporal lobes showed that almost all phonology-related genes, including our top findings, were not differentially expressed between Broca's region and premotor region (6d1–6d3) in the frontal lobe, and between Wernicke's region and fusiform gyrus (Fg1-Fg4) in the temporal lobe (**Supplementary Tables 9A,B**). The only follow-up analysis showing a significant and FWE correction-stable expression difference, was the frontal lobe comparison, revealing a higher expression of *CNTNAP2* and *DCDC2* in Broca suggesting their activity in this part of the language network. Because none of our candidate genes was significantly upregulated after correction in the non-language areas, we hypothesize that *ATP2C2, DNAAF4,* and *FOXP2* were specifically expressed in cortical regions being language and/or phonology relevant. To further evaluate the biological specificity of these results, we performed two additional control analyses. Neither the genes of a random selection from the whole transcriptome nor the genes of human body coloration achieved a correction stable result. Both negative results, together with knowledge about the disorders, brain regions, and gene functions, supported the specificity of regional expressions of *ATP2C2, DNAAF4*, and *FOXP2*.

The literature analysis suggested an overlap between dyslexia and SLI for *ATP2C2* (Newbury et al., 2011; Müller et al., 2017; Martinelli et al., 2021). In the enrichment analysis, it did not show up among our top findings but provided nominal significance in a gene set with *ROBO1* for a non-brain related biological process (**Supplementary Table 8**). Different studies provided evidence that *ATP2C2* is involved in phonological processing, for instance, regarding a modulation of phonological working

memory in language impairment (Newbury et al., 2009; Smith et al., 2015). *ATP2C2* encodes a magnesium-dependent calcium transporter. Regarding a translation of our *ATP2C2* finding to a clinical level, it seems to be important that imbalances of magnesium and calcium ions in blood serum were reported in patients with dyslexia and other communication disorders (Kurup and Kurup, 2003).

For *DNAAF4*, the literature analysis provided a link between dyscalculia and dyslexia. In the enrichment analysis, the gene was part of the GO term "cognition" highlighting the topic *learning*. *DNAAF4*, formerly known as *DYX1C1* (dyslexia susceptibility 1 candidate 1), was described as axonemal dynein assembly factor required for ciliary motility (Tarkar et al., 2013). More relevant for our study was a previous finding of a protein-protein interaction with estrogen receptors possibly linking its well-known role in neuronal migration during cortical development to an involvement of hormonal pathways in the development of dyslexia (Wang et al., 2006; Massinen et al., 2009). In this line, *DNAAF4* was found to be associated with phonological memory in dyslexia (Lim et al., 2014) as well as with phonological working memory in healthy participants (Marino et al., 2007). Of note, knockdown of *Dnaaf4* in rat embryos demonstrated effects on auditory processing, visual attention as well as cortical and thalamic anatomy (Szalkowski et al., 2013). In humans, two SNPs, rs17819126 in *DNAAF4* and rs8053211 in *ATP2C2*, represented the only correction stable results in an association screen of ten candidate genes tagged by 23 independent SNPs for event-related potential mismatch response, an indicator for auditory discrimination capabilities in dyslexia patients (Müller et al., 2017). Müller et al. (2017) provided evidence that genetic variation in *ATP2C2* and *DNAAF4* may be a putative modulator of mismatch response in dyslexia. This aspect is highly interesting since auditory discrimination is an essential prerequisite for phonological processing and should be investigated in a future study, especially in context with disease-dependent changes of structural and functional connectivity between Broca's and Wernicke's regions.

FOXP2 is considered to be one of the most important genes for speech development and disorder. Its relevance was hypothesized when rare variation (a missense mutation) was discovered in members of a British family with frequent problems in articulating, formulating, and understanding of speech (Lai et al., 2001). Subsequently, common variation (SNPs) was investigated at this gene locus and associations between SNPs and dyslexia as well as other language and/or learning disorders were identified (Mascheretti et al., 2017). *FOXP2* expression is relevant during brain development, when the transcription factor controls the transcriptional activity of different target genes, e.g., *CNTNAP2* (Castro Martínez et al., 2019). Our literature evaluation provided a link between *FOXP2* and dyslexia and SLI (Eicher et al., 2013; Doust et al., 2020). In our enrichment analysis, the gene contributed to the best findings of the topic *learning*. The significantly higher expression of *FOXP2* in Wernicke's region may fit to a finding of a study by Wilcke et al. (2012). The authors report that the dyslexia-associated SNP rs12533005 in *FOXP2* was associated with grapheme-phoneme correspondence abilities (linking letters to speech sounds) in written language in an inferior parietal area near Wernicke's region involved in phonological processing (Wilcke et al., 2012). We speculate whether the higher activity of *FOXP2* in Wernicke's region could support the concept of regional specificity. Currently, *FOXP2* is mainly known as a gene linked to childhood apraxia of speech and speech motor planning deficits (Morgan et al., 2016). The possible link between *FOXP2* and phonology could be a new aspect to investigate further in the future.

Limitations

The search criteria ("clinical categories") of the literature evaluation were rather broad to cover the terminological variability between published studies of the four different disorders as much as possible. Consequently, we had to make the compromise of obtaining results at the genomic level that contained broader findings in addition to the desired disorders, e.g., genes for arithmetical weakness in case of dyscalculia. Basically, we only extracted markers and genes from a study that were self-reported as best findings by the study authors. We specified $p < 0.05$ for criterion (c) as a general threshold for significance; for GWAS, we tried to stick to genome-wide significant findings ($p < 5 \times 10^{-8}$) if reported. Thus, we always stayed within the logic of the respective study and did not make an arbitrary decision for or against a selection. This is the reason why we did not consider negative findings in our study. Many phonology-related genes have been selected from traditional candidate gene studies rather than large studies such as GWAS. The main reason is that we studied four disorders for which the literature is very diverse. Some disorder phenotypes already have GWAS, while others do not yet. Therefore, we did not prioritize study types in the design (GWAS, candidate gene study, linkage study). This may be a limitation, but in practice it was not feasible otherwise. Therefore, our gene selection may be interpreted with caution. To minimize the risk of unrecognized studies and genes, we performed a supporting search in the GWAS Catalog database for common genetic variants and their mapped genes across the four disorders during the period of the primary literature search (2010–2021). Despite thorough mining, we could not prevent the selection of gene markers with weak replication evidence in independent studies, e.g., *RBFOX2*. Again, we urge caution in interpreting the results. Ultimately, only meta-analyses will help to separate the robust associations from the false positives.

The assumption of the enrichment analysis was that the phonology-related genes we have yet to find will be consistent with what is already known about phonological processing and/or its genetic basis which may not always be true. The enrichment analysis can only be as accurate as the underlying annotations (GO categories) since not all genes, especially in humans, have phenotype annotations and there are many genes whose functions are not defined yet. As a result of these limitations, enrichments may arise in GO terms where certain genes show noticeable dominance that may bias interpretation, e.g., *CNTNAP2* and *FOXP2* in the terms of the topic "learning." This is a caveat to keep in mind when interpreting results.

In the expression analysis, we focused on Broca's and Wernicke's regions. This does not mean that we ignore the broader network including the subcortical regions from which we did not include basal ganglia and striatum because these structures are associated with speech motor processes rather than phonology (Eickhoff et al., 2009). A similar reason applies for the cerebellum which is mainly responsible for speech motor control (Houde and Nagarajan, 2011). Because of the left hemispheric dominance for language for left- and right-handed people (Branch et al., 1964; Mazoyer et al., 2014), and the fact that there is more data for the left hemisphere in the Allen Human Brain Atlas expression data, only data from the left hemisphere were analyzed. Although the exclusive use of left hemispheric data is based on a strong biological assumption, this should still be considered as a possible limitation and taken into account when interpreting the data. Areas 44 and 45 were combined into one single VOI, considering the spatial constraints of availability of gene expression data, which did not allow searching in a more detailed way. At the same time, differences between both areas at the level of cyto- and receptorarchitecture (Amunts et al., 2010) as well as connectivity and function (Anwander et al., 2007; Friederici and Gierhan, 2013) have been described in the past, and the functional specialization of both areas undergoes changes during ontogeny until it is finally differentiated (Amunts et al., 2003; Skeide and Friederici, 2016). Therefore, it can be hypothesized that both areas may also differentially contribute to the findings of the present study. In addition, it cannot be excluded that the detected expression differences between Broca's and Wernicke's regions were influenced, to a certain degree, by differences in their normal cell type proportions of the bulk tissue used by Allen Brain. Further studies will be necessary to more precisely elucidate the role of the different cortical areas underlying Broca's and Wernicke's regions. The strength of the dataset used is the dense spatial coverage of the tissue samples whose gene expressions were analyzed. Together with the probability-based location information contained in the Julich-Brain maps, a meaningful differential gene expression analysis can be calculated. However, the relatively small number of six donors is also a statistical limitation that would suggest further molecular genetic analyses.

Conclusion

In the present study, we gathered previously published evidence for genetic factors underlying phonological processing symptoms of the language and learning disorders dyslexia, dyscalculia, and SLI and performed expression fine-mapping in two key regions of the language network. While most previous studies sought to link candidate genes and phonological aspects of a single disorder, we focused on a more general aim, to understand whether a symptom, i.e., phonological processing, may have a common genetic regulation in different disorders. Overall, the identified regional expression of *ATP2C2*, *DNAAF4*, and *FOXP2* together with markers from the literature provide evidence of a putative role not only in impaired phonological processing but also for the healthy subjects. In this regard, our study may be a use-case for larger studies on the genetics of phonological processing in the future. To investigate new hypotheses for such gene-phenotype correlates *in vivo*, one option would be to test for association between DNA variation (SNPs, copy-number variants) at candidate gene loci and effects on phonological processing in cortical areas like Broca's and Wernicke's regions, and also in subcortical areas of the language network using large samples of the three disorders and beyond at different ages.

DATA AVAILABILITY STATEMENT

Data from Allen Human Brain Atlas are available at http://human.brain-map.org/ and data from Julich-Brain are available at https://www.jubrain.fz-juelich.de. A stand-alone version of JuGEx is available at http://www.fz-juelich.de/inm/inm-1/jugex. JuGEx is also part of the Atlas of the Human Brain Project, available at https://www.humanbrainproject.eu/en/explore-the-brain/atlases/.

ETHICS STATEMENT

The study computationally analyzed data from the Allen Human Brain Atlas and Julich-Brain Atlas. For Allen Brain: Brain tissues were collected after obtaining informed consent from the decedent's next-of-kin. Institutional Review Board review and approval were obtained for the collection of tissue and non-identifying case information at the tissue banks and repositories that provided tissue for this project (http://help.brain-map.org/display/humanbrain/Documentation). For Julich-Brain: The brains were obtained through the body donor program of the Department of Anatomy at the University of Düsseldorf in accordance with the rules of the local ethics committee (#4863). The patients/participants' next of kind provided their written informed consent to participate in this study.

AUTHOR CONTRIBUTIONS

NU, DIH, and TWM conducted analyses. NU, SH, KA, and TWM analyzed and interpreted the results. SB supported the JuGEx analyses. PP provided digital versions of the cytoarchitectonic probability maps. SH, SC, KA, and TWM supervised all aspects of the study. NU wrote a first draft of the manuscript. All authors critically revised the manuscript and approved its publication.

FUNDING

This research was supported by the European Union's Horizon 2020 Research and Innovation Program [Specific Grant Agreement No. 785907 (Human Brain Project SGA2) and Specific Grant Agreement No. 945539 (Human Brain Project SGA3) to SC and KA] as well as by the Swiss National Science Foundation (SNSF, grant 156791 to SC).

SUPPLEMENTARY MATERIAL

The Supplementary Material for this article can be found online at: https://www.frontiersin.org/articles/10.3389/fnins.2021.680762/full#supplementary-material

Supplementary Table 1 | Overview of phonological deficits in the four investigated disorders.

Supplementary Table 2 | Overview of studies on Broca's and Wernicke's regions in humans and model organisms.

Supplementary Table 3 | Literature evaluation—The eleven single searches using PubMed Advanced Search.

Supplementary Table 4 | Literature evaluation—PubMed Advanced Search combining clinical categories and genetic terms for the identification of phonology-related genes.

Supplementary Table 5 | Literature evaluation—Clinical categories found in research articles.

Supplementary Table 6A | Gene expression analysis—Random genes used as negative control.

Supplementary Table 6B | Gene expression analysis—Color genes used as negative control.

Supplementary Table 7A | Literature evaluation—The 36 excluded review articles.

Supplementary Table 7B | Literature evaluation—The 71 research articles providing the 77 candidate genes.

Supplementary Table 7C | Literature evaluation—The 77 candidate genes from the remaining 71 research articles.

Supplementary Table 7D | Literature evaluation—Basic annotation of the 21 phonology-related genes.

Supplementary Table 7E | Literature evaluation—The genetic items extracted from the 21 phonology-related genes.

Supplementary Table 8 | Total results of the functional enrichment analysis of phonology-related genes.

Supplementary Table 9A | Follow-up gene expression analysis in the frontal lobe—Phonology-related genes—Broca's region vs. premotor areas.

Supplementary Table 9B | Follow-up gene expression analysis in the temporal lobe—Phonology-related genes—Wernicke's region vs. fusiform gyrus.

Supplementary Table 9C | Follow-up gene expression analysis—Random genes—Broca's region vs. Wernicke's region.

Supplementary Table 9D | Follow-up gene expression analysis—Color genes—Broca's region vs. Wernicke's region.

REFERENCES

Aboitiz, F., Aboitiz, S., and García, R. R. (2010). The phonological loop: a key innovation in human evolution. *Curr. Anthropol.* 51, S55–S65. doi: 10.1086/650525

Adams, A. K., Smith, S. D., Truong, D. T., Willcutt, E. G., Olson, R. K., DeFries, J. C., et al. (2017). Enrichment of putatively damaging rare variants in the DYX2 locus and the reading-related genes CCDC136 and FLNC. *Hum. Genet.* 136, 1395–1405. doi: 10.1007/s00439-017-1838-z

Allen Human Brain Atlas (2013). *Case Qualification and Donor Profiles. Technical White Paper*. v7. 2013. Seattle, WA: Allen Human Brain Atlas.

American Psychiatric Association (1994). *Diagnostic and Statistical Manual of Mental Disorders: (DSM-IV)*, 4th Edn. Washington, DC: American Psychiatric Publishing.

American Psychiatric Association (2013). *Diagnostic and Statistical Manual of Mental Disorders: (DSM-5)*, 5th Edn. Washington, DC: American Psychiatric Publishing.

Amunts, K., Lenzen, M., Friederici, A. D., Schleicher, A., Morosan, P., Palomero-Gallagher, N., et al. (2010). Broca's region: novel organizational principles and multiple receptor mapping. *PLoS Biol.* 8:e1000489. doi: 10.1371/journal.pbio.1000489

Amunts, K., Mohlberg, H., Bludau, S., and Zilles, K. (2020). Julich-brain: a 3D probabilistic atlas of human brain's cytoarchitecture. *Science* 369, 988–992. doi: 10.1126/science.abb4588

Amunts, K., Schleicher, A., and Zilles, K. (2004). Outstanding language competence and cytoarchitecture in Broca's speech region. *Brain Lang.* 89, 346–353. doi: 10.1016/S0093-934X(03)00360-2

Amunts, K., Schleicher, A., Bürgel, U., Mohlberg, H., Uylings, H. B. M., Zilles, K., et al. (1999). Broca's region revisited: cytoarchitecture and intersubject variability. *J. Comp. Neurol.* 412, 319–341. doi: 10.1002/(SICI)1096-9861(19990920)412:2<319::AID-CNE10<3.0.CO;2-7

Amunts, K., Schleicher, A., Ditterich, A., and Zilles, K. (2003). Broca's region: cytoarchitectonic asymmetry and developmental changes. *J. Comp. Neurol.* 465, 72–89. doi: 10.1002/cne.10829

Anwander, A., Tittgemeyer, M., von Cramon, D. Y., Friederici, A. D., and Knösche, T. R. (2007). Connectivity-based parcellation of Broca's area. *Cereb. Cortex* 17, 816–825. doi: 10.1093/cercor/bhk034

Attout, L., and Majerus, S. (2015). Working memory deficits in developmental dyscalculia: the importance of serial order. *Child Neuropsychol.* 21, 432–450. doi: 10.1080/09297049.2014.922170

Bates, T. C., Lind, P. A., Luciano, M., Montgomery, G. W., Martin, N. G., and Wright, M. J. (2010). Dyslexia and DYX1C1: deficits in reading and spelling associated with a missense mutation. *Mol. Psychiatry* 15, 1190–1196. doi: 10.1038/mp.2009.120

Bates, T. C., Luciano, M., Medland, S. E., Montgomery, G. W., Wright, M. J., and Martin, N. G. (2011). Genetic variance in a component of the language acquisition device: ROBO1 polymorphisms associated with phonological buffer deficits. *Behav. Genet.* 41, 50–57. doi: 10.1007/s10519-010-9402-9

Berthier, M. L., Lambon Ralph, M. A., Pujol, J., and Green, C. (2012). Arcuate fasciculus variability and repetition: the left sometimes can be right. *Cortex* 48, 133–143. doi: 10.1016/j.cortex.2011.06.014

Binder, J. R. (2017). Current controversies on Wernicke's area and its role in language. *Curr. Neurol. Neurosci.* 17:58. doi: 10.1007/s11910-017-0764-8

Bishop, D. V. M. (2009). Specific language impairment as a language learning disability. *Child Lang. Teach. Ther.* 25, 163–165. doi: 10.1177/0265659009105889

Bludau, S., Mühleisen, T. W., Eickhoff, S. B., Hawrylycz, M. J., Cichon, S., and Amunts, K. (2018). Integration of transcriptomic and cytoarchitectonic data implicates a role for MAOA and TAC1 in the limbic-cortical network. *Brain Struct. Funct.* 223, 2335–2342. doi: 10.1007/s00429-018-1620-6

Branch, C., Milner, B., and Rasmussen, T. (1964). Intracarotid sodium Amytal for the lateralization of cerebral speech dominance: observations in 123 patients. *Neurosurgery* 21, 399–405. doi: 10.3171/jns.1964.21.5.0399

Brodmann, K. (1909). *Vergleichende Lokalisationslehre der Großhirnrinde*. Leipzig: Barth.

Buchsbaum, B. R., Hickok, G., and Humphries, C. (2001). Role of left posterior superior temporal gyrus in phonological processing for speech perception and production. *Cogn. Sci.* 25, 663–678. doi: 10.1207/s15516709cog2505_2

Carrion-Castillo, A., Maassen, B., Franke, B., Heister, A., Naber, M., Van Der Leij, A., et al. (2017). Association analysis of dyslexia candidate genes in a Dutch longitudinal sample. *Eur. J. Hum. Genet.* 25, 452–460. doi: 10.1038/ejhg.2016.194

Castro Martínez, X. H., Moltó Ruiz, M. D., Morales Marin, M. E., Flores Lázaro, J. C., González Fernández, J., Gutiérrez Najera, N. A., et al. (2019). FOXP2 and language alterations in psychiatric pathology. *Salud Mental* 42, 297–308. doi: 10.17711/sm.0185-3325.2019.039

Catani, M., Jones, D. K., and Ffytche, D. H. (2005). Perisylvian language networks of the human brain. *Ann. Neurol.* 57, 8–16. doi: 10.1002/ana.20319

Centanni, T. M., Booker, A. B., Sloan, A. M., Chen, F., Maher, B. J., Carraway, R. S., et al. (2014). Knockdown of the dyslexia-associated gene Kiaa0319 impairs

temporal responses to speech stimuli in rat primary auditory cortex. *Cereb. Cortex* 24, 1753–1766. doi: 10.1093/cercor/bht028

Centanni, T. M., Pantazis, D., Truong, D. T., Gruen, J. R., Gabrieli, J. D. E., and Hogan, T. P. (2018). Increased variability of stimulus-driven cortical responses is associated with genetic variability in children with and without dyslexia. *Dev. Cogn. Neurosci.* 34, 7–17. doi: 10.1016/j.dcn.2018.05.008

Chen, J., Bardes, E. E., Aronow, B. J., and Jegga, A. G. (2009). ToppGene suite for gene list enrichment analysis and candidate gene prioritization. *Nucleic Acids Res.* 37, W305–W311. doi: 10.1093/nar/gkp427

Child, A. E., Cirino, P. T., Fletcher, J. M., Willcutt, E. G., and Fuchs, L. S. (2019). A cognitive dimensional approach to understanding shared and unique contributions to reading, math, and attention skills. *J. Learn. Disabil.* 52, 15–30. doi: 10.1177/0022219418775115

Cicchini, G. M., Marino, C., Mascheretti, S., Perani, D., and Morrone, M. C. (2015). Strong motion deficits in dyslexia associated with DCDC2 gene alteration. *J.Neurosci.* 35, 8059–8064. doi: 10.1523/JNEUROSCI.5077-14.2015

Claessen, M., and Leitão, S. (2012). Phonological representations in children with SLI. *Child Lang. Teach. Ther.* 28, 211–223. doi: 10.1177/0265659012436851

Classon, E., Rudner, M., and Rönnberg, J. (2013). Working memory compensates for hearing related phonological processing deficit. *J. Commun. Disord.* 46, 17–29. doi: 10.1016/j.jcomdis.2012.10.001

Cope, N., Eicher, J. D., Meng, H., Gibson, C. J., Hager, K., Lacadie, C., et al. (2012). Variants in the DYX2 locus are associated with altered brain activation in reading-related brain regions in subjects with reading disability. *NeuroImage* 63, 148–156. doi: 10.1016/j.neuroimage.2012.06.037

Couto, J. M., Livne-Bar, I., Huang, K., Xu, Z., Cate-Carter, T., Feng, Y., et al. (2010). Association of reading disabilities with regions marked by acetylated H3 histones in KIAA0319. *Am. J. Med. Genet.* 153, 447–462. doi: 10.1002/ajmg.b

Crespi, B. J. (2017). "Autism as a disorder of high intelligence," in *Autism Spectrum Disorders (ASD) – Searching for the Biological Basis for Behavioral Symptoms and New Therapeutic Targets*, eds B. Gesundheit, J. Rosenzweig, and Y. Shoenfeld (Lausanne: Frontiers Media), 68–94. doi: 10.3389/978-2-88945-112-8

Czamara, D., Bruder, J., Becker, J., Bartling, J., Hoffmann, P., Ludwig, K. U., et al. (2011). Association of a rare variant with mismatch negativity in a region between KIAA0319 and DCDC2 in dyslexia. *Behav. Genet.* 41, 110–119. doi: 10.1007/s10519-010-9413-6

De Carvalho, C. A. F., Kida, A. D. S. B., Capellini, S. A., and de Avila, C. R. B. (2014). Phonological working memory and reading in students with dyslexia. *Front. Psychol.* 5:746. doi: 10.3389/fpsyg.2014.00746

De Smedt, B. (2018). "Language and arithmetic: the potential role of phonological processing," in *Heterogeneity of Function in Numerical Cognition*, eds A. Henik and W. Fias (San Diego, CA: Academic Press), 51–74. doi: 10.1016/C2016-0-00729-5

De Smedt, B., and Boets, B. (2010). Phonological processing and arithmetic fact retrieval: evidence from developmental dyslexia. *Neuropsychologia* 48, 3973–3981. doi: 10.1016/j.neuropsychologia.2010.10.018

Dehaene, S. (1992). Varieties of numerical abilities. *Cognition* 44, 1–42. doi: 10.1016/0010-0277(92)90049-n

Dehaene, S., Piazza, M., Pinel, P., and Cohen, L. (2003). Three parietal circuits for number processing. *Cogn. Neuropsychol.* 20, 487–506. doi: 10.1080/02643290244000239

DeWitt, I., and Rauschecker, J. P. (2013). Wernicke's area revisited: parallel streams and word processing. *Brain Lang.* 127, 181–191. doi: 10.1016/j.bandl.2013.09.014

Dinkel, P. J., Willmes, K., Krinzinger, H., Konrad, K., and Koten, J. W. (2013). Diagnosing developmental dyscalculia on the basis of reliable single case FMRI methods: promises and limitations. *PLoS One* 8:e83722. doi: 10.1371/journal.pone.0083722

Doust, C., Gordon, S. D., Garden, N., Fisher, S. E., Martin, N. G., Bates, T. C., et al. (2020). The association of dyslexia and developmental speech and language disorder candidate genes with reading and language abilities in adults. *Twin Res. Hum. Genet.* 23, 23–32. doi: 10.1017/thg.2020.7

Eicher, J. D., Powers, N. R., Miller, L. L., Akshoomoff, N., Amaral, D. G., Bloss, C. S., et al. (2013). Genome-wide association study of shared components of reading disability and language impairment. *Genes Brain Behav.* 12, 792–801. doi: 10.1111/gbb.12085

Eicher, J. D., Powers, N. R., Miller, L. L., Mueller, K. L., Mascheretti, S., Marino, C., et al. (2014). Characterization of the DYX2 locus on chromosome 6p22 with reading disability, language impairment, and IQ. *Hum. Genet.* 133, 869–881. doi: 10.1007/s00439-014-1427-3

Eicher, J. D., Stein, C. M., Deng, F., Ciesla, A. A., Powers, N. R., Boada, R., et al. (2015). The DYX2 locus and neurochemical signaling genes contribute to speech sound disorder and related neurocognitive domains. *Genes Brain Behav.* 14, 377–385. doi: 10.1111/gbb.12214

Eickhoff, S. B., Heim, S., Zilles, K., and Amunts, K. (2009). A systems perspective on the effective connectivity of overt speech production. *Philos. Trans. A Math. Phys. Eng. Sci.* 367, 2399–2421. doi: 10.1098/rsta.2008.0287

Elbert, A., Lovett, M. W., Cate-Carter, T., Pitch, A., Kerr, E. N., and Barr, C. L. (2011). Genetic variation in the KIAA0319 5' region as a possible contributor to dyslexia. *Behav. Genet.* 41, 77–89. doi: 10.1007/s10519-010-9434-1

Evans, A. C., Janke, A. L., Collins, D. L., and Baillet, S. (2012). Brain templates and atlases. *NeuroImage* 62, 911–922. doi: 10.1016/j.neuroimage.2012.01.024

Fraser, J., Goswami, U., and Conti-Ramsden, G. (2010). Dyslexia and specific language impairment: the role of phonology and auditory processing. *Sci. Stud. Read.* 14, 8–29. doi: 10.1080/10888430903242068

Friederici, A. D. (2009). Pathways to language: fibre tracts in the human brain. *Trends Cogn. Sci.* 13, 175–181. doi: 10.1016/j.tics.2009.01.001

Friederici, A. D. (2011). The brain basis of language processing: from structure to function. *Physiol. Rev.* 91, 1357–1392. doi: 10.1152/physrev.00006.2011

Friederici, A. D. (2012). Language development and the ontogeny of the dorsal pathway. *Front. Evol. Neurosci.* 4:3. doi: 10.3389/fnevo.2012.00003

Friederici, A. D., and Gierhan, S. M. E. (2013). The language network. *Curr. Opin. Neurobiol.* 23, 250–254. doi: 10.1016/j.conb.2012.10.002

Galaburda, A. M., LoTurco, J., Ramus, F., Fitch, R. H., and Rosen, G. D. (2006). From genes to behavior in developmental dyslexia. *Nat. Neurosci.* 9, 1213–1217. doi: 10.1038/nn1772

Gehman, L. T., Meera, P., Stoilov, P., Shiue, L., O'Brien, J. E., Meisler, M. H., et al. (2012). The splicing regulator Rbfox2 is required for both cerebellar development and mature motor function. *Genes Dev.* 26, 445–460. doi: 10.1101/gad.182477.111

Gene Ontology Consortium (2021). The gene ontology resource: enriching a gold mine. *Nucleic Acids Res.* 49, D325–D334. doi: 10.1093/nar/gkaa1113

Gialluisi, A., Guadalupe, T., Francks, C., and Fisher, S. E. (2017). Neuroimaging genetic analyses of novel candidate genes associated with reading and language. *Brain Lang.* 172, 9–15. doi: 10.1016/j.bandl.2016.07.002

Gialluisi, A., Newbury, D. F., Wilcutt, E. G., Olson, R. K., DeFries, J. C., Brandler, W. M., et al. (2014). Genome-wide screening for DNA variants associated with reading and language traits. *Genes Brain Behav.* 13, 686–701. doi: 10.1111/gbb.12158

Gori, S., Mascheretti, S., Giora, E., Ronconi, L., Ruffino, M., Quadrelli, E., et al. (2015). The DCDC2 intron 2 deletion impairs illusory motion perception unveiling the selective role of magnocellular-dorsal stream in reading (dis)ability. *Cereb. Cortex* 25, 1685–1695. doi: 10.1093/cercor/bhu234

Gorno-Tempini, M. L., Brambati, S. M., Ginex, V., Ogar, B. J., Dronkers, N. F., Marcone, A., et al. (2008). The logopenic/phonological variant of primary progressive aphasia. *Neurology* 71, 1227–1234. doi: 10.1212/01.wnl.0000320506.79811.da

Gorno-Tempini, M. L., Dronkers, N. F., Rankin, K. P., Ogar, J. M., Phengrasamy, L., Rosen, H. J., et al. (2004). Cognition and anatomy in three variants of primary progressive aphasia. *Ann. Neurol.* 55, 335–346. doi: 10.1002/ana.10825

Gorno-Tempini, M. L., Hillis, A. E., Weintraub, S., Kertesz, A., Mendez, M., Cappa, S. F., et al. (2011). Classification of primary progressive aphasia and its variants. *Neurology* 76, 1006–1014. doi: 10.1212/WNL.0b013e31821103e6

Goswami, U. (2011). A temporal sampling framework for developmental dyslexia. *Trends Cogn Sci.* 15, 3–10. doi: 10.1016/j.tics.2010.10.001

Gray, S., Fox, A. B., Green, S., Alt, M., Hogan, T. P., Petscher, Y., et al. (2019). Working memory profiles of children with dyslexia, developmental language disorder, or both. *J. Speech Lang. Hear. Res.* 62, 1839–1858. doi: 10.1044/2019_JSLHR-L-18-0148

Hagoort, P., and Indefrey, P. (2014). The neurobiology of language beyond single words. *Annu. Rev. Neurosci.* 37, 347–362. doi: 10.1146/annurev-neuro-071013-013847

Hannula-Jouppi, K., Kaminen-Ahola, N., Taipale, M., Eklund, R., Nopola-Hemmi, J., Kääriäinen, H., et al. (2005). The axon guidance receptor gene ROBO1 is a candidate gene for developmental dyslexia. *PLoS Genet.* 1:e50. doi: 10.1371/journal.pgen.0010050

Hartwigsen, G. (2015). The neurophysiology of language: insights from non-invasive brain stimulation in the healthy human brain. *Brain Lang.* 148, 81–94. doi: 10.1016/j.bandl.2014.10.007

Hartwigsen, G. (2016). Adaptive plasticity in the healthy language network: implications for language recovery after stroke. *Neural Plast.* 2016:9674790. doi: 10.1155/2016/9674790

Hartwigsen, G., Stockert, A., Charpentier, L., Wawrzyniak, M., Klingbeil, J., Wrede, K., et al. (2020). Short-term modulation of the lesioned language network. *Elife* 9:e54277. doi: 10.7554/eLife.54277

Hasselhorn, M., Schuchardt, K., and Mähler, C. (2010). Phonological working memory in children with specific learning disorders in reading and/or spelling: the effect of word length and lexicality on memory span. *Z. Entwicklungspsychol. Padagog. Psychol.* 42, 211–216. doi: 10.1026/0049-8637/a000024

Hawrylycz, M. J., Lein, E. S., Guillozet-Bongaarts, A. L., Shen, E. H., Ng, L., Miller, J. A., et al. (2012). An anatomically comprehensive atlas of the adult human brain transcriptome. *Nature* 489, 391–399. doi: 10.1038/nature11405

Hawrylycz, M., Miller, J. A., Menon, V., Feng, D., Dolbeare, T., Guillozet-Bongaarts, A. L., et al. (2015). Canonical genetic signatures of the adult human brain. *Nat. Neurosci.* 18, 1832–1844. doi: 10.1038/nn.4171

Heim, S., Eickhoff, S. B., and Amunts, K. (2008). Specialisation in Broca's region for semantic, phonological, and syntactic fluency? *NeuroImage* 40, 1362–1368. doi: 10.1016/j.neuroimage.2008.01.009

Heim, S., Eickhoff, S. B., and Amunts, K. (2009a). Different roles of cytoarchitectonic BA 44 and BA 45 in phonological and semantic verbal fluency as revealed by dynamic causal modelling. *NeuroImage* 48, 616–624. doi: 10.1016/j.neuroimage.2009.06.044

Heim, S., Eickhoff, S. B., Ischebeck, A. K., Friederici, A. D., Stephan, K. E., and Amunts, K. (2009b). Effective connectivity of the left BA 44, BA 45, and inferior temporal gyrus during lexical and phonological decisions identified with DCM. *Hum. Brain Map.* 30, 392–402. doi: 10.1002/hbm.20512

Heim, S., Grande, M., Meffert, E., Eickhoff, S. B., Schreiber, H., Kukolja, J., et al. (2010). Cognitive levels of performance account for hemispheric lateralisation effects in dyslexic and normally reading children. *NeuroImage* 53, 1346–1358. doi: 10.1016/j.neuroimage.2010.07.009

Heim, S., Opitz, B., Müller, K., and Friederici, A. D. (2003). Phonological processing during language production: fMRI evidence for a shared production-comprehension network. *Brain Res. Cogn. Brain Res.* 16, 285–296. doi: 10.1016/s0926-6410(02)00284-7

Henry, M. L., and Gorno-Tempini, M.-L. (2010). The logopenic variant of primary progressive aphasia. *Curr. Opin. Neurol.* 23, 633–637. doi: 10.1097/WCO.0b013e32833fb93e

Henry, M. L., Wilson, S. M., Babiak, M. C., Mandelli, M. L., Beeson, P. M., Miller, Z. A., et al. (2016). Phonological processing in primary progressive aphasia. *J. Cogn. Neurosci.* 28, 210–222. doi: 10.1162/jocn_a_00901

Hensler, B. S., Schatschneider, C., Taylor, J., and Wagner, R. K. (2010). Behavioral genetic approach to the study of dyslexia. *J. Dev. Behav. Pediatr.* 31, 525–532. doi: 10.1097/DBP.0b013e3181ee4b70

Houde, J. F., and Nagarajan, S. S. (2011). Speech production as state feedback control. *Front. Hum. Neurosci.* 5:82. doi: 10.3389/fnhum.2011.00082

Indefrey, P. (2011). The spatial and temporal signatures of word production components: a critical update. *Front. Psychol.* 2:255. doi: 10.3389/fpsyg.2011.00255

Indefrey, P., and Levelt, W. J. M. (2004). The spatial and temporal signatures of word production components. *Cognition* 92, 101–144. doi: 10.1016/j.cognition.2002.06.001

Jarvis, E. D. (2019). Evolution of vocal learning and spoken language. *Science* 366, 50–54. doi: 10.1126/science.aax0287

Johnson, J. C. S., Jiang, J., Bond, R. L., Benhamou, E., Requena-Komuro, M. C., Russell, L. L., et al. (2020). Impaired phonemic discrimination in logopenic variant primary progressive aphasia. *Ann. Clin. Transl. Neurol.* 7, 1252–1257. doi: 10.1002/acn3.51101

Johnson, M. B., Kawasawa, Y. I, Mason, C. E., Krsnik, Ž, Coppola, G., Bogdanović, D., et al. (2009). Functional and evolutionary insights into human brain development through global transcriptome analysis. *Neuron* 62, 494–509. doi: 10.1016/j.neuron.2009.03.027

Katzev, M., Tüscher, O., Hennig, J., Weiller, C., and Kaller, C. P. (2013). Revisiting the functional specialization of left inferior frontal gyrus in phonological and semantic fluency: the crucial role of task demands and individual ability. *J. Neurosci.* 33, 7837–7845. doi: 10.1523/JNEUROSCI.3147-12.2013

Kim, G., Ahmadian, S. S., Peterson, M., Parton, Z., Memon, R., Weintraub, S., et al. (2016). Asymmetric pathology in primary progressive aphasia with progranulin mutations and TDP inclusions. *Neurology* 86, 627–636. doi: 10.1212/WNL.0000000000002375

Klaus, J., and Hartwigsen, G. (2019). Dissociating semantic and phonological contributions of the left inferior frontal gyrus to language production. *Hum. Brain Map.* 40, 3279–3287. doi: 10.1002/hbm.24597

König, I. R., Schumacher, J., Hoffmann, P., Kleensang, A., Ludwig, K. U., Grimm, T., et al. (2011). Mapping for dyslexia and related cognitive trait loci provides strong evidence for further risk genes on chromosome 6p21. *Am. J. Med. Genet. B Neuropsychiatr. Genet.* 156, 36–43. doi: 10.1002/ajmg.b.31135

Kurup, R. K., and Kurup, P. A. (2003). Hypothalamic digoxin and hemispheric chemical dominance: relation to speech and language dysfunction. *Int. J. Neurosci.* 113, 797–814. doi: 10.1080/00207450390200936

Lai, C. S. L., Fisher, S. E., Hurst, J. A., Vargha-Khadem, F., and Monaco, A. P. (2001). A forkhead-domain gene is mutated in a severe speech and language disorder. *Nature* 413, 519–523. doi: 10.1038/35097076

Lambert, N., Lambot, M. A., Bilheu, A., Albert, V., Englert, Y., Libert, F., et al. (2011). Genes expressed in specific areas of the human fetal cerebral cortex display distinct patterns of evolution. *PLoS One* 6:e17753. doi: 10.1371/journal.pone.0017753

Lamminmäki, S., Massinen, S., Nopola-Hemmi, J., Kere, J., and Hari, R. (2012). Human ROBO1 regulates interaural interaction in auditory pathways. *J. Neurosci.* 32, 966–971. doi: 10.1523/JNEUROSCI.4007-11.2012

Landerl, K., Fussenegger, B., Moll, K., and Willburger, E. (2009). Dyslexia and dyscalculia: two learning disorders with different cognitive profiles. *J. Exp. Child Psychol.* 103, 309–324. doi: 10.1016/j.jecp.2009.03.006

Lewis, B. A., Avrich, A. A., Freebairn, L. A., Taylor, H. G., Iyengar, S. K., and Stein, C. M. (2011). Subtyping children with speech sound disorders by endophenotypes. *Top. Lang. Disord.* 31, 112–127. doi: 10.1097/TLD.0b013e318217b5dd

Liakakis, G., Nickel, J., and Seitz, R. J. (2011). Diversity of the inferior frontal gyrus – a meta-analysis of neuroimaging studies. *Behav. Brain Res.* 225, 341–347. doi: 10.1016/j.bbr.2011.06.022

Lim, C. K. P., Wong, A. M. B., Ho, C. S. H., and Waye, M. M. Y. (2014). A common haplotype of KIAA0319 contributes to the phonological awareness skill in Chinese children. *Behav. Brain Funct.* 10:23. doi: 10.1186/1744-9081-10-23

Lind, P. A., Luciano, M., Wright, M. J., Montgomery, G. W., Martin, N. G., and Bates, T. C. (2010). Dyslexia and DCDC2: normal variation in reading and spelling is associated with DCDC2 polymorphisms in an Australian population sample. *Eur. J. Hum. Genet.* 18, 668–673. doi: 10.1038/ejhg.2009.237

López-Barroso, D., Catani, M., Ripollés, P., Dell'Acqua, F., Rodríguez-Fornells, A., and de Diego-Balaguer, R. (2013). Word learning is mediated by the left arcuate fasciculus. *Proc. Natl. Acad. Sci. U.S.A.* 110, 13168–13173. doi: 10.1073/pnas.1301696110

Luciano, M., Gow, A. J., Pattie, A., Bates, T. C., and Deary, I. J. (2018). The influence of dyslexia candidate genes on reading skill in old age. *Behav. Genet.* 48, 351–360. doi: 10.1007/s10519-018-9913-3

Ludwig, K. U., Sämann, P., Alexander, M., Becker, J., Bruder, J., Moll, K., et al. (2013). A common variant in Myosin-18B contributes to mathematical abilities in children with dyslexia and intraparietal sulcus variability in adults. *Transl. Psychiatry* 3:e229. doi: 10.1038/tp.2012.148

Magnin, E., Démonet, J. F., Wallon, D., Dumurgier, J., Troussière, A. C., Jager, A., et al. (2016). Primary progressive aphasia in the network of French Alzheimer plan memory centers. *J. Alzheimer's Dis.* 54, 1459–1471. doi: 10.3233/JAD-160536

Marino, C., Citterio, A., Giorda, R., Facoetti, A., Menozzi, G., Vanzin, L., et al. (2007). Association of short-term memory with a variant within DYX1C1 in developmental dyslexia. *Genes Brain Behav.* 6, 640–646. doi: 10.1111/j.1601-183X.2006.00291.x

Marino, C., Mascheretti, S., Riva, V., Cattaneo, F., Rigoletto, C., Rusconi, M., et al. (2011). Pleiotropic effects of DCDC2 and DYX1C1 genes on language and mathematics traits in nuclear families of developmental dyslexia. *Behav. Genet.* 41, 67–76. doi: 10.1007/s10519-010-9412-7

Marino, C., Meng, H., Mascheretti, S., Rusconi, M., Cope, N., Giorda, R., et al. (2012). DCDC2 genetic variants and susceptibility to developmental dyslexia. *Psychiatr. Genet.* 22, 25–30. doi: 10.1097/YPG.0b013e32834acdb2

Marino, C., Scifo, P., Della Rosa, P. A., Mascheretti, S., Facoetti, A., Lorusso, M. L., et al. (2014). The DCDC2/intron 2 deletion and white matter disorganization: focus on developmental dyslexia. *Cortex* 57, 227–243. doi: 10.1016/j.cortex.2014.04.016

Martinelli, A., Rice, M. L., Talcott, J. B., Diaz, R., Smith, S., Raza, M. H., et al. (2021). A rare missense variant in the ATP2C2 gene is associated with language impairment and related measures. *Hum. Mol. Genet.* 30, 1160–1171. doi: 10.1093/hmg/ddab111

Mascheretti, S., Bureau, A., Battaglia, M., Simone, D., Quadrelli, E., Croteau, J., et al. (2013). An assessment of gene-by-environment interactions in developmental dyslexia-related phenotypes. *Genes Brain Behav.* 12, 47–55. doi: 10.1111/gbb.12000

Mascheretti, S., Bureau, A., Trezzi, V., Giorda, R., and Marino, C. (2015). An assessment of gene-by-gene interactions as a tool to unfold missing heritability in dyslexia. *Hum. Genet.* 134, 749–760. doi: 10.1007/s00439-015-1555-4

Mascheretti, S., De Luca, A., Trezzi, V., Peruzzo, D., Nordio, A., Marino, C., et al. (2017). Neurogenetics of developmental dyslexia: from genes to behavior through brain neuroimaging and cognitive and sensorial mechanisms. *Transl. Psychiatry* 7:e987. doi: 10.1038/tp.2016.240

Mascheretti, S., Riva, V., Giorda, R., Beri, S., Lanzoni, L. F. E., Cellino, M. R., et al. (2014). KIAA0319 and ROBO1: evidence on association with reading and pleiotropic effects on language and mathematics abilities in developmental dyslexia. *J. Hum. Genet.* 59, 189–197. doi: 10.1038/jhg.2013.141

Massinen, S., Tammimies, K., Tapia-Páez, I., Matsson, H., Hokkanen, M. E., Söderberg, O., et al. (2009). Functional interaction of DYX1C1 with estrogen receptors suggests involvement of hormonal pathways in dyslexia. *Hum. Mol. Genet.* 18, 2802–2812. doi: 10.1093/hmg/ddp215

Matsson, H., Huss, M., Persson, H., Einarsdottir, E., Tiraboschi, E., Nopola-Hemmi, J., et al. (2015). Polymorphisms in DCDC2 and S100B associate with developmental dyslexia. *J. Hum. Genet.* 60, 399–401. doi: 10.1038/jhg.2015.37

Mazoyer, B., Zago, L., Jobard, D., Crivello, F., Joliot, M., Perchey, G., et al. (2014). Gaussian mixture modeling of hemispheric lateralization for language in a large sample of healthy individuals balanced for handedness. *PLoS One* 9:e101165. doi: 10.1371/journal.pone.0101165

McCrone, J. (2002). Dyscalculia. *Lancet Neurol.* 1:266. doi: 10.1016/S1474-4422(02)00113-8

Morgan, A., Fisher, S. E., Scheffer, I., and Hildebrand, M. (2016). "FOXP2-related speech and language disorders. 2016 Jun 23 [Updated 2017 Feb 2]," in *GeneReviews® [Internet]*, eds M. P. Adam, H. H. Ardinger, R. A. Pagon, S. E. Wallace, L. J. H. Bean, G. Mirzaa, et al. (Seattle, WA: University of Washington), 1993–2021.

Morosan, P., Schleicher, A., Amunts, K., and Zilles, K. (2005). Multimodal architectonic mapping of human superior temporal gyrus. *Anat. Embryol.* 210, 401–406. doi: 10.1007/s00429-005-0029-1

Mozzi, A., Riva, V., Forni, D., Sironi, M., Marino, C., Molteni, M., et al. (2017). A common genetic variant in FOXP2 is associated with language-based learning (dis)abilities: evidence from two Italian independent samples. *Am. J. Med. Genet. B Neuropsychiatr. Genet.* 174, 578–586. doi: 10.1002/ajmg.b.32546

Müller, B., Schaadt, G., Boltze, J., Emmrich, F., Skeide, M. A., Neef, N. E., et al. (2017). ATP2C2 and DYX1C1 are putative modulators of dyslexia-related MMR. *Brain Behav.* 7:e00851. doi: 10.1002/brb3.851

Müller, N. G., and Knight, R. T. (2006). The functional neuroanatomy of working memory: contributions of human brain lesion studies. *Neuroscience* 139, 51–58. doi: 10.1016/j.neuroscience.2005.09.018

Neef, N. E., Müller, B., Liebig, J., Schaadt, G., Grigutsch, M., Gunter, T. C., et al. (2017). Dyslexia risk gene relates to representation of sound in the auditory brainstem. *Dev. Cogn. Neurosci.* 24, 63–71. doi: 10.1016/j.dcn.2017.01.008

Newbury, D. F., Paracchini, S., Scerri, T. S., Winchester, L., Addis, L., Richardson, A. J., et al. (2011). Investigation of dyslexia and SLI risk variants in reading- and language-impaired subjects. *Behav. Genet.* 41, 90–104. doi: 10.1007/s10519-010-9424-3

Newbury, D. F., Winchester, L., Addis, L., Paracchini, S., Buckingham, L. L., Clark, A., et al. (2009). CMIP and ATP2C2 modulate phonological short-term memory in language impairment. *Am. J. Hum. Genet.* 85, 264–272. doi: 10.1016/j.ajhg.2009.07.004

Oguro-Ando, A., Rosensweig, C., Herman, E., Nishimura, Y., Werling, D., Bill, B. R., et al. (2015). Increased CYFIP1 dosage alters cellular and dendritic morphology and dysregulates mTOR. *Mol. Psychiatry* 20, 1069–1078. doi: 10.1038/mp.2014.124

Papagno, C., Comi, A., Riva, M., Bizzi, A., Vernice, M., Casarotti, A., et al. (2017). Mapping the brain network of the phonological loop. *Hum. Brain Mapp.* 38, 3011–3024. doi: 10.1002/hbm.23569

Paracchini, S., Ang, Q. W., Stanley, F. J., Monaco, A. P., Pennell, C. E., and Whitehouse, A. J. O. (2011). Analysis of dyslexia candidate genes in the Raine cohort representing the general Australian population. *Genes Brain Behav.* 10, 158–165. doi: 10.1111/j.1601-183X.2010.00651.x

Pennington, B. F., and Bishop, D. V. M. (2009). Relations among speech, language, and reading disorders. *Annu. Rev. Psychol.* 60, 283–306. doi: 10.1146/annurev.psych.60.110707.163548

Peschansky, V. J., Burbridge, T. J., Volz, A. J., Fiondella, C., Wissner-Gross, Z., Galaburda, A. M., et al. (2010). The effect of variation in expression of the candidate dyslexia susceptibility gene homolog Kiaa0319 on neuronal migration and dendritic morphology in the rat. *Cereb. Cortex* 20, 884–897. doi: 10.1093/cercor/bhp154

Peter, B., Raskind, W. H., Matsushita, M., Lisowski, M., Vu, T., Berninger, V. W., et al. (2011). Replication of CNTNAP2 association with nonword repetition and support for FOXP2 association with timed reading and motor activities in a dyslexia family sample. *J. Neurodev. Disord.* 3, 39–49. doi: 10.1007/s11689-010-9065-0

Pettigrew, K. A., Frinton, E., Nudel, R., Chan, M. T. M., Thompson, P., Hayiou-Thomas, M. E., et al. (2016). Further evidence for a parent-of-origin effect at the NOP9 locus on language-related phenotypes. *J. Neurodev. Dis.* 8:24. doi: 10.1186/s11689-016-9157-6

Pinel, P., Fauchereau, F., Moreno, A., Barbot, A., Lathrop, M., Zelenika, M., et al. (2012). Genetic variants of FOXP2 and KIAA0319/TTRAP/THEM2 locus are associated with altered brain activation in distinct language-related regions. *J. Neurosci.* 32, 817–825. doi: 10.1523/JNEUROSCI.5996-10.2012

Pollack, C., and Ashby, N. C. (2018). Where arithmetic and phonology meet: the meta-analytic convergence of arithmetic and phonological processing in the brain. *Dev. Cogn. Neurosci.* 30, 251–264. doi: 10.1016/j.dcn.2017.05.003

Powers, N. R., Eicher, J. D., Butter, F., Kong, Y., Miller, L. L., Ring, S. M., et al. (2013). Alleles of a polymorphic ETV6 binding site in DCDC2 confer risk of reading and language impairment. *Am. J. Hum. Genet.* 93, 19–28. doi: 10.1016/j.ajhg.2013.05.008

Powers, N. R., Eicher, J. D., Miller, L. L., Kong, Y., Smith, S. D., Pennington, B. F., et al. (2016). The regulatory element READ1 epistatically influences reading and language, with both deleterious and protective alleles. *J. Med. Genet.* 53, 163–171. doi: 10.1136/jmedgenet-2015-103418

Raghubar, K. P., Barnes, M. A., and Hecht, S. A. (2010). Working memory and mathematics: a review of developmental, individual difference, and cognitive approaches. *Learn. Individ. Differ.* 20, 110–122. doi: 10.1016/j.lindif.2009.10.005

Rice, M. L., Taylor, C. L., Zubrick, S. R., Hoffman, L., and Earnest, K. K. (2020). Heritability of specific language impairment and nonspecific language impairment at ages 4 and 6 years across phenotypes of speech, language, and nonverbal cognition. *J. Speech Lang. Hear. Res.* 63, 793–813. doi: 10.1044/2019_JSLHR-19-00012

Riva, V., Cantiani, C., Benasich, A. A., Molteni, M., Piazza, C., Giorda, R., et al. (2018). From CNTNAP2 to early expressive language in infancy: the mediation role of rapid auditory processing. *Cereb. Cortex* 28, 1–9. doi: 10.1093/cercor/bhx115

Riva, V., Mozzi, A., Forni, D., Trezzi, V., Giorda, R., Riva, S., et al. (2019). The influence of DCDC2 risk genetic variants on reading: testing main and haplotypic effects. *Neuropsychologia* 130, 52–58. doi: 10.1016/j.neuropsychologia.2018.05.021

Rogalski, E., Johnson, N., Weintraub, S., and Mesulam, M. (2008). Increased frequency of learning disability in patients with primary progressive aphasia and their first-degree relatives. *Arch. Neurol.* 65, 244–248. doi: 10.1001/archneurol.2007.34

Rogalsky, C., and Hickok, G. (2011). The role of Broca's area in sentence comprehension. *J. Cogn. Neurosci.* 23, 1664–1680. doi: 10.1162/jocn.2010.21530

Sánchez-Morán, M., Hernández, J. A., Duñabeitia, J. A., Estévez, A., Bárcena, L., González-Lahera, A., et al. (2018). Genetic association study of dyslexia and ADHD candidate genes in a Spanish cohort: implications of comorbid samples. *PLoS One* 13:e0206431. doi: 10.1371/journal.pone.0206431

Scerri, T. S., Morris, A. P., Buckingham, L. L., Newbury, D. F., Miller, L. L., Monaco, A. P., et al. (2011). DCDC2, KIAA0319 and CMIP are associated with reading-related traits. *Biol. Psychiatry* 70, 237–245. doi: 10.1016/j.biopsych.2011.02.005

Skeide, M. A., and Friederici, A. D. (2016). The ontogeny of the cortical language network. *Nat. Rev. Neurosci.* 17, 323–332. doi: 10.1038/nrn.2016.23

Smith, A. W., Holden, K. R., Dwivedi, A., Dupont, B. R., and Lyons, M. J. (2015). Deletion of 16q24.1 supports a role for the ATP2C2 gene in specific language impairment. *J. Child Neurol.* 30, 517–521. doi: 10.1177/0883073814545113

Sonty, S. P., Mesulam, M. M., Weintraub, S., Johnson, N. A., Parrish, T. B., and Gitelman, D. R. (2007). Altered effective connectivity within the language network in primary progressive aphasia. *J. Neurosci.* 27, 1334–1345. doi: 10.1523/JNEUROSCI.4127-06.2007

Stefansson, H., Meyer-Lindenberg, A., Steinberg, S., Magnusdottir, B., Morgen, K., Arnarsdottir, S., et al. (2014). CNVs conferring risk of autism or schizophrenia affect cognition in controls. *Nature* 505, 361–366. doi: 10.1038/nature12818

Stefansson, H., Rujescu, D., Cichon, S., Pietiläinen, O. P. H., Ingason, A., Steinberg, S., et al. (2008). Large recurrent microdeletions associated with schizophrenia. *Nature* 455, 232–236. doi: 10.1038/nature07229

Steinbrink, C., Schwanda, S., and Vogt, K. (2008). Relations between cognitive skills and reading and spelling performance in first graders with poor spelling abilities. *Nervenheilkunde* 27, 644–651. doi: 10.1055/s-0038-1627124

Szalkowski, C. E., Booker, A. B., Truong, D. T., Threlkeld, S. W., Rosen, G. D., and Fitch, R. H. (2013). Knockdown of the candidate dyslexia susceptibility gene homolog dyx1c1 in rodents: effects on auditory processing, visual attention, and cortical and thalamic anatomy. *Dev. Neurosci.* 35, 50–68. doi: 10.1159/000348431

Tam, G. W. C., Van De Lagemaat, L. N., Redon, R., Strathdee, K. E., Croning, M. D. R., Malloy, M. P., et al. (2010). Confirmed rare copy number variants implicate novel genes in schizophrenia. *Biochem. Soc. Trans.* 38, 445–451. doi: 10.1042/BST0380445

Tarkar, A., Loges, N. T., Slagle, C. E., Francis, R., Dougherty, G. W., Tamayo, J. V., et al. (2013). DYX1C1 is required for axonemal dynein assembly and ciliary motility. *Nat. Genet.* 45, 995–1003. doi: 10.1038/ng.2707

Thompson, P. A., Hulme, C., Nash, H. M., Gooch, D., Hayiou-Thomas, E., and Snowling, M. J. (2015). Developmental dyslexia: predicting individual risk. *J. Child Psychol. Psychiatry* 56, 976–978. doi: 10.1111/jcpp.12412

Torrens, V., and Yagüe, E. (2016). The role of phonological working memory in children with SLI. *Lang. Acquis.* 25, 102–117. doi: 10.1080/10489223.2016.1187617

Tosto, M. G., Hayjiou-Thomas, M. E., Harlaar, N., Prom-Wormley, E., Dale, P. S., and Plomin, R. (2017). The genetic architecture of oral language, reading fluency, and reading comprehension: a twin study from 7 to 16 years. *Dev. Psychol.* 53, 1115–1129. doi: 10.1037/dev0000297

Träff, U., and Passolunghi, M. C. (2015). Mathematical skills in children with dyslexia. *Learn. Individ. Differ.* 40, 108–114. doi: 10.1016/j.lindif.2015.03.024

Tran, C., Wigg, K. G., Zhang, K., Cate-Carter, T. D., Kerr, E., Field, L. L., et al. (2014). Association of the ROBO1 gene with reading disabilities in a family-based analysis. *Genes Brain Behav.* 13, 430–438. doi: 10.1111/gbb.12126

Treiman, R. (2017). Learning to spell: phonology and beyond. *Cogn. Neuropsychol.* 34, 83–93. doi: 10.1080/02643294.2017.1337630

Troung, D. T., Adams, A. K., Paniagua, S., Frijters, J. C., Boada, R., Hill, D. E., et al. (2019). Multivariate genome-wide association study of rapid automatised naming and rapid alternating stimulus in Hispanic American and African-American youth. *J. Med. Genet.* 56, 557–566. doi: 10.1136/jmedgenet-2018-105874

Ulfarsson, M. O., Walters, G. B., Gustafsson, O., Steinberg, S., Silva, A., Doyle, O. M., et al. (2017). 15q11.2 CNV affects cognitive, structural and functional correlates of dyslexia and dyscalculia. *Transl. Psychiatry* 7:e1109. doi: 10.1038/tp.2017.77

Verhoeven, J. S., Rommel, N., Prodi, E., Leemans, A., Zink, I., Vandewalle, E., et al. (2012). Is there a common neuroanatomical substrate of language deficit between autism spectrum disorder and specific language impairment? *Cereb. Cortex* 22, 2263–2271. doi: 10.1093/cercor/bhr292

Vernes, S. C., Newbury, D. F., Abrahams, B. S., Winchester, L., Nicod, J., Groszer, M., et al. (2008). A functional genetic link between distinct developmental language disorders. *N. Engl. J. Med.* 359, 2337–2345. doi: 10.1056/NEJMoa0802828

Wadsworth, S. J., Olson, R. K., and Defries, J. C. (2010). Differential genetic etiology of reading difficulties as a function of IQ: an update. *Behav. Genet.* 40, 751–758. doi: 10.1007/s10519-010-9349-x

Wagner, S., Sebastian, A., Lieb, K., Tüscher, O., and Tadić, A. (2014). A coordinate-based ALE functional MRI meta-analysis of brain activation during verbal fluency tasks in healthy control subjects. *BMC Neurosci.* 15:19. doi: 10.1186/1471-2202-15-19

Wallace, M. T. (2009). Dyslexia: bridging the gap between hearing and reading. *Curr. Biol.* 19, R260–R262. doi: 10.1016/j.cub.2009.01.025

Wang, Y., Paramasivam, M., Thomas, A., Bai, J., Kaminen-Ahola, N., Kere, J., et al. (2006). DYX1C1 functions in neuronal migration in developing neocortex. *Neuroscience* 143, 515–522. doi: 10.1016/j.neuroscience.2006.08.022

Wei, C. H., Kao, H. Y., and Lu, Z. (2013). PubTator: a web-based text mining tool for assisting biocuration. *Nucleic Acids Res.* 41, W518–W522. doi: 10.1093/nar/gkt441

Whitehouse, A. J. O., Bishop, D. V. M., Ang, Q. W., Pennell, C. E., and Fisher, S. E. (2011). CNTNAP2 variants affect early language development in the general population. *Genes Brain Behav.* 10, 451–456. doi: 10.1111/j.1601-183X.2011.00684.x

Wilcke, A., Ligges, C., Burkhardt, J., Alexander, M., Wolf, C., Quente, E., et al. (2012). Imaging genetics of FOXP2 in dyslexia. *Eur. J. Hum. Genet.* 20, 224–229. doi: 10.1038/ejhg.2011.160

Yi, H. G., Leonard, M. K., and Chang, E. F. (2019). The encoding of speech sounds in the temporal gyrus. *Neuron* 102, 1096–1110. doi: 10.1016/j.neuron.2019.04.023

Zou, L., Chen, W., Shao, S., Sun, Z., Zhong, R., Shi, J., et al. (2012). Genetic variant in KIAA0319, but not in DYX1C1, is associated with risk of dyslexia: an integrated meta-analysis. *Am. J. Med. Genet. B Neuropsychiatr. Genet.* 159, 970–976. doi: 10.1002/ajmg.b.32102

Conflict of Interest: The authors declare that the research was conducted in the absence of any commercial or financial relationships that could be construed as a potential conflict of interest.

Publisher's Note: All claims expressed in this article are solely those of the authors and do not necessarily represent those of their affiliated organizations, or those of the publisher, the editors and the reviewers. Any product that may be evaluated in this article, or claim that may be made by its manufacturer, is not guaranteed or endorsed by the publisher.

3 Diskussion

Die vorliegende Arbeit trägt zur Parzellierung des posterioren FOp und weiterer sprachverarbeitender Cortexabschnitte bei. Im Zuge dessen wurden die Areale Op5, Op6 und Op7 identifiziert und zytoarchitektonische Wahrscheinlichkeitskarten berechnet (Unger et al., 2021a; Unger et al., 2021b; Unger et al., 2021c). Es schloss sich eine multimodale Charakterisierung des FOp an, innerhalb welcher sich Area Op6 links als funktionell am stärksten von den drei betrachteten Arealen in Netzwerke der Musik- und Sprachverarbeitung eingebunden zeigte (Unger et al., 2023). Während Area Op5-Op7 innerhalb von Unger et al. (2023) zunächst nach Schleicher et al. (1999, 2005, 2009) kartiert wurden, konnte zusätzlich ein automatisierter auf Deep-Learning mit CNNs basierender Mapping-Ansatz für die Areale Op5-Op7 und Area 44+45 angewendet werden (Schiffer et al., 2021). Area 44+45 sowie Area Te3 wurden hinsichtlich ihrer Genexpression untersucht; hierbei standen mit phonologischer Verarbeitung assoziierte Gene im Fokus (Unger et al., 2021d). Insgesamt trägt das Projekt zur zytoarchitektonischen Analyse von Sprache sowie zur Erweiterung multimodaler Informationen des FOp und der klassischen Sprachareale Broca und Wernicke im Rahmen des Julich-Brain Atlasses sowie des Multilevel Human Brain Atlasses bei.

3.1 Multimodale Abgrenzung der FOp-Areale zu anderen Sprachareale n

In früheren Studien konnten das FOp und das klassische Sprachareal Broca auf Basis der Rezeptorarchitektonik (Amunts et al., 2010) und der Konnektivität (Anwander et al., 2007; Jung et al., 2017) voneinander abgegrenzt werden. Dies wurde in der vorliegenden Arbeit durch die zytoarchitektonische Unterteilung des posterioren FOp in die Areale Op5-Op7 bestätigt; Area 44+45 (Amunts et al., 1999; Amunts et al., 2004) sowie das anteriore FOp (Area Op8 und Op9; Saal et al., 2021a; Saal et al., 2021b) stellten sich als Nachbarareale von Op6 und Op7 heraus (Unger et al., 2023). Somit konnten durch die von unserer Arbeitsgruppe betrachteten Modalitäten Rezeptorarchitektonik und Zytoarchitektonik innerhalb des Areals FOp konzeptionelle Veränderungen auf zwei Ebenen innerhalb des Cortex aufgezeigt werden (Amunts et al., 2010; Unger et al., 2023). Zusätzlich wurden

Area 44+45 genetisch abgegrenzt und charakterisiert (Unger et al., 2021d), was auf abweichende zugrundeliegende organisatorische Prinzipien hindeutet.

Mikrostrukturell betrachtet zeigte Area Op6 die größte Ähnlichkeit mit der makroanatomisch benachbarten und ebenso dysgranulären Area 44 durch sehr große Zellen in den Laminae III und V (Amunts et al., 1999; Amunts et al., 2004; Unger et al., 2023). Für Area Op6 links konnte innerhalb von Unger et al. (2023) die stärkste funktionelle und strukturelle Einbindung in Musik- und Sprachnetzwerke gefunden werden. Analysierte Konnektivitätsdaten umfassten darüber hinaus Verbindungen zwischen Area 44 und dem Areal Op6 links (Unger et al., 2023), ggf. als Teil der anterioren Sprachregion (Amunts et al., 2010). Eine Positronen-Emissions-Tomographie (PET)-Studie bestätigte dies durch eine parallele Aktivität im linken FOp und in den BA 44+45 bei der Generierung von Sätzen sowie im rechten FOp, im BA 44 rechts und im BA 45 links bei der Verarbeitung von Tönen (Brown et al., 2006). Auch eine Reihe fMRT-basierter Sprachexperimente zeigte Co-Aktivierungen des FOp mit Broca (u. a. Friederici et al., 2000), sodass wiederholt der Eindruck eines engen inhaltlichen Zusammenhangs der Areale als reine Erweiterung des klassischen Sprachareals Broca entstand.

Basierend auf zytoarchitektonischen Kriterien wies Area 44 im Vergleich zu Area Op6 deutlich größere Pyramidenzellen mit einer höheren Zelldichte auf (Amunts et al., 1999; Amunts et al., 2004). Eine weitere Abweichung bestand darin, dass für die sprachlich relevante Area 44 links ein signifikant höheres Volumen festgestellt wurde (Amunts et al., 2004), während für Area Op6 links keine signifikante Lateralisierung zugunsten der linken Hemisphäre vorlag (Unger et al., 2023). Darüber hinaus zeigte das Areal Op6 links neben der Assoziation mit Musikverarbeitung eine zusätzliche funktionelle Spezialisierung in Form der Muskelkontraktion (Unger et al., 2023), aufgrund derer derzeit nicht davon ausgegangen werden kann, dass es sich bei dem posterioren FOp um eine reine strukturelle und funktionelle Erweiterung des Broca-Areals handelt.

Die Annahme wird bekräftigt durch feine differentielle sprachbezogene Aussagen zwischen dem FOp und dem klassischen Broca-Areal. Für den Bereich Syntax zeigte sich dies durch eine Beteiligung des linken FOp an der Bildung lokaler Phrasenstrukturen (Nominal-, Verbal- und Präpositionalphrasen), während sich Broca in Abhängigkeitsbeziehungen zwischen den Konstituenten eines Satzes involviert zeigte und eine entscheidende Rolle bei der Verarbeitung von syntaktisch komplexen Satzhierarchien spielte (Friederici et al., 2003; Friederici, 2006; Friederici et al., 2006a; Grodzinsky, 2000; Grodzinsky & Friederici, 2006). Im Bereich Phonologie stellte sich Broca als an phonologischen Wortproduktionsaufgaben

(z. B. für phonologische Wortflüssigkeitsparadigmen) beteiligt heraus, während das FOp u. a. in phonologische Entscheidungsaufgaben involviert war (Friederici et al., 2000). In einer Studie zur strukturellen Konnektivität zeigten Friederici et al. (2006a) unterschiedliche Konnektivitätssignaturen für das FOp und das Broca-Areal im linken inferioren frontalen Cortex, was zusätzlich für eine Segregation spricht.

Zusammenfassend deuten die Ergebnisse darauf hin, dass Broca und das FOp bei komplexen sprachlichen Funktionen wie Syntax zusammenarbeiten (Friederici et al., 2000) und für die Ausführung verschiedener Teilfunktionen verantwortlich sind (Friederici et al., 2006a; Friederici et al., 2006b). Assoziativen Arealen kann oft keine eindeutige funktionelle Einbindung zugeordnet werden (Draguhn, 2019). Da das FOp dem präfrontalen Assoziationscortex (Birbaumer & Schmidt, 2019) zugeschrieben werden kann und darüber hinaus phylogenetisch älter ist als das Broca-Areal (Friederici, 2006), kann angenommen werden, dass die funktionelle Spezialisierung weniger stark ausgeprägt ist als die des Broca-Areals.

Nach einer Vielzahl von Studien, die eine sprachbasierte Co-Aktivierung zwischen dem FOp und der anterioren Insula zeigten (u. a. Hurschler et al., 2013), konnten innerhalb von Unger et al. (2023) die operculären Areale Op5-Op7 neben der Abgrenzung zu Broca auch klar von Arealen der anterioren Insula unterschieden werden. Die zytoarchitektonische Grenze zum FOp konnte jeweils im Sulcus circularis insulae identifiziert werden und das FOp ging medial in keiner der betrachteten Hemisphären über den Sulcus hinaus (Unger et al., 2023). Innerhalb der Brodmannschen Karte (1909) konnte der Bereich der Insula nicht präzise dargestellt werden (Zilles & Amunts, 2010); Quabs et al. (2022) kartierten die anteriore Insula kürzlich in sieben Areale (Ig3, Ia1 und Id2-Id6). Da sich mit Area Id7 insbesondere eines der Areale durch Beteiligung an der Funktion der lokalen Negation als zuständig zeigte (Grodzinsky et al., 2020), und dies ohne weitere Beteiligung sowie in Abgrenzung zum FOp, wird zwischen der Insula und dem FOp ebenfalls eine Grenze gezogen und das FOp nicht als reine Erweiterung der (anterioren) Insula angesehen.

Eine ähnliche Annahme kann für den Bereich des PMC getroffen werden. Rezeptorarchitektonisch konnte Area 6r1 bereits vom FOp abgegrenzt werden (Amunts et al., 2010); zytoarchitektonisch konnte dieser Aspekt bestätigt werden (Unger et al., 2023). Das Areal 6r1 wurde als Teil der anterioren Sprachregion identifiziert. Darüber hinaus ist der PMC auch in motorische Prozesse und weitere kognitive Funktionen involviert (für ein Review siehe Fine & Hayden, 2022).

3.2 Rolle des FOp als funktionelles Übergangsareal

Da in mehreren Modalitäten deutliche Unterschiede zwischen den Arealen Op5-Op7 und ihrer unmittelbaren Umgebung festgestellt wurden, könnte der posteriore Teil des FOp als Übergangszone fungieren. Dies wird durch die regional unterschiedlichen Ergebnisse zur Funktion und Konnektivität belegt, die diese Annahme unterstützen (Unger et al., 2023).
So grenzt das Areal Op6 ventral an Area 44; beide Areale sind in Musik- bzw. Sprachnetzwerke eingebunden (Chiang et al., 2018; Unger et al., 2023). In Bezug auf die funktionelle Konnektivität zeigten sich insbesondere Verbindungen zu Area 44 der linken Hemisphäre (Unger et al., 2023). Die strukturellen Konnektivitätsdaten aus der 1000BRAINS-Studie bestätigten dies, indem sie in der Literatur (Catani et al., 2005; Friederici, 2009; Friederici, 2011) bereits beschriebene Verbindungen von Area Op6 links zu Area 44 links und Area 45 links und somit in das Musik- bzw. Sprachnetzwerk aufzeigten. Demnach ist das Areal Op6 links qualitativ eher der anterioren Sprachregion zuzuordnen als das Areal Op5, das funktionell eher der somatosensorischen Region des POp zugeschrieben werden kann (Unger et al., 2023).
Das Areal Op6 befindet sich lateral angrenzend an Area 6 des PMC. Linkshemisphärisch sind die Areale Op6 links und Op5 rechts laut BrainMap mit isometrischer Muskelkraft verbunden (Unger et al., 2023), während der PMC motorische Funktionen übernimmt (Fine & Hayden, 2022). Durch eine auf MACM basierende funktionelle Konnektivität zu Area 44 links sowie zu den Arealen hIP1 (Choi et al., 2006) und hIP3 (Scheperjans et al., 2008a; Scheperjans et al., 2008b) des Sulcus intraparietalis (Ward & Frackowiak, 2003) konnten motorische Verbindungen belegt werden (Unger et al., 2023). Die Ergebnisse der strukturellen Konnektivität bestätigten dies zwischen dem linken Areal Op6 zur linken Area 44. Weitere strukturelle Verbindungen konnten zu den Arealen 1 (Geyer et al., 1999; Geyer et al., 2000) und 4a (Geyer et al., 1996) in Kombination mit Teilen des Areals 6 (Sigl et al., 2021a; Sigl et al., 2021b) und des Lobus parietalis inferior nachgewiesen werden, die ebenfalls für motorische Funktionen relevant sind (Caspers et al., 2006; Caspers et al., 2008). Aufgrund dieser Einbettung kann Area Op5 rechts zusammen mit dem Areal Op6 links motorischen Funktionen zugeordnet werden (Unger et al., 2023).
Area Op5 grenzt hingegen rostral an die Areale OP1 und OP4 des POp. Rechtshemisphärisch ist Area Op5 laut BrainMap mit sexueller Verarbeitung assoziiert (Unger et al., 2023), während Area OP1 (Eickhoff et al., 2006a; Eickhoff et al., 2006c) und OP4 (Eickhoff et al., 2006a; Eickhoff et al., 2006c) somatosensorische Funktionen aufweisen (Eickhoff et al.,

2010). Für Area Op5 rechts zeigte sich der Zusammenhang insbesondere durch die funktionellen Verbindungen auf Basis von MACM (Unger et al., 2023) zu den Arealen 3a (Geyer et al., 1999; Geyer et al., 2000), 3b (Geyer et al., 1999; Geyer et al., 2000), 4a, 4p (Geyer et al., 1996), Id4 (Quabs et al., 2022), OP1 und OP3 (Eickhoff et al., 2006a; Eickhoff et al., 2006c) sowie zum Corpus geniculatum mediale des Metathalamus (Kiwitz et al., 2022) und präzentralen Bereichen (Georgiadis et al., 2010; Moulier et al., 2006).

3.3 Einsatzmöglichkeiten zytoarchitektonischer Wahrscheinlichkeitskarten

Im klinischen Kontext der Neurologie und Psychiatrie bieten sich vielfältige Einsatzmöglichkeiten für die zytoarchitektonischen Wahrscheinlichkeitskarten, u. a. hinsichtlich sprachbezogener Fragestellungen. Das vorhandene neuroanatomische Wissen aus der Grundlagenforschung kann so aktiv genutzt werden (Zachlod et al., 2023). Darüber hinaus können, ähnlich wie von Palomero-Gallagher et al. (2020) für den Bereich des Hippocampus vorgeschlagen, Vergleiche der molekularen Organisation von physiologischem und pathologischem Gewebe aus dem neurologischen und psychiatrischen Bereich zu translationalen neurowissenschaftlichen Strategien und zur Entwicklung von Medikamenten beitragen. Da die Karten eine präzise Lokalisation der jeweiligen Hirnregion ermöglichen, erlauben sie bei Area Op5-Op7 eine klare Unterscheidung zwischen dem FOp und benachbarten Arealen.

3.3.1 Klinisch-neurologischer Bereich

Durch die Einbindung in den MNI-Referenzraum sind die Julich-Brain Atlas-Karten interoperabel und könnten u. a. zur Beschreibung neuronaler Aktivierungsmuster (Amunts et al., 2020) innerhalb von fMRT-Sprachexperimenten herangezogen werden. Da Area Op6 links aufgrund ihrer strukturellen und funktionellen Konnektivität mit der Verarbeitung von Musik in Verbindung gebracht wurde und sich als unterstützend für sprachliche Funktionen herausstellte (Unger et al., 2023), könnte diese Annahme durch weitere Studien im Bereich der Sprachverarbeitung mithilfe der auf mikrostrukturellem

Detailgrad basierenden Karte untersucht werden, um die sprachliche Rolle genauer zu definieren.

Ergänzend könnte durch die schwerpunktmäßige Assoziation des Areals Op6 links mit der Musikverarbeitung (Unger et al., 2023) die Frage nach morphologischen Charakteristika des FOp bei musikalisch begabten Personen gestellt werden. Abdul-Kareem et al. (2011) zeigten u. a. ein höheres Volumen der grauen Substanz innerhalb des linken Pars opercularis als Teilbereich des Broca-Areals bei männlichen Orchestermusikern, positiv korreliert mit den Jahren der musikalischen Erfahrung. Da Broca und das FOp in der Musik- und Sprachverarbeitung zusammenwirken (Levitin & Menon, 2003), könnte ein weiterer Anwendungskontext für die Karte von Op6 links im Bereich des Cortexvolumens von Musiker:innen innerhalb des FOp liegen. Zudem könnte der Schwerpunkt auf eine voxel-basierte Morphometrie gesetzt werden, um die Dichte der grauen Substanz zu messen, die sich im Broca-Areal bei männlichen Symphonieorchestermusikern erhöht zeigte (Sluming et al., 2002).

Eine weitere Einsatzmöglichkeit zytoarchitektonischer Wahrscheinlichkeitskarten wurde in einer einjährigen fMRT-Longitudinalstudie durch Heim et al. (2014) aufgezeigt. Die Studie untersuchte die Entwicklung der lexikalischen Verarbeitung auf neuronaler Basis bei vier Patient:innen mit der neurodegenerativen Sprachstörung PPA. Dazu wurde eine Wörter und Pseudowörter umfassende Entscheidungsaufgabe in Verbindung mit einer Betrachtung von Atrophiemustern durchgeführt. Mithilfe von fMRT- und Blood-Oxygenation-Level Dependent-Messungen wurden Gruppenunterschiede bzgl. des Lexikalitätseffekts untersucht. Zur Erfassung von Gehirnatrophien wurde eine hochauflösende 3D-T1-gewichtete MRT-Aufnahme mittels Magnetization Prepared Rapid Acquisition with Gradient Echoes durchgeführt und anhand der deformations-basierten Morphometrie ausgewertet. Eines der Hauptergebnisse war eine erhöhte Aktivität im linken Gyrus temporalis medius sowie im Übergang vom Sulcus frontalis inferior zum Sulcus praecentralis inferior bei zunehmender Atrophie in diesen Bereichen. Die lexikalische Performanz war etwa gleichbleibend (Heim et al., 2014). Bei Ausweitung der Studie hinsichtlich phonologischer Symptome, welche sich insbesondere bei der lvPPA zeigen (Gorno-Tempini et al., 2011), könnte in einem ähnlichen Studiendesign der spezifische Bereich des FOp betrachtet werden.

Durch eine Längsschnittanalyse (Pieperhoff et al., 2022) auf Grundlage einer deformationsbasierten Morphometrie, erhoben im MRT, wurden für die Erkrankung Morbus Parkinson durch den Einsatz zytoarchitektonischer Karten aus dem Julich-Brain Atlas

regionale Veränderungen nachgewiesen. Diese zeigten sich in Form signifikant beschleunigter Volumenabnahmen im Lobus occipitalis, Lobus temporalis, Lobus parietalis inferior sowie in der Insula, dem Putamen und dem Nucleus basalis im Gegensatz zur Kontrollgruppe. Baseline-Gruppenvergleiche betrafen auch das anteriore FOp (Pieperhoff et al., 2022). Im Bereich der Bewegungsstörungen bei Parkinson könnten in weiteren Untersuchungen gezielt Aktivierungen in den u. a. mit Bewegung assoziierten Arealen Op5 und Op6 (Unger et al., 2023) betrachtet werden.

Neben ihrem Einsatz in MRT-Experimenten könnten die zytoarchitektonischen Wahrscheinlichkeitskarten auch zur Analyse schlaganfallbedingter Läsionsmuster (Zhao et al., 2020) oder zur Lokalisation von Läsionen bei taktilen Agnosien (Hömke et al., 2009) angewendet werden. Im weiteren Verlauf könnten die Karten des FOp in der Neurochirurgie für die Lokalisation und Operation von Hirntumoren, einschließlich Wachoperationen mit Sprachmonitoring, eingesetzt werden. Hier könnten sie bei der Abgrenzung benachbarter sprachlich relevanter und nicht relevanter Areale behilflich sein.

Damit zusammenhängend befasste sich eine Studie von Duong et al. (2023) mit einer umfassenden Dekodierung der funktionellen Organisation der Insula mittels intrakranieller elektrischer Stimulation und aufgabenbezogener intrakranieller EEG-Aufzeichnungen, was eine weitere Anwendungsmöglichkeit darstellt. Durch den Einsatz probabilistischer zytoarchitektonischer Wahrscheinlichkeitskarten der Insula konnten den Arealen lg2/ld2, ld3, Id6 und Id7 spezifische Funktionen im viszeralen bzw. autonomen Bereich sowie in den Domänen Angst, Geschmack bzw. Olfaktorik, Schmerz bzw. Temperatur und Somatosensorik auf Basis von 17 neurochirurgischen Patient:innen zugeordnet werden. Ein vergleichbarer Ansatz könnte für die Areale des FOp angewandt werden, u. a. um die Spezialisierung hinsichtlich Musik bzw. Sprache für nur eines der Areale zu überprüfen und ggf. zu verifizieren.

Ein weiteres neurologisch relevantes Anwendungsgebiet könnte die nichtinvasive Hirnstimulation sein. Dies umfasst die transkranielle Gleichstromstimulation (tDCS) und die transkranielle Magnetstimulation (TMS), welche u. a. zur sprachlichen Rehabilitation bei Aphasie nach Schlaganfall in Verbindung mit Benenntherapie und somit im neurologisch-sprachtherapeutischen Bereich eingesetzt werden können (u. a. Meinzer et al., 2016; Naeser et al., 2011). Als Maske zur Platzierung der Elektroden bzw. des Stimulationsaustrittsortes wird häufig das Elektroenzephalographie (EEG)-System (10-20-System) eingesetzt (Antal et al., 2017). Die Nutzung von MRT-unterstützter Neuronavigation kann Lokalisationsungenauigkeiten verringern (De Witte et al., 2018;

Sack et al., 2009). Um neue Methoden zur Platzierung der Elektroden bzw. TMS mit bestmöglichem Ergebnis zu entwickeln, wäre es wünschenswert, das neuroanatomische Wissen der neu gewonnenen zytoarchitektonischen Wahrscheinlichkeitskarten zu nutzen.
Nicht nur bei Patient:innen mit Aphasie nach Schlaganfall, sondern auch bei einer Vielzahl neurologischer Erkrankungen wie z. B. der PPA (Nissim et al., 2020) konnte gezeigt werden, dass nichtinvasive Hirnstimulation beitragen kann, sprachliche Symptome zu lindern. Das Prinzip der tDCS zielt auf die Stimulation funktioneller Netzwerkanteile ab, z. B. zur Unterstützung sprachlicher Funktionen (u. a. Meinzer et al., 2016). Die Identifizierung neuer sprachlicher Areale basierend auf zytoarchitektonischen Kriterien, die u. a. für Phonologie und Syntax relevant sind, könnte dazu beitragen, relevante Netzwerke zu identifizieren und potentiell zu stimulieren. Darüber hinaus könnte das Einbeziehen des neuroanatomischen Wissens je nach Störungsbild und medizinisch-therapeutischer Zielsetzung Aufschluss darüber geben, welche im Netzwerk zur Stimulation geeigneten Areale in welchem Umfang intakt oder betroffen sind.

3.3.2 Klinisch-psychiatrischer Bereich

Eine MRT-Studie im klinisch-psychiatrischen Bereich, die sowohl eine voxel-basierte Morphometrie als auch eine regionenbasierte Morphometrie umfasste (Bludau et al., 2016), untersuchte die zytoarchitektonisch definierten Areale Fp1 und Fp2 genetisch, da der menschliche Frontalpol in der Vergangenheit als Knotenpunkt im dysfunktionalen Netzwerk der Major Depression identifiziert wurde. In die Studie wurden insgesamt 73 Menschen mit schwerer Depression und 73 gesunde Kontrollpersonen eingeschlossen. In der Patient:innengruppe zeigten sich morphologische Veränderungen in Form eines signifikant kleineren medialen Frontalpols (Fp2, linke Hemisphäre), darüber hinaus war eine negative Korrelation zwischen Krankheitsschwere und -dauer zu beobachten.
In einer Arbeit zur Schizophrenie untersuchten Zimmermann et al. (2024) insgesamt 478 Patient:innen und 236 Kontrollpersonen. Es konnte ein Zusammenhang zwischen reduzierten Asymmetrien der bilateralen zytoarchitektonisch definierten Areale 44+45 und dem Grad der individuellen Psychopathologie, z. B. in Form von Psychosen, gezeigt werden. Darüber hinaus wurden spezifische Reduktionen der grauen Substanz innerhalb der Areale mit einem kognitiven und negativen Subtyp der Schizophrenie assoziiert. Eine Genexpressionsanalyse ergab eine Hochregulierung des Gens *MET* in den betrachteten Bereichen, woraus die Autor:innen einen Zusammenhang zwischen sich unterscheidenden

Genvarianten, strukturellen Veränderungen innerhalb von Area 44+45 und einer spezifischen Psychopathologie bei Schizophrenie folgerten. Ausgehend von dieser Studie könnten die zytoarchitektonischen Wahrscheinlichkeitskarten des FOp als Maske zur Untersuchung weiterer Symptome der Schizophrenie herangezogen werden. Da eine Studie des auditiven Arbeitsgedächtnisses im fMRT bei Schizophrenie von Menon et al. (2001) signifikante auf die weiße Substanz zurückzuführende Aktivierungsdefizite im bilateralen FOp zeigte, könnte die Forschung in diesem Bereich fortgesetzt werden.
Ein ergänzendes psychiatrisches Anwendungsfeld könnte die Weiterführung von Studien wie der von Kaulen et al. (2022) sein. Die Autor:innen stellten einen PET-Atlas vor, der die Verteilung von Glutamat und $GABA_A$ *in vivo* zeigt, mit potenziellem Nutzen für psychiatrische Erkrankungen. Die Verknüpfung der rezeptorspezifischen Erkenntnissen mit den mikrostrukturellen Karten des Julich-Brain Atlasses oder Genexpressionsdaten des Allen Human Brain Atlasses, wie in den Limitationen der Arbeit erwähnt, könnte zur weiteren Validierung der Informationen beitragen (Kaulen et al., 2022).

3.4 Offene Fragen und Ausblick

Neben Einsatzmöglichkeiten der zytoarchitektonischen Wahrscheinlichkeitskarten im klinischen Bereich ergeben sich aus der hier vorgestellten Arbeit konkrete neurowissenschaftliche Fragestellungen. Diese betreffen insbesondere die multimodale Perspektive, neurobiologische Grundlagenforschung sowie den Bereich der künstlichen Intelligenz.

3.4.1 Neurowissenschaftliche Fragestellungen

Mithilfe der zytoarchitektonischen Wahrscheinlichkeitskarten von Op5-Op7, die die interindividuelle Variabilität des menschlichen Gehirns berücksichtigen, könnten weitere multimodale Analysen zur strukturellen und funktionellen Charakterisierung der Areale durchgeführt werden (Unger et al., 2023). Neben Aussagen zur Zytoarchitektonik (Unger et al., 2023) und Rezeptorarchitektonik (Amunts et al., 2010) zum FOp könnten gezielt genetische und funktionelle Analysen für die spätere Aufnahme in den EBRAINS Multilevel Human Brain Atlas ergänzt werden. Auch eine Unterteilung hinsichtlich weiterer Modalitäten, u. a. Myeloarchitektonik, Rezeptorarchitektonik und Genexpression sowie eine

Betrachtung ihrer Kohärenz sind von hoher Relevanz. So könnte das FOp in einem noch umfangreicheren multimodalen Kontext diskutiert werden.

Weiterhin wäre es interessant, welche strukturellen Verbindungen sich auf konnektiver Ebene für die bisherigen identifizierten Areale des gesamten Operculums ergeben. Auf diese Weise könnten Verbindungen im nächsten Schritt funktionell eingeordnet und interpretiert werden, beispielsweise im anterior-posterior-Vergleich. Zur Sichtbarmachung von Faserorientierungen könnte u. a. die Methode des Polarized Light Imaging (Axer & Amunts, 2022) eingesetzt werden.

In Bezug auf die Idee des posterioren FOp als funktionelle Übergangsregion zwischen Sprache (Broca), Motorik (PMC) und somatosensorischen Funktionen (POp) (siehe **Kapitel 3.2**), wäre es interessant, JuGEx-Analysen mithilfe von Karten des FOp durchzuführen und das strukturelle Wissen so zu erweitern. Genetische Profile könnten weiteren Aufschluss über die Verbindungen zwischen den Hirnregionen geben.

Hinsichtlich der Genexpression, äquivalent zu der Analyse von Area 44+45 und Te3 (Unger et al., 2021d), ergibt sich darüber hinaus die Frage, wie sich die Expression sprachrelevanter Gene innerhalb des FOp im Vergleich zu den bereits untersuchten Arealen Broca und Wernicke darstellt. Hierbei könnte aufgrund der Zuordnung des FOp zu phonologischer Verarbeitung (Bohland & Guenther, 2006; Fiez et al., 2006; Hurschler et al., 2013) der Schwerpunkt aus Unger et al. (2021d) beibehalten werden und z. B. um Area Op6 links (Unger et al., 2023) erweitert werden. Ein genetischer Vergleich zwischen den benachbarten Arealen Op6 und Area 44 links wäre aufgrund der zytoarchitektonischen Ähnlichkeit relevant. Da sich die räumliche Topographie des Neocortex in seiner molekularen Topographie widerspiegelt (Hawrylycz et al., 2012), ist anzunehmen, dass kortikale Regionen, die ähnlich nah beieinander liegen wie Area Op6 und Area 44, vergleichbare Transkriptome aufweisen; aufgrund des in **Kapitel 1.2** thematisierten phylogenetischen Unterschieds zwischen den Gebieten ist der Vergleich dennoch besonders interessant.

Neben der Betrachtung von Daten gesunder Proband:innen könnte als erweiterter Schritt die multimodale Betrachtung der Areale Op5-Op7 im erkrankten Gehirn in Erwägung gezogen werden. In diesem Zuge könnte z. B. das linke Areal Op6 bei Proband:innen mit einer syntaktischen bzw. phonologischen Störung strukturell untersucht werden, um Abweichungen von der zuvor untersuchten Physiologie aufzuzeigen.

Darüber hinaus könnten mögliche zukünftige Forschungsaktivitäten anterior zu Area Op8+Op9 gelegene Bereiche untersuchen, um herauszufinden, ob das FOp aus

weiteren Arealen besteht als dem in Unger et al. (2023) beschriebenen posterioren Teil (Op5-Op7) und dem anterioren Teil (Op8+Op9). Im Zuge der Arbeit von Saal et al. (2021a, 2021b) wurden Hinweise auf bislang unerforschte Areale im FOp gefunden. Langfristig wäre dieser Aspekt für die Gesamtgröße und Lokalisation des FOp entscheidend. Zudem könnte dies Aufschluss zu strukturellen und funktionellen Charakteristika des gesamten FOp bzw. Operculums im Vergleich zur Umgebung geben.

Für das FOp (Op5-Op7) befinden sich im EBRAINS Multilevel Human Brain Atlas neben der zytoarchitektonischen Wahrscheinlichkeitskarten und Konnektivitätsdaten pro Hemisphäre (Unger et al., 2023) u. a. strukturelle Daten zur 3D-Rekonstruktion von Pyramidenzellen, Nervenfaserrekonstruktionen in Mikrometer-Auflösung sowie eine Segmentierung des Gehirnvolumens auf Basis eines 7-Tesla-MRT-Scans. Bzgl. funktioneller Messungen liegen u. a. im Schlaf erhobene EEG-Daten mit intermittierendem Aufwachen sowie EEG-Daten für Schlafentzug vor (Julich-Brain Atlas, 2023a). All diese Daten könnten Ansatzpunkte liefern für strukturelle und funktionelle Folgeanalysen mit dem kompletten FOp, mit dem vollständigen posterioren FOp oder mit einzelnen Arealen anhand zytoarchitektonischer Wahrscheinlichkeitskarten.

3.4.2 Deep Learning im multimodalen Kontext

Derzeit existiert ein Zuwachs von Methoden, die auf Deep-Learning-Algorithmen basieren, u. a. CNNs (Schiffer et al., 2021; Spitzer et al., 2017; Spitzer et al., 2018). Vorhandene Ergebnisse zum automatisierten zytoarchitektonischen Mapping müssen in diesem Zuge erweitert und präzisiert werden, für zuverlässige und mit dem bisherigen Ansatz vergleichbare Aussagen (Schiffer et al., 2021). Es wäre interessant, dieses CNN-basierte Wissen in Zukunft auch auf andere Modalitäten anzuwenden, die eine bildbasierte Methode nutzen können. Das BigBrain stellt mit seiner hohen Auflösung und durch das enthaltende dichte Mapping ein geeignetes 3D-Modell dar, um Analysen im Mikrometerbereich der kortikalen Schichten durchzuführen. Außerdem fungiert es als Referenzsystem zur Integration multimodaler Daten sowie für Modellierungen und Simulationen, welche die regionale Heterogenität der Organisation des menschlichen Gehirns miteinbeziehen (Amunts et al., 2013).

Das Thema des automatisierten Mappings mittels eines Algorithmus bringt Vor- und Nachteile mit sich. Vorteile sind automatisierte Prozesse, Zeitersparnis durch höhere

Produktivität sowie zeitliche Effizienz (Schiffer et al., 2021). Nachteilig kann eine mangelnde Transparenz bzgl. der Arbeitsweise von Algorithmen sein (Kiwitz et al., 2020). Bzgl. ultrahochaufgelöster Gehirnmodelle wie z. B. dem BigBrain und dem automatisierten Mapping von Schnitten innerhalb dieser Modelle ist zu beachten, dass aufgrund der hohen Auflösung große Datenmengen entstehen. Die Disziplinen Big Data und Supercomputing sind hier von großer Bedeutung, da die Daten ansonsten schwer speicher- und nutzbar sind (Amunts et al., 2013; Amunts & Lippert, 2021).

Langfristig könnten Deep-Learning-basierte Methoden, die sich auf Sprachfunktionen und Sprachstörungen beziehen, deutlich erweitert werden, z. B. im Hinblick auf genetische Analysen. Es wäre wünschenswert, Methoden zu entwickeln, die eine Vorhersage der physiologischen Expression von sprachrelevanten Genen und ihren Abweichungen in spezifischen Gehirnregionen ermöglichen. Auf der Grundlage identifizierter Profile von Personen mit Sprach- und Lernstörungen könnten genetische Profile für die Diagnose von Sprachstörungen verwendet werden.

Es könnten außerdem Modelle entwickelt werden, um die Auswirkungen von Läsionen innerhalb von Sprachareale auf die Sprachleistung abzuschätzen, z. B. bei Auftreten einer Aphasie. Hierbei könnte beispielsweise das „Virtual Brain“ als Teil von EBRAINS genutzt werden, das eine Möglichkeit zur Konstruktion, Simulation und Analyse von Gehirnnetzwerkmodellen bietet (Schirner et al., 2022). Die Sprachtherapie als für die Behandlung von Sprachstörungen verantwortliche Disziplin könnte von diesem Wissen profitieren und die Behandlung individuell auf die Läsion der Patient:innen ausrichten.

3.5 Schlussfolgerungen

Durch die zytoarchitektonische Kartierung von Area Op5, Op6 und Op7 konnte die vorliegende Arbeit zur Identifizierung der Areale im posterioren Teil des FOp auf mikrostruktureller Ebene beitragen. Es zeigte sich ein breites Spektrum an assoziierten Funktionen von Area Op5-Op7. Daher kann das posteriore FOp derzeit nicht als reine Erweiterung des klassischen Sprachareals Broca, das zusätzlich anhand der Genexpression definiert werden konnte, angesehen werden. Die deutlichsten Hinweise auf eine Einbindung des posterioren FOp in das Musik- bzw. Sprachnetzwerk ergaben sich für Area Op6 links. In Folgestudien wird es aufgrund der nun vorliegenden zytoarchitektonischen Wahrscheinlichkeitskarte für das Areal Op6 links möglich sein, dies klinisch weiter zu

untersuchen und die Sprachfunktion in Abgrenzung zu benachbarten Arealen weiter zu präzisieren. Weitere Anwendungsfelder im neurologischen, psychiatrischen und neurowissenschaftlichen Bereich ergeben sich aus der Verfügbarkeit der mikrostrukturellen Karten.

Die Zusammenfassung multimodalen Wissens innerhalb des EBRAINS Multilevel Human Brain Atlasses bietet übersichtlich strukturiertes, umfassendes und multimodales Wissen pro zytoarchitektonisch definiertem Bereich. Es handelt sich dabei um einen integrativen Ansatz sowie eine innovative Infrastruktur, die sich in den kommenden Jahren und Jahrzehnten erheblich erweitern wird und die die traditionelle Kartierung ergänzen wird. Durch den Einsatz von auf Deep Learning basierenden Verfahren können zukünftig sowohl die Grundlagenforschung als auch die translationale und klinische Forschung profitieren.

Literaturverzeichnis

Abdul-Kareem, I. A., Stancak, A., Parkes, L. M., & Sluming, V. (2011). Increased gray matter volume of left pars opercularis in male orchestral musicians correlate positively with years of musical performance. *Journal of Magnetic Resonance Imaging*, *33*(1), 24–32. https://doi.org/10.1002/jmri.22391

Amunts, K., Hawrylycz, M. J., Van Essen, D. C., Van Horn, J. D., Harel, N., Poline, J. B., De Martino, F., Bjaalie, J. G., Dehaene-Lambertz, G., Dehaene, S., Valdes-Sosa, P., Thirion, B., Zilles, K., Hill, S. L., Abrams, M. B., Tass, P. A., Vanduffel, W., Evans, A. C., & Eickhoff, S. B. (2014). Interoperable atlases of the human brain. *NeuroImage*, *99*, 525–532. https://doi.org/10.1016/j.neuroimage.2014.06.010

Amunts, K., Lenzen, M., Friederici, A. D., Schleicher, A., Morosan, P., Palomero-Gallagher, N., & Zilles, K. (2010). Broca's region: Novel organizational principles and multiple receptor mapping. *PLoS Biology*, *8*(9), e1000489. https://doi.org/10.1371/journal.pbio.1000489

Amunts, K., Lepage, C., Borgeat, L., Mohlberg, H., Dickscheid, T., Rousseau, M.-É., Bludau, S., Bazin, P.-L., Lewis, L. B., Oros-Peusquens, A.-M., Shah, N. J., Lippert, T., Zilles, K., & Evans, A. C. (2013). BigBrain: An ultrahigh-resolution 3D human brain model. *Science, 340*(6139), 1472–1475. https://doi.org/10.1126/science.1235381

Amunts, K., & Lippert, T. (2021). Brain research challenges supercomputing. *Science*, *374*(6571), 1054–1055. https://doi.org/10.1126/science.abl8519

Amunts, K., Mohlberg, H., Bludau, S., & Zilles, K. (2020). Julich-Brain: A 3D probabilistic atlas of the human brain's cytoarchitecture. *Science*, *368*(6506), 988–992. https://doi.org/10.1126/science.abb4588

Amunts, K., Schleicher, A., Bürgel, U., Mohlberg, H., Uylings, H. B. M., Zilles, K., & Vogt, O. (1999). Broca's region revisited: Cytoarchitecture and intersubject variability. J*ournal of Comparative Neurology, 412*(2), 319–341.

Amunts, K., Schleicher, A., & Zilles, K. (2004). Outstanding language competence and cytoarchitecture in Broca's speech region. *Brain and Language*, *89*(2), 346–353.

https://doi.org/10.1016/S0093-934X(03)00360-2

Amunts, K., Schleicher, A., & Zilles, K. (2007). Cytoarchitecture of the cerebral cortex – More than localization. *NeuroImage*, *37*(4), 1061–1065. https://doi.org/10.1016/j.neuroimage.2007.02.037

Amunts, K., & Zilles, K. (2006). A multimodal analysis of structure and function in Broca's region. In Y. Grodzinsky, & K. Amunts (Hrsg.), *Broca's region.* (S. 17–46). Oxford, UK: Oxford University Press.

Amunts, K., & Zilles, K. (2012). Architecture and organizational principles of Broca's region. *Trends in Cognitive Sciences*, *16*(8), 418–426. https://doi.org/10.1016/j.tics.2012.06.005

Amunts, K., & Zilles, K. (2015). Architectonic mapping of the human brain beyond Brodmann. *Neuron*, *88*(6), 1086–1107. https://doi.org/10.1016/j.neuron.2015.12.001

Antal, A., Alekseichuk, I., Bikson, M., Brockmöller, J., Brunoni, A. R., Chen, R., Cohen, L. G., Dowthwaite, G., Ellrich, J., Flöel, A., Fregni, F., George, M. S., Hamilton, R., Haueisen, J., Herrmann, C. S., Hummel, F. C., Lefaucheur, J. P., Liebetanz, D., Loo, C. K., … Paulus, W. (2017). Low intensity transcranial electric stimulation: Safety, ethical, legal regulatory and application guidelines. *Clinical Neurophysiology*, *128*(9), 1774–1809. https://doi.org/10.1016/j.clinph.2017.06.001

Anwander, A., Tittgemeyer, M., Von Cramon, D. Y., Friederici, A. D., & Knösche, T. R. (2007). Connectivity-based parcellation of Broca's area. *Cerebral Cortex*, *17*(4), 816–825. https://doi.org/10.1093/cercor/bhk034

Axer, M., & Amunts, K. (2022). Scale matters: The nested human connectome. *Science*, *378*(6619), 500–504. https://doi.org/10.1126/science.abq2599

Bailey, P., & Von Bonin, G. (1951). *The isocortex of man*. Illinois: University of Illinois Press.

Binder, J. R. (2017). Current controversies on Wernicke's area and its role in language. *Current Neurology and Neuroscience Reports*, *17*(8), 58. https://doi.org/10.1007/s11910-017-0764-8

Birbaumer, N., & Schmidt, R. F. (2019[32]). Kognitive Prozesse (Denken) und Sprache.

In R. Brandes, F. Lang, & R. F. Schmidt (Hrsg.), *Physiologie des Menschen mit Pathophysiologie* (864–876). Berlin: Springer.

Bludau, S., Bzdok, D., Gruber, O., Kohn, N., Riedl, V., Sorg, C., Palomero-Gallagher, N., Müller, V. I., Hoffstaedter, F., Amunts, K., & Eickhoff, S. B. (2016). Medial prefrontal aberrations in major depressive disorder revealed by cytoarchitectonically informed voxel-based morphometry. *American Journal of Psychiatry*, *173*(3), 291–298. https://doi.org/10.1176/appi.ajp.2015.15030349

Bludau, S., Eickhoff, S. B., Mohlberg, H., Caspers, S., Laird, A. R., Fox, P. T., Schleicher, A., Zilles, K., & Amunts, K. (2014). Cytoarchitecture, probability maps and functions of the human frontal pole. *NeuroImage*, *93*(Pt 2), 260–275. https://doi.org/10.1016/j.neuroimage.2013.05.052

Bludau, S., Mühleisen, T. W., Eickhoff, S. B., Hawrylycz, M. J., Cichon, S., & Amunts, K. (2018). Integration of transcriptomic and cytoarchitectonic data implicates a role for MAOA and TAC1 in the limbic-cortical network. *Brain Structure and Function*, *223*(5), 2335–2342. https://doi.org/10.1007/s00429-018-1620-6

Bohland, J. W., & Guenther, F. H. (2006). An fMRI investigation of syllable sequence production. *NeuroImage*, *32*(2), 821–841. https://doi.org/10.1016/j.neuroimage.2006.04.173

Brodmann, K. (1909). *Vergleichende Lokalisationslehre der Großhirnrinde*. Leipzig: Barth.

Brodmann, K. (1914). Physiologie des Gehirns. In A. Knoblauch, & K. Brodmann (Hrsg.), *Die allgemeine Chirurgie der Gehirnkrankheiten* (S. 86–426). Stuttgart: Verlag von Ferdinand Enke.

Brown, S., Martinez, M. J., & Parsons, L. M. (2006). Music and language side by side in the brain: A PET study of the generation of melodies and sentences. *European Journal of Neuroscience*, *23*(10), 2791–2803. https://doi.org/10.1111/j.1460-9568.2006.04785.x

Campbell, A. W. (1905). *Histological studiens on the localisation of cerebral function*. Cambridge, UK: Cambridge University Press.

Caspers, S., Eickhoff, S. B., Geyer, S., Scheperjans, F., Mohlberg, H., Zilles, K., &

Amunts, K. (2008). The human inferior parietal lobule in stereotaxic space. *Brain Structure and Function*, *212*(6), 481–495. https://doi.org/10.1007/s00429-008-0195-z

Caspers, S., Geyer, S., Schleicher, A., Mohlberg, H., Amunts, K., & Zilles, K. (2006).The human inferior parietal cortex: Cytoarchitectonic parcellation and interindividual variability. *NeuroImage*, *33*(2), 430–448. https://doi.org/10.1016/j.neuroimage.2006.06.054

Caspers, S., Moebus, S., Lux, S., Pundt, N., Schütz, H., Mühleisen, T. W., Gras, V., Eickhoff, S. B., Romanzetti, S., Stöcker, T., Stirnberg, R., Kirlangic, M. E., Minnerop, M., Pieperhoff, P., Mödder, U., Das, S., Evans, A. C., Jöckel, K. H., Erbel, R., … Amunts, K. (2014). Studying variability in human brain aging in a population-based German cohort-rationale and design of 1000BRAINS. *Frontiers in Aging Neuroscience*, *6*, 149. https://doi.org/10.3389/fnagi.2014.00149

Catani, M., Jones, D. K., & Ffytche, D. H. (2005). Perisylvian language networks of the human brain. *Annals of Neurology*, *57*(1), 8–16. https://doi.org/10.1002/ana.20319

Chiang, J. N., Rosenberg, M. H., Bufford, C. A., Stephens, D., Lysy, A., & Monti, M. M. (2018). The language of music: Common neural codes for structured sequences in music and natural language. *Brain and Language, 185,* 30–37. https://doi.org/10.1016/j.bandl.2018.07.003

Chikazoe, J., Lee, D. H., Kriegeskorte, N., & Anderson, A. K. (2019). Distinct representations of basic taste qualities in human gustatory cortex. *Nature Communications*, *10*(1), 1048. https://doi.org/10.1038/s41467-019-08857-z

Choi, H. J., Zilles, K., Mohlberg, H., Schleicher, A., Fink, G. R., Armstrong, E., & Amunts, K. (2006). Cytoarchitectonic identification and probabilistic mapping of two distinct areas within the anterior ventral bank of the human intraparietal sulcus. *Journal of Comparative Neurology*, *495*(1), 53–69. https://doi.org/10.1002/cne.20849

De Witte, S., Klooster, D., Dedoncker, J., Duprat, R., Remue, J., & Baeken, C. (2018). Left prefrontal neuronavigated electrode localization in tDCS: 10–20 EEG system versus MRI-guided neuronavigation. *Psychiatry Research - Neuroimaging*, *274*, 1–6. https://doi.org/10.1016/j.pscychresns.2018.02.001

Draguhn, A. (2019[32]). Höhere zentralnervöse Funktionen. In R. Brandes, F. Lang, &

R. F. Schmidt (Hrsg.), *Physiologie des Menschen mit Pathophysiologie* (S. 791–803). Berlin: Springer.

Duong, A., Quabs, J., Kucyi, A., Lusk, Z., Buch, V., Caspers, S., & Parvizi, J. (2023). Subjective states induced by intracranial electrical stimulation matches the cytoarchitectonic organization of the human insula. *Brain Stimulation*, *16*(6), 1653–1665. https://doi.org/10.1016/j.brs.2023.11.001

Eickhoff, S. B., Amunts, K., Mohlberg, H., & Zilles, K. (2006a). The human parietal operculum. II. Stereotaxic maps and correlation with functional imaging results. *Cerebral Cortex*, *16*(2), 268–279. https://doi.org/10.1093/cercor/bhi106

Eickhoff, S. B., Jbabdi, S., Caspers, S., Laird, A. R., Fox, P. T., Zilles, K., & Behrens, T. E. J. (2010). Anatomical and functional connectivity of cytoarchitectonic areas within the human parietal operculum. *Journal of Neuroscience*, *30*(18), 6409–6421. https://doi.org/10.1523/JNEUROSCI.5664-09.2010

Eickhoff, S. B., Lotze, M., Wietek, B., Amunts, K., Enck, P., & Zilles, K. (2006b). Segregation of visceral and somatosensory afferents: An fMRI and cytoarchitectonic mapping study. *NeuroImage*, *31*(3), 1004–1014. https://doi.org/10.1016/j.neuroimage.2006.01.023

Eickhoff, S. B., Schleicher, A., Scheperjans, F., Palomero-Gallagher, N., & Zilles, K. (2007). Analysis of neurotransmitter receptor distribution patterns in the cerebral cortex. *NeuroImage*, *34*(4), 1317–1330. https://doi.org/10.1016/j.neuroimage.2006.11.016

Eickhoff, S. B., Schleicher, A., Zilles, K., & Amunts, K. (2006c). The human parietal operculum. I. Cytoarchitectonic mapping of subdivisions. *Cerebral Cortex*, *16*(2), 254–267. https://doi.org/10.1093/cercor/bhi105

Eickhoff, S. B., Stephan, K. E., Mohlberg, H., Grefkes, C., Fink, G. R., Amunts, K., & Zilles, K. (2005). A new SPM toolbox for combining probabilistic cytoarchitectonic maps and functional imaging data. *NeuroImage*, *25*(4), 1325–1335. https://doi.org/10.1016/j.neuroimage.2004.12.034

Eickhoff, S. B., Yeo, B. T. T., & Genon, S. (2018). Imaging-based parcellations of the human brain. *Nature Reviews Neuroscience*, *19*(11), 672–686.

https://doi.org/10.1038/s41583-018-0071-7

Evans, A. C., Janke, A. L., Collins, D. L., & Baillet, S. (2012). Brain templates and atlases. *NeuroImage*, *62*(2), 911–922. https://doi.org/10.1016/j.neuroimage.2012.01.024

Fiez, J. A., Tranel, D., Seager-Frerichs, D., & Damasio, H. (2006). Specific reading and phonological processing deficits are associated with damage to the left frontal operculum. *Cortex*, *42*(4), 624–643. https://doi.org/10.1016/S0010-9452(08)70399-X

Fine, J. M., & Hayden, B. Y. (2022). The whole prefrontal cortex is premotor cortex. *Philosophical Transactions of the Royal Society B: Biological Sciences*, *377*(1844), 20200524. https://doi.org/10.1098/rstb.2020.0524

Flechsig, P. (1898). Neue Untersuchungen über die Marbildung in den menschlichen Grosshirnlappen. *Neurologisches Zentralblatt (Leipzig)*, *21*, 977–996.

Friederici, A. D. (2006). Broca's area and the ventral premotor cortex in language: Functional differentiation and specificity. *Cortex*, *42*(4), 472–475. https://doi.org/10.1016/S0010-9452(08)70380-0

Friederici, A. D. (2009). Pathways to language: fiber tracts in the human brain. *Trends in Cognitive Sciences*, *13*(4), 175–181. https://doi.org/10.1016/j.tics.2009.01.001

Friederici, A. D. (2011). The brain basis of language processing: From structure to function. *Physiological Reviews*, *91*(4), 1357–1392. https://doi.org/10.1152/physrev.00006.2011

Friederici, A. D. (2017). *Language in our brain: The origins of a uniquely human capacity.* Cambridge, MA: MIT Press.

Friederici, A. D., Bahlmann, J., Heim, S., Schubotz, R. I., & Anwander, A. (2006a). The brain differentiates human and non-human grammars: Functional localization and structural connectivity. *Proceedings of the National Academy of Sciences of the United States of America*, *103*(7), 2458–2463. https://doi.org/10.1073/pnas.0509389103

Friederici, A. D., Fiebach, C. J., Schlesewsky, M., Bornkessel, I. D., & Von Cramon, D. Y. (2006b). Processing linguistic complexity and grammaticality in the left frontal cortex. *Cerebral Cortex*, *16*(12), 1709–1717. https://doi.org/10.1093/cercor/bhj106

Friederici, A. D., Opitz, B., & Von Cramon, D. Y. (2000). Segregating semantic and syntactic aspects of processing in the human brain: An fMRI investigation of different word types. *Cerebral Cortex*, *10*(7), 698–705. https://doi.org/10.1093/cercor/10.7.698

Friederici, A. D., Rüschemeyer, S. A., Hahne, A., & Fiebach, C. J. (2003). The role of left inferior frontal and superior temporal cortex in sentence comprehension: Localizing syntactic and semantic processes. *Cerebral Cortex*, *13*(2), 170–177. https://doi.org/10.1093/cercor/13.2.170

Georgiadis, J. R., Farrell, M. J., Boessen, R., Denton, D. A., Gavrilescu, M., Kortekaas, R., Renken, R. J., Hoogduin, J. M., & Egan, G. F. (2010). Dynamic subcortical blood flow during male sexual activity with ecological validity: A perfusion fMRI study. *NeuroImage*, *50*(1), 208–216. https://doi.org/10.1016/j.neuroimage.2009.12.034

Geyer, S., Ledbergt, A., Schleicher, A., Kinomurat, S., & Schormann, T. (1996). Two different areas within the primary motor cortex of man. *Nature*, *530*(1995), 1995–1997. https://doi.org/10.1038/382805a0

Geyer, S., Schleicher, A., & Zilles, K. (1999). Areas 3a, 3b, and 1 of human primary somatosensory cortex: 1. Microstructural organization and interindividual variability. *NeuroImage*, *10*(1), 63–83. https://doi.org/10.1006/nimg.1999.0440

Geyer, S., Schormann, T., Mohlberg, H., & Zilles, K. (2000). Areas 3a, 3b, and 1 of human primary somatosensory cortex. 2. Spatial normalization to standard anatomical space. *NeuroImage*, *11*(6 Pt1), 684–696. https://doi.org/10.1006/nimg.2000.0548

Glasser, M. F., Coalson, T. S., Robinson, E. C., Hacker, C. D., Harwell, J., Yacoub, E., Ugurbil, K., Andersson, J., Beckmann, C. F., Jenkinson, M., Smith, S. M., & Van Essen, D. C. (2016). A multi-modal parcellation of human cerebral cortex. *Nature*, *536*(7615), 171–178. https://doi.org/10.1038/nature18933

Gorno-Tempini, M. L., Hillis, A. E., Weintraub, S., Kertesz, A., Mendez, M., Cappa, S. F., Ogar, J. M., Rohrer, J. D., Black, S., Boeve, B. F., Manes, F., Dronkers, N. F., Vandenberghe, R., Rascovsky, K., Patterson, K., Miller, B. L., Knopman, D. S., Hodges, J. R., Mesulam, M. M., & Grossman, M. (2011). Classification of primary progressive aphasia and its variants. *Neurology*, *76*(11), 1006–1014. https://doi.org/10.1212/WNL.0b013e31821103e6

Gratton, C., Sun, H., & Petersen, S. E. (2018). Control networks and hubs. *Psychophysiology*, *55*(3), 10.1111/psyp.13032. https://doi.org/10.1111/psyp.13032

Grodzinsky, Y. (2000). The neurology of syntax: Language use without Broca's area. *Behavioral and Brain Sciences*, *23*(1), 1–71. https://doi.org/10.1017/S0140525X00002399

Grodzinsky, Y., Deschamps, I., Pieperhoff, P., Iannilli, F., Agmon, G., Loewenstein, Y., & Amunts, K. (2020). Logical negation mapped onto the brain. *Brain Structure and Function*, *225*(1), 19–31. https://doi.org/10.1007/s00429-019-01975-w

Grodzinsky, Y., & Friederici, A. D. (2006). Neuroimaging of syntax and syntactic processing. *Current Opinion in Neurobiology*, *16*(2), 240–246. https://doi.org/10.1016/j.conb.2006.03.007

Hagoort, P. (2014). Nodes and networks in the neural architecture for language: Broca's region and beyond. *Current Opinion in Neurobiology*, *28*, 136–141. https://doi.org/10.1016/j.conb.2014.07.013

Hawrylycz, M. J., Lein, E. S., Guillozet-Bongaarts, A. L., Shen, E. H., Ng, L., Miller, J. A., Van de Lagemaat, L., N., Smith, K. A., Ebbert, A., Riley, Z. L., Abajian, C., Beckmann, C. F., Bernard, A., Bertagnolli, D., Boe, A. F., Cartagena, P. M., Chakravarty, M. M., Chapin, M., Chong, J., … Jones, A. R. (2012). An anatomically comprehensive atlas of the adult human brain transcriptome. *Nature*, *489*(7416), 391–399. https://doi.org/10.1038/nature11405

Hawrylycz, M. J., Miller, J. A., Menon, V., Feng, D., Dolbeare, T., Guillozet-Bongaarts, A. L., Jegga, A. G., Aronow, B. J., Lee, C.-K., Bernard, A., Glasser, M. F., Dierker, D. L., Menche, J., Szafer., Collman, F., Grange, P., Berman, K. A., Mihalas, S., Yao, Z., … Lein, E. (2015). Canonical genetic signatures of the adult human brain. *Nature Neuroscience*, *18*(12), 1832–1844. https://doi.org/10.1038/nn.4171

Heim, S., Pieperhoff, P., Grande, M., Kuijsten, W., Wellner, B., Sáez, L. E., Schulte, S., Südmeyer, M., Caspers, S., Minnerop, M., Binkofski, F., Huber, W., & Amunts, K. (2014). Longitudinal changes in brains of patients with fluent primary progressive aphasia. *Brain and Language*, *131*, 11–19. https://doi.org/10.1016/j.bandl.2013.05.012

Higo, T., Mars, R. B., Boorman, E. D., Buch, E. R., & Rushworth, M. F. S. (2011). Distributed and causal influence of frontal operculum in task control. *Proceedings of the National Academy of Sciences of the United States of America*, *108*(10), 4230–4235. https://doi.org/10.1073/pnas.1013361108

Hömke, L., Amunts, K., Bönig, L., Fretz, C., Binkofski, F., Zilles, K., & Weder, B. (2009). Analysis of lesions in patients with unilateral tactile agnosia using cytoarchitectonic probabilistic maps. *Human Brain Mapping*, *30*(5), 1444–1456. https://doi.org/10.1002/hbm.20617

Holmes, C., Hoge, R., Collins, L., Woods, R., Toga, A., & Evans, A. (1998). Enhancement of MR images using registration for signal averaging. *Journal of Computer Assisted Tomography*, *22*(2), 324–333.

Hurschler, M. A., Liem, F., Jäncke, L., & Meyer, M. (2013). Right and left perisylvian cortex and left inferior frontal cortex mediate sentence-level rhyme detection in spoken language as revealed by sparse fMRI. *Human Brain Mapping*, *34*(12), 3182–3192. https://doi.org/10.1002/hbm.22134

Johnson, M. B., Kawasawa, Y. I., Mason, C. E., Krsnik, Ž., Coppola, G., Bogdanovi, D., Geschwind, D. H., Mane, S. M., State, W., & Šestan, N. (2009). Functional and evolutionary insights into human brain development through global transcriptome analysis. *Neuron, 62*(4), 494–509. https://doi.org/10.1016/j.neuron.2009.03.027

Julich-Brain Atlas (2023a). *Area Op5 (Frontal Operculum) left.* Zugriff am 01.08.2023 unter https://atlases.ebrains.eu/viewer/

Julich-Brain Atlas (2023b). *Parcellation-based structural and resting-state functional brain connectomes of a healthy cohort.* Zugriff am 01.08.2023 unter https://atlases.ebrains.eu/viewer/

Jung, J. Y., Cloutman, L. L., Binney, R. J., & Lambon Ralph, M. A. (2017). The structural connectivity of higher order association cortices reflects human functional brain networks. *Cortex*, *97*, 221–239. https://doi.org/10.1016/j.cortex.2016.08.011

Kaulen, N., Rajkumar, R., Régio Brambilla, C., Mauler, J., Ramkiran, S., Orth, L., Sbaihat, H., Lang, M., Wyss, C., Rota Kops, E., Scheins, J., Neumaier, B., Ermert, J., Herzog, H., Langen, K. J., Lerche, C., Shah, N. J., Veselinović, T., & Neuner, I.

(2022). $mGluR_5$ and $GABA_A$ receptor-specific parametric PET atlas construction – PET/MR data processing pipeline, validation, and application. *Human Brain Mapping*, *43*(7), 2148–2163. https://doi.org/10.1002/hbm.25778

Kiwitz, K., Brandstetter, A., Schiffer, C., Bludau, S., Mohlberg, H., Omidyeganeh, M., Massicotte, P., & Amunts, K. (2022). Cytoarchitectonic maps of the human metathalamus in 3D space. *Frontiers in Neuroanatomy*, *16*, 837485. https://doi.org/10.3389/fnana.2022.837485

Kiwitz, K., Schiffer, C., Spitzer, H., Dickscheid, T., & Amunts, K. (2020). Deep learning networks reflect cytoarchitectonic features used in brain mapping. *Scientific Reports*, *10*(1), 22039. https://doi.org/10.1038/s41598-020-78638-y

Laird, A. R., Eickhoff, S. B., Kurth, F., Fox, P. M., Uecker, A. M., Turner, J. A., Robinson, J. L., Lancaster, J. L., & Fox, P. T. (2009). ALE meta-analysis workflows via the BrainMap database: Progress towards a probabilistic functional brain atlas. *Frontiers in Neuroinformatics*, *3*, 23. https://doi.org/10.3389/neuro.11.023.2009

Lambert, N., Lambot, M. A., Bilheu, A., Albert, V., Englert, Y., Libert, F., Noel, J. C., Sotiriou, C., Holloway, A. K., Pollard, K. S., Detours, V., & Vanderhaeghen, P. (2011). Genes expressed in specific areas of the human fetal cerebral cortex display distinct patterns of evolution. *PLoS ONE*, *6*(3), e17753. https://doi.org/10.1371/journal.pone.0017753

Lashley, K. S., & Clark, G. (1946). The cytoarchitecture of the cerebral cortex of ateles: A critical examination of architectonic studies. *Journal of Comparative Neurology*, *85*(2), 223–305. https://doi.org/ 10.1002/cne.900850207

Levitin, D. J., & Menon, V. (2003). Musical structure is processed in “language” areas of the brain: A possible role for Brodmann Area 47 in temporal coherence. *NeuroImage*, *20*(4), 2142–2152. https://doi.org/10.1016/j.neuroimage.2003.08.016

Mahalanobis, P. C., Majumdar, D. N., & Rao, C. R. (1949). Anthropometric survey of the united provinces, 1941: A statistical study. *Sankhyā: The Indian Journal of Statistics*, *9*(2–3), 90–324.

Mai, J. K., Paxinos, G., & Voss, T. (2008³). *Atlas of the human brain.* Oxford, UK: Elsevier.

Meinzer, M., Darkow, R., Lindenberg, R., & Flöel, A. (2016). Electrical stimulation of the motor cortex enhances treatment outcome in post-stroke aphasia. *Brain*, *139*(4), 1152–1163. https://doi.org/10.1093/brain/aww002

Menon, V., Anagnoson, R. T., Mathalon, D. H., Glover, G. H., & Pfefferbaum, A. (2001). Functional neuroanatomy of auditory working memory in schizophrenia: Relation to positive and negative symptoms. *NeuroImage*, *13*(3), 433–446. https://doi.org/10.1006/nimg.2000.0699

Morosan, P., Schleicher, A., Amunts, K., & Zilles, K. (2005). Multimodal architectonic mapping of human superior temporal gyrus. *Anatomy and Embryology*, *210*(5–6), 401–406. https://doi.org/10.1007/s00429-005-0029-1

Moulier, V., Mouras, H., Pélégrini-Issac, M., Glutron, D., Rouxel, R., Grandjean, B., Bittoun, J., & Stoléru, S. (2006). Neuroanatomical correlates of penile erection evoked by photographic stimuli in human males. *NeuroImage*, *33*(2), 689–699. https://doi.org/10.1016/j.neuroimage.2006.06.037

Naeser, M. A., Martin, P. I., Theoret, H., Kobayashi, M., Fregni, F., Nicholas, M., Tormos, J. M., Steven, M. S., Baker, E. H., & Pascual-Leone, A. (2011). TMS suppression of right pars triangularis, but not pars opercularis, improves naming in aphasia. *Brain and Language*, *119*(3), 206–213. https://doi.org/10.1016/j.bandl.2011.07.005

Nissim, N. R., Moberg, P. J., & Hamilton, R. H. (2020). Efficacy of noninvasive brain stimulation (tDCS or TMS) paired with language therapy in the treatment of primary progressive aphasia: An exploratory meta-analysis. *Brain Sciences*, *10*(9), 597. https://doi.org/10.3390/brainsci10090597

Novick, J. M., Trueswell, J. C., & Thompson-Schill, S. L. (2005). Cognitive control and parsing: Reexamining the role of Broca's area in sentence comprehension. *Cognitive, Affective and Behavioral Neuroscience*, *5*(3), 263–281. https://doi.org/10.3758/CABN.5.3.263

Palomero-Gallagher, N., Kedo, O., Mohlberg, H., Zilles, K., & Amunts, K. (2020). Multimodal mapping and analysis of the cyto- and receptorarchitecture of the human hippocampus. *Brain Structure and Function*, *225*(3), 881–907. https://doi.org/10.1007/s00429-019-02022-4

Pieperhoff, P., Südmeyer, M., Dinkelbach, L., Hartmann, C. J., Ferrea, S., Moldovan, A. S., Minnerop, M., Diaz-Pier, S., Schnitzler, A., & Amunts, K. (2022). Regional changes of brain structure during progression of idiopathic Parkinson's disease – A longitudinal study using deformation based morphometry. *Cortex*, *151*, 188–210. https://doi.org/10.1016/j.cortex.2022.03.009

Quabs, J., Caspers, S., Schöne, C., Mohlberg, H., Bludau, S., Dickscheid, T., & Amunts, K. (2022). Cytoarchitecture, probability maps and segregation of the human insula. *NeuroImage*, *260*, 119453. https://doi.org/10.1016/j.neuroimage.2022.119453

Quirmbach, F., & Limanowski, J. (2022). A crucial role of thefrontal operculum in task-set dependent visuomotor performance monitoring. *eNeuro*, *9*(2), ENEURO.0524-21.2021. https://doi.org/10.1523/ENEURO.0524-21.2021

Riegele, L. (1931). Die Cytoarchitektonik der Felder der Broca'schen Region. *Journal für Psychologie und Neurologie*, *42*, 496–514.

Robinson, J. L., Laird, A. R., Glahn, D. C., Lovallo, W. R., & Fox, P. T. (2010). Metaanalytic connectivity modeling: Delineating the functional connectivity of the human amygdala. *Human Brain Mapping*, *31*(2), 173–184. https://doi.org/10.1002/hbm.20854

Rolls, E. T., Sienkiewicz, Z. J., & Yaxley, S. (1989). Hunger modulates the responses to gustatory stimuli of single neurons in the caudolateral orbitofrontal cortex of the macaque monkey. *European Journal of Neuroscience*, *1*(1), 53–60. https://doi.org/10.1111/j.1460-9568.1989.tb00774.x

Saal, M., Bludau, S., Mohlberg, H., Caspers, S., & Amunts, K. (2021a). Probabilistic cytoarchitectonic map of Area OP8 (Frontal Operculum) (v6.2) [Data set]. EBRAINS. DOI: 10.25493/1CTC-2GS

Saal, M., Bludau, S., Mohlberg, H., Caspers, S., & Amunts, K. (2021b). Probabilistic cytoarchitectonic map of Area OP9 (Frontal Operculum) (v6.2) [Data set]. EBRAINS. DOI: 10.25493/9TCJ-JZ3

Sack, A. T., Kadosh, R. C., Schuhmann, T., Moerel, M., Walsh, V., & Goebel, R. (2009). Optimizing functional accuracy of TMS in cognitive studies: A comparison of methods. *Journal of Cognitive Neuroscience*, *21*(2), 207–221.

https://doi.org/10.1162/jocn.2009.21126

Sarkisov, S. A., Filimonoff, I. N., & Preobrashenskaya, N. S. (1949). *Cytoarchitecture of the human cortex cerebri (Russ.)*. Moskau: Medgiz.

Scheperjans, F., Eickhoff, S. B., Hömke, L., Mohlberg, H., Hermann, K., Amunts, K., & Zilles, K. (2008a). Probabilistic maps, morphometry, and variability of cytoarchitectonic areas in the human superior parietal cortex. *Cerebral Cortex*, *18*(9), 2141–2157. https://doi.org/10.1093/cercor/bhm241

Scheperjans, F., Hermann, K., Eickhoff, S. B., Amunts, K., Schleicher, A., & Zilles, K. (2008b). Observer-independent cytoarchitectonic mapping of the human superior parietal cortex. *Cerebral Cortex*, *18*(4), 846–867. https://doi.org/10.1093/cercor/bhm116

Schiffer, C., Spitzer, H., Kiwitz, K., Unger, N., Wagstyl, K., Evans, A. C., Harmeling, S., Amunts, K., & Dickscheid, T. (2021). Convolutional neural networks for cytoarchitectonic brain mapping at large scale. *NeuroImage*, *240*, 118327. https://doi.org/10.1016/j.neuroimage.2021.118327

Schirner, M., Domide, L., Perdikis, D., Triebkorn, P., Stefanovski, L., Pai, R., Prodan, P., Valean, B., Palmer, J., Langford, C., Blickensdörfer, A., Van der Vlag, M., Diaz-Pier, S., Peyser, A., Klijn, W., Pleiter, D., Nahm, A., Schmid, O., Woodman, M., … Ritter, P. (2022). Brain simulation as a cloud service: The Virtual Brain on EBRAINS. *NeuroImage*, *251*, 118973. https://doi.org/10.1016/j.neuroimage.2022.118973

Schleicher, A., Amunts, K., Geyer, S., Morosan, P., & Zilles, K. (1999). Observer-independent method for microstructural parcellation of cerebral cortex: A quantitative approach to cytoarchitectonics. *NeuroImage*, *9*(1), 165–177. https://doi.org/10.1006/nimg.1998.0385

Schleicher, A., Morosan, P., Amunts, K., & Zilles, K. (2009). Quantitative architectural analysis: A new approach to cortical mapping. *Journal of Autism and Developmental Disorders*, *39*(11), 1568–1581. https://doi.org/10.1007/s10803-009-0790-8

Schleicher, A., Palomero-Gallagher, N., Morosan, P., Eickhoff, S. B., Kowalski, T., De Vos, K., Amunts, K., & Zilles, K. (2005). Quantitative architectural analysis:

A new approach to cortical mapping. *Anatomy and Embryology*, *210*(5–6), 373–386. https://doi.org/10.1007/s00429-005-0028-2

Sigl, B., Caspers, S., Bludau, S., Mohlberg, H., Eickhoff, S. B., & Amunts, K. (2021a). Probabilistic cytoarchitectonic map of Area 6d1 (PreCG) (v7.1) [Data set]. EBRAINS. DOI: 10.25493/KSY8-H3F

Sigl, B., Caspers, S., Bludau, S., Mohlberg, H., Eickhoff, S. B., & Amunts, K. (2021b). Probabilistic cytoarchitectonic map of Area 6d2 (PreCG) (v7.1) [Data set]. EBRAINS. DOI: 10.25493/WJQ5-HWC

Sluming, V., Barrick, T., Howard, M., Cezayirli, E., Mayes, A., & Roberts, N. (2002). Voxel-based morphometry reveals increased gray matter density in Broca's area in male symphony orchestra musicians. *NeuroImage*, *17*(3), 1613–1622. https://doi.org/10.1006/nimg.2002.1288

Smith, E. G. (1907). A new topographical survey of the human cerebral cortex, being an account of the distribution of the anatomically distinct cortical areas and their relationship to te cerebral sulci. *Journal of Anatomy, 41*(Pt 4), 237–254.

Spitzer, H., Amunts, K., Harmeling, S., & Dickscheid, T. (2017). Parcellation of visual cortex on high-resolution histological brain sections using convolutional neural networks. In *2017 IEEE 14th International Symposium on Biomedical Imaging (ISBI 2017)* (S. 920–923). IEEE. https://doi.org/10.1109/ISBI.2017.7950666

Spitzer, H., Kiwitz, K., Amunts, K., Harmeling, S., & Dickscheid, T. (2018). Improving cytoarchitectonic segmentation of human brain areas with self-supervised siamese networks. In A. Frangi, J. Schnabel, C. Davatzikos, C. Alberola-López, & G. Fichtinger (Hrsg.), *Medical Image Computing and Computer Assisted Intervention – MICCAI 2018: Vol. 11072 (S. 663–671).* Cham, CH: Springer. https://doi.org/10.1007/978-3-030-00931-1_76

Stengel, E. (1930). Morphologische und cytoarchitektonische Studien über den Bau der unteren Frontalwindung bei Normalen und Taubstummen: Ihre individuellen und Seitenunterschiede. *Zeitschrift für experimentelle und angewandte Psychologie*, *42*, 496–514.

Talairach, J., & Tournoux, P. (1988). Co-planar stereotaxic atlas of the human brain.

Clinical Neurology and Neurosurgery, *91*(3), 277–278. https://doi.org/10.1016/0303-8467(89)90128-5

Thompson-Schill, S. L., D'Esposito, M., Aguirre, G. K., & Farah, M. J. (1997). Role of left inferior prefrontal cortex in retrieval of semantic knowledge: A reevaluation. *Proceedings of the National Academy of Sciences of the United States of America*, *94*(26), 14792–14797. https://doi.org/10.1073/pnas.94.26.14792

Toga, A. W., Thompson, P. M., Mori, S., Amunts, K., & Zilles, K. (2006). Towards multimodal atlasses of the human brain. *Nature Reviews Neuroscience*, *7*(12), 952–966. https://doi.org/10.1038/nrn2012

Tremblay, P., & Dick, A. S. (2016). Broca and Wernicke are dead, or moving past the classic model of language neurobiology. *Brain and Language*, *162*, 60–71. https://doi.org/10.1016/j.bandl.2016.08.004

Unger, N., Bludau, S., Mohlberg, H., Caspers, S., & Amunts, K. (2021a). Probabilistic cytoarchitectonic map of Area OP5 (Frontal Operculum) (v3.2) [Data set]. EBRAINS. DOI: 10.25493/KN1A-YX4

Unger, N., Bludau, S., Mohlberg, H., Caspers, S., & Amunts, K. (2021b). Probabilistic cytoarchitectonic map of Area OP6 (Frontal Operculum) (v3.2) [Data set]. EBRAINS. DOI: 10.25493/RQKR-WE4

Unger, N., Bludau, S., Mohlberg, H., Caspers, S., & Amunts, K. (2021c). Probabilistic cytoarchitectonic map of Area OP7 (Frontal Operculum) (v3.2) [Data set]. EBRAINS. DOI: 10.25493/W2D1-DJF

Unger, N., Haeck, M., Eickhoff, S. B., Camilleri, J. A., Dickscheid, T., Mohlberg, H., Bludau, S., Caspers, S., & Amunts, K. (2023). Cytoarchitectonic mapping of the human frontal operculum – New correlates for a variety of brain functions. *Frontiers in Human Neuroscience*, *17*, 1087026. https://doi.org/10.3389/fnhum.2023.1087026

Unger, N., Heim, S., Hilger, D. I., Bludau, S., Pieperhoff, P., Cichon, S., Amunts, K., & Mühleisen, T. W. (2021d). Identification of phonology-related genes and functional characterization of Broca's and Wernicke's regions in language and learning disorders. *Frontiers in Neuroscience*, *15*, 680762. https://doi.org/10.3389/fnins.2021.680762

Veldhuizen, M. G., Albrecht, J., Zelano, C., Boesveldt, S., Breslin, P., & Lundström, J. N. (2011). Identification of human gustatory cortex by activation likelihood estimation. *Human Brain Mapping*, *32*(12), 2256–2266. https://doi.org/10.1002/hbm.21188

Vogt, C., & Vogt, O. (1919). Allgemeinere Ergebnisse unserer Hirnforschung. *Journal für Psychologie und Neurologie*, *25*, 292–398.

Von Economo, C., & Koskinas, G. (1925). *Die Cytoarchitektonik der Hirnrinde des erwachsenen Menschen.* Wien: Springer.

Ward, N. S., & Frackowiak, R. S. J. (2003). Age-related changes in the neural correlates of motor performance. *Brain*, *126*(4), 873–888. https://doi.org/10.1093/brain/awg071

Zachlod, D., Palomero-Gallagher, N., Dickscheid, T., & Amunts, K. (2023). Mapping Cytoarchitectonics and receptor architectonics to understand brain function and connectivity. *Biological Psychiatry*, *93*(5), 471–479. https://doi.org/10.1016/j.biopsych.2022.09.014

Zhao, Y., Halai, A. D., & Lambon Ralph, M. A. (2020). Evaluating the granularity and statistical structure of lesions and behaviour in post-stroke aphasia. *Brain Communications*, *2*(2), fcaa062. https://doi.org/10.1093/braincomms/fcaa062

Zilles, K., & Amunts, K. (2010). Centenary of Brodmann's map conception and fate. *Nature Reviews Neuroscience*, *11*(2), 139–145. https://doi.org/10.1038/nrn2776

Zilles, K., & Amunts, K. (2018). Cytoarchitectonic and receptorarchitectonic organization in Broca's region and surrounding cortex. *Current Opinion in Behavioral Sciences*, *21*, 93–105. https://doi.org/10.1016/j.cobeha.2018.02.011

Zilles, K., Palomero-Gallagher, N., Grefkes, C., Scheperjans, F., Boy, C., Amunts, K., & Schleicher, A. (2002). Architectonics of the human cerebral cortex and transmitter receptor fingerprints: Reconciling functional neuroanatomy and neurochemistry. *European Neuropsychopharmacology*, *12*(6), 587–599. https://doi.org/10.1016/S0924-977X(02)00108-6

Zilles, K., Schleicher, A., & Kretschmann, H. J. (1978). A quantitative approach to cytoarchitectonics: I. The areal pattern of the cortex of Tupaia belangeri. *Anatomy and Embryology, 153*(2), 195–212.

Zilles, K., Stephan, H., & Schleicher, A. (1982). Quantitative cytoarchitectonics of the cerebral cortices of several prosimian species. In E. Armstrong & D. Falk (Hrsg.), *Primate Brain Evolution: Methods and Concepts* (S. 177–201). New York: Plenum Press.

Zilles, K., Zilles, B., & Schleicher, A. (1980). A quantitative approach to cytoarchitectonics - VI. The areal pattern of the cortex of the albino rat. *Anatomy and Embryology*, *159*(3), 335–360. https://doi.org/10.1007/BF00317655

Zimmermann, S., Sakreida, K., Bludau, S., Camilleri, J. A., Hoffstaedter, F., Pelzer, D. I., Aleman, A., Brückner, T., Derntl, B., Frank, E., Frodl, T., Fuentes-Claramonte, P., García-León, M. A., Gruber, O., Hajak, G., Heim, S., Jardri, R., Kogler, L., Kreuzer, P. M., … Poeppl, T. B. (2024). Asymmetry, cytoarchitectonic morphology and genetics associated with Broca's area in schizophrenia. *Nature Mental Health, 2,* 310–319. https://doi.org/10.1038/s44220-023-00200-2

Danksagung

Meiner Doktormutter **Frau Universitätsprofessorin Dr. med. Katrin Amunts** möchte ich für ihre umfassende Betreuung und stete Unterstützung bei der Entstehung dieser Dissertation sehr herzlich danken. Danke, dass Du mein Interesse für die Zytoarchitektonik geweckt hast und mir die Promotion in Düsseldorf und Jülich ermöglicht hast. Ich hätte mir keine bessere Doktormutter vorstellen können. Du bist ein großes wissenschaftliches Vorbild für mich und ich danke Dir für die vielen wertvollen Ratschläge, die konstruktive und aufbauende Kritik und die Möglichkeit zur Weiterentwicklung.

Meinem Zweitbetreuer **Herrn Universitätsprofessor Dr. med. Simon Eickhoff** möchte ich für seine Hilfe in allen Phasen dieser Arbeit sehr herzlich danken. Für die motivierenden Gespräche und den Input zu den Themen der Dissertation bin ich sehr dankbar. Für die Berechnungen der MACM-Analyse möchte ich mich ebenfalls bedanken.

Ganz herzlich bedanke ich mich außerdem bei meinen **Mitdoktorand:innen und Kolleg:innen** aus dem **Cécile und Oskar Vogt-Institut für Hirnforschung in Düsseldorf** und aus dem **Institut für Neurowissenschaften und Medizin (INM-1) des Forschungszentrums Jülich** für die gemeinsame Zeit, die positive Atmosphäre und die produktive Zusammenarbeit bei der Umsetzung gemeinsamer Projekte.

Besonderer Dank gilt…

- **Dr. Sebastian Bludau** für die stete Unterstützung bei der Entstehung dieser Dissertation. Danke für Dein wertvolles Feedback zu schriftlichen Ausarbeitungen und dass Du mir bei kurzfristigen Deadlines immer motivierend zur Seite standest.
- **Universitätsprofessor Dr. Stefan Heim** für die zahlreichen fachlichen Gespräche im neurolinguistischen Bereich und seine Unterstützung seit meinem Studium der Logopädie an der Rheinisch-Westfälischen Technischen Hochschule Aachen. Danke, dass Du mein Interesse für die Wissenschaft geweckt hast.
- **Universitätsprofessorin Dr. Dr. Svenja Caspers** für die Unterstützung bei der zytoarchitektonischen Kartierung.
- **Hartmut Mohlberg** für die Berechnung der Wahrscheinlichkeitskarten.

- **Dr. Thomas Mühleisen** und **Dominique Pelzer** für die Einführung in die Genetik und für die zahlreichen interdisziplinären Gespräche.
- **Dr. Manuel Marx** für den konstruktiven fachlichen Input zu schriftlichen Ausarbeitungen im Zuge der Dissertation.
- **Dr. Julian Quabs, Dr. Martin Saal** und **Jeanette Stangier** für die gemeinsame Arbeit an unseren benachbarten zytoarchitektonischen Arealen.
- **Anna Stössel** für ihre organisatorische Unterstützung bei der Entstehung dieser Arbeit.
- **René Hübbers** für die Unterstützung bei methodischen und technischen Fragen.
- **Ulrich Opfermann-Emmerich** für die technische Betreuung und das Ausleihen der Gehirnschnitte für die Mikroskopie. Wir werden Dich immer in unserer Erinnerung behalten.

Mein größter Dank gilt meiner Familie und meinen Freund:innen. Danke, dass Ihr immer an meiner Seite seid.